Pre-assembled Complexes of naRNA and LL37 Redefine Neutrophil Extracellular Traps as Inflammatory Agents

Dissertation

der Mathematisch-Naturwissenschaftlichen Fakultät

der Eberhard Karls Universität Tübingen

zur Erlangung des Grades eines

Doktors der Naturwissenschaften

(Dr. rer. nat.)

vorgelegt von

M.Sc. Francesca Bork

aus Frankfurt am Main

Tübingen

2022

Gedruckt mit Genehmigung der Mathematisch-Naturwissenschaftlichen Fakultät der Eberhard Karls Universität Tübingen.

Tag der mündlichen Qualifikation:	03.04.2023
Dekan:	Prof. Dr. Thilo Stehle
1. Berichterstatter:	Prof. Alexander N.R. Weber (Ph.D.)
2. Berichterstatterin:	Apl. Prof. Dr. Christiane Wolz
3. Berichterstatterin:	Prof. Dr. Luise Erpenbeck

Acknowledgements

At first, I would like to thank my professor and supervisor Alexander Weber for offering me the opportunity to perform my PhD in his lab and providing me this interesting project, which has really grown on me. I would like to thank him for teaching me a lot about research, helping me to perform experiments needed to fulfil this study, but also pushing me to my limits and thereby teaching me a lot about myself, trusting me to perform well even during rough times. I can definitely say I have learned a lot in the past three years!

Additionally, I would like to thank Professor Hans-Georg Rammensee for giving me the opportunity to perform my PhD at his department. It was a pleasure to be part of the Department of Immunology and to work in such a fantastic environment with great colleagues who became friends.

I would also like to thank Professor Christiane Wolz for being my second PhD examinator, providing me additional supervision.

Furthermore, I want to thank the DFG for funding through the SFB TR156 'The skin as a sensor and effector organ orchestrating local and systemic immune responses'.

This study could not have been performed without all the people who drew blood for me (Markus, Joseph, Malte, Sarah, Jonas) and all the 'Elks' who donated their neutrophils for my experiments, thank you!

I would further like to thank everyone who contributed to this study: Carsten Greve for performing experiments on BlaER1 cells, THP-1 cells, and keratinocytes; Christine Youn, Yu Wang, and Nathan Archer for performing the *in vivo* experiments; Sirui Chen for performing the DLR assay and the PBMC experiments; Pujan Engels for performing the NK cell experiments; Masoud Nasri and Julia Skokowa for providing and differentiating stem cells into neutrophils; Jule Focken for performing the *S. aureus* killing assay; Birgit Schittek and Jasmin Scheurer for providing the 3D human skin equivalent; Marissa Dubbelaar for helping me with the RNASeq analysis; Katharina Hipp and her team for the Electron Microscopy and IF of ultrathin sections; Reinhild Klein and Beate Preuß for providing patient sera and granulocytes, as well as for performing the RNA ELISA; Gimi Latifi for helping me with the RNA isolation from blood; Tzu-Hsuan Chang for culturing *C.albicans*; and Natalya Korn for providing bacterial RNA. I greatly appreciate your work and your contribution; it was a pleasure to cooperate with you!

I would further like to thank all current and former members of AG Weber, who are not only colleagues but friends to me. It was a pleasure to work in such a great, reliable team, in which you can always find a person to joke around with but also help and support if you need it!

Last but not least, I would like to thank my family and friends for always supporting me, listening to me when I had problems, and helping me to get on my feet again to always continue and never give up. I could have not managed it without you!

Summary

Neutrophils, being the most abundant leukocyte population in circulation and mediating the first line of innate immunity, exert different host mechanisms for pathogen clearance, such as the release of neutrophil extracellular traps (NETs). Although first described as a mechanism to trap and kill bacteria, NETs have been additionally reported to be released upon detection of damage-associated molecular patterns (DAMPs). DAMPs consist of non-microbial molecules and can be of exogenous or endogenous origin, e.g. occur after apoptotic cell death. Hence, NETs can be advantageous for the host by fighting invading microbes but also detrimental, as implied by their association with many diseases, such as psoriasis. They are known as drivers of persisting inflammation, although some of the exact underlying mechanisms remain to be explored. With the first report about NET-associated RNA (naRNA) by Herster et al. in 2020, a novel, potential driver of sustained, self-mediated NET formation was introduced. However, until now, naRNA has not been well characterized and its effects in immune modulation not been investigated into detail. This study therefore aimed to gain novel insights into the features and role of naRNA in the human immune system.

First, naRNA was observed to be a common, i.e. canonical, component of NETs, independent of the NET formation pathway (suicidal vs. vital) induced by various stimuli. Furthermore, naRNA was found to be the crucial driver of the self-amplifying properties of NETs, namely extracellular trap release in naïve PMNs. This process was dependent on the RNA receptors TLR8 (in human cells) and Tlr13 (in mouse). Of note, this effect was associated with the complexation of naRNA with the antimicrobial peptide LL37, as isolated, ‘naked’ naRNA was no sufficient NET stimulus, whereas LL37 was able to restore its pro-inflammatory properties. It was therefore investigated if naRNA-LL37 complexes can be found in NETs, since LL37 is known to be a highly abundant component of the latter. Surprisingly, in co-localization analysis and high-resolution electron microscopy imaging, naRNA-LL37 complexes were not only found in NETs, but also in unstimulated PMNs. The pre-assembly in vesicles of resting neutrophils indicated that these complexes not just ‘accidentally’ combine after release of both components during the NET formation process. Moreover, naRNA was not observed to be essential for the well-studied antibacterial properties of NETs, as characterized by a killing assay. Thus, the pro-inflammatory roles of naRNA continued to be a focus of this underlying study. It was hereby observed that NETs mediate IL-8 release in macrophages in a TLR8- and naRNA-dependent fashion. Moreover, NETs induced naRNA-dependent NK cell activation, measured by the secretion of IFN-γ. Additionally, incubation of keratinocyte cultures and of a 3D human skin equivalent with NETs led to a naRNA-dependent activation of these cells, characterized by cytokine ELISA and qPCR. Therefore, naRNA does not only modulate classical immune cells but also epidermal cells with immune functions, such as keratinocytes. Hence, naRNA was considered to play an important role in psoriasis, a disease manifesting mainly in cutaneous inflammation. *In vivo* intradermal injection of naRNA-containing NET content indeed induced psoriasis-like skin inflammation in mice, which was reduced in *Tlr13* KO animals that lack RNA-sensing. Using the well-established murine imiquimod psoriasis model further showed that RNA-sensing was essential for disease progression, since *Tlr13*-deficient mice were protected from sustained inflammation.

Summary

In conclusion, this study characterizes naRNA as a novel composite DAMP, which is pre-packed in neutrophil vesicles and gets extruded during NET formation. This re-defines extracellular trap release from an antimicrobial host defense mechanism to a primary source of inflammatory agents: our data provide evidence for NETs as an abundant origin of immunostimulatory extracellular RNAs. The observation that naRNA modulates various immune responses in a TLR8-dependent manner additionally highlights this TLR and its downstream signaling as novel potential therapeutic target for treatment of NET-related diseases.

Zusammenfassung

Neutrophile Granulozyten sind Teil des angeborenen Immunsystems. Sie stellen die am häufigsten vorkommenden Leukozyten im Blutkreislauf dar und sind die ersten Immunzellen, welche gegen Pathogene ankämpfen, sobald diese in den Körper gelangen. Ein Abwehrmechanismus, der hierfür durch diese Zellen ausgeführt wird, ist die Freisetzung der sogenannten neutrophilen extrazellulären Fallen (neutrophil extracellular traps (NETs)). Obwohl sie ursprünglich als Mechanismus zum Fangen und Abtöten von Bakterien beschrieben wurden, ist zusätzlich bekannt, dass NETs bei der Erkennung von schädigungsassoziierten molekularen Mustern (damage-associated molecular patterns (DAMPs)) freigesetzt werden. DAMPs bestehen aus nicht-mikrobiellen Molekülen und können exogenen oder endogenen Ursprungs sein, z. B. treten sie nach dem apoptotischen Zelltod auf. Daher können NETs von Vorteil sein, indem sie eindringende Mikroben bekämpfen, aber auch schädlich, wie ihre Assoziation mit vielen Krankheiten, z. B. Psoriasis, zeigt. Sie sind dafür bekannt, dass sie anhaltende Entzündungen fördern, obwohl einige der genauen zugrunde liegenden Mechanismen noch erforscht werden müssen. Mit dem ersten Bericht über NET-assoziierte RNA (naRNA) von Herster et al. im Jahr 2020 wurde ein neuartiger, potenzieller Auslöser für eine anhaltende, selbstvermittelte NET-Bildung vorgestellt. Bislang wurde naRNA jedoch nicht weiter charakterisiert und deren Auswirkung auf Immunantworten nicht näher untersucht. Es war daher das Ziel dieser Studie, neue Erkenntnisse über die Eigenschaften und die Rolle von naRNA im menschlichen Immunsystem zu gewinnen.

Zunächst wurde festgestellt, dass naRNA ein allgemeiner, kanonischer Bestandteil von NETs ist, unabhängig vom Typ der NET-Bildung (suizidal oder vital) und der eingesetzten Stimuli. Darüber hinaus hat sich gezeigt, dass naRNA die entscheidende Rolle in den selbstinduzierenden Eigenschaften von NETs spielt. Dieser Prozess war abhängig von den RNA-Rezeptoren TLR8 (in menschlichen Zellen) und Tlr13 (in Mäusen). Diese Wirkung war mit der Komplexierung von naRNA mit dem antimikrobiellen Peptid LL37 verbunden, da isolierte, "nackte" naRNA keinen ausreichenden NET-Stimulus darstellte, während LL37 die pro-inflammatorischen Eigenschaften wiederherstellen konnte. Es wurde daher untersucht, ob naRNA-LL37-Komplexe in NETs gefunden werden können, da LL37 bekanntermaßen ein sehr häufig vorkommender Bestandteil von NETs ist. Überraschenderweise wurden naRNA-LL37-Komplexe bei der Ko-Lokalisierungsanalyse und der hochauflösenden elektronenmikroskopischen Bildgebung nicht nur in NETs, sondern auch in nicht-stimulierten PMNs gefunden. Die Präassoziierung in Vesikeln ruhender Neutrophiler Granulozyten deutet darauf hin, dass sich diese Komplexe nicht nur "zufällig" nach der Ausschüttung der beiden Komponenten während der NET-Freisetzung bilden. In einem Test zur antimikrobiellen Wirkung wurde festgestellt, dass naRNA für die gut charakterisierten, antibakteriellen Eigenschaften von NETs nicht wesentlich ist. Die pro-inflammatorischen Funktionen von naRNA, wie z. B. die bereits erwähnte Selbstamplifikation von NETs, standen daher fortan im Mittelpunkt der zugrunde liegenden Studie. Dabei wurde beobachtet, dass NETs die Freisetzung von IL-8 in Makrophagen in einer TLR8- und naRNA-abhängigen Weise vermitteln, sowie eine naRNA-abhängige NK-Zell-Aktivierung induzieren, welche durch die Ausschüttung von IFN-γ detektiert wurde. Darüber hinaus führte die Inkubation von Keratinozyten und einem menschlichen 3D-Hautäquivalent mit NETs zu einer naRNA-abhängigen Aktivierung dieser Zellen, was durch einen Zytokin-ELISA und eine qPCR ermittelt wurde.

Daher moduliert naRNA nicht nur klassische Immunzellen, sondern auch epidermale Zellen mit Immunfunktionen, wie z. B. Keratinozyten, die in Erkrankungen wie Psoriasis eine entscheidende Rolle spielen. Die intradermale Injektion von naRNA-haltigen NETs löste bei Mäusen eine Psoriasis-ähnliche Hautentzündung aus, die bei *Tlr13* (dem murinen Äquivalent zum menschlichen TLR8) KO-Tieren reduziert war, welchen die Möglichkeit zur RNA-Erkennung fehlt. Die Verwendung des etablierten Imiquimod-Psoriasis-Maus-Modells zeigte außerdem, dass RNA-Erkennung für das Fortschreiten der Krankheit essenziell ist, da Tlr13-defiziente Mäuse vor anhaltenden Entzündungen geschützt waren.

Zusammenfassend lässt sich sagen, dass diese Studie naRNA als neuartiges zusammengesetztes DAMP charakterisiert, welches in neutrophilen Vesikeln vorverpackt ist und während der NET-Bildung extrudiert wird. Dadurch stellen NETs eine mögliche Quelle für das Immunsystem-modulierende, extrazelluläre RNAs dar und die hier gezeigten Daten definieren die extrazellulären Fallen neu: vom Mechanismus des angeboren Immunsystems als Abwehr gegen Pathogene zur Freisetzung eines körpereigenen, Entzündungs-vermittelnden Wirkstoffs. Die Beobachtung, dass naRNA verschiedene Immunreaktionen in einer TLR8-abhängigen Weise moduliert, hebt diesen TLR und dessen Signalwege zusätzlich als neue, potenzielle therapeutische Ziele für die Behandlung von NET-assoziierten Krankheiten hervor.

Table of contents

Acknowledgements I
Summary II
Zusammenfassung IV
Table of contents VI
Figures XI
Tables XII
Movies XII
Abbreviations XIII
1 Introduction 1
1.1 The human immune system 1
1.1.1 Providing rapid host defense – innate immunity 2
1.1.2 The specific arm of the immune system – the adaptive immunity 4
1.2 Polymorphonuclear neutrophils (PMNs) – the first line of host defense 6
1.2.1 About Neutrophils 6
1.2.2 Crosstalk between PMNs and other immune cells – a highly orchestrated system 9
1.2.3 Neutrophils in pathogen clearance 10
1.3 Neutrophil extracellular traps 12
1.3.1 Characteristics of NETs 12
1.3.2 Interactions of NETs with immune cells 17
1.3.3 NETs and diseases – the downside of extracellular trap formation 19
1.3.3.1 NETs in inflammatory conditions 20
1.3.3.2 NETs in autoimmunity 21
1.3.3.3 NETs and cancer 22
1.3.3.4 NETs in psoriasis and its comorbidities: first insights into molecular mechanisms 22
1.4 Pattern recognition receptors 24
1.4.1 General hallmarks of pattern recognition receptors 24
1.4.2 Toll-like receptors and their roles in immunity 26
1.4.3 Endosomal TLRs – the nucleic acid sensors 29
1.4.4 TLRs and their roles in driving autoimmune diseases 30

1.4.5 Neutrophil TLRs and their roles in inflammatory stages 31
1.5 Extracellular RNA as a DAMP shaping immune responses 33
1.5.1 Definition, origin, and significance of exRNA 33
1.5.2 exRNAs modulate neutrophil activation and NET formation 34
1.6 Aims of this study 35
2 Materials and Methods 37
2.1 Materials 37
2.1.1 Reagents and chemicals 37
2.1.1.1 Reagents and chemicals 37
2.1.1.2 Click chemistry reagents 38
2.1.1.3 Commercial TLR ligands and inhibitors 38
2.1.1.4 Nucleic acid TLR agonists 39
2.1.2 Buffers and media 39
2.1.3 Enzymes 40
2.1.4 Antibodies 41
2.1.5 Plasmids used for transfection of HEK cells 41
2.1.6 Primers used for qPCR 42
2.1.7 Kits 42
2.1.8 Special instruments, equipment, software, and settings 43
2.1.8.1 Special instruments, equipment, and software 43
2.1.8.2 Confocal Microscope Zeiss LSM800 settings 44
2.1.8.3 FACS Canto II settings 44
2.2 Cell biology methods 45
2.2.1 RNA-LL37 complex/RNA/CpG+DOTAP preparation 45
2.2.2 Preparation of fungal RNA from *C. albicans* 45
2.2.3 Mice 45
2.2.4 Isolation and stimulation of bone marrow-derived PMNs (BM-PMNs) 46
2.2.5 Study participants and human blood acquisition 46
2.2.6 Isolation of primary human neutrophils (PMNs) 47
2.2.7 Stimulation of primary human neutrophils (PMNs) 47
2.2.8 Preparation and isolation of NETs and purification of naRNA/whole PMN RNA 47
2.2.9 RNA sequencing analysis of naRNA 48

2.2.10 Extracellular bacterial killing of *S. aureus* 48
2.2.11 Isolation of peripheral blood mononuclear cells (PBMCs) and subsequent stimulation ... 48
2.2.12 Isolation and preparation of primary human stem cell-derived neutrophils 49
2.2.13 Cell culture, transdifferentiation, and stimulation of BlaER1 cells 50
2.2.14 Cell culture, differentiation, and stimulation of THP-1 cells 50
2.2.15 Cell culture and stimulation of N/TERT-1 keratinocytes 50
2.2.16 Culturing and stimulation of primary normal human epidermal keratinocyte (NHEK) cells 51
2.2.17 Preparation of the 3D human skin equivalent 51
2.2.18 qPCR analysis of *IL-8* mRNA of the 3D human skin equivalent 51
2.2.19 Culturing and stimulation of NK-92 MI cells 52
2.2.20 Transient transfection of HEK293T cells 52
2.2.21 Dual luciferase reporter assay 52
2.3 Immunochemical methods 53
2.3.1 Flow cytometry analysis of purity and pre-activation state of PMNs 53
2.3.2 Immunofluorescence (IF) microscopy of fixed human or murine primary neutrophils 53
2.3.3 Quantification of NET formation 54
2.3.4 Quantification of naRNA-LL37-colocalization by using Pearson's Correlation Coefficient. 54
2.3.5 Line plot analysis of high resolution and ultrathin section images 55
2.3.6 Live fluorescence microscopy of RNase digest of human NETs 55
2.3.7 Electron microscopy of NETs, naRNA, and LL37 55
2.3.8 Preparation of ultrathin sections for IF 56
2.3.9 Click chemistry of stem cell-derived human PMNs and IF microscopy 57
2.3.10 Enzyme-linked Immunosorbent Assay (ELISA) 58
2.3.11 Leukocyte RNA-ELISA for detection of anti-RNA autoantibodies 58
2.3.12 Detection of autoantibody-binding to naRNA on resting/NET forming PMNs 59
2.3.13 Quantification of autoantibody-binding to naRNA on resting PMNs 60
2.4 *In vivo* experiments 60
2.4.1 Analysis of naRNA DAMP effects in skin inflammation 60
2.4.2 Fluorescence imaging of neutrophil infiltration after intradermal NET-injection 60
2.4.3 Imiquimod model of psoriatic skin inflammation 61
2.4.4 Histologic analysis of mouse ear skin 61

2.5 Data analysis and statistics 61
3 Results 62
3.1 naRNA is a highly abundant and canonical NET-component 62
3.1.1 naRNA is released independent of the stimulus and type of NET formation 62
3.1.2 Antibody-independent click chemistry labeling of naRNA validates its presence 66
3.1.3 Confirmation of naRNA in NET-fibers by high resolution imaging 68
3.1.4 naRNA consists of different types of RNA 71
3.2 NET formation in primary PMNs is propagated by naRNA, a potent DAMP 72
3.2.1 naRNA does not play a crucial role in the antibacterial properties of NETs 72
3.2.2 naRNA is the main driver of self-propagation of NETs 73
3.3 Human TLR8 and murine Tlr13 are the DAMP-receptors sensing naRNA 75
3.3.1 NETs readily induce TLR8-sensing and self-amplification in a TLR8/Tlr13-dependent manner 75
3.3.2 naRNA induces TLR8-dependent immune responses in macrophages, as well as activation of other immune cells 81
3.3.3 NETs induce naRNA-dependent keratinocyte activation 85
3.4 NET-related *in vivo* inflammation is highly naRNA-dependent 87
3.4.1 naRNA potently triggers Tlr13-dependent inflammatory responses *in vivo* 87
3.4.2 RNA-sensing mediates disease progression in the IMQ psoriasis model 90
3.5 naRNA-LL37 complexes represent a pre-assembled composite DAMP 92
3.5.1 LL37 restores the NET-inducing properties of naRNA 92
3.5.2 naRNA-LL37 complexes are found in resting PMNs as a pre-assembled composite DAMP 94
4 Discussion 97
4.1 The properties of naRNA 98
4.1.1 naRNA is a common component of NETs, independent of the NET-formation pathway .. 98
4.1.2 The composition of naRNA 100
4.1.3 naRNA as an endogenous, sterile NET-inducing agent 100
4.1.4 NET-related TLR8 signaling: which pathway does naRNA induce? 101
4.2 naRNA acts as a novel class of composite DAMP 103
4.2.1 naRNA rather acts pro-inflammatory than providing host defense 104
4.2.2 naRNA-related DAMP activities could be linked to early NET responses 106

4.3 Re-defining NETs: intentional release of DAMP webs 108
4.4 naRNA as a potential driver of (autoimmune) diseases 108
4.4.1 naRNA as a source of exRNA modulating autoimmune diseases 108
4.4.2 SLE-patient sera contain anti-RNA autoantibodies with naRNA-binding affinities 110
4.4.3 naRNA as a possible driver of disease progression in psoriasis 112
4.4.4 COVID-19 pathologies might be naRNA-mediated 112
4.5 Therapeutic implications – targeting naRNA to prevent disease progression 113
4.6 Conclusion 117
5 Appendix 118
5.1 Secondary antibody controls of electron microscopy 118
5.2 Supplemental movies of 3D analysis of naRNA in NET-fibers and naRNA digest by RNase A .. 119
5.2.1 3D reconstruction of NETs: naRNA is speckled on DNA-fibers 119
5.2.2 naRNA digest by RNase A in PMA-induced NETs 119
Statutory Declaration 120
References 121

Figures

Figure 1.1: The stages of granulopoiesis. 8
Figure 1.2: Neutrophil killing mechanisms to clear pathogens. 10
Figure 1.3: Detailed molecular mechanism of NET formation. 13
Figure 1.4: Three proposed mechanisms of NET formation: Suicidal, vital, and mitochondrial NET release. 14
Figure 1.5: NET-associated pathologies: an overview. 19
Figure 1.6: TLRs and their signaling pathways: an overview. 28
Figure 1.7: Hypothesis and aims of this study: naRNA as a DAMP inducing TLR8-dependent inflammatory responses. 36
Figure 3.1: FACS analysis of human PMNs. 63
Figure 3.2: naRNA is an abundant and common component of human and murine NETs. 66
Figure 3.3: Validation of differentiation of stem cell-derived neutrophils. 67
Figure 3.4: Metabolic labeling of naRNA in NETs of stem cell-derived neutrophils. 68
Figure 3.5: High resolution imaging of NETs proves existence of naRNA. 70
Figure 3.6: naRNA consists of different types of RNA. 71
Figure 3.7: naRNA has no antibacterial properties on Staphylococcus aureus. 72
Figure 3.8: naRNA is the main driver of self-propagation of NETs. 75
Figure 3.9: NETs readily induce TLR8-sensing and self-amplification in a TLR8-dependent manner. 78
Figure 3.10: NETs are sensed via Tlr13 in murine BM-PMNs. 81
Figure 3.11: naRNA activates macrophages in a TLR8-dependent manner. 82
Figure 3.12: NETs induce a naRNA-dependent cytokine release in PBMCs and NK cells. 84
Figure 3.13: NETs induce naRNA-dependent keratinocyte activation. 86
Figure 3.14: naRNA potently triggers Tlr13-dependent inflammatory responses in vivo. 89
Figure 3.15: RNA-sensing mediates disease progression in the IMQ psoriasis model. 91
Figure 3.16: LL37 restores the NET-inducing properties of and co-localizes with naRNA. 93
Figure 3.17: Line plot analysis of naRNA and LL37 in human PMNs reveals colocalization in unstimulated cells. 95
Figure 3.18: naRNA-LL37 complexes can be found pre-assembled in intact neutrophils. 96
Figure 4.1: Open questions. 98
Figure 4.2: naRNA as an early inflammation-enhancing DAMP. 107
Figure 4.3: SLE patient sera contain autoantibodies directed against leukocyte RNA, specifically PMN RNA. 111
Figure 4.4: Therapeutic implications – targeting naRNA and its signaling to prevent disease progression. 116
Figure 5.1: Secondary antibody controls of electron microscopy. 118

Tables

Table 1.1: NET formation pathways, possible inducers, and signaling involved. 15
Table 1.2: Interactions of NETs with immune cells. 17
Table 1.3: Pathologies and diseases mediated and driven by NETs. 20
Table 1.4: An overview of human TLRs and their corresponding ligands. 27
Table 2.1: Reagents and chemicals 37
Table 2.2: Click chemistry reagents 38
Table 2.3: Commercial TLR ligands and inhibitors 38
Table 2.4: Nucleic acid TLR agonists 39
Table 2.5: Buffers and media 39
Table 2.6: Enzymes 40
Table 2.7: Antibodies 41
Table 2.8: Plasmids used for transfection of HEK cells 41
Table 2.9: Primers used for qPCR 42
Table 2.10: Kits 42
Table 2.11: Special instruments, equipment, and software 43
Table 2.12: Confocal Microscope Zeiss LSM800 settings 44
Table 2.13: FACS Canto II settings 44
Table 4.1: Sterile NET-inducing agents. 101
Table 4.2: NET-associated DAMPs. 105
Table 4.3: NET-derived autoantigens and associated diseases. 109

Movies

Supplemental Movie S 1: 3D reconstruction of NETs: naRNA is speckled on DNA-fibers. 119
Supplemental Movie S 2: naRNA digest by RNase A in PMA-induced NETs. 119

Abbreviations

5-EU	5-ethynyluridine
A	Adenosine
ACE2	Angiotensin converting enzyme 2
ACPA	Anti-citrullinated protein antibodies
ADAR1	Adenosine deaminase RNA-specific binding protein
AMI	Acute myocardial infarction
AMP	Adenosine monophosphate
ANA	Antinuclear antibodies
ANCA	Anti-neutrophil cytoplasmic antibody
AP1	Activator protein 1
APC	Antigen presenting cell
ARDS	Acute respiratory distress syndrome
ATP	Adenosine 5’-triphosphate
BAFF	B cell activating factor
Bb	Complement factor Bb
BCR	B cell receptor
BET	Basophil extracellular traps
BM	Bone marrow
bRNA	Bacterial RNA
C	Cytidine
C. albicans	*Candida albicans*
cAMP	Cyclic adenosine monophosphate
CD	Cluster of differentiation
CDK	Cyclin-dependent kinase
cfDNA	Cell-free DNA
CLR	C-type lectin-like receptor
CNPY3	Canopy FGF signaling regulator 3
COPII	Coat protein complex II
CREB	Cyclic AMP-responsive element-binding protein
DAMP	Damage-associated molecular pattern
DC	Dendritic cell
DLR	Dual luciferase reporter
dsRNA	Double-stranded RNA
EBI3	Epstein-Barr virus induced gene 3
eCIRP	Extracellular cold-inducible RNA-binding protein
E. coli	*Escherichia coli*
EGFP	Enhanced green fluorescent protein
ELISA	Enzyme-linked immunosorbent assay
EM	Electron microscopy
ER	Endoplasmic reticulum
ERK	Extracellular signal-regulated kinase

ET	Extracellular trap
exRNA	Extracellular RNA
FACS	Fluorescence-activated cell sorting
FGF	Fibroblast growth factor
fRNA	Fungal RNA
G-CSF	Granulocyte colony-stimulating factor
GM-CSF	Granulocyte macrophage colony-stimulating factor
Gp96	Glycoprotein 96
GPCR	G-protein coupled receptors
GSDMD	Gasdermin D
hCAP-18	Human cationic antimicrobial protein 18
H&E	Hematoxylin and eosin
HLA	Histocompatibility leukocyte antigens
HMGB1	High mobility group box protein 1
HPSC	Hematopoietic stem cell
ICAM-1	Intercellular adhesion molecule 1
IF	Immunofluorescence
IFN	Interferon
IgG	Immunoglobulin G
IgM	Immunoglobulin M
IL	Interleukin
IL-36R	IL-36 receptor
IMQ	Imiquimod
iODN	Inhibitory oligodeoxynucleotide
IRAK	IL-1R-associated kinases
JNK	JUN N-terminal kinase
KC	Keratinocyte chemoattractant
KO	Knock-out
LAMP2	Lysosomal membrane protein 2
LCN2	Lipocalin 2
LGP2	Laboratory of genetics and physiology-2
LN	Lupus nephritis
lncRNA	Long non-coding RNA
LPP	Lipoprotein
LPS	Lipopolysaccharide
LTB_4	Leukotriene B_4
MAL	MYD88-adaptor-like protein
MAMP	Microbe-associated molecular pattern
MAPK	Mitogen-activated protein kinase
MC	Mast cell
MCET	Mast cell extracellular trap
MDA5	Melanoma differentiation-associated antigen 5
MEK	MAPK/ERK kinase
MET	Macrophage extracellular trap
MHC	Major histocompatibility complex

MIP-2	Macrophage inflammatory protein 2
miRNA	Micro RNA
MMP	Matrix metalloproteinase
MNC	Mononuclear cell
MPO	Myeloperoxidase
MYD88	Myeloid differentiation primary response 88
NADPH	Nicotinamide adenine dinucleotide phosphate
naRNA	NET-associated RNA
ncRNA	Non-coding RNA
NE	Neutrophil elastase
NET	Neutrophil extracellular trap
NK	Natural killer
NLR	NOD-like receptor
NOD	Nucleotide-binding oligomerization domain
NSP	Neutrophil serine protease
OPA1	Optic atrophy 1
PAD4	Peptidyl arginine deiminase 4
PDK1	Phosphoinositide-dependent kinase-1
piRNA	Piwi-interacting RNA
PKC	Protein kinase C
PMA	Phorbol-12-myristate-13-acetate
PMN	Polymorphonuclear neutrophil
Poly I:C	Polyinosinic-polycytidylic acid
PR3	Proteinase 3
PRR	Pattern recognition receptor
PTEN	Phosphatase and tensin homolog deleted on chromosome 10
R848	Resiquimod
RA	Rheumatoid arthritis
Rab	Ras-related in brain
Rb	Retinoblastoma protein
RIG-I	Retinoic acid-inducible gene I
RLR	RIG-I like receptor
RNP	Ribonucleoprotein
ROS	Reactive oxygen species
rRNA	Ribosomal RNA
RT	Room temperature
S. aureus	*Staphylococcus aureus*
SEM	Scanning electron microscopy
SGEC	Salivary gland epithelial cells
siRNA	Small interfering RNA
SLE	Systemic lupus erythematosus
SLPI	Secretory leukocyte protease inhibitor
Sm	Smith
snoRNA	Small nucleolar RNA
SNP	Single nucleotide polymorphism

snRNA	Small nuclear RNA
snRNP	Small nuclear RNP
SR	Scavenger receptor
SS	Sjögren's Syndrome
SSA	Sjögren's Syndrome antigen-A
ssRNA	Single-stranded RNA
STAT3	Signal transducer and activator of transcription 3
TCR	T cell receptor
TF	Tissue factor
Th	T helper
TIR	Toll IL-1R homology
TLR	Toll-like receptor
TNF	Tumor necrosis factor
TRAF	TNF receptor-associated factors
Treg	Regulatory T cell
TREM-1	Triggering receptor expressed on myeloid cells
TRIF	TIR domain-containing adaptor protein inducing IFN-β
tRNA	Transfer RNA
U	Uridine
UNC93B1	Unc-93 homolog B1
WT	Wild-type

1 Introduction

1.1 The human immune system

Around 8.7 million different eukaryotic species are predicted to live on planet earth (Mora et al. 2011), organisms built of cells containing a nucleus, an endomembrane and a cytoskeleton (Vellai and Vida 1999). However, it is proposed that only a tiny amount of species on earth (~14%) and in the ocean (~9%) has so far been discovered (Mora et al. 2011). Besides eukaryotes, estimated amounts of 4-6 x 10^{30} prokaryotes, single-celled species, which lack a nucleus and other specialized cell organelles, are living on our planet (Hugon et al. 2015). Large multicellular organisms (eukaryotes), like humans, can provide habitats for microbes (prokaryotes), such as bacteria. This interplay can be beneficial for both organisms, i.e. symbiotic or mutualistic, or, alternatively, pathogenic for the host (Moran 2006).

Our body is permanently exposed to countless microbes: there are around 1,400 species known to be pathogenic to humans, including viruses, bacteria, fungi, protozoa, and helminths ('Microbiology by numbers' 2011). Being constantly exposed to those organisms, which are inhaled, swallowed, or can penetrate our skin and mucous membranes (Parkin and Cohen 2001), one can imagine that there must be a highly orchestrated system to defend the body for humans to survive. Besides humans, plants (Ngou, Ding, and Jones 2022), fish (Rauta, Nayak, and Das 2012), and insects (Yang et al. 2021), amongst many more species, are fighting pathogens in a similar and highly conserved manner: with the help of an immune system. The human immune system is defined by a complex and unique interplay between numerous molecules and cell types, which communicate dependent on their cell-surface proteome (Rieckmann et al. 2017).

Determined by the speed and specificity of the reaction, immunity can be divided into two parts, namely the innate and the adaptive immunity (Parkin and Cohen 2001). The innate immune system became of interest in science more than 100 years ago and is described to be composed of the afferent (sensing) arm detecting infections on one, and the efferent (effector) arm eradicating infections on the other hand (Beutler 2004). Physical, chemical, and microbiological barriers are considered elements of the innate immune system. Besides those barriers, innate immune cells, like neutrophils, monocytes, or macrophages, and soluble mediators, like cytokines and acute phase proteins, provide immediate host defense (Janeway and Medzhitov 2002). These relatively general components fight the majority of infections. However, the immune system of higher animals does not only carry out innate but also adaptive responses, i.e. responses that are tailored (adapted) to a specific threat, in case innate defenses are insufficient. The adaptive immune response is thus much more specific, but this precise response can take several days or weeks to develop (Parkin and Cohen 2001). T lymphocytes and antibody-producing B lymphocytes are the main effectors of the cellular part of the adaptive immunity (Bonilla and Oettgen 2010), providing microbe-specific responses and immune memory (Nicholson 2016).

1.1.1 Providing rapid host defense – innate immunity

The two parts of the immune system, although they act together, fulfil distinct roles and have unique properties. Whereas innate immunity provides the first line of host defense and is operational from birth (hence termed “innate”), the adaptive arm becomes prominent after several days post infection, providing pathogen-specific host responses, and matures with age (Chaplin 2010). Innate immunity mediates immediate defensive responses to invading pathogens and cannot only be divided into the afferent and efferent arm but further into anatomic barriers, and humoral as well as cellular components, respectively (Beutler 2004; Murphey, Weaver, and Berg 2022).

Anatomic barriers, such as the skin and mucosa, as well as the intestine and respiratory epithelium are defined as the very first host defense mechanisms, with the aim to avoid contact of external threats with internal tissues. In addition, antimicrobial proteins which act as natural antibiotics are produced by anatomic barriers, e.g. the mucosa, to enhance their host protective effect. However, many microbes overcome those barriers, which leads to the activation of humoral innate immunity, namely the complement system. The complement system consists of more than 30 proteins in plasma and on the cell surface and was first discovered in the 1890s. It involves a signaling cascade resulting in the formation of soluble anaphylatoxins and chemoattractants C3a and C5a and the stable deposition of ‘complement’ (C3b) on the microbe surface, which enables pore formation by other complement factors or better recognition by phagocytes. Three different mechanisms are known to lead to the activation of the complement system: the lectin pathway, the classical pathway, and the alternative pathway. Upon detection of pathogens by the in blood and extracellular fluids circulating receptors mannose-binding lectin (MBL), which recognize microbial carbohydrates, and ficolin, which recognize acetylated sugar containing oligosaccharides, activation of the lectin pathway occurs. The classical pathway is homologous to the lectin one and is activated upon binding to the receptor C1, which can either directly sense the microbe or antibodies opsonizing it and therefore is part of both, the innate and adaptive immune system. The third mechanism, the alternative pathway, is antibody-independent and can be activated by the lectin or classical pathway. Hereby, C3b protein is generated through those pathways and initiates the formation of the alternative C3 convertase C3bBb. C3bBb, which is composed of C3b, in turn can then produce C3b, thereby amplifying generation of itself and C3b. In addition, spontaneous hydrolysis of C3 to C3(H_2O) and subsequent formation of C3(H_2O)Bb fluid-phase C3 convertase can lead to the activation of the alternative pathway (Murphey, Weaver, and Berg 2022). Defects in complement regulation can result in various diseases, like hemolytic uremic syndrome, hereditary angioedema, or systemic lupus erythematosus (SLE) (Sarma and Ward 2011).

Increasingly, innate immune responses mediated by tissue cells are gaining interest, but typically professional innate immune cells are in view when talking about the innate immune system. Neutrophils are the first innate immune cells to be recruited to the side of infection, where they exert pathogen clearance through phagocytosis, degranulation, and the release of neutrophil extracellular traps (NETs). Moreover, macrophages, which can be found in almost all tissues and mature from circulating monocytes, are professional innate immune cells fighting invading microbes directly via phagocytosis and activation of bactericidal mechanisms, as well as indirectly via antigen presentation and production of cytokines which activates other immune cells. The main role of dendritic cells (DCs) is the production of mediators

which act on various immune cells to start their specific defense functions after the uptake and degradation of pathogens in their immature state, as well as the presentation of antigens to T lymphocytes as specialized cells after maturation. Furthermore, eosinophils and basophils, which belong together with neutrophils to the family of granulocytes, are part of the innate immune cells. Antibody-coated parasites are detected and eliminated by eosinophils, whereas basophils can enhance anti-parasitic mechanisms but mainly promote allergic responses. In addition, natural killer (NK) cells can kill other cells through the release of lytic granules, e.g. virus-infected or tumor cells. Last but not least, mast cells are important innate immune cells. These cells are mainly located in barrier tissues, where they release granules which contain inflammatory mediators, like histamine and proteases (Murphey, Weaver, and Berg 2022). The afore mentioned cells can be categorized into phagocytes (neutrophils, monocytes/macrophages), cytotoxic cells (NK cells) and antigen-presenting cells (DCs) (Chaplin 2010), which all bear germline-encoded recognition receptors (Janeway and Medzhitov 2002). Whereas NK cells, a lymphoid lineage, use several types of receptors (e.g. Killer Cell Lectin-Like Receptors) to detect self-patterns on host cells that may be altered as a result of infection or oncogenic transformation (‘altered self’), most innate immune cells and some tissue cells primarily detect non-self by so-called pattern recognition receptors (PRRs) (Murphey, Weaver, and Berg 2022).

These pattern recognition receptors (PRRs) were first described by C. Janeway in 1982. They can be expressed on the cell surface, intracellularly, or secreted into the bloodstream and tissue fluids, and play a role in opsonization, the complement system, in phagocytosis, the activation of proinflammatory signaling pathways, as well as the induction of apoptosis (Janeway and Medzhitov 2002; Gewurz et al. 1982). Toll-like receptors (TLRs) are the most studied PRRs and sense microbe-associated molecular patterns (MAMPs), like gram-negative bacteria-derived lipopolysaccharide (LPS) (Ray et al. 2013), fungal chitin, bacterial flagellin (Ye and Murata 2016) or proteins, nucleic acids, and peptidoglycans of gram-positive bacteria-derived membrane vesicles (Bitto et al. 2021), which leads to the secretion of inflammatory cytokines and ultimately pathogen clearance (Newton and Dixit 2012; Kawai and Akira 2010).

1.1.2 The specific arm of the immune system – the adaptive immunity

Once microbes successfully evade or overcome innate immunity, the adaptive immune responses are activated (Murphey, Weaver, and Berg 2022). Manifesting exquisite specificity for target antigens and the ability to adapt to threats not encountered before are the hallmarks of the adaptive immune system. These characteristics are mediated by antigen-specific receptors expressed on the surfaces of T and B lymphocytes, the main drivers of adaptive immune responses. Generally, cells of the immune system develop from pluripotent hematopoietic stem cells into myeloid stem cells or the common lymphoid progenitor, the latter differentiating further into the major mature lymphocyte populations: B cells, T cells, and NK cells (Chaplin 2010). Maturation of B cells occurs in the bone marrow, whereas T cells mature in the thymus (Murphey, Weaver, and Berg 2022).

Lymphocytes can be divided into naïve ones, which have not been activated through antigen interaction yet, and effector lymphocytes, which are fully functional mature cells after antigen contact. B lymphocytes (B cells) and T lymphocytes (T cells) express different antigen receptors, which are used to distinguish those cells. B cells express the so-called B-cell receptor (BCR), a membrane-anchored immunoglobulin encoded by genes assembled from re-arranged germline elements, giving rise to massive amounts of receptors specific for virtually any structure. B cell receptors recognize antigens via their cell-surface variable region (V region). The subsequent transmitted signal activates the cell, which leads to its clonal expansion and antibody production. B cells which express antibodies are called plasma cells, the effector form of B lymphocytes. Hereby, the antibodies expressed by the plasma cell have the exact same specificity as its B cell receptor. Antibodies released by B cells are crucial for pathogen clearance in adaptive immune responses. Viruses can e.g. be neutralized through antibody-binding, as well as opsonization of pathogens marks those for destruction through phagocytic cells and the complement system. The expression of a cell-surface T-cell receptor (TCR), which is needed for the discrimination between self-derived antigens and foreign ones thereby maintaining self-tolerance, defines T cells. By the arrangement of many hundred germline-encoded gene elements, millions of different antigen receptors can be assembled. The difference between BCRs and TCRs is that TCRs cannot recognize whole antigens but instead short protein antigen fragments, namely peptides. Those antigen peptides are presented to T lymphocytes by major histocompatibility complex (MHC) molecules on the host cell surface of all nucleated cells. Additionally, so-called antigen-presenting cells (APCs), e.g. macrophages or DCs, expose antigens taken up from the outside to T cells. After interaction of the T cell with an antigen specific for its TCR, the cell differentiates into an effector T lymphocyte. Those in turn can be divided into three broad classes, dependent on their activity: cytotoxic T cells, helper T (Th) cells, and regulatory T (Treg) cells. Virus-infected or pathogen-bearing cells are killed by cytotoxic T cells, whereas Th cells serve as signal-mediators and activate functions of other cells via specific cytokines. The production of antibodies by B cells e.g. is mediated by Th cell-derived signals. To limit immune responses and prevent excessive immune cell activation, Treg cells can suppress lymphocyte activity (Murphey, Weaver, and Berg 2022). Besides that, T lymphocytes can be divided by their expression of the so-called cluster of differentiation (CD) markers, which can be described as the ‘molecular fingerprint’ of immune cell types and are used for immunophenotyping (Gabius et al. 2015). CD4-expressing ($CD4^+$) T cells are Th cells which promote humoral and cell-mediated immune responses, e.g. by providing help to B cells or macrophages, respectively. The activation of Th cells is carefully regulated by Tregs and occurs only after naïve $CD4^+$ cells

get presented with antigens of histocompatibility leukocyte antigens (HLA) class II and appropriate co-stimulatory molecules on the surface of professional APCs (Andersen et al. 2006). HLAs are encoded by the major histocompatibility complex (MHC) genes and involved in various immune responses. Class II HLAs are limited in their distribution and only found on certain cell types, whereas HLA class I molecules can be found on all cell types, except red blood cells (Touraine et al. 1989). The latter are derived from MHC class I molecules and get detected by $CD8^+$ T cells, which monitor all cells of the human body, destroying those considered to be a threat to the host. Those dangerous, altered cells can be e.g. virally infected or tumorous cells, which show quantitative and qualitative antigenic differences in the presentation of the MHC class I peptides derived from intracellular protein degradation products of the infected or damaged cell (Andersen et al. 2006). B cells and T cells are not independent from each other, they tightly interact: an antibody response to protein antigens requires the recognition of the same antigen particle by both, B cells and T cells. B cells present specific antigens to the T cell which get recognized by the T lymphocytes leading to their activation, in turn activating the antigen-presenting B cell (Parker 1993).

In addition, creating memory is a hallmark of adaptive immunity. Hereby, some B and T lymphocytes differentiate into memory cells after antigen exposure. Those memory cells can rapidly develop into effector cells after a second contact with the same antigen. Thus, they mediate long-lasting immunity after disease or vaccination (Murphey, Weaver, and Berg 2022).

NK cells express germline-encoded receptors which recognize cell-surface molecules of infected or tumorous cells. Compared to naïve B and T lymphocytes, NK cells are larger and contain cytoplasmic granules. These granules contain cytotoxic molecules, like granzymes and the pore-forming protein perforin, which directly act on the target cell. Thereby, the target cell membrane is penetrated by these cytotoxic effector molecules and programmed cell death is induced (Murphey, Weaver, and Berg 2022). After their discovery, NK cells were initially considered as innate immune cells. However, long-lived NK cells were found and thus, these cells are now considered to be part of both, the innate and the adaptive immune system. As players of the adaptive immune system, NK cells can shape T cell responses and, depending on the immune status, stimulate or inhibit T lymphocytes (O'Brien and Finlay 2019).

1.2 Polymorphonuclear neutrophils (PMNs) – the first line of host defense

1.2.1 About Neutrophils

Neutrophils belong, just as eosinophils and basophils, to the granulocyte family, are the largest leukocyte population in peripheral blood (Murphey, Weaver, and Berg 2022) (50-70% (Liew and Kubes 2019)), and play essential roles in sterile and pathogen-induced inflammation. Eosinophils and basophils make up only a small proportion of peripheral blood cells (6% eosinophils (Murphey, Weaver, and Berg 2022), 0.5-1% basophils (Borzova 2020)) and share biological features, such as roles in allergic inflammation, with rather damaging than protective effects. They are further critical players in host defense against parasites which are too large to be cleared by phagocytes. Neutrophils show distinct functions: they are the most important innate immune cells and classical phagocytes (Murphey, Weaver, and Berg 2022).

Around 60% of hematopoietic stem cells of the bone marrow are granulocyte precursors and will later on mature into polymorphonuclear neutrophils (PMNs) (Kennedy and DeLeo 2009). Thereby, common myeloid progenitor cells develop into common granulocyte monocyte progenitors and further into PMNs in a well-characterized, strictly regulated process (Bartels et al. 2015). Around 10^9 cells/kg of body weight are leaving the bone marrow every day, probably due to the relatively short life span of PMNs (Manz and Boettcher 2014). Once in the blood stream, PMNs can be easily isolated for research purposes and sorted by their CD markers. Neutrophils are regarded $CD11b^+CD14^-CD15^+CD66b^+$ and, if not pre-activated, $CD62L^+$ (Lakschevitz et al. 2016). CD62L is considered a sensitive and early marker which is shed upon PMN activation (Simon et al. 1995). Due to the massive amounts of neutrophils daily released into circulation, the balance between granulopoiesis, bone marrow storage and release, intravascular margination (Manz and Boettcher 2014)(pool of neutrophils which left the circulation into tissue but can be mobilized back into blood stream (Liew and Kubes 2019)), and migration into peripheral tissues is essential and tightly regulated depending on and impacting the hosts health (Manz and Boettcher 2014). For instance, impaired maturation of neutrophils, which can be e.g. caused by mutations in the *ELANE* gene encoding neutrophil elastase (NE) or mutations in *HAX1*, affecting the granulocyte colony-stimulating factor (G-CSF) signaling pathway, can lead to so-called severe congenital neutropenias (SCNs). Patients suffering from hereditary SCNs are susceptible to life-threatening, recurrent infections (Skokowa et al. 2017).

The regulation of neutrophil maturation can be described by differentiating between steady-state homeostasis and emergency granulopoiesis, which is modulated by external stimuli (Hirai et al. 2015). Apoptotic neutrophils are ingested by tissue macrophages during steady-state granulopoiesis, which activates e.g. the transcription of C/EBP-α, a transcription factor that is involved in many biological processes, such as regulating neutrophil development. C/EBP-α activity leads to the suppression of proinflammatory cytokine expression and lowers G-CSF levels. G-CSF is a growth factor released by DCs that participates in and regulates PMN homeostasis and distribution. During infection, emergency granulopoiesis occurs: in the presence of bacteria, C/EBP-β is induced, playing an important role in granulopoiesis induction, as well as in the release of early inflammatory mediators, such as interleukin-1β (IL-1β), tumor necrosis factor (TNF), G-CSF, and granulocyte-macrophage (GM)-CSF (Lawrence, Corriden, and Nizet 2018). In turn, immature ($CD15^+CD16^{low}CD66b^+$) and mature ($CD15^+CD16^{high}CD66b^+$) neutrophils (Ai and Udalova 2020) are released from bone marrow into the blood, leading to neutrophilia, an increased number of circulating neutrophils with elevated amounts of immature cells (Lawrence,

Corriden, and Nizet 2018). It has been suggested that TLRs link steady-state and emergency granulopoiesis by detection of MAMPs of hematopoietic stem and progenitor cells, subsequently stimulating the proliferation and differentiation of PMNs (Nauseef and Borregaard 2014). Additionally, reactive oxygen species (ROS) can be produced by bone marrow myeloid cells through enhanced nicotinamide adenine dinucleotide phosphate (NADPH) oxidase activation, induced via proinflammatory chemokines such as keratinocyte chemoattractant (KC), macrophage inflammatory protein (MIP)-2, G-CSF, and TNF. ROS in turn trigger the oxidation and deactivation phosphatase and tensin homolog deleted on chromosome 10 (PTEN) (Kwak et al. 2015), a tumor suppressor with growth and survival regulatory functions and metabolic regulator (Chen et al. 2018). Finally, this leads to increased G-CSF production and the induction of emergency granulopoiesis (Lawrence, Corriden, and Nizet 2018).

The formation of granules within the developing neutrophil begins between the myeloblast and promyelocyte stages of development, proceeds over four to six days, and is characterized by the stepwise emergence of neutrophil granules and secretory vesicles (Fig. 1.1). In myeloblasts and promyelocytes, which contain large round nuclei, azurophilic (primary) granules occur. These primary granules are packed with defensins, acidic hydrolases, microbicidal proteins, serine proteases, and high amounts of myeloperoxidase (MPO), a lysosomal enzyme triggering proinflammatory functional activities (Lawrence, Corriden, and Nizet 2018). Microorganisms phagocytosed by leukocytes are digested with the help of these enzymes sequestered in the azurophilic granules (Cieutat et al. 1998). In a next maturation step, myelocytes and metamyelocytes produce specific granules, while the round nucleus becomes kidney shaped. Those specific or secondary granules are rich in antimicrobial substances, e.g. lactoferrin, metalloproteinases, and the cathelicidin LL37, which are either mobilized within the phagosome or released into the extracellular milieu, providing microbicidal activities. During the transition of metamyelocytes into band neutrophils, the nucleus becomes band-shaped and gelatinase granules are formed. Those tertiary granules are mobilized when the cell establishes primary rolling contact with the activated endothelium and contain matrix-degrading enzymes, such as gelatinase, as well as membrane receptors. Thus, they are helping in the extravasation of neutrophils into the inflamed tissue during the earliest phases of neutrophil inflammatory responses. In a last step, ficolin-1 granules and secretory vesicles are formed in cells containing the characteristic segmented nucleus of neutrophils. Secretory vesicles are significantly smaller than granules, contain an important reservoir of membrane-associated receptors, actin, actin-binding proteins, and alkaline phosphatase, required in the earliest phases of neutrophil-mediated inflammatory responses. These small vesicles are located throughout the cytoplasm and are the most exocytosed cell organelles of neutrophils, being essential for establishing firm contact with activated vascular endothelium, extravasation from the blood vessels, and chemotaxis-directed migration to the side of inflammation (Lawrence, Corriden, and Nizet 2018).

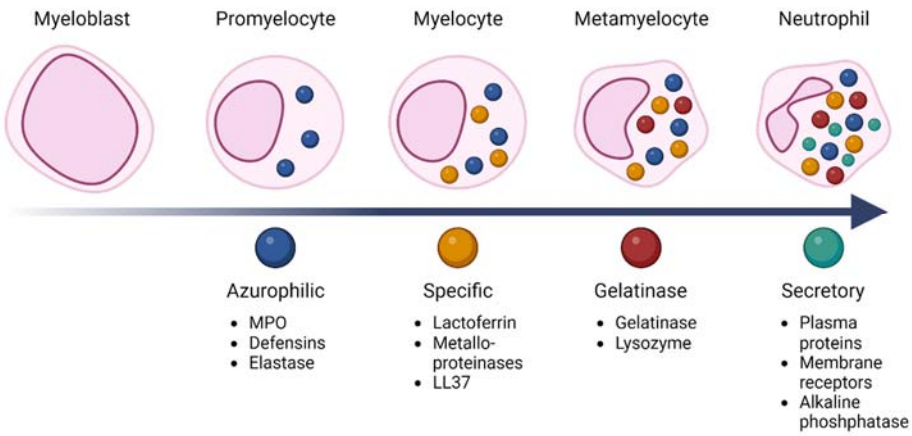

Figure 1.1: The stages of granulopoiesis.

Neutrophil granulopoiesis occurs during maturation of myeloblasts to neutrophils in the bone marrow. At first, myeloblasts develop into promyelocytes with large round nuclei and which contain azurophilic granules. These primary granules are packed with myeloperoxidase (MPO), defensins, and elastase. Afterwards, promyelocytes develop into myelocytes, which additionally contain specific (secondary) granules carrying lactoferrin, metalloproteinases, and LL37. During further maturation, the nucleus becomes more kidney-shaped, a characteristic of metamyelocytes. At those stages, additional gelatinase-containing tertiary granules are formed. Mature neutrophils contain a segmented nucleus, their hallmark. Secretory granules carry plasma proteins, membrane receptors, and alkaline phosphatase, are significantly smaller than the earlier granules and found in mature neutrophils. Created with BioRender.com, adapted from Lawrence et al. (2018) (Lawrence, Corriden, and Nizet 2018).

The formation of granules during neutrophil maturation is needed to fulfill one of their major functions as the first line of host defense during inflammation: their antimicrobial properties. Pathogen clearance of neutrophils is mediated via phagocytosis, degranulation, and the formation of neutrophil extracellular traps (NETs) (discussed in detail in section 1.2.3). To date, PMNs are further considered to exert immunoregulatory functions. In both, healthy and pathological conditions, the latter including cancer, infections, and autoimmune diseases, heterogenous populations of circulating neutrophils have been described, displaying their phenotypic and functional plasticity. Furthermore, tissue-based PMN populations have been characterized, acquiring specialized phenotypes and functions depending on the tissue microenvironment (Silvestre-Roig et al. 2019). To elicit the various functions of neutrophils, coordinated crosstalk between many cell populations is needed and it has been shown that the tissue environment and cellular interactions can have significant impact on neutrophil function (Richardson, Calo, and Hind 2021).

1.2.2 Crosstalk between PMNs and other immune cells – a highly orchestrated system

Within minutes of infection or injury, neutrophils get activated and migrate from the blood vessel to the site of inflammation. This multi-step process is mediated by an intricate meshwork of cellular interactions, including crosstalk between further PMNs, endothelial cells, other immune cells, and/or the pathogen. Hereby, the migration of PMNs to the site of infection or injury is induced by various factors: products of tissue breakdown, as well as chemokines released by other cells can activate granulocyte recruitment. Additionally, complement factors and lipid mediators contribute to neutrophil migration (Kruger et al. 2015). Once arrived at the blood vessel site of infection or tissue injury, PMNs escape the circulation through a series of interactions with endothelial cells, which line the blood vessel lumen, in a process known as the leukocyte adhesion cascade (Richardson, Calo, and Hind 2021). Those endothelial cells upregulate selectin expression, which in turn binds and captures circulating neutrophils (Kanwar et al. 1997; Richardson, Calo, and Hind 2021). The subsequent extravasation into tissue, which can occur through an endothelial cell (transcellular) or between two endothelial cells (paracellular), is mediated by the binding of neutrophil ligands to adhesion molecules on the surface of endothelial cells. Except endothelial cells, other cell types, such as monocytes (Richardson, Calo, and Hind 2021), but also platelets, which are anucleated cells released from bone marrow megakaryocytes into the circulation, regulate the process of neutrophil extravasation. Platelets have been described as pathfinders guiding leukocytes to their exit points in the microvasculature: they were observed to immediately adhere at distinct sites in microvessels, enabling the capturing of PMNs upon onset of inflammation (Zuchtriegel et al. 2016). Others have described the role of platelets in orienting neutrophils for directional extravasation. After extravasation into the tissue, PMNs follow chemoattractant gradients to locate and migrate to the site of inflammation. This is mediated by the over 30 cell surface receptors recognizing proinflammatory signals, e.g. cytokines released by tissue resident cells or damage-associated molecular patterns (DAMPs). Not only neutrophils but also tissue resident cells like macrophages and mast cells recognize DAMPs, MAMPs, and inflammatory cytokines, which in turn leads to their activation and the subsequent production and secretion of additional inflammatory cytokines like IL-8 (also known as CXCL8), a potent PMN chemoattractant. Moreover, a neutrophil-mediated feedback loop leads to further PMN recruitment to the site of infection: the granulocytes release IL-1β, a cytokine activating macrophages, DCs, T cells, and endothelial cells. Those activated cells in turn release further chemokines leading to supplementary neutrophil recruitment (Richardson, Calo, and Hind 2021). In addition, the release of IL-1β and IL-6, as well as the chemokines CXC chemokine ligands (CXCL)1-3 and IL-8 by PMNs themselves leads to self-attraction of further cells within the neutrophil population (Bouchery and Harris 2019). But not only chemokines induce neutrophil attraction. Lipid mediators, such as leukotriene B_4 (LTB_4), produced by both, tissue resident cells and PMNs, are well-known contributors to sustained neutrophil responses. To prevent an overactive immune response, interaction with other immune cells is important for PMN resolution after they have fulfilled their job in pathogen clearance. Monocyte-derived macrophages play an important role in PMN clearance, and dysregulation of this process can lead to autoimmune diseases, such as SLE. Tissue resident macrophages can further downregulate neutrophil swarming and activity by hiding microlesions or, e.g. in fungal infections, by preventing fungal germination, a process which would activate PMNs (Richardson, Calo, and Hind 2021).

Besides bearing innate immune functions, neutrophils interact with cells of the adaptive immune system and can regulate their responses. Large amounts of arginase 1, an enzyme carried in azurophilic granules, as well as ROS can mediate suppression of T cell proliferation and activation. Furthermore, conventional PMNs can become B cell 'helper' neutrophils which release molecules stimulating those cells, such as B cell-activating factor (BAFF) and CD40 ligand (CD40L), and thereby promote the secretion of immunoglobulin (Ig)M and IgG. Additionally, neutrophils have recently been described as APCs, which interact with resident myeloid APCs, prime $CD8^+$ T cells, and elicit anti-tumor responses in mice (Mysore et al. 2021).

1.2.3 Neutrophils in pathogen clearance

Of all the aforementioned functions, the killing mechanisms of neutrophils, which play crucial roles in pathogen clearance and have a high impact on the host's health, are probably the best-studied and most well-known hallmarks of these cells. When microbes penetrate host tissues, they get rapidly recognized by neutrophils, attacked, and subsequently eliminated. The identification of pathogens is mediated via neutrophil PRRs and additionally the help of soluble proteins, like antibodies or complement, opsonizing microbes and thus allowing efficient recognition and uptake or degranulation by PMNs. The binding of pathogenic ligands leads to switching on of diverse signal transduction machineries, coordinating various cellular pathways to initiate antimicrobial responses (Burn et al. 2021). The mechanisms, by which neutrophils elicit pathogen killing, can be divided into phagocytosis, degranulation, and the release of NETs (Fig. 1.2) (Gierlikowska et al. 2021).

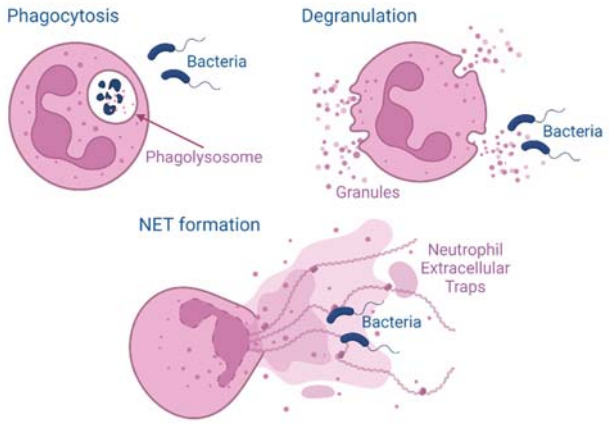

Figure 1.2: Neutrophil killing mechanisms to clear pathogens.

Neutrophils use phagocytosis, degranulation, and the formation of neutrophil extracellular traps (NETs) to protect the host from invading pathogens. During phagocytosis, the pathogens are taken up into the phagosome, which is later on fused to granules containing antimicrobial peptides and lysozymes. In the phagolysosome, an oxidative burst is induced, leading to the killing of the phagocytosed microbe. During degranulation, neutrophils release their granules containing e.g. serine proteases, lactoferrin, and antimicrobial peptides, acting directly (e.g. bacterial membrane lysis) or indirectly (e.g. receptor competition) on the bacteria and their virulence factors, thus providing host defense. In the third mechanism, neutrophils release NETs, which are mesh-like structures composed of nuclear/mitochondrial DNA, histones, and granular contents into the extracellular space. Pathogens get trapped in those sticky chromatin fibers and are killed by the enzymes contained in NETs (Gierlikowska et al. 2021). Created with BioRender.com, adapted from Gierlowska et al. (2021) (Gierlikowska et al. 2021).

Phagocytosis enables the clearance of microbes, as well as dead cells and tissue debris by neutrophils. It is a fundamental mechanism for the effective elimination of disease-causing agents and therefore a crucial component responsible for tissue homeostasis and innate immune responses. During the process of phagocytosis, target organisms or particles can be internalized by two different mechanisms. In the first, the trigger mechanism, discreet signaling initiates the formation of plasma membrane protrusions, shaped by actin and surrounding nearby material. The second mechanism is the so-called 'zipper mechanism', in which cell surface receptors sequentially bind to ligands on the target particle, in turn leading to the complete enveloping of the target molecule by the plasma membrane. Many phagocytic receptors are involved in the latter mechanism, allowing the binding of a wide spectrum of species of pathogens/particles. Receptors of the Fcγ class are essential mediators of phagocytosis and recognize e.g. IgG, whereas TLRs and nucleotide-binding oligomerization domain (NOD)-like receptors (NLRs) do not play a role here. Receptor binding and subsequent activation leads to the initiation of a signaling cascade re-modeling cell membrane lipids. Furthermore, the actin cytoskeleton gets rearranged, and the cell membrane is extended around the target particles, leading to their internalization. This process is highly dependent on several regulators, like Ras-related in brain (Rab) proteins (Gierlikowska et al. 2021), which are membrane proteins coordinating vesicle formation (Zerial and McBride 2001). Rab5 and Rab7 are directly involved in the regulation of phagosome functions. By precise trafficking and fusion/fission processes, membrane proteins and granule contents are directed to distinct locations for fusion of phagosomes with preformed granules. The subsequent activation of granules is assisted by the recruitment of NADPH oxidase, and it is suggested that an oxidative burst in the phagosomes is mediated by their early alkalization (Gierlikowska et al. 2021). NADPH oxidase is a multi-protein complex and mutations in genes of its subunits cause the pathology chronic granulomatous disease (CGD). Granulocytes of CGD patients are impaired in ROS production and thus lack the ability for an oxidative burst. Therefore, a rapid release of high levels of bactericidal reactive chemical species leading to pathogen killing is not possible, which makes patients more susceptible to infections, especially to *Staphylococcus* and *Aspergillus* induced ones (Kruger et al. 2015).

In addition to the intracellular killing of pathogens and clearance of danger molecules by phagocytosis, the extracellular process of degranulation is a well-studied mechanism for neutrophil-mediated antimicrobial host defense and modulation of immune responses by various ways. At first, the afore described tertiary granules are released, then secondary granules, and finally primary (azurophilic) granules, which contain the most pro-inflammatory and antimicrobial proteins, like elastase, MPO, cathepsin G, and defensins (Gierlikowska et al. 2021). These azurophilic granule-derived neutrophil serine proteases (NSPs) can destroy bacterial cells: e.g. neutrophil elastase (NE) has been shown to directly kill the bacteria *Escherichia coli* (*E. coli*) by the cleavage of its outer membrane protein A (OmpA), resulting in the loss of membrane integrity and subsequent cell death. Furthermore, NSPs can cleave host proteins to generate active antimicrobial peptides like LL37 through cleavage of its inactive precursor human cationic antimicrobial protein (hCAP)-18 by proteinase 3 (PR3). Additionally, NSPs can attenuate bacterial virulence by inactivation of pathogenic factors. Moreover, lactoferrin, derived from specific/secondary granules, can block the entry of bacterial pathogens by competitive binding to cell surface receptors, thereby providing antibacterial activity. It has furthermore proteolytic effects, e.g. the degradation of protein virulence factors of *E. coli*, and can prevent adhesion of bacteria by competing with bacterial

adhesion sites directly on the microbe or on host cells. Besides lactoferrin, further secondary granule antimicrobial compounds directly act on bacteria, like calprotectin and lysozymes, whereas tertiary granules mainly serve as storage compartments for a number of metalloproteases, such as gelatinase and leukolysin (Teng et al. 2017). In homeostatic states, primary and secondary granules are mainly released into phagosomes, preventing host tissue damage. This balance can be disrupted and dysregulated by microbes, leading to excessive neutrophil degranulation, even to an extent where host protective effects are diminished. This may benefit the pathogen and extend the disease course (Gierlikowska et al. 2021).

As a third mechanism besides phagocytosis and degranulation, neutrophils have been described to release so-called neutrophil extracellular traps (NETs) as a rapid way of trapping and killing pathogens (Brinkmann et al. 2004). Whether neutrophils undergo NET formation or use another pathogenic killing mechanism like phagocytosis highly depends on the size of the target microbe (Branzk, Lubojemska et al. 2014), but 'multi-tasking', e.g. phagocytosis post-NET release, has also been described (Yipp et al. 2012). As they are a primary focus of this thesis, NETs are next discussed in greater detail.

1.3 Neutrophil extracellular traps

1.3.1 Characteristics of NETs

NETs are mesh-like structures mainly composed of a decondensed DNA backbone, decorated with citrullinated histones and antimicrobial enzymes and peptides. They serve as a rapid and highly effective mechanism to trap pathogens and subsequently kill them. This third mechanism of the neutrophil host defense system was first described and discovered by Arturo Zychlinsky's group in 2004 (Brinkmann et al. 2004). To date, investigating the fundamental mechanisms of NET formation as a novel cell death pathway *in vitro* and *in vivo*, as well as its physiological relevance, has been of great research interest.

The majority of potent inducers of NET formation are of microbial origin, such as gram positive and negative bacteria, LPS, or fungi, or synthetic substances, such as the calcium ionophore A23187 or ionomycin. In addition, cytokines like IL-6 or IL-8 are considered to mediate NET formation (Hoppenbrouwers et al. 2017). However, not many sterile NET inducers, such as sialyl Lewis(X), a tetrasaccharide and ligand for L-selectin found on neutrophil surfaces (Mohanty et al. 2015), have been discovered and characterized to date.

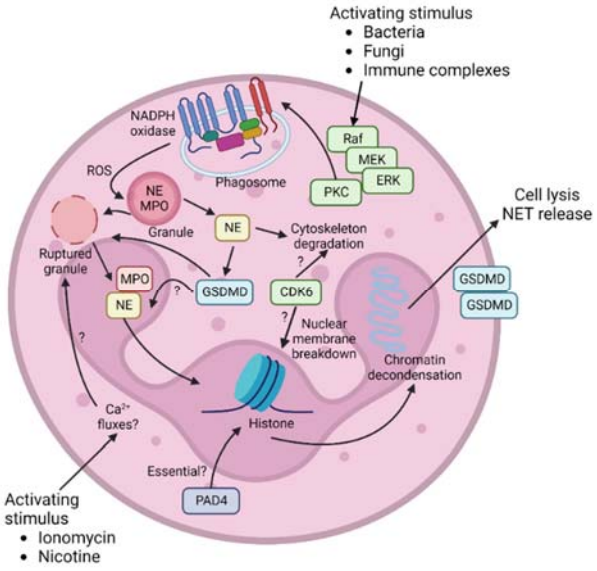

Figure 1.3: Detailed molecular mechanism of NET formation.

The formation of NETs can be NADPH oxidase-dependent (upper half of the figure) or independent (lower half of the figure). During NADPH oxidase dependent NET formation, the Raf-Mek-Erk pathway gets activated, leading to the activation of protein kinase C (PKC) and subsequent ROS production, mediated by NADPH oxidase. ROS in turn trigger the release of NE from granules, which degrades the actin cytoskeleton and activates the protein gasdermin D (GSDMD). GSDMD acts in a feed-forward loop allowing additional NE release. NE translocates to the nucleus cleaving histones and allowing chromatin expansion. In the NADPH oxidase-independent NET formation, granule rupture and release of NE are mediated by Ca^{2+}, which additionally activates PAD4, leading to citrullination of histones and chromatin decondensation. Finally, in both pathways the nuclear membrane breaks down and chromatin fills the cell, getting released as NETs after cell lysis occurs (Rosazza, Warner, and Sollberger 2021). Created with BioRender.com, adapted from Rosazza et al. (2021) (Rosazza, Warner, and Sollberger 2021).

In resting conditions, most of the neutrophil DNA is transcriptionally inactive and condensed into heterochromatin within the nucleus, wrapped around histones forming nucleosomes and further organized into chromatin. The peptidyl arginine deiminase 4 (PAD4) mediates heterochromatin decondensation by catalyzing the conversion of histone arginines to citrullines, a mechanism being considered as one essential initiating step of NET formation. The citrullination of histones reduces their strong positive charges and thus weakens their binding to DNA, leading to the unwrapping of the nucleosomes. Ca^{2+} has been shown to activate PAD4 as an important mediator of intracellular signal transduction during physiological neutrophil activation. Consequently, PAD4-deficicient mice were shown to be unable to form NETs in response microbial activators such as bacteria, highlighting the role of PAD4 in *in vivo* NET formation. During NET formation, NE was also detected to cleave histones, and thus, besides PAD4, is considered as essential for the release of NETs. This was confirmed by an observed loss of the ability to form NETs during *in vivo* experiments in elastase-deficient mice (Sorensen and Borregaard 2016). In detail, NET formation requires the following steps (Fig. 1.3): NADPH oxidase activation, which occurs after binding of DAMPs or MAMPs to neutrophils, leads to the formation of ROS. This can be mediated by various stimuli, their corresponding receptors, and subsequent downstream pathways, such as binding of bacteria to TLR2 or TLR4, the binding of fungi to Dectin2, or the detection of immune complexes by Fcγ

receptors, all leading to the activation of the mitogen-activated protein kinase (MAPK)/ extracellular signal-regulated kinase (ERK)/MAPK/ERK kinase (MEK1 or MEK2) pathway and subsequent protein kinase C (PKC) and therefore NADPH oxidase activation. These ROS stimulate MPO to trigger the activation and translocation of NE from azurophilic granules to the nucleus, where NE performs the afore mentioned histone cleavage. MPO can furthermore bind chromatin and synergizes with NE in its decondensation, independently of the enzymatic activity. This MPO-NE pathway is induced by various stimuli, e.g. fungi and crystals. Of note, in response to some stimuli, mitochondrial ROS are sufficient to drive NET formation, independent of NADPH oxidase activity. Such stimuli being proposed to induce NET formation dependent on mitochondrial ROS are immune complexes, the Ca^{2+} ionophore ionomycin, and nicotine (Papayannopoulos 2018).

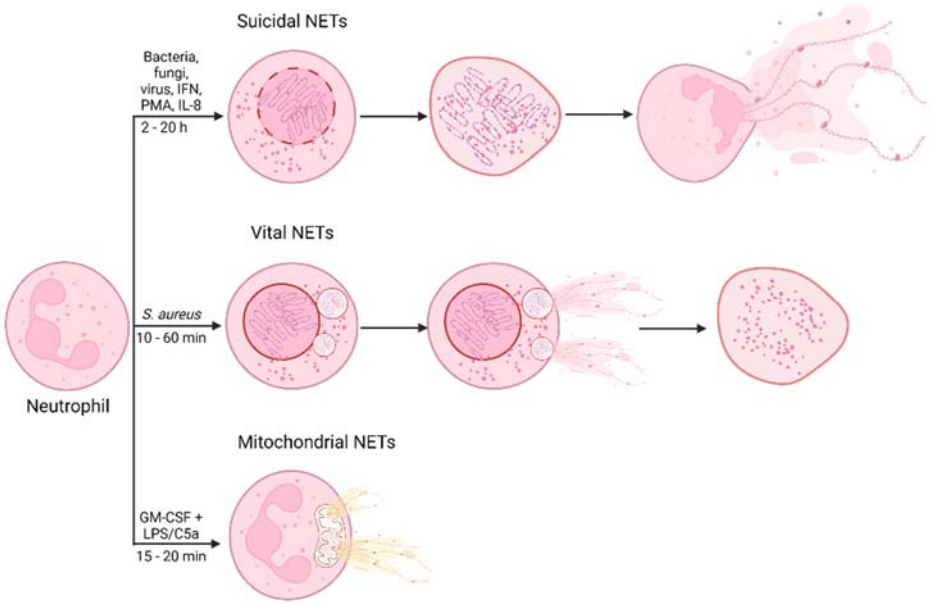

Figure 1.4: Three proposed mechanisms of NET formation: Suicidal, vital, and mitochondrial NET release.

During suicidal NET formation, the neutrophil plasma membrane ruptures upon NET release, which leads to the death of the cell. It occurs 2-20 h after stimulation with various pathogens and DAMPs. In the process of vital NET formation, the neutrophil stays intact after NET release and can even fulfill other functions, like phagocytosis. It occurs rapidly after contact with the target microbe (10-60 min), leaving an anucleated cell behind. The third mechanism, mitochondrial NET formation, relies on the release of mitochondrial DNA and also occurs rapidly after stimulation (Tan, Aziz, and Wang 2021). Created with BioRender.com, adapted from Tan et al. (2021) (Tan, Aziz, and Wang 2021).

Depending on the morphologic changes occurring in neutrophils during NET formation, this process can be classified into three types (Fig. 1.4, Table 1.1): The first type is called suicidal NETosis, in which NETs are released through a cell death mechanism, which takes relatively long (2 – 20 h) and is mediated by pathogens, e.g. bacteria, fungi, or viruses, as well as by cytokines, like IL-8, or the phorbol ester phorbol-12-myristate-13-acetate (PMA), an activator of PKC commonly used as a potent NET inducer. The suicidal NET formation is the most commonly studied and relies on the previously described NADPH oxidase-dependent mechanism. After chromatin decondensation, it disperses into the cytoplasm, where it mixes

with cytoplasmic proteins. In a final step, the plasma membrane ruptures and NETs are released into the extracellular space (Tan, Aziz, and Wang 2021). NADPH oxidase-dependent NETosis has further been observed after infection with human immunodeficiency virus-1 (HIV-1) and characterized to be TLR7/8-mediated (Saitoh et al. 2012).

The second form of NET formation is called vital NET formation, which happens more rapidly than the suicidal form and is induced by certain pathogens, such as *Staphylococcus aureus* (*S. aureus*). It occurs, as the name indicates, without cell death, and the plasma membrane stays intact. Vital NET formation is oxidant-independent and suggested to rely on TLR2-mediated signaling. Furthermore, neutrophils undergoing vital NET formation retain some normal functions, such as phagocytosis (Tan, Aziz, and Wang 2021).

Lastly, the above-mentioned mitochondrial NET formation, in which, as the name implies, mitochondrial DNA is extruded, was observed. The latter happens rapidly, e.g. after pre-treatment of neutrophils with GM-CSF and subsequent stimulation with bacteria derived lipopolysaccharides (LPS) or the complement factor C5a (Tan, Aziz, and Wang 2021), and was first described in 2009 by Yousefi et al. (Yousefi et al. 2009). The release of mitochondrial DNA occurs in a ROS-dependent manner but does not yield in lytic cell death. The process of mitochondrial NET formation has recently been observed in other pathogenic conditions, such as anaplastic thyroid cancers or neutrophils derived of trauma patients (Tan, Aziz, and Wang 2021).

To date, RNA-LL37 complexes have been reported as potent NET inducers but have not been investigated yet regarding the type of NETs they mediate to release after 3 h *in vitro* incubation with neutrophils. Due to their TLR8-dependent signaling (Herster et al. 2020), RNA-LL37 complexes might induce, just as HIV-1 induces NADPH oxidase-dependent NETosis in a TLR7/8-dependent way (Saitoh et al. 2012), the suicidal form of NET formation.

Table 1.1: NET formation pathways, possible inducers, and signaling involved.

Abbreviations: PMA - phorbol-12-myristate-13-acetate, HIV-1 – Human Immunodeficiency Virus-1. Adapted from Tan et al. (2021) (Tan, Aziz, and Wang 2021; Yousefi et al. 2009; Saitoh et al. 2012; Herster et al. 2020; Kenny et al. 2017).

NET formation pathway	(Possible) Inducers	Signaling
Suicidal	Bacteria, fungi, virusses, cytokines (IL-8), PMA HIV-1 RNA-LL37 complexes?	NADPH oxidase-dependent TLR7/8 TLR8
Vital	*Staphylococcus aureus* *Candida albicans*	NADPH oxidase independent, TLR2 PKC, NE, MPO; PAD4-independent
Mitochondrial	GM-CSF + LPS/C5a	NADPH oxidase-dependent

Additionally to the classification of NET formation dependent on the morphological differences, NETs can be characterized by the molecular pathways involved in their release, as suggested by the above described PAD4- and NE-dependency (Sorensen and Borregaard 2016). To date, there exists a controversy as to

whether histone citrullination by PAD4 is required for NADPH oxidase-dependent and -independent NET formation. This is based on the demonstration that the formation of NETs upon stimulation with the NADPH oxidase-independent NET-inducer A23187, a calcium ionophore, shows histone citrullination rather than PMA-mediated NADPH oxidase-dependent NET release (Kenny et al. 2017). Additionally, PAD4-independent NET formation processes have been described more recently: Guiducci *et al.* observed PAD4 to be dispensable in *Candida albicans* (*C. albicans*)-induced NET formation (Guiducci et al. 2018). Moreover, Diaz-Godinez et al. observed a non-classical NET formation process upon stimulation of PMNs with the trophozoite *Entamoeba histolytica*, in which NADPH oxidase2-derived ROS and PAD4-activity is redundant (Diaz-Godinez et al. 2018). Additionally, in an *in vivo* study comparing wild-type (WT) to PAD4-deficient mice, NET formation was found in both animals after infection with the bacteria *Klebsiella pneumoniae* (Claushuis et al. 2018). In contrast, PAD4 was found to be essential in inflammasome-related NET formation: the NLR family pyrin domain containing 3 (NLRP3) inflammasome was reported to be involved in NET formation under sterile conditions. It was hereby observed that PAD4 is necessary for adequate NLRP3 assembly after nigericin stimulation (Munzer et al. 2021). Besides NADPH oxidase, PAD4, and NE, NET formation was described to be, in some cases, dependent on cell cycle molecules. It was found that NET-releasing neutrophils exhibit the expression of various cell-cycle markers, such as Ki-67, a proliferation marker, as well as phosphorylation of Rb, and the cyclin-dependent kinases (CDK)4/6. In addition, NET formation was successfully blocked by CDK4/6 inhibitors by suppressing the translocation of elastase to the nucleus. Furthermore, neutrophils derived of CDK6 knock-out (KO) mice showed impaired NET production upon stimulation with PMA or *C. albicans,* and the KO animals were more susceptible to infections of the latter. Moreover, metabolism was observed to be involved in the process of NET formation, as e.g. neutrophils were not able to form NETs in glucose-free culture medium. Addition of glucose restored this capability, and it was further observed that glycolysis is required for both, NADPH oxidase-dependent and NADPH oxidase-independent NET formation. Besides glucose, optic atrophy (OPA1)-dependent glycolytic adenosine triphosphate (ATP) production was considered essential in the NET formation process (Tan, Aziz, and Wang 2021). In addition to the afore mentioned, Rho GTPase activation leads to NET formation upon stimulation of PMNs with extracellular cold-inducible RNA-binding protein (eCIRP) by increasing intercellular adhesion molecule 1 (ICAM-1) expression via triggering receptor expressed on myeloid cells (TREM-1) (Murao et al. 2020; Tan, Aziz, and Wang 2021).

Taken together, it is evident that the formation of NETs is dependent on many molecular factors and more research on underlying pathways is needed to fully understand this process.

Additionally, although NETs are known to prevent the host from invading pathogens, they are considered as a double edged sword and found to be drivers of many different pathologies, like acute respiratory distress syndrome (ARDS), autoimmune diseases such as vasculitis and SLE, as well as thrombosis and diabetes, amongst others (Sorensen and Borregaard 2016). It is therefore logical that NET formation has an impact on other players of the immune system, e.g. macrophages (Farrera and Fadeel 2013).

1.3.2 Interactions of NETs with immune cells

An overview of the interaction of NETs with immune cells is given in the following table (Table 1.2).

Table 1.2: Interactions of NETs with immune cells.

Abbreviation: pDCs – plasmacytoid DCs.

Immune cell	Effect	Species	*In vitro/in vivo*	Signaling mechanism	Reference
Macrophages	Clearance of dead PMNs after NET release	Human	*In vitro*	Cytochalasin D-dependent Opsonization with C1q	(Farrera and Fadeel 2013)
Macrophages	Activation of caspase 1, release of IL-1β and IL-18, NET induction through IL-18	Human	*In vitro*	-	(Kahlenberg et al. 2013)
Macrophages	NET-associated microRNAs induce TNF production	Human	*In vitro*	-	(Linhares-Lacerda et al. 2020)
pDC	IFN-α release	Human	*In vitro*	DNA uptake	(Garcia-Romo et al. 2011)
Macrophages and DCs	Decrease LPS-induced secretion of proinflammatory cytokines	Human	*In vitro*	-	(Domer et al. 2021)
DCs	Induce expression of antigen presenting molecules				
T cells	Priming of $CD4^+$ T cells				
PMNs	Release of granules, ROS production, NET formation, increased phagocytosis				

After NET release by PMNs, it is crucial to remove those to prevent the triggering of autoimmune diseases (Farrera and Fadeel 2013). Generally, when cells undergo a more common form of cell death, like apoptosis, they are exposing 'eat-me' signals on their surface, which are subsequently recognized by phagocytes, leading to the engulfment and clearance of the dead cell (Lauber et al. 2004). A similar mechanism was shown for clearance of dead neutrophils after the release of NETs: human monocyte-derived macrophages were able to engulf NETs in a cytochalasin D-dependent manner, indicating an active, endocytic process. Furthermore, C1q, a component of the complement system, was found to opsonize NETs to facilitate their uptake (Farrera and Fadeel 2013). However, NETs are not only acting on macrophages and stimulate them to induce their own clearance: they were also shown to induce proinflammatory processes in many ways (Domer et al. 2021). It was observed in SLE patients that PMNs are primed *in vivo* by type I IFN and release NETs upon exposure to SLE-derived anti-ribonucleoprotein antibodies *in vitro*. Those NETs contain DNA, as well as high amounts of LL37 and high mobility group box protein 1 (HMGB1), facilitate uptake of DNA by plasmacytoid DCs (pDCs), activating them to produce great levels of IFN-α (Garcia-Romo et al. 2011). In human macrophages, NETs were shown to directly activate caspase-1, the central enzyme of the inflammasome, leading to the release of active IL-1β and IL-18. In turn, IL-18 was found to induce naïve NET formation, suggesting a feed-forward loop (Kahlenberg et al.

2013). Additionally, microRNAs (miRNAs) associated with NETs were found to induce the production of TNF by macrophages (Linhares-Lacerda et al. 2020), but NETs were also shown to exert anti-inflammatory effects on macrophages and DCs, e.g. by decreasing LPS-induced secretion of proinflammatory cytokines. Moreover, NETs were reported to induce the expression of antigen-presenting molecules by DCs and can even directly act on T cells modulating their functions, as shown by the NET-induced enhanced expression of CD69 and CD25, resulting in $CD4^+$ T cell priming. Taken together, these findings highlight the immunomodulatory roles of NETs, which can actively shape an innate inflammatory, as well as an adaptive response, and should not only be considered as a primitive mechanism to kill invading pathogens (Domer et al. 2021). However, the mechanisms or components of NETs mediating these properties have not been clearly identified and *in vivo* studies are missing.

Additionally to activating other immune cells, NETs can directly act on further neutrophils, inducing proinflammatory activities, thus initiating a positive feedback loop. NETs isolated from PMA-exposed neutrophils induced exocytosis of granules, NADPH-dependent ROS production, NADPH oxidase2-dependent NET formation, as well as increased phagocytosis and killing of microbial pathogens. Furthermore, the secretion of the proinflammatory chemokine IL-8 and the B-cell activating cytokine BAFF was observed after stimulating naïve neutrophils with NETs (Domer et al. 2021). Again, the underlying molecular mechanisms remain to be elucidated.

Looking at the potential effects of NETs on other immune cells and PMNs themselves, of which the ones listed here are only a couple examples, strikingly shows that this orchestrated system needs to be kept in balance to prevent detrimental effects on the host, caused by excessive NET formation.

1.3.3 NETs and diseases – the downside of extracellular trap formation

Besides the functions of NETs in host defense and their immune-protective roles, pathologies caused by NETs have been studied by many research groups and the list of diseases that are linked to NETs is continuously expanding (Papayannopoulos 2018). Examples of pathologies driven and mediated by NETs are given in Figure 1.5 and Table 1.3 and are discussed in more detail in the sections below.

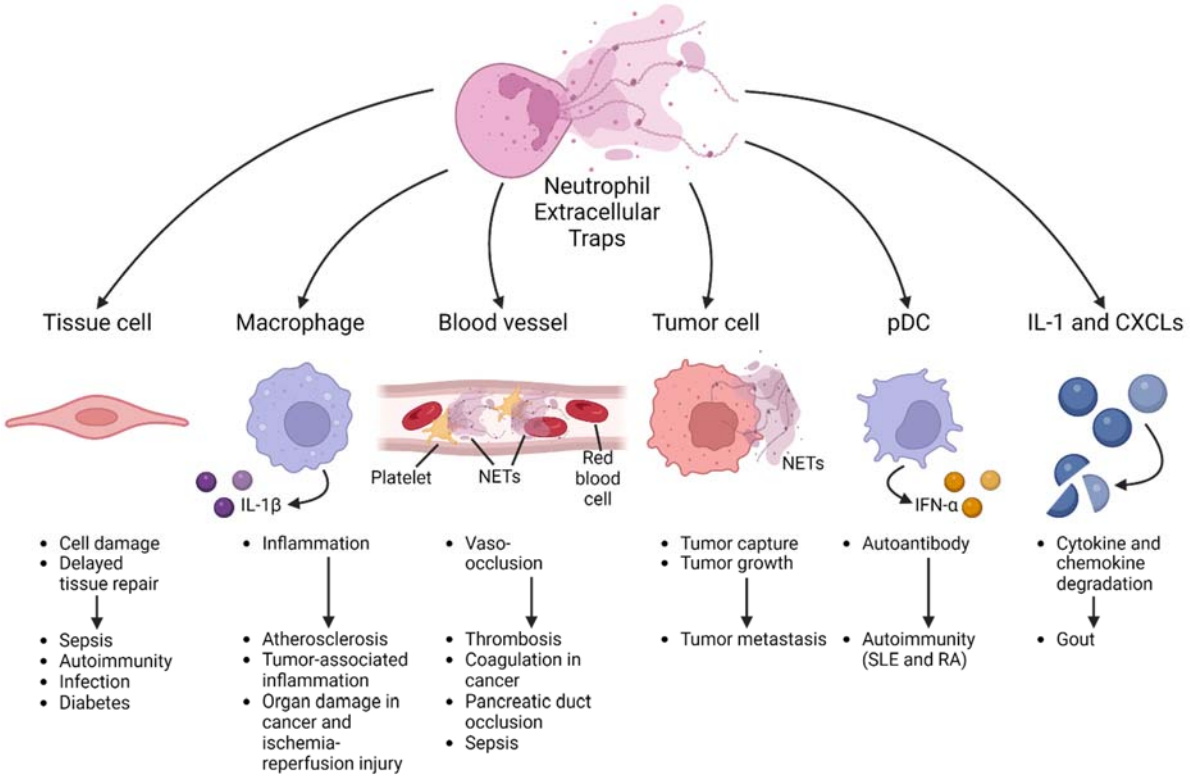

Figure 1.5: NET-associated pathologies: an overview.

Several pathologies are associated with NETs, such as direct cell damage which occurs in infection, sepsis, and diabetes. During inflammation, NETs license macrophages (Papayannopoulos 2018) through priming via exposure of decondensed and proinflammatory DNA (Warnatsch et al. 2015), leading to atherosclerosis, tumor-associated inflammation, and organ damage. In vaso-occlusion, NETs were observed to be drivers of thrombus formation, e.g. via the activation of platelets (Papayannopoulos 2018) through the release of HMGB1 (Kim and Jenne 2016). Additionally, NETs were found to directly act on tumor progression and metastasis formation, as well as serving as a source for autoantigens in autoantibody-mediated autoimmune diseases. Furthermore, NETs were shown to degrade cytokines and chemokines, leading to disease progression in gout (Papayannopoulos 2018). Created with BioRender.com, adapted from Papayannopoulos (2018) (Papayannopoulos 2018).

Table 1.3: Pathologies and diseases mediated and driven by NETs.

Pathology/disease	Effect of NETs	Reference
COVID-19	Thrombus formation	(Yaqinuddin and Kashir 2020; Cicco et al. 2020; Barnes et al. 2020; Golonka et al. 2020)
	Lung tissue damage through induction of endothelial to mesenchymal transition and apoptotic cell death	(Ackermann et al. 2021; Obermayer et al. 2021; Veras et al. 2020)
Atherosclerosis	NETs pile up in sclerotic lesions fueling plaque progression	(Dhawan et al. 2021)
Acute myocardial infarction	Promotion of fibrin deposition and platelet activation	(Bonaventura et al. 2020)
Systemic lupus erythematosus	Impaired clearance of NETs, break of self-tolerance, and interactions with other immune cells, activate complement system and inflammasome, serve as DAMP	(Fousert, Toes, and Desai 2020)
	Source of autoantigens	(Khandpur et al. 2013)
Rheumatoid arthritis		
Anti-neutrophil cytoplasmic antibody (ANCA)-associated vasculitis	Source of autoantigens	(Kessenbrock et al. 2009)
Cancer	Modulate invasion and evasion of cancer cells, as well as metastasis	(Demkow 2021)
Psoriasis	NETs in skin lesions	(Herster et al. 2020; Shao et al. 2019)
	NETs in circulation creating extremely immunogenic environment, activation of TH17 cells and further PMN and keratinocyte activation, type I IFN production of pDCs, release of proinflammatory mediators by DCs	(Chiang et al. 2019)
	Activation of epidermal TLR4/IL-36R crosstalk in keratinocytes and subsequent accumulation of immunocytes	(Shao et al. 2019)
	IFN-α and IFN-β release from pDCs	(Greb et al. 2016)

1.3.3.1 NETs in inflammatory conditions

In addition to well-studied diseases, NETs are of great research interest regarding the relatively novel pathology, COVID-19, mediated by the SARS-CoV-2 coronavirus, a severe contagious respiratory disease causing a pandemic since early 2020 (Janiuk, Jablonska, and Garley 2021). COVID-19-related pathologies include thrombo-inflammatory states, like sepsis, thrombosis, and respiratory failure. Circulating NETs have been found in plasma of hospitalized COVID-19 patients (Zuo et al. 2020) and linked to thrombus formation by several research groups (Yaqinuddin and Kashir 2020; Cicco et al. 2020; Barnes et al. 2020; Golonka et al. 2020). Besides thrombosis, respiratory failure is the leading cause of poor disease outcome after SARS-CoV-2 infection (Xu, Shi, et al. 2020) and NETs have been tightly linked to lung tissue damage

causing this disease pathology (Ackermann et al. 2021; Veras et al. 2020; Obermayer et al. 2021). It was found that SARS-CoV-2 enters cells through angiotensin converting enzyme 2 (ACE2) expressed on renal and pulmonary endothelial cells. Infected endothelial cells release paracrine factors, altering functions of neighboring cells, including neutrophils. Thereby, NET formation is induced. NETs in turn can directly activate endothelial cells, inducing endothelial to mesenchymal transition and apoptotic cell death. Thus, endothelial integrity and barrier functions are compromised, and endothelial dysfunction is further promoted (Ackermann et al. 2021).

Additionally, NET accumulation was described in vascular diseases, like atherosclerosis, in which NET-forming cells pile up in atherosclerotic lesions fueling plaque progression (Dhawan et al. 2021). Moreover, besides the roles of monocytes and macrophages, which have been well-characterized, neutrophils came into focus of acute myocardial infarction (AMI) research, being described to be directly involved in atherothrombosis. During thrombosis, NETs were found to promote fibrin deposition and formation of fibrin networks and additionally activate platelets, leading to further thrombin formation, subsequent plaque rupture finally resulting in AMI (Bonaventura et al. 2020).

Furthermore, NETs have been well characterized in autoinflammatory diseases, such as rheumatoid arthritis (RA) (Khandpur et al. 2013) and systemic lupus erythematosus (SLE) (Fousert, Toes, and Desai 2020). Moreover, NETs have been frequently reported to mediate pathologies in psoriasis (Chiang et al. 2019) and are regarded as potential drivers of disease progression in cancer (Demkow 2021).

1.3.3.2 NETs in autoimmunity

It has been observed in various studies that NETs are present in abundance at inflammatory sites of many autoimmune diseases, making their active involvement in driving autoimmune responses plausible. It is suggested that both, impaired clearance of NETs (e.g. observed in SLE), as well as interactions of NETs with other immune cells lead to the development of autoimmunity and the break of self-tolerance (Fousert, Toes, and Desai 2020). In anti-neutrophil cytoplasmic antibody (ANCA)-associated vasculitis (AAV), NET-associated MPO and PR3 enzymes were characterized as target antigens of autoantibodies (Kessenbrock et al. 2009). In SLE, NET-derived extracellular nucleic acids and dsDNA were observed to be autoantibody targets, as well as citrullinated H3 is considered to be an autoantigen for anti-citrullinated protein antibodies (ACPA) in rheumatoid arthritis (RA) (Khandpur et al. 2013), highlighting NETs as a crucial source of host-derived antigens in these autoimmune diseases. Despite strong evidence that NETs are involved in autoimmune diseases, it is noteworthy that the understanding of the exact mechanisms how NET autoantigens drive autoimmune responses is still in pre-mature state. The lack of knowledge and several missing links to define common mechanisms of NET-derived autoimmunity requires further research, although the currently proposed theory describes a ‘vicious loop of inflammation and autoimmunity’. In the latter, inflammation-mediated NET formation leads to the release of various components, being sources of autoantigens for the production of autoantibodies. It is suggested that these autoantibodies and associated immune complexes may induce additional NET formation, feeding a self-amplifying loop of autoimmune inflammation. Additionally to serving as sources of autoantigens, NETs have been observed to activate the complement system in SLE, serve as DAMPs in SLE and AAV, and activate the inflammasome in SLE or adult-onset Still’s disease (Fousert, Toes, and Desai 2020).

Further to directly serving as target molecules and triggers of inflammatory responses, impaired clearance of NETs usually mediated via macrophages or DNase1 can enhance pathologic processes in the host. In SLE, reduced DNase 1 activity was reported, leading to dysregulated NET clearance. In addition, the deposition of the complement factor C1q on NETs was found to further inhibit the function of this enzyme. Impaired NET clearance leads to their accumulation, in turn leading to increased inflammation and prolonged presence of NET-derived autoantigens (Fousert, Toes, and Desai 2020).

1.3.3.3 NETs and cancer

Besides playing a role in autoimmune and cardiovascular diseases, NETs have been described as drivers of cancer, modulating invasion, evasion, and metastasis. It was found that dormant cancer cells can be awakened by extracellular traps released from neutrophils. Additionally, NETs were found to regulate the tumor microenvironment and add to the aggressiveness of cancer by enhancing its migration and invasion capacity. It was observed that NETs can induce the epithelial to mesenchymal transition in tumor cells and can degrade the extracellular matrix, promoting extravasation of cancer cells. By physically trapping circulating cancer cells, NETs can further facilitate metastasis, thus being detrimental for the host (Demkow 2021).

1.3.3.4 NETs in psoriasis and its comorbidities: first insights into molecular mechanisms

In most of the above-mentioned scenarios, the mechanistic influence of NETs remains to be investigated. However, for psoriasis recently some new insights have been gleaned. It has been reported that NETs are driving disease progression and cause comorbidities, combining some of the previously mentioned NET-related pathologies, such as arthritis or cardiovascular disorders. Psoriasis is a common, chronic, immune-mediated disease manifesting mainly as skin lesions, though being associated with extracutaneous pathologies, affecting more than 125 million people worldwide. Disease outbreaks usually start between the age of 20 to 30, although children and teenagers can be affected, too, manifesting in men and women equally. Clinically, psoriasis can be classified in the following types, depending on the areas of affected skin and plaque phenotype: psoriasis vulgaris, guttate psoriasis, inverse psoriasis, pustular psoriasis, and erythrodermic psoriasis. Erythematous, indurated, and scaling plaques, which are painful, itchy, and have burning sensation, are disease hallmarks. The unpleasant symptoms but also the skin appearance contributes to decreased patients' quality of life, even leading to psychological issues, such as depressions. Thus, long-term physical and psychological treatments are required. However, there is no cure for psoriasis to date, only a reduction of symptoms can be achieved (Chiang et al. 2019).

Immune reactions in psoriasis involve T cell imbalance, keratinocyte proliferation, angiogenesis, and autoantigen formation, initiated by endogenous and exogenous stimuli and neutrophil-derived ROS (Chiang et al. 2019). The abnormal proliferation and differentiation of keratinocytes, leading to epidermal hyperplasia, infiltration of the dermis by various immune cells, and increased dermal capillary density with enhanced permeability in wide-caliber vessels, are hallmarks of the disease (Benhadou, Mintoff, and Del Marmol 2019). Psoriasis patient-derived neutrophils were shown to be pre-activated (Schon, Broekaert, and Erpenbeck 2017; Herster et al. 2020) and NETs were found in high abundancy in skin lesions (Shao et al. 2019; Herster et al. 2020). In addition, increased levels of NETs were detected in patient blood samples with their amount correlating to disease severity and they are suggested to create an extremely

immunogenic environment, participating in the initial and maintenance phases of the disease (Chiang et al. 2019). In the epidermis, NETs drive inflammatory responses by activating epidermal TLR4/IL-36 receptor (IL-36R) crosstalk in keratinocytes. Activation of TLR4/IL-36R crosstalk leads to downstream signaling of myeloid differentiation primary response 88 (MYD88)/nuclear factor-kappa B (NF-κB), resulting in proinflammatory keratinocyte responses. The latter include the expression and release of lipocalin 2 (LCN2), IL-36γ, IL-8 and CXCL1, inflammatory mediators which induce increased accumulation of immunocytes, including neutrophils, resulting in amplification and sustenance of the psoriatic inflammatory cascade (Shao, Fang et al. 2019). pDCs were shown to release IFN-α and IFN-β upon detection of NET-derived chromatin accompanied by LL37, released from keratinocytes (Greb et al. 2016), inducing mDCs to release many proinflammatory mediators, such as IL-6, IL-12, IL-23 and TNF, playing important roles in the initiation of Th17 (IL-17-expressing Th) cell immune responses. Neutrophils, which release PR3 that cleaves pro-IL-36 to its activated form (IL-36), TNF, and IFN-γ, are even amplifying this mDC response. The activation of Th17 cells leads to IL-17 production, in turn activating keratinocytes and neutrophils. pDCs can be further activated to produce type I IFNs thereby regulating autoimmune responses in psoriasis: Secretory leukocyte protease inhibitor (SLPI), a component of NETs with inhibitory effects on NET formation, might bind to DNA and NE in psoriatic skin lesions. Besides, neutrophil antigens are readily sensed by mDCs and NETs allow T cells to be primed directly. Taken together, NETs link the innate and adaptive immunity in psoriasis, therefore playing an important role in the pathophysiology of this disease (Chiang et al. 2019).

To perform *in vivo* studies on psoriasis disease pathogenies, the well-established imiquimod (IMQ)-induced psoriasis-like skin inflammation mouse model is commonly used. Hereby, topical application of the TLR7/8 ligand and potent immune activator IMQ induces and exacerbates inflamed scaly skin lesions in mice (Gilliet et al. 2004). Those lesions show increased epidermal proliferation, abnormal differentiation, epidermal accumulation of neutrophils in microabcesses, neoangiogenesis, and infiltrates consisting of T cells and DCs, comparable to the findings in human plaque type psoriasis. The treatment of the animals with IMQ further leads to epidermal expression of IL-23, IL-17A, and IL-17F, as well as increased amounts of Th17 cells. Additionally, IL-23 or IL-17 receptor-deficient mice were observed to be protected from disease progression, highlighting the pivotal role of the IL-23/IL-17 axis, just as in humans. Thus, topical treatment of mice with IMQ provides a rapid and convenient model, allowing further elucidation of pathogenic mechanisms and evaluation of new therapies in psoriasis (van der Fits et al. 2009).

Depending on the severeness of the disease, different treatment options for psoriasis patients are available. Patients suffering from mild psoriasis can be treated with topical corticosteroids, vitamin D analogues, calcineurin inhibitors, keratolytics, and targeted phototherapy. In moderate to severe cases, phototherapy is the treatment of choice. Alternatively or additionally, patient medication with biologicals is performed. Phototherapy uses narrowband ultraviolet (UV)-B, broadband UV-B, or UV-A irradiation to decrease DNA synthesis, leading to keratinocyte apoptosis and decreased production of proinflammatory cytokines by T cells. Psoralens, like methoxalen, are additionally administered orally or topically prior to UV-A irradiation, intercalating into DNA to suppress its synthesis. Adverse effects of phototherapy include erythema, pruritus, blistering, photoaging, and photocarcinogenesis. Biologicals used to treat psoriasis can be classified into four groups, depending on the target they are acting on, and are mostly administered

subcutaneously: TNF inhibitors, IL-12/23 inhibitors, IL-17 inhibitors, and IL-23 inhibitors. Adverse effects of these medications include injection site reactions, nasopharyngitis, and upper respiratory tract infections. All treatment options cannot provide cure and have to be administered continuously throughout the patient's life, impairing its quality (Armstrong and Read 2020), why further research on psoriasis disease progression and pathogenesis, as well as on novel treatment options is crucial.

For detection of the afore mentioned DAMPs, e.g. NETs, in inflammatory states, which might later on progress to autoimmune diseases, TLRs are essential, as suggested by several studies. Regarding psoriasis it was observed that TLR1 and TLR2 are upregulated on keratinocytes of skin lesions. Since TLRs are major players in immune modulation and absolutely crucial for the overall functioning of the immune system, being beneficial and not only detrimental for the host in many ways (Chen, Szodoray, and Zeher 2016), it is worth to take a closer look at this PRR family.

1.4 Pattern recognition receptors

1.4.1 General hallmarks of pattern recognition receptors

The discrimination between self and non-self is crucial for all multi-cellular organisms exposed to potentially harmful microorganisms. They therefore possess a system for recognition of distinct microbe-associated molecular patterns (MAMPs) present in microbes but not in the host itself (Janeway 1992). This recognition is mediated by the so-called pattern recognition receptors (PRRs), a term coined by Charles Janeway Jr. in 1989 (Janeway 1989). The recognition of microbe-associated molecules by PRRs triggers an immune response in the host, activates conserved host defense signaling pathways, and thereby controls the expression of various immune response genes (Prochazkova et al. 2020; Janeway 1989, 1992). The concept of pattern recognition not only includes detection of the presence of microbes by MAMPs, but also of host molecules modified by microbial enzymes. Another theory suggests that the immune system is not responding only to non-self MAMPs, but additionally to dangerous molecules or cellular damage, regardless of self or non-self origin. Hereby, damage-associated molecular patterns (DAMPs) alert the body of cell and tissue injury by acting as PRR ligands. If the discrimination between non-self and the self-tolerance breaks down, endogenous damage signals can lead to the induction of inappropriate innate immune responses, leading to autoimmunity (Prochazkova et al. 2020).

PRRs can be divided in their subfamilies: TLRs, which are the most characterized PRRs, C-type lectin-like receptors (CLRs), retinoic acid-inducible gene (RIG)-I-like receptors (RLRs), nucleotide-binding oligomerization domain (NOD)-like receptors (NLRs) (Chen, Szodoray, and Zeher 2016) and cytoplasmic DNA sensors (Hopfner and Hornung 2020). Whilst TLRs will be discussed in the next section, a brief overview of the other PRR families is given here:

RLRs mainly sense viral genomic RNA or transcriptional intermediates in the cytoplasm, leading to activation of immunological responses against viral infections: the activation of the NF-κB and type I IFN signaling pathway. The family of RLRs includes three members: RIG-I, melanoma differentiation-associated antigen 5 (MDA5), and laboratory of genetics and physiology-2 (LGP2). RLRs use an RNA helicase-like domain to bind to viral double-stranded (ds)RNAs. Hereby, differences at the 5'end of RNA

transcripts are used by RIG-I to discriminate between host-derived and virus-derived nucleic acids. In contrast to RIG-I, MDA5 does not require a 5'-triphosphate for recognition and generally senses longer dsRNA fragments. LGP2 cooperates with RIG-I and MDA5 for RNA recognition via its helicase domain. Overall, induction of RLRs leads to the activation of mitochondrial antiviral-signaling protein (MAVS) and subsequent type I IFN and proinflammatory cytokine production (Murphey, Weaver, and Berg 2022).

The family of NLRs is a big group of innate sensors which can recognize a broad variety of ligands, such as microbial pathogens, as well as host-derived DAMPs. They are located in the cytosol and consist of a nucleotide-binding and oligomerization domain (NOD), as well as leucine rich repeats (LRRs). Additional domains in the respective NLR results in its distinct function and it is worth noting that not all NLRs are involved in the detection of pathogens, as e.g. NLRC5 and CIITA are regulators of the transcription of MCH class I and II genes. Some NLRs, like NOD1 and NOD2, need only one stimulus for activation: they can directly recognize cell-wall peptidoglycans of bacteria, as NOD1 senses γ-glutamyl diaminopimelic acid (iE-DAP) of e.g. *Salmonella* or *Listeria* and NOD2 binds muramyl dipeptide (MDP), a component of plenty bacteria. Their activation results in NF-κB-activation and leads to the release of proinflammatory cytokines. Other NLRs respond to stimuli with the assembly of a multiprotein complex, the inflammasome. Such a NLR forming an inflammasome is NLR family pyrin domain containing 3 (NLRP3). NLRP3, like most NLRs, is triggered by multiple stimuli, probably in an indirect manner. Thereby, efflux of cellular potassium has been suggested to underpin these different agonists, which can be mediated by e.g. *Staphylococcus aureus*, an intracellular bacterium which produces pore-forming toxins. The inflammasome formation results in proinflammatory cytokine production and induces pyroptotic cell death (Murphey, Weaver, and Berg 2022).

CLRs have been demonstrated to recognize a diverse range of ligands of endogenous and exogenous origin, thereafter regulating a broad repertoire of physiological functions. They mediate innate and adaptive antimicrobial immune responses, mainly by detecting fungal derived MAMPs, but were further observed to contribute to autoimmune disease progression. CLRs can be divided into 17 subgroups depending on the basis of their phylogeny and domain organization and are found as secreted molecules or transmembrane proteins in mammals. Notable examples are dendritic cell-associated C-type lectin 1 (Dectin1) and the mannose receptor. Dectin1 is a receptor for β-glucans of bacterial or fungal cell walls, is mainly expressed in myeloid cells, and signals via RAS/RAF, leading to the activation of NF-κB (Brown, Willment, and Whitehead 2018). Macrophages and dendritic cells express the mannose receptor, which recognizes, as the name indicates, mannosylated ligands that can be present on fungi, bacteria, or viruses. However, the mannose receptor on macrophages is thought to mainly serve as a clearance receptor for host glycoproteins rather than for pathogens. Hereby, β-glucuronidase and lysosomal hydrolases, which are elevated during inflammation, can be detected via their mannose-containing carbohydrate side chains (Murphey, Weaver, and Berg 2022).

During different stages of infection with various pathogens, the microbial, viral, or protozoan DNA might be found in the cytosol of host cells. The main sensor of cytosolic DNA is cyclic guanosine monophosphate-adenosine monophosphate (GAMP) synthase (cGAS), an enzyme. cGAS directly binds to DNA, which leads to the production of cyclic GAMP (cGAMP). cGAMP in turn binds to stimulator of interferon genes (STING), thereby causing a conformational change of STING from its inactive homodimer to its active dimeric form.

Sensing of DNA via the cGAS-STING pathway finally results in the production of type I IFN (Murphey, Weaver, and Berg 2022).

1.4.2 Toll-like receptors and their roles in immunity

The research on the PRR family most-studied to date, the Toll-like receptors (TLRs), started with the discovery of the *Toll* gene in *Drosophila melanogaster* by Katherina Anderson and Christiane Nüsslein-Volhard in 1985. The *Toll* gene was described as a central component of the complex pathway regulating dorsoventral polarity and pattern of the *Drosophila* embryo, thus playing a role in developmental biology (Anderson, Bokla, and Nusslein-Volhard 1985). In the meantime, researchers in immunology reported in the 1980s the discovery of IL-1, a pleiotropic proinflammatory cytokine involved in T cell activation, pyrogenicity, the promotion of cartilage breakdown, and the activation of active phase response. The gene encoding the receptor for IL-1, *IL-1R type 1* (*IL-1R1*), was cloned in 1988 and the sequence was shown to be homologous to the cytosolic domain of the *Drosophila* protein Toll in 1991 (Gay and Keith 1991). This finding led to the observation of Toll playing a role in *Drosophila* antifungal immunity (Lemaitre et al. 1996), the identification of a Toll homologue in human cells (Taguchi et al. 1996), and finally the first observation and description of Toll-like receptors in mammals (Medzhitov, Preston-Hurlburt, and Janeway 1997).

Since then, thousands of papers have investigated the role of different TLRs in various organisms. In humans, 10 different TLR genes are expressed (*TLR1-10*). TLRs recognize MAMPs, which can be components of pathogenic but also nonpathogenic microorganisms, as well as DAMPs. They are transmembrane proteins and either located on the plasma membrane surface (TLR1, TLR2, TLR4-6), or on the endosomal membrane (TLR3, TLR7-9). Mice express Tlr1-9, but not Tlr10. Moreover, mice express Tlr11-13, which are localized in the endosomal membrane and absent in humans. The extracellular region of a TLR consists of 18-25 copies of LRRs of which multiple create a horseshoe-shaped protein scaffold, which serves as the ligand binding site. TLR1, TLR2, and TLR6 form heterodimers, whereas the others form homodimers upon ligand binding, which leads to the activation of the respective TLRs (Murphey, Weaver, and Berg 2022). An overview of the human TLRs and their ligands is given in Table 1.4.

Table 1.4: An overview of human TLRs and their corresponding ligands.

Abbreviations: dsRNA – double-stranded RNA; LPS – lipopolysaccharide; ssRNA – single-stranded RNA. Adapted from Takeuchi et al. (2010) and Janeway's Immunobiology 10th Edition (Takeuchi and Akira 2010; Murphey, Weaver, and Berg 2022).

TLR	Localization	Ligand	Ligand origin
TLR1	Plasma membrane	Triacylated lipopeptides (with TLR2)	Bacteria
TLR2	Plasma membrane	Lipoprotein, oligomeric chitin	Bacteria, viruses, parasites, self
TLR3	Endosome	dsRNA	Viruses
TLR4	Plasma membrane	LPS	Bacteria, viruses, self
TLR5	Plasma membrane	Flagellin	Bacteria
TLR6	Plasma membrane	Diacylated lipopeptides (with TLR2)	Bacteria, viruses
TLR7/8	Endosome	ssRNA/RNA breakdown products	Virus, bacteria, self
TLR9	Endosome	DNA	Virus, bacteria, protozoa, self
TLR10	unknown		

TLR2 was shown to sense bacterial lipopeptides by heterodimerization with either TLR1 to recognize triacylated lipopetides, or with TLR6 to recognize diacylated lipopetides. Besides that, TLR2 has been observed to recognize a wide variety of other non-lipopeptidic MAMPs of various pathogens. Bacteria-derived lipopolysaccharides (LPS) were found to be recognized by the plasma membrane-localized TLR4, which can be endocytosed upon ligand-binding. Flagellin, a protein component of bacterial flagella, was reported to be sensed by TLR5 and this specific TLR was additionally characterized as a modulator of innate and adaptive immune responses upon bacterial sensing in the intestine. The sequence of the TLR10 receptor was observed to be most similar to TLR1, but a role for TLR10 has not been discovered yet (Murphey, Weaver, and Berg 2022).

Besides these abovementioned cytoplasmic TLRs, endosomal TLRs are well characterized. TLR3 was found to recognize dsRNA, a major virus component. TLR7 and TLR8 were both shown to recognize single-stranded (ss)RNA, which can be derived endogenously from host, or exogenously from bacteria or viruses. Additionally, TLR9 was observed to bind exogenous, as well as endogenous DNA. In mice, Tlr11 has been shown to detect a component of uropathogenic bacteria and can cooperate with Tlr12 to bind the *Toxoplasma gondii*-derived profilin protein (O'Neill, Golenbock, and Bowie 2013). The murine Tlr13 has a specificity for bacterial ribosomal RNA rather than for viral RNA sequences (Murphey, Weaver, and Berg 2022). An overview of the different human and murine TLRs and their downstream signaling pathways is given in Figure 1.6.

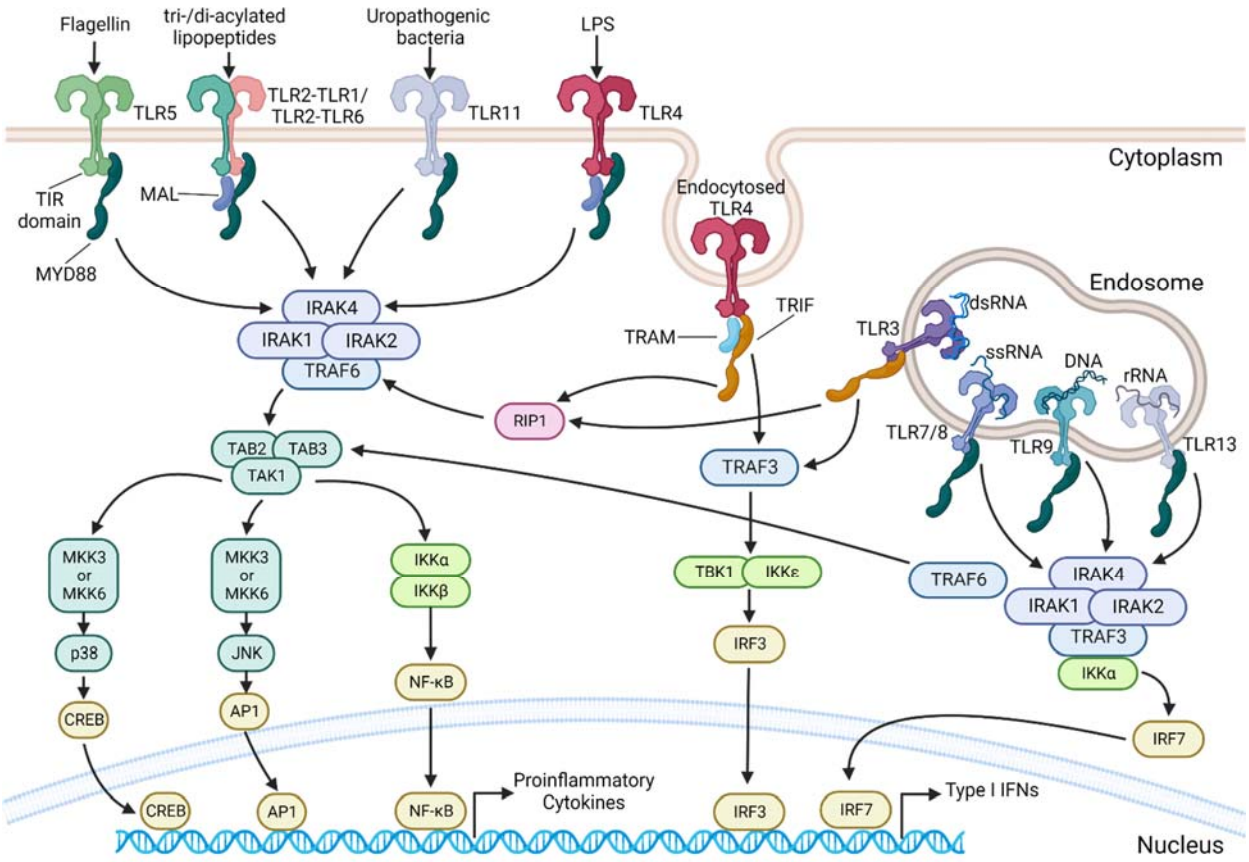

Figure 1.6: TLRs and their signaling pathways: an overview.

TLR2 can heterodimerize with TLR1 or TLR6 to detect triacylated or diacylated lipopeptides, respectively. TLR4 recognizes LPS, whereas TLR5 senses flagellins. Murine Tlr11 was observed to sense uropathogenic bacteria. The endosomal TLRs (TLR3, TLR7/8, and TLR9) detect dsRNA, ssRNA, and DNA, respectively, whereas the murine endosomal Tlr13 was found to detect ribosomal RNA (rRNA). Downstream of TLR signal transduction, transcription factors like NF-κB, interferon-regulatory factors (IRFs), cyclic adenosine monophosphate (AMP)-responsive element-binding protein (CREB), and activator protein 1 (AP1) are induced, which leads to the production of proinflammatory cytokines and type I IFNs in the case of endosomal TLRs (O'Neill, Golenbock, and Bowie 2013). Created with BioRender.com, adapted from O'Neill et al. (2013) (O'Neill, Golenbock, and Bowie 2013).

Following the binding of various ligands by the corresponding TLRs, their TIR domains engage TIR-domain containing adaptor proteins, such as Myeloid differentiation (MYD88), MYD88-adaptor-like protein (MAL), or TIR domain-containing adaptor protein inducing IFN-β (TRIF) and TRIF-related adaptor molecule (TRAM). The TIR domains of the different TLRs interact with distinct combinations of the adaptor proteins, which influences the activation of downstream signals. MAL and TRAM do not directly participate in downstream signal transduction, but rather act as recruiters for MYD88 and TRIF, respectively. Those, either alone or in combination, control most of the downstream TLR signaling. Of note, MYD88 is the most prominent TLR adaptor protein (Murphey, Weaver, and Berg 2022). In the special case of TLR4, this certain receptor moves from the plasma membrane to the endosomes in order to switch signaling from MYD88 to TRIF. Downstream signaling pathways of the adaptor molecules involve interactions between IL-1R-associated kinases (IRAKs) and TNF receptor-associated factors (TRAFs), which in turn lead to the activity

of the MAPKs JUN (transcription factor) N-terminal kinase (JNK) and p38. This furthermore leads to the activation of the transcription factors NF-κB, interferon-regulatory factors (IRFs), cyclic adenosine monophosphate (AMP)-responsive element-binding protein (CREB), and activator protein 1 (AP1) and finally to the expression of proinflammatory cytokines. Activation of endosomal TLRs initiates the expression of type I IFNs and pro-inflammatory cytokines upon the described induction of transcription factors in dependence of cell type (O'Neill, Golenbock, and Bowie 2013).

1.4.3 Endosomal TLRs – the nucleic acid sensors

The endosome provides a hostile environment capable of detecting and reporting infections, after internalization of microbes by the phagocytic cell, which search the extracellular milieu for signs of threats. This uptake is fulfilled by receptor-mediated endocytosis, phagocytosis, or nonspecific fluid phase endocytosis. Macrophages and PMNs are more active than other cells in performing phagocytosis, which requires the reorganization of the cytoskeleton and formation of membrane protrusions for target engulfment. Suspended or cell-adherent target particles can be taken up via fluid phase endocytosis or micropinocytosis, which also require the rearrangement of the actin cytoskeleton but allow the uptake of multiple small particles in a bolus of liquid (Blasius and Beutler 2010). The human intracellular TLRs (TLR3, TLR7, TLR8, and TLR9) are capable of detecting nucleic acids and are therefore acting within the endosomal compartment: microbe-derived nucleic acids are products of phagocytosed and degraded pathogens, whereas host-derived nucleic acids are usually not found in these cellular structures, since they are mainly located in the nucleus and cytoplasm. However, in abnormal situations, endosomal TLRs might detect self-derived nucleic acids, which can be released into the extracellular space during tissue damage or NET formation, leading to autoimmunity. Thus, the localization of nucleic acid sensing TLRs to the endosome has a protective function (Murphey, Weaver, and Berg 2022).

Macrophages, DCs, and epithelial cells of the intestine express TLR3, which recognizes dsRNA, mainly derived of dsRNA-containing viruses. Moreover, dsRNA of ssRNA-viruses can be detected which occurs during gene expression or replication. The recognition takes place either directly after endocytosis of dsRNA-containing viruses or phagocytosis of virus-infected dying cells. Mutations in TLR3, more specifically in its ectodomain, are e.g. associated with encephalitis, caused by failed control over herpes simplex virus infections. Of note, herpes simplex is a DNA virus. It is suggested that dsRNA is generated after transcription of overlapping viral genes, making TLR3-mediated detection possible (Murphey, Weaver, and Berg 2022).

Degradation products of ssRNA activate the closely related TLRs TLR7 and TLR8, which share similar amino acid sequences. After degradation of ssRNA-containing viruses, such as influenza or SARS-CoV-2, small fragments of ssRNA are detected within the endosome. TLR7 has a specificity for guanosine-rich fragments, whereas TLR8 especially binds short RNA fragments containing uridine (Murphey, Weaver, and Berg 2022). Moreover, TLR8 was described to sense RNA degradation products: in 2019, exogenous RNA was incubated with the lysosomal endoribonuclease RNase T2, which led to detectable TLR8-ligands *in cellulo* (Greulich et al. 2019). Additionally, RNase T2 and RNase 2 were observed to cooperate for digestion of synthetic, bacterial, and protozoan RNA in 2020. This degradation led to the release of uridine, therefore being considered as essential for the creation of fragments detectable by TLR8 (Ostendorf et al. 2020).

TLR9 was initially reported to only bind unmethylated CpG-motifs in DNA sequences, which are much more abundant in prokaryotes. However, it has later on been observed that the recognition by this certain TLR also includes the 2'-deoxyribose phosphate backbone of DNA. For example, if one transfects nondenatured vertebrate DNA using liposome transfection reagents and thereby delivering it to the endosome, TLR9 gets stimulated (Yasuda et al. 2006). This highlights the crucial part of intracellular nucleic acid uptake and receptor compartmentalization to prevent autoimmunity due to breakdown of discrimination between self and non-self antigens and shows that the localization of the DNA rather than its sequence dictates TLR9 activation.

Although intracellular TLRs are not only expressed in the endosome but also in the endoplasmic reticulum (ER), multivesicular bodies, and lysosomes, activation primarily occurs within acidified endolysosomal compartments (Blasius and Beutler 2010). The trafficking of the nucleic acid sensing TLRs from the ER to the endosome, where they can induce downstream signaling and inflammatory responses, is seen as a regulatory mechanism for activation of self versus non-self discrimination. One important factor involved in this trafficking is Unc-93 homolog B1 (UNC93B1), a protein residing in the ER that helps the TLRs to exit this cellular compartment to get loaded into coat protein complex II (COPII) vesicles, which transport cargo from the ER to the Golgi. Upon reaching the latter, the nucleic acid sensing TLRs are sorted to the endosomes (Lee and Barton 2014). The need for Unc93B1 function for efficient signaling by endosomal TLRs is evidenced by failed Tlr3, Tlr7, and Tlr9 responses in mice with a triple D (3d) mutation of *Unc93B1*, thus lacking the functional protein (Tabeta et al. 2006). Besides UNC93B1, additional factors regulate TLR exit from the ER, generally functioning as folding chaperones, such as glycoprotein 96 (gp96) and canopy fibroblast growth factor (FGF) signaling regulator 3 (CNPY3), of which the latter, unlike UNC93B1, does not discriminate between intracellular and surface TLRs (Lee and Barton 2014).

Being described that the differentiation between self and non-self is a crucial function of TLRs, it is coherent that a disbalance in this sensitively orchestrated discrimination system can lead to various autoimmune diseases (Chen, Szodoray, and Zeher 2016).

1.4.4 TLRs and their roles in driving autoimmune diseases

Many autoimmune diseases are associated with TLR signaling, such as SLE, a systemic disease affecting organs and joints. Patients suffering from SLE display higher concentration of antibodies to self nucleic acids or nucleoproteins. Those autoantibodies can bind to the nucleic acid structures, thus building complexes which can be internalized via FcγRIIa receptors recognizing IgGs on DCs, which in turn leads to their delivery to TLR7- and TLR9-containing vesicles, resulting in type I IFN production. In addition, B cell antigen receptors are able to bind these immune complexes, which contributes to the activation of autoreactive B cells, thus driving disease progression (Pan et al. 2020).

Sjögren's syndrome (SS) is a slowly progressive systemic autoimmune inflammatory disease in which impaired salivary and lachrymal gland functions occur. It is associated with comorbidities, such as fatigue, Raynaud's phenomenon, as well as muscle and joint pains. SS salivary gland epithelial cells (SGECs) showed overexpression of TLR1, TLR2, and TLR4, and increased amounts of TLR2, TLR3, TLR4, and MYD88 were observed in labial salivary glands. It is suggested that peptidoglycans activate TLR2, which leads to activation of IL-6, signal transducer and activator of transcription 3 (STAT3), and NF-κB pathways, inducing

IL-17 and IL-23 production in peripheral blood mononuclear cells (PBMCs), which results in proinflammatory responses (Chen, Szodoray, and Zeher 2016).

In cohorts of patients suffering from RA, a disease which primarily affects synovial joints with chronic inflammatory processes causing destruction of the articular tissue, single nucleotide polymorphisms (SNPs) in TLR9 and TLR8 associated genes were found. Furthermore, increased activation of TLRs and an essential role of MYD88 in disease progression have been reported. It was shown that TLR3 upregulates receptor activator of NF-κB ligand (RANKL), leading to osteoclastogenesis in synovial fluids which promotes chronic inflammation. Additionally, necrotic cells located in synovial fluids have been reported to release RNA, which acts as an endogenous ligand for TLR3. Besides, massive secretion of TLR8-mediated TNF from RA synovium has been observed and antimalarial drugs, such as chloroquine and hydroxychloroquine, which inhibit endosomal acidification, are successfully used as treatment options for RA, highlighting the role of endosomal TLRs in this autoimmune disease (Chen, Szodoray, and Zeher 2016).

In 2007 the group of Michel Gilliet showed LL37, which has been found in high abundance in psoriatic skin lesions, to bind to self-DNA, resulting in a complex which can activate DCs in a TLR9-dependent manner (Lande et al. 2007). Two years later, they further observed self-RNA-LL37 complexes behaving in a similar manner, activating DCs in a TLR7/8-dependent fashion, driving disease progression. LL37 was hence described as a “tolerance” breaker but the sources of self-RNA and LL37, as well as their physiological complex formation *in vivo* remained to be elucidated. This emphasizes again the role of endosomal TLR signaling in autoimmune diseases and their crucial ability to discriminate between self and non-self (Ganguly et al. 2009).

Since both, TLRs and PMNs, are playing essential roles in host defense and are related to the scope of this work, taking a more detailed look at TLR-mediated signaling in neutrophils is necessary to understand this complex interplay.

1.4.5 Neutrophil TLRs and their roles in inflammatory stages

Several classes of receptors are expressed on the surface of neutrophils, such as G-protein coupled receptors (GPCRs), Fc-receptors, adhesion molecules, such as selectins/selectin ligands and integrins, a variety of cytokine receptors, and the innate immune receptors C-type lectins and TLRs (Futosi, Fodor, and Mocsai 2013). Human neutrophils lack TLR3 (Gan et al. 2018) and the existence of TLR7 and TLR9 is debated, but TLR1, TLR2, TLR4-6, and TLR8 are well-accepted (Futosi, Fodor, and Mocsai 2013). The most studied neutrophil TLRs are located on the cell surface, due to the primary role of PMNs in host defense against bacteria. For instance, TLR2 and TLR4 mediate responses to gram-positive and gram-negative bacteria, respectively, and cooperate with co-receptors, including CD14 and CD11b/CD18 to facilitate this immune mechanism. TLR5, also expressed on neutrophil surfaces, detects bacterial flagellin (Prince et al. 2011).

The endosomal TLR9 in neutrophils can be activated by binding of bacterial DNA, which in turn leads to enhanced phagocytotic functions, regulation of adhesion molecules, cytokine production (predominantly IL-8, but also TNF and IL-6), as well as induction of ROS and (similar to TLR8 activation) suppression of neutrophil apoptosis. Furthermore, dsRNA in neutrophils was observed to be detected through the intracellular receptors RIG-I and MDA-5 (Prince et al. 2011).

TLR8 signaling plays an important role in neutrophil activation and subsequent immune modulations, as shown by different studies. Virus derived ssRNA agonists can inhibit neutrophil apoptosis in a TLR8-dependent manner, stimulating cytokine generation and ROS formation, as well as degranulation and priming for inflammatory lipid mediator biosynthesis (Prince et al. 2011). It was further reported that neutrophils express IL-12B and IL-23A in a TLR8-dependent manner and that supernatants of neutrophils containing these cytokines can induce differentiation of naïve T cells into Th17 cells in an IL-23-dependent fashion. Thus, PMNs stimulated with TLR8 agonists play key roles in the IL-17/IL-23 network and Th17 responses, therefore mediate the neutrophil/Th17 cell crosstalk (Tamassia et al. 2019). The latter e.g. plays an important role in psoriasis, as previously mentioned (Chiang et al. 2019). Additionally to secretion of cytokines belonging to the IL-12 family, PMNs were observed to release Epstein-Barr virus induced gene 3 (EBI3) (Cassatella et al. 2020), a subunit of the composite cytokines IL-27 and IL-35, which belong to the IL-6/IL-12 family of cytokines. Those have been shown to fulfill beneficial functions or effects in models of infectious and autoimmune diseases in a TLR8-dependent manner (Chehboun et al. 2017).

As a more physiologically relevant source, extracellular nucleic acids present in *C. albicans* biofilms were observed to trigger the release of NETs in human PMNs. By using CU-CPT9a, a compound preventing the formation of an active conformation of TLR8, Smolarz et al. confirmed the important role of this particular endosomal TLR in NET formation upon *C. albicans* sensing (Smolarz et al. 2021). However, it remained unclear which TLR8 agonist contained in *Candida* was involved.

In 2020, Herster et al. showed that bacterial and synthetic RNA complexed with LL37 leads to cytokine and chemokine release in human PMNs, which was efficiently blocked by TLR8-targeting inhibitory oligonucleotides (iODNs). Additionally, stimulation of PMNs with RNA-LL37 complexes led to NET release. Moreover, they reported NETs to be a physiological source of RNA and introduced the so-called NET-associated RNA (naRNA) not only as a novel component of NETs, but further suggested it as a possible driver of TLR8-mediated neutrophil immune responses (Herster et al. 2020), although proof of principle was missing so far.

To date, the effects of various types of RNAs, especially extracellular RNAs (exRNAs), regarding neutrophil activation and NET formation, thereby modulating the human immune system, are of great research interest (Aguila et al. 2021). However, exact underlying mechanisms are unknown and remain to be elucidated.

1.5 Extracellular RNA as a DAMP shaping immune responses

1.5.1 Definition, origin, and significance of exRNA

RNA is often considered to be a short-lived biomolecule that is rapidly integrated, degraded, or processed due to and with the help of multiple in cellular and extracellular fluids existing RNases, helicases, polymerases, and chaperones (Houseley and Tollervey 2009). Nevertheless, it has been reported for decades that RNA can exist in the human body outside of cells. However, the functionality of extracellular RNAs (exRNAs) has been elusive until researchers found a functional transfer of messenger RNAs (mRNAs) and micro (mi)RNAs between cells. Although outside of a cellular environment, RNA may also remain stable when associated to proteins. It is suggested that exRNAs are mainly packed in extracellular vesicles (EVs), which can be plasma membrane- or endosome-derived. Hereby, extracellular miRNAs have been found to be rather distinct from their expression in parental cells. This observation suggests that specific miRNAs are actively selected for extrusion. Other reports claim that RNAs are released in a nonselective way, depending on their local concentration. In a third hypothesis it is assumed that exRNA might be generated from precursors in the extracellular space and is not directly released from cells, as unpacked non-vesicular RNAs were observed. Of note, the source of the latter still remains to be elucidated. If the exRNA was actively released by a cell or not does not necessarily determine its later functions (Tosar, Witwer, and Cayota 2021), which can include macrophage polarization, leukocyte recruitment to the site of inflammation and their rolling at the vascular endothelium, integrin-mediated firm adhesion of immune cells, and thrombosis promotion (Preissner, Fischer, and Deindl 2020).

Many different types of exRNAs have been reported to travel through body fluids carrying information from cell to cell acting as signaling molecules: mRNAs, long non-coding RNAs (lncRNAs), as well as various types of small non-coding RNAs (ncRNAs), which can be divided into regulatory and housekeeping RNAs. lncRNAs, miRNAs, piwi-interacting (pi)RNA, siRNA, transfer (t)RNA-derived fragments, and Y RNAs belong to the group of regulatory RNAs, whereas housekeeping RNAs include rRNA, tRNA, small nuclear RNA (snRNA), and small nucleolar RNA (snoRNA). exRNAs can be found in a variety of biofluids, like plasma, serum, breast milk, saliva, cerebrospinal fluid, bile, semen, and urine and can be secreted/derived by all cell types. Besides EVs, ribonucleoprotein complexes (RNPs) and lipoprotein complexes (LPPs) can be carriers of exRNAs, transferring them from the donor to the recipient cell to elicit functional responses and regulate biological processes (Happel, Ganguly, and Tagle 2020).

exRNAs can be used as biomarkers to monitor disease states, e.g. of cancer patients in so-called ‘liquid biopsies’. Due to their availability in most body fluids, they can be collected in a non-invasive way, and are used for both, diagnostic and prognostic purposes. miRNAs play a central role as biomarkers in cancer, since their expression patterns are unique to individual tissues and differ between malignant and healthy cells (Happel, Ganguly, and Tagle 2020). EV-related exRNA is further found in high amounts in diseases affecting elderly, e.g. Parkinson’s and Alzheimer’s disease, therefore being of diagnostic value (Kim et al. 2017). Additionally, another approach to use exRNAs as biomarkers is made for post-MI risk evaluation and asymptomatic atherosclerosis (pre-MI risk), since they are suggested to play a role in cardiac remodeling. Moreover, exRNAs are used as markers for detection of placental dysfunction, diseases of the central nervous system, intracranial hemorrhage, multiple sclerosis, and renal disease, which occurs in autoimmune disorders like SLE or lupus nephritis (LN) (Quinn et al. 2015).

Although many diseases are linked to exRNAs and exRNAs therefore provide diagnostic and prognostic purposes as biomarkers (Happel, Ganguly, and Tagle 2020; Kim et al. 2017; Quinn et al. 2015), only little is known about the physiological sources of self-derived exRNAs. Stress- or injury-induced cell necrosis, sterile inflammation-induced tissue damage, as well as cell activation or tissue injury mediated by hypoxia, infection, inflammation, or tumor growth are suggested to induce the release of host-derived exRNAs. As afore described, exRNAs are extruded by cells in an either free or bound form. The binding of exRNA to various proteins can prevent its degradation by extracellular RNases on one hand, but can further modulate the reactivity and immunogenicity of the exRNA, therefore shaping the corresponding immune response on the other hand (Preissner, Fischer, and Deindl 2020). Such an immunogenicity-modulating peptide binding to exRNA is LL37. LL37, which has an exclusive structure consisting of cationic α-helical residues, has first been reported to bind to the anionic phosphate backbone of DNA in a stable way, preventing it from nuclease degradation (Kubo and Fujii 2001). Later on, LL37 was not only found to stabilize and protect DNA, but to further transport host-derived DNA into the cytosol of monocytes, leading to type I IFN responses (Chamilos et al. 2012). In addition, the group of Michel Gilliet showed that complex formation of DNA and RNA with LL37 induces immune responses in DCs (Lande et al. 2007; Ganguly et al. 2009). More recently, LL37 was reported to bind to exRNA, e.g. derived from necrotic cells (Preissner, Fischer, and Deindl 2020). A further link between a physiologically relevant exRNA and LL37 was made by Herster et al. in 2020, who proposed that NET-derived naRNA can form complexes with the highly abundant NET component LL37 to fuel a vicious cycle of inflammation in the context of psoriasis (Herster et al. 2020). However, if, when, and how naRNA-LL37 complexes assemble and if they are actually of immunomodulatory function has not been investigated to date. Thus, further research is needed to prove this hypothesis.

1.5.2 exRNAs modulate neutrophil activation and NET formation

As previously mentioned, exRNAs can serve as stimulants for neutrophils, inducing their activation and/or NET formation. A well-studied exRNA known to modulate neutrophil responses is miR-146a, a small ncRNA (Aguila et al. 2021). It was observed that miR-146a is capable of inducing NET formation (Arroyo et al. 2018) on one hand, but also to reduce it on the other hand (Hsieh et al. 2022), therefore further investigation on the exact modulation properties is needed. Besides miR-146a, miR-155 is a relevant inflammation-modulating miRNA, mainly expressed in hematopoietic cells. miR-155 can inhibit PAD4, therefore regulating NET formation in a negative manner (Hawez et al. 2019). Another miRNA, miR-505, which is involved in the development of different cancer types, such as breast or pancreatic cancer, was observed to downregulate NAD-dependent deacetylase sirtuin-3 (SIRT3), a mitochondrial protein implicated in regulation of ROS production, thereby increasing NET formation. The platelet derived exosomal miR-15b-5p and miR-378a-3p were described to regulate the expression of phosphoinositide-dependent kinase-1 (PDK1), subsequently activating autophagy and thus promoting NET formation (Aguila et al. 2021). In the context of gout, NET formation was observed to be mediated by miR-3146, thereby providing a potential therapeutic target for disease treatment options (Shan et al. 2021). Due to the sheer amounts of exRNAs known to exist (Tosar, Witwer, and Cayota 2021), it is coherent that many more PMN function-modulating exRNAs will be reported in the future.

1.6 Aims of this study

Many studies describe the involvement of NETs in various disease pathologies, such as autoimmune diseases like SLE and RA, or cancer, cardiovascular diseases and thrombosis, as well as sepsis. It has further been well-characterized that NETs are not only involved in those diseases but are drivers of severe disease progression. Therefore, NETs can be detrimental for the host's health (Papayannopoulos 2018). Additionally to NETs, exRNAs have been ascribed to the same afore mentioned pathologies (Quinn et al. 2015; Kim et al. 2017; Happel, Ganguly, and Tagle 2020) and found to induce immune responses related to inflammation and infection (Preissner, Fischer, and Deindl 2020). Nevertheless, the hypothesis that NETs provide a highly abundant source of exRNAs, and hence DAMPs, which drive immune responses in various diseases and thereby link the parallel observation of NETs and exRNAs to play crucial roles in the same pathologies, has never been investigated.

With observing NETs to not only release DNA, histones, and antimicrobial peptides, but also NET-associated RNA, Herster et al. kickstarted the assumption that naRNA can fuel inflammation (Herster et al. 2020). It was herein hypothesized that naRNA might be a canonical component of NETs, which could initiate self-propagation of NET formation and further responses of other immune cells in many physiological settings by serving as a DAMP and source of exRNA (see Fig. 1.7).

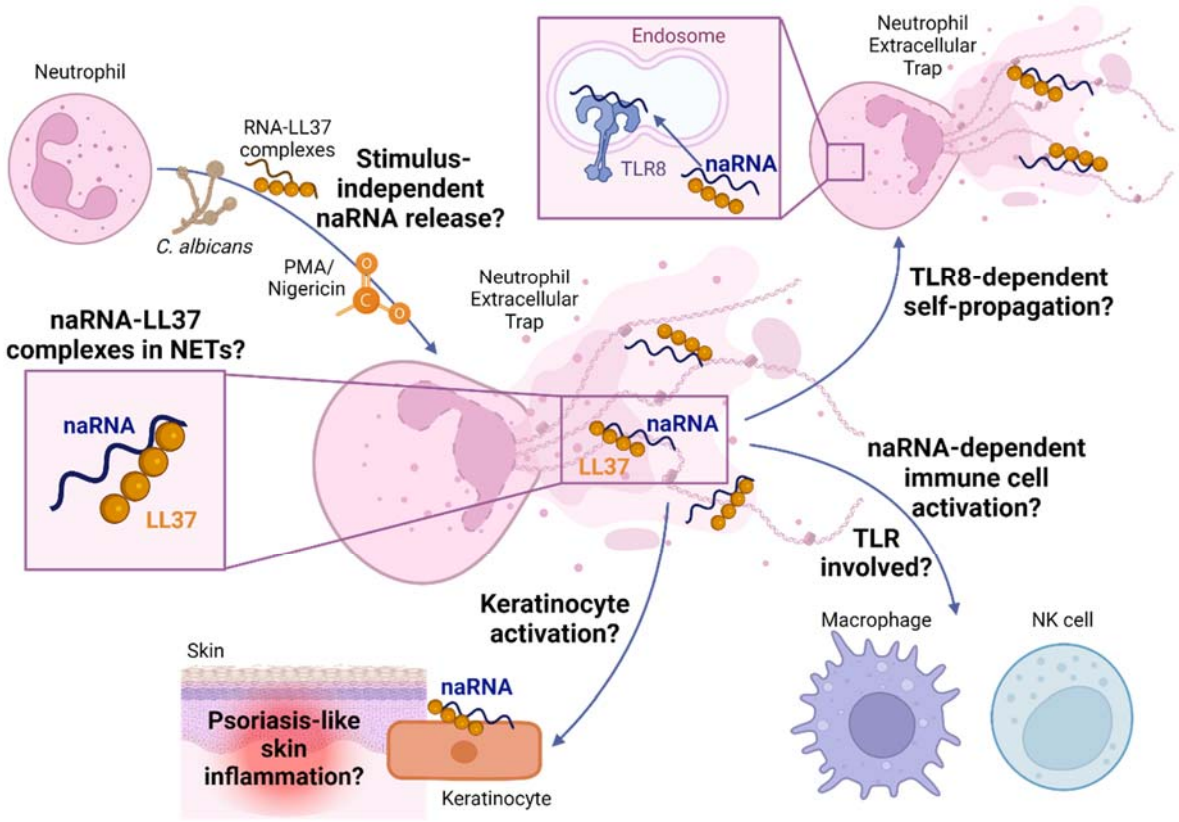

Figure 1.7: Hypothesis and aims of this study: naRNA as a DAMP inducing TLR8-dependent inflammatory responses.

It was hypothesized that naRNA is an abundant component of NETs, independent of the stimulus and the type of NET formation, thereby being a common source of exRNA serving as a potent DAMP. This study aimed to investigate, whether naRNA-LL37 complexes can be found in NETs and how LL37 contributes to the immunomodulatory functions of naRNA. Furthermore, naRNA was suggested to induce self-propagation of NET formation in a TLR8-dependent manner, as well as activation of immune cells like macrophages. It was additionally anticipated to investigate the *in vivo* effects of naRNA in psoriasis-like skin inflammation. Created with BioRender.com.

The aims of the underlying study therefore were:

- prove the existence of naRNA in all types of NETs by different methods, independent of the stimulus used and type of NET formation induced (suicidal vs. vital).
- investigate whether naRNA and LL37 can be found in complexed form in NETs and how LL37 contributes to the immunomodulatory roles of naRNA.
- explore the effect of naRNA on naïve PMNs, other immune cells, as well as keratinocytes.
- characterize the TLRs involved in naRNA mediated signaling in different cell types.
- study the effects of naRNA *in vivo*, in order to ascertain if psoriasis-related disease progression can be directly linked to this novel DAMP.

2 Materials and Methods

2.1 Materials

2.1.1 Reagents and chemicals

2.1.1.1 Reagents and chemicals

Table 2.1: Reagents and chemicals

Reagent/Chemical	Company	Product no.
Acetone	Applichem	A1582.2500PE
Ampuwa	Fresenius Kabi	1833
β-estradiol	Sigma	E2758
Blocking buffer for electron microscopy	Jackson ImmunoResearch	115-195-166
Bovine Serum Albumin	Biomol	01400.100
$CaCl_2$	Roth	CN93.1
Chloroform	Merck	288306
Citric acid ($C_6H_8O_7$)	Carl Roth	X863.2
CnT-07 medium	CELLnTEC	CnT-07
Cytochalasin D	Sigma	C8273-1MG
DEPC	Roth	K028.2
DMEM	Sigma	D5796-24X500ML
DOTAP	Roth	L787.2
EDTA (pH = 8)	Thermo Fisher	15575020
Ethanol	VWR	20821.330
FCS (heat inactivated, sterile filtered)	Th. Geyer	11682258
FITC conjugate	BioRad	30446
Fixation buffer	BioLegend	420801
HEPES	Sigma	H0887
Histopaque/ Ficoll 1.077 g/mL	Sigma	10771
IMDM-Medium	Lonza	12-722F
hIL-3 (recombinant)	Peprotech	200-03
hM-CSF (recombinant)	Peprotech	300-25
IFN-γ	Sigma	I-3265
Imiquimod (5%)	Taro Pharmaceuticals Industries, NY	-
Isopropanol	VWR	1.09634.1011P
Keratinocyte Growth Medium 2	PromoCell	C-20111
$KHCO_3$	Fluka	60220
L-glutamine	Gibco	25030081
Methanol	Honeywell	32213-2.5L
NH_4Cl	Roth	5470.1
Normal Chicken Serum Blocking Solution	Biozol/Vectorlabs	VEC-S-3000-20
Opti-MEM™ Reduced Serum Medium	Thermo Fisher	31985062
Passive lysis buffer (1x)	Promega	E194A
PBS	Thermo Fisher	14190-169
Pencicillin/Streptomycin	Gibco	15140122
Platinum	Safematic	CCU-010
Poly-L-lysine	Sigma	A-005-C
Poly-L-lysine	Sigma (for RNA ELISA)	P8920

ProLong™ Diamond Antifade Mountant	Thermo Fisher	P36961
Pooled human serum	Transfusion medicine Tübingen	-
RNase/DNase free water	Thermo Fisher	10977049
RPMI culture medium	Sigma	R8758
RPMI culture medium without phenol red	Sigma	R7509
RPMI-1640	PAN Biotech	P04-18525
Saponin	Applichem	A4518.0100
Sodium pyruvate	Gibco	11360070
Stemline® II Hematopoietic Stem Cell Expansion medium	Sigma	S0192
TaqMan™ Gene Expression Assay	Thermo Fisher	4448892
TaqMan™ Universal Mastermix II	Thermo Fisher	4440040
Trisodium citrate dihydrate ($C_6H_5Na_3O_7$*2 H_2O)	Carl Roth	4088.1
TRIzol™	Thermo Fisher	15596018
X-tremeGENE™ HP DNA Transfection Reagent	Merck	6366236001

2.1.1.2 Click chemistry reagents

Table 2.2: Click chemistry reagents

Reagent	Company	Product no.
AF546-azide	Jena Bioscience	CLK-1283-1
Aminoguanidine-Hydrochloride	Merck	396494-25G
$CuSO_4$-click chemistry grade	Jena Bioscience	CLK-MI004-50.1
5-Ethynyluridine	Jena Bioscience	CLK-N002-10
Na-Ascorbate-click chemistry grade	Jena Bioscience	CLK-MI005-1G
THPTA (Tris((1-hydroxy-propyl-1H-1,2,3-triazol-4-yl)methyl)amine)	Jena Bioscience	CLK-1010-25

2.1.1.3 Commercial TLR ligands and inhibitors

Table 2.3: Commercial TLR ligands and inhibitors

Component	Company	Product no.
Cl-amidine	Merck	506282
CpG PTO 2006	TIB Molbiol	n/a, see Table 2.5
CU-CPT9a	Invivogen	inh-cc9a
Dnase inhibitor 50 mM EDTA	Thermo Fisher	EN0521
DOTAP	Roth	L787.2
Ionomycin	Sigma	I0634-1MG
LL37	Invivogen	tlrl-l37
LPS-EK (ultrapure)	Invivogen	tlrl-peklps
Nigericin	Invivogen	tlrl-nig
PMA	Invivogen	tlrl-pma
R848 (Resiquimod)	Invivogen	tlrl-r848
RNase A	Thermo Fisher	EN0531
RNase inhibitor	Promega	N2615
TL8-506	Invivogen	tlrl-tl8506

2.1.1.4 Nucleic acid TLR agonists

Table 2.4: Nucleic acid TLR agonists

Component	Sequence	Backbone	Company
RNA40	5'GsCsCsCsGsUsCsUsGsUsUsGsUsGsUsGsAsCsUsC3'	Phosphorothioate	Eurogentec
CpG PTO 2006	5'TsCsGsTsCsGsTsTsTsTsGsTsCsGsTsTsTsTsGsTsCsGsTsT3'	Phosphorothioate	TIB

2.1.2 Buffers and media

Table 2.5: Buffers and media

Buffer/media	Components
BlaER1 culture medium	• RPMI-1640 (PAN Biotech) • 10% FCS • 1% Pen./Strep. • 1% Sodium pyruvate • 1% HEPES
BlaER1 transdifferentiation medium	• RPMI-1640 (PAN Biotech) • 10% FCS • 1% Pen./Strep. • 1% Sodium pyruvate • 1% HEPES • 10 ng/mL hIL-3 • 10 ng/mL M-CSF • 150 nM β-estradiol
Blocking buffer for Immunofluorescence	• 1x PBS • 0.1% DEPC (heat inactivated) • 0.1% Saponin • 10 U/µL RNase inhibitor • 10% Normal Chicken Serum
BM-PMN culture medium	• RPMI (Sigma) • 10% FCS • 1% L-glutamine
$CD34^+$ culture medium	• Stemline II Hematopoietic Stem Cell Expansion medium • 10% FCS • 1% L-glutamine • 1% Pen./Strep. • 20 ng/mL IL-3 • 20 ng/mL IL-6 • 20 ng/mL TPO • 50 ng/mL SCF • 50 ng/mL FLT-3L
Citrate buffer	• 0.1 M $C_6H_5Na_3O_7$*2 H_2O • pH adjusted to 6.0 with 0.1 M $C_6H_8O_7$
Complete DMEM	• DMEM • 10% FCS • 1% Pen./Strep. • 1% L-glutamine

Complete RPMI	• RPMI (Sigma) • 10% FCS • 1% Pen./Strep. • 1% L-glutamine
Erythrocyte lysis buffer (ACK, 10x)	• 1.54 M NH_4Cl • 100 mM $KHCO_3$ • 1 mM EDTA, pH=8 • dissolved in Ampuwa water, pH adjusted to 7.3, sterile filtered (0.22 µm) • dilute in sterile H_2O for 1x
MACS buffer	• PBS • 0.5% Bovine Serum Albumin • 0.2 mM EDTA • Sterile filtered
PBMC culture medium	• RPMI (Sigma) • 10% FCS • 1% Pen./Strep. • 1% L-glutamine
PMN culture medium	• RPMI (Sigma) • 10% FCS

2.1.3 Enzymes

Table 2.6: Enzymes

Enzyme	Company	Product no.
DNase I	Thermo Fisher	EN0521
RNase A	Thermo Fisher	EN0531

2.1.4 Antibodies

Table 2.7: Antibodies

Abbreviations: EM – Electron Microscopy; IF – Immunofluorescence; FACS – Fluorescence Activated Cell Sorting

Antibody/Dye	Fluorophore	Species	Isotype	Company	Product no.	Assay
Anti-hLL37	DyLight 550	rabbit	IgG	LSBio	LS-B6696-500	EM/IF
Anti-rRNA (Y10b)	unconjugated	mouse	IgG_{2a} κ	Santa Cruz Biotechnology	sc-33678	EM/IF
Anti-rRNA (Y10b) Alexa Fluor® 647	AF647	mouse	IgG_{2a} κ	Santa Cruz Biotechnology	sc-33678 AF647	IF
Anti-mouse IgG	AF647	chicken	IgY	Thermo Fisher	A-21463	IF
Hoechst 33342	-	-	-	Thermo Fisher	H21492	IF
SYTO RNAselect Green fluorescent dye	-	-	-	Thermo Fisher	S32703	Live cell IF
Anti-mouse Cy3	Cy3	goat	IgG	Jackson ImmunoResearch	115-165-146	IF (ultrathin sections)
Anti-rabbit AF488	AF488	goat	IgG	Molecular Probes	A-11008	IF (ultrathin sections)
Anti-mouse 6 nm gold	-	goat	IgG	Jackson ImmunoResearch	115-195-166	EM
Anti-rabbit 12 nm gold	-	goat	IgG	Jackson ImmunoResearch	111-205-144	EM
Anti-hCD15	PE	mouse	IgG1 κ	BioLegend	323006	FACS
Anti-hCD66b	FITC	mouse	IgG1 κ	BioLegend	305103	FACS
Anti-hCD62L	BV421	mouse	IgG1 κ	BioLegend	30482	FACS
Anti-hCD14	PE	mouse	IgG1 κ	ImmunoTools	21620144	FACS
Isotype control	PE	mouse	IgG1 κ	eBioscience	12471442	FACS
Isotype control	FITC	muse	IgM	BioLegend	401605	FACS
Isotype control	BV421	mouse	IgG1 κ	BioLegend	400157	FACS
Anti-human IgG/HRP	-	goat	-	Dianova	109-035-098	RNA-ELISA
Anti-mouse IgG/HRP	--	rabbit	-	Agilent, Dako	P0260	RNA-ELISA

2.1.5 Plasmids used for transfection of HEK cells

Table 2.8: Plasmids used for transfection of HEK cells

Plasmid name insert	Vector backbone	Insert	pEX number
NF-κB reporter	pGL3	6x NF-κB response element	pEX449
Renilla	pRL-TK	*Renilla*	pEX351
hTLR7	pcDNA3.1 (+)	hTLR7	pEX045
hTLR8	pcDNA3.1 (+)	hTLR8	pEX011
hTLR9	pSEM-hTLR9	hTLR9	pEX169

2.1.6 Primers used for qPCR

Table 2.9: Primers used for qPCR

Gene	Assay number
IL-8	Hs00174103_m1
TBP (housekeeper)	HS00427620_m1

2.1.7 Kits

Table 2.10: Kits

Kit	Company	Product no.
CD34 MicroBead Kit human	Miltenyi	130-046-702
Dual luciferase kit	Promega	E1980
DyLight 550 Conjugation Kit (Fast)	Abcam	ab201800
ELISA MAX™ Deluxe Set Human IL-8	BioLegend	431504
ELISA MAX™ Deluxe Set Human IL-6	BioLegend	430504
ELISA MAX™ Deluxe Set Human IFN-γ	BioLegend	430104
High-Capacity RNA-to-cDNA-Kit	Thermo Fisher	4387406
Mouse Neutrophil Isolation Kit	Miltenyi	130-097-658
NucleoSpin miRNA isolation Kit	Macherey-Nagel	740971.50
RNeasy Mini Kit	Qiagen	74106
TNF alpha Human Uncoated ELISA Kit	Invitrogen	88-7346-88

2.1.8 Special instruments, equipment, software, and settings

2.1.8.1 Special instruments, equipment, and software

Table 2.11: Special instruments, equipment, and software

Instrument/Equipment/Software	Company	Product no./Version
4-well glass bottom microscopy cell culture dish	Greiner	627871
Axioplan microscope	Zeiss	-
Compact coating unit	Safematic	CCU-010
Confocal microscope	Zeiss	LSM800
Critical point dryer	Leica Microsystems	CPD300
Cytofunnel™	Thermo Fisher, Shandon	-
Cytospin centrifuge	Shandon	-
Cytoclip™ slide clips	Thermo Fisher, Shandon	-
EDTA blood collection tubes (S-Monovette)	Sarstedt	04.1931.010
Excel	Microsoft	2019
FACS Canto II	BD Bioscience	-
FACSDiva	BD Bioscience	Version 6
FlowJo	FlowJo LLC	Version 10
GENECODE	EMBL-EBI	-
Half-area 96-well plate	Greiner	675061
ImageJ	NIH	Win64
IVIS Lumina II imaging system	Caliper	-
Living Image software	Caliper	-
Manual Caliper	Peacock, Japan	0.01-10 mm
Microtube homogenizer	Merck	BeadBug™
Nanozoomer microscope	Hamamatsu	-
NEBNext® Ultra™ II Directional RNA Library Prep Kit	Illumina	protocol for use with rRNA Depleted FFPE RNA
Plate reader for dual luciferase reporter assay	BMG Labtech	FLUOstar OPTIMA
Poly-L-lysine coated glass coverslips	Electron Microscopy Sciences	72292-04
PowerPoint	Microsoft	2019
Prism	GraphPad	Version 8
QuantStudio Real-Time-PCR software	Thermo Fisher	Version 1.3
Salmon	-	Version 1.5.0
Scanning electron microscope (field emission)	Hitachi High Technologies	Regulus 8230
SIS cell software	Olympus	-
Tapestation	Agilent	4200
tximport	Bioconductor	-
U-bottom 96-well plate	Greiner	650101
V-bottom 96-well plate	Greiner	651101
Zen Blue	Zeiss	Version 3

2.1.8.2 Confocal Microscope Zeiss LSM800 settings

Table 2.12: Confocal Microscope Zeiss LSM800 settings

Parameter		**Setting**			
Fluorophore	Hoechst	Laser (nm)	405	Filter	DAPI
	AF647		640		AF647
	Dylight550		561		AF550
	SYTO RNAselect		488		FITC
Objective	40x	Acquisition mode	AiryScan (AiryScan processing performed in Zen Blue 3 software after image acquisition)	Multidimensional acquisition	Tiles (3x) (stitching performed in Zen Blue 3 software after image acquisition)
	63x				z-stack (10); 3 z-stacks and time series for live cell imaging (one image every 5 min for a duration of 30 min total)
Frame size		1024 x 1024 pixels (super resolution for high resolution imaging)			
Scan speed		Max			
Scanning		Bidirectional			
Averaging		None			
Live cell imaging	Temperature	37°C			
	CO_2	5%			

2.1.8.3 FACS Canto II settings

Table 2.13: FACS Canto II settings

Fluorophore	**Laser**	**Wavelength (nm)**
BV421	Violet	450/50
FITC/AF488	Blue	530/30
PE	Blue	585/42
APC/AF647	Red	660/20

2.2 Cell biology methods

2.2.1 RNA-LL37 complex/RNA/CpG+DOTAP preparation

Nataly Korn from the group of Christiane Wolz, Department of Microbiology and Infection medicine, University of Tübingen, kindly isolated bacterial RNA (bRNA) from *S. aureus (USA300)* as previously described by this group (Herster et al. 2020). naRNA isolated from PMA-induced NETs and fungal RNA (fRNA) from *C. albicans* strain SC5314 was isolated as described below. To stimulate cells in a volume of 500 µL, 10 µg LL37 was incubated with 5.8 µM ssRNA40 (see Table 2.4; ~ 34.4 µg/mL), fRNA (125 ng/mL), bRNA (10 µg/mL), or PMA NET-derived naRNA (~ 600 ng/mL) for 1 h at RT for complex formation. For smaller volumes of cells, according fractional amounts of complexes were used. For naRNA-only control, the same amount and volume was used replacing LL37 with sterile, endotoxin-free water. The transfection reagent DOTAP was incubated with ssRNA40 or CpG-DNA (see Table 2.4) for 10 min at RT for complex formation (amounts of DOTAP and ssRNA40/CpG-DNA used are stated in the according sections).

2.2.2 Preparation of fungal RNA from *C. albicans*

Tzu-Hsuan Chang from the group of Alexander Weber, Department of Immunology, University of Tübingen, kindly cultured the fungi *C. albicans* SC5314. Therefore, the fungi was plated in a YPD agar containing slant tube and grown overnight at 30 °C as previously described (Chang et al. 2022). For fRNA isolation, one colony from the slant tube was picked and resuspended in 500 µL YPD medium in a 1.5 mL Eppendorf tube. Afterwards, the tube was centrifuged at 10,000 rpm for 1 min and the supernatant was removed. To wash the fungi, the centrifugation step was repeated with 1 mL PBS. Afterwards, the fungal cells were resuspended in 200 µL RLT buffer (derived from RNeasy Mini Kit, Qiagen, see Table 2.10) and transferred into a 0.5 mm diameter ceramic beads-containing 2 mL reaction tube. 1 mL additional RLT buffer was further added. The fungal cell walls were subsequently cracked open by homogenization using a microtube homogenizer (BeadBug™, Merck, see Table 2.11) with an interval of seven times 2 min shaking at 2800 rpm and 1 min cooling break on ice. Afterwards, the fRNA-containing supernatant was transferred into a new tube and 1 mL 75% ethanol was added. The RNA isolation was then performed according to the manufacturer's instructions using the Qiagen RNeasy Mini Kit for purification of Total RNA from Animal Tissues (see Table 2.10). At last, the fungal RNA was eluted in 30 µL RNase DNase-free H_2O and the concentration was measured using a Nanodrop Spectrophotometer.

2.2.3 Mice

Unc93b1$^{3d/3d}$ mice lacking functional endosomal TLRs (Tabeta et al. 2006), *Tlr13*$^{-/-}$ mice lacking the murine equivalent to the human ssRNA-sensing TLR8 (Li and Chen 2012) (both kindly provided by Tatjana Eigenbrod, Heidelberg and on C57BL/6 background) and WT C57BL/6 mice between the age of 8 to 20 weeks were used in accordance with local institutional guidelines on animal experiments, regular hygiene monitoring, and specific locally approved protocols compliant with the German regulations of the Gesellschaft für Versuchstierkunde/Society for Laboratory Animal Science (GV-SOLAS) and the European Health Law of the Federation of Laboratory Animal Science Associations (FELASA) for sacrificing and *in vivo* work. *Unc93b1*$^{3d/3d}$, *Tlr13*$^{-/-}$, and WT C57BL/6 control mice were housed in controlled specific-pathogen-free animal facilities at the Interfaculty Institute of Cell Biology, University of Tübingen. Local federal authority for the approval of experimental protocols was the Regierungspräsidium Tübingen.

These mice were used for *ex vivo* experiments. *Tlr9*$^{-/-}$ mice lacking the DNA-sensing endosomal TLR and matched WT C57BL/6 control mice were a kind gift from Birgit Schittek, Department of Dermatology, University Hospital Tübingen, and also used for *ex vivo* experiments. LysM$^{EGFP/+}$ mice expressing green fluorescent labeled myeloid cells (Faust et al. 2000), *Tlr13*$^{-/-}$ mice (Li and Chen 2012) (kindly provided by James Chen, Houston and David Nemazee, La Jolla), and WT (all on a C57BL/6 background) mice were bred and maintained under the specific pathogen-free conditions with air isolated cages at an American Association for the Accreditation of Laboratory Animal Care (AAALAC)-accredited animal facility at Johns Hopkins University and handled according to procedures described in the Guide for the Care and Use of Laboratory Animals as well as Johns Hopkins University's policies and procedures as set forth in the Johns Hopkins University Animal Care and Use Training Manual, and all animal experiments were approved by the Johns Hopkins University Animal care and Use Committee (MO21M378). Sex-and age-matched 6–8-week-old mice were used for each experiment. All of the *in vivo* experiments on these mice were performed by Christine Youn, Yu Wang, and Nathan Archer from the Department of Dermatology, Johns Hopkins University School of Medicine, Baltimore, USA.

2.2.4 Isolation and stimulation of bone marrow-derived PMNs (BM-PMNs)

Bone-marrow (BM)-PMNs were isolated from mice as previously described by this group (Herster et al. 2020). At first, bones were isolated from the respective mice after CO_2 and subsequent cervical dislocation-sacrifice. Femur and tibia of all four legs were used and the bone marrow was flushed out using RPMI containing 10% FCS. Afterwards, the cells were centrifuged at 509 x g for 5 min, resuspended in 1 mL 1x erythrocyte lysis buffer (ACK, see Table 2.5) and incubated at 4 °C for 5 min on a roller shaker. After erythrocyte lysis, the tube was filled up to 25 mL with MACS buffer (see Table 2.5) to inactivate the ACK buffer and for washing. The cells were centrifuged again at 509 x g for 5 min and resuspended with the appropriate volume of MACS buffer, according to the kits instructions (mouse Neutrophil Isolation Kit, Miltenyi, see Table 2.10). Subsequently, neutrophils were isolated using magnetic separation (MACS) (mouse Neutrophil Isolation Kit, Miltenyi, see Table 2.10) following the manufacturer's instructions. After magnetic separation using negative selection, BM-PMNs were resuspended in culture medium for BM-PMNs (see Table 2.5) and 1×10^5 cells/well were seeded in a 24-well plate containing poly-L-lysine-coated coverslips (Electron Microscopy Sciences, see Table 2.11). Finally, stimulation was performed with PMA (600 nM), ssRNA+LL37 complex (as previously described), nigericin (50 µM), live *C. albicans* (MOI1), or human NET content (Mock/PMA NETs, 1:50 dilution) for 16 h at 37°C and 5% CO_2. Subsequently, cells were stained for immunofluorescence as described below.

2.2.5 Study participants and human blood acquisition

All healthy donors included in this study provided their written informed consent before participation. Approval for use of biomaterials was obtained for this project by the local ethics committee of the Medical Faculty Tübingen in accordance with the principles laid down in the Declaration of Helsinki as well as applicable laws and regulations.

2.2.6 Isolation of primary human neutrophils (PMNs)

Neutrophils of healthy human donors were isolated as previously described by this group (Herster et al. 2020). Therefore, ~9 mL EDTA-anticoagulated whole blood (drawn in EDTA blood collection tubes (S-Monovette), see Table 2.11) was diluted 1:2 in 20 mL PBS and loaded on 20 mL Ficoll (1.077 g/mL) in a 50 mL Falcon tube. For density gradient separation, the blood was centrifuged for 25 min at 509 x g at RT without brake and acceleration. Afterwards, all layers except the erythrocyte-granulocyte layer (most lowest layer) were discarded using a vacuum pump. To perform erythrocyte lysis, the tube was carefully filled up to 50 mL with 1x ACK (see Table 2.5) and incubated for 20 min at 4 °C on a roller shaker. Afterwards, the cells were centrifuged for 10 min at 509 x g without brake and acceleration. The supernatant was carefully removed using a vacuum pump and discarded. To ensure the removal of remaining red blood cells, a second erythrocyte lysis step was performed. Therefore, the tube was carefully filled up to 25 mL with 1x ACK and incubated for 10 min at 4°C on a roller shaker. Subsequently, the tube was centrifuged for 5 min at 509 x g without brake and acceleration. The supernatant was carefully removed with a vacuum pump to not disturb the cell pellet and the remaining neutrophils were resuspended in PMN culture medium (see Table 2.5) to a density of 1.6 x 10^6 cells/mL, or 5 x 10^6 cells/mL. After isolation, PMNs were analyzed for purity and activation status by flow cytometry analysis before every experiment, as described in section 2.3.1.

2.2.7 Stimulation of primary human neutrophils (PMNs)

500 µL cells/well were seeded in a 24-well plate (containing poly-L-lysine-coated coverslips (Electron Microscopy Sciences, see Table 2.11)) for immunofluorescence microscopy, or 8 mL of 5 x 10^6 cells/mL were seeded in uncoated 10 cm petri-dishes for NET preparation and naRNA isolation/isolation of whole PMN RNA. The cells were rested for 30 min at 37°C and 5% CO_2 and subsequently stimulated with PMA (600 nM), nigericin (50 µM), live *C. albicans* (MOI2), RNA+LL37 complexes (as previously described), or NET content (Mock/PMA +/-RNase inhibitor) at indicated dilutions for 3 h for immunofluorescence microscopy, with PMA (1200 nM) for 3 h for electron microscopy, or with PMA (600 nM) for 4 h for preparation of NET content and naRNA isolation. The cells were additionally incubated with 100 nM TLR8-inhibitor CU-CPT9a or 200 µM PAD4-inhibitor Cl-amidine 30 min before stimulation where indicated. In these conditions, medium was not replaced with fresh medium without inhibitor for incubation with the respective stimuli.

2.2.8 Preparation and isolation of NETs and purification of naRNA/whole PMN RNA

To induce NET formation for preparation of NET content, PMNs were seeded in uncoated petri dishes and treated with 600 nM PMA for 4 h at 37°C and 5% CO_2, or left unstimulated during the incubation time as the Mock control. Afterwards, to get rid of residual PMA used as the stimulus for NET formation, any cytokines released by the cells, and unstimulated PMNs (which do not adhere to the uncoated dish), the cells were washed three times with 5 mL PBS/plate very carefully. Where indicated and for isolation of naRNA, naRNA was protected by addition of 10 U/µL RNase inhibitor (Promega, see Table 2.1) (= Mock/PMA NETs + RNase Inhibitor) during the NET preparation process and for storage. For digest of naRNA in NETs, the NET content was incubated for 30 min at 37 °C with 100 µg/mL RNase A (Thermo Fisher, see Table 2.6, EDTA for DNase inhibition added). For isolation of naRNA, PMA or Mock NETs were

resuspended in 300 µL of ML lysis buffer after the above described washing steps and RNA isolation was performed according to the manufacturer's instructions (NucleoSpin miRNA isolation kit, Macherey-Nagel, see Table 2.10). Subsequently, naRNA was eluted in 50 µL RNase DNase-free H_2O and the concentration was determined using a Nanodrop Spectrophotometer. For isolation of whole PMN RNA, untreated PMNs were directly lysed in 300 µL ML buffer and the RNA was isolated from the cells according to the manufacturer's instructions (NucleoSpin miRNA isolation kit, Macherey-Nagel, see Table 2.10).

2.2.9 RNA sequencing analysis of naRNA

Quality control of isolated naRNA was run using the Agilent 4200 TapeStation system. Subsequently, sequencing was performed according to NEBNext® Ultra™ II Directional RNA Library Prep Kit for Illumina® using the protocol for use with rRNA Depleted FFPE RNA at the Core Facility for Genomics, Medical Faculty, University Münster. The data was quantified and analyzed by Marissa Dubbelaar (PostDoc in the group of Juliane Walz, Department of Immunology, University of Tübingen/Quantitative Biology Center (QbiC), University of Tübingen) using Salmon Version 1.5.0. tximport was used to obtain the transcript-level quantification. For transcript classification, GENECODE annotation was performed.

2.2.10 Extracellular bacterial killing of *S. aureus*

The killing assay of *S. aureus* with human PMNs was kindly performed by Jule Focken, a PhD student of the group of Birgit Schittek, Division of Dermatooncology, Department of Dermatology, University Hospital Tübingen, and performed as described according to Brinkmann *et al.*, 2004 (Brinkmann et al. 2004). Therefore, PMNs were seeded at a density of 2 x 10^6 cells/mL and incubated with PMA (600 nM) for 2 h at 37°C. The medium was carefully replaced afterwards with serum-free culture medium containing 2% heat-inactivated pooled human serum and cytochalasin D (10 µg/mL) and incubated further for 15 min before infection with bacteria. Cytochalasin D treatment did not affect NET formation and the concentration used in this study was effective to block phagocytosis of the bacteria. To investigate whether naRNA of NETs is necessary for extracellular bacterial killing, samples were either treated with 100 µg/mL RNase A (Thermo Fisher, see Table 2.6) or 1 U/10 µL DNase I (Thermo Fisher, see Table 2.6) for 2 h during NET formation, or after NET formation during the 30 min bacteria incubation and killing process. Bacteria were added, samples were centrifuged at 700 x g for 10 min, and afterwards incubated at 37°C and 5% CO_2 for 30 minutes. Bacterial killing was measured as percentages of control values (bacteria incubated alone in media without neutrophils).

2.2.11 Isolation of peripheral blood mononuclear cells (PBMCs) and subsequent stimulation

All PBMC assays were performed by the former master student of AG Weber, Sirui Chen, Department of Immunology, University of Tübingen, under my supervision. PBMCs were isolated from whole blood as previously described by this group (Herster et al. 2020). Therefore, ~9 mL EDTA-anticoagulated blood was diluted 1:2 in PBS (20 mL) and density gradient separation was performed as described above (see section 2.2.6). The serum layer (upper most layer) was removed using a vacuum pump and the PBMC layer (second layer from top, white) was then carefully transferred with Pasteur pipettes into another 50 mL reaction tube. The tube was filled up to 50 mL with PBS and the cell suspension was spun down at 1800 rpm for 8 min. The supernatant was discarded using a vacuum pump and 30 mL PBS were added for

washing. The cells were again centrifuged for 8 min at 1500 rpm and the supernatant was removed using a vacuum pump. For a last washing step, 30 mL PBS were added and the PBMCs were centrifuged one more time at 1100 rpm for 8 min. The supernatant was again discarded and the cells were resuspended in PBMC culture medium (see Table 2.5) at a density of 1 x 10^6 cells/mL. Afterwards, 200 µL/well of PBMCs were seeded in a 96-well plate and stimulated with LPS (100 ng/mL), R848 (5 µg/mL), TL8 (100 ng/mL), ssRNA (1.6 µg/mL) + DOTAP (50 µg/mL), ssRNA+LL37 complex (as described above), and respective NET content (Mock/PMA NETs +/-RNase inhibitor, 1:20 dilution) for 24 h at 37°C and 5% CO_2. Where indicated, the TLR8 inhibitor CU-CPT9a was added to the cells at a concentration of 1 µM 2 h before stimulation. The inhibitor was not removed for the incubation of the cells with the respective stimuli. After the stimulation, the plate was centrifuged for 5 min at 1500 rpm, the supernatant was transferred into a new plate and stored at -80 °C until the respective cytokine ELISA was performed.

2.2.12 Isolation and preparation of primary human stem cell-derived neutrophils

The isolation and preparation, as well as differentiation of primary human stem cell-derived neutrophils was kindly performed by Masoud Nasri, a PostDoc of the group of Julia Skokowa, Division of Translational Oncology, Department of Oncology, Hematology, Clinical Immunology and Rheumatology, University Hospital Tübingen. The stem cells (cord blood-derived) used were obtained under the according ethics approval of AG Skokowa. All reagents used for the preparation of stem cells were kindly provided by AG Skokowa. Stem cells derived from human healthy donors were prepared and differentiated as described (Sioud 2020). Therefore, bone marrow was diluted in PBS, carefully layered on Ficoll-Paque medium (density: 1.077 g/mL) and centrifuged at 500 x g for 25 min at RT without brake and acceleration to perform density gradient separation. The interphase layer containing the mononuclear cell fraction was then transferred to a new 50 mL tube. Washing was performed twice with 30 mL ice-cold PBS and subsequent centrifugation at 300 x g at 8 °C for 8 min. Furthermore, the cells were resuspended, counted, and isolated using Human CD34 MicroBead Kit (Miltenyi, see Table 2.10) for MACS isolation of $CD34^+$ cells from BM-mononuclear cells (MNCs). Afterwards, the number of $CD34^+$ hematopoietic stem cells (HPSCs) was determined and the isolated cells were cultured in $CD34^+$ culture medium (see Table 2.5) at a density of 2 x 10^5/mL at 37 °C and 5% CO_2 for two weeks. Thereby, the medium was replaced every second day. During the differentiation process, the cells were fed with 100 µM 5-ethynyluridine, an analogue of uridine which gets incorporated into RNA but not DNA (Presolski, Hong, and Finn 2011), for 14 days for subsequent click chemistry labeling of endogenous RNA, or were left untreated as controls. To verify differentiation, cell morphology was assessed using Cytospin assay (see Table 2.11). In brief, the Cytoclip™ slide clips were loaded by assembling the filter card, the sample chamber, and the glass slide. An assembled Cytoclip™ slide clip was then placed in the slide clip support plate of the Cytospin centrifuge. 2 x 10^4 cells from liquid differentiation culture were pipetted into Cytofunnel™ and centrifuged for 3 min at 200 x g. The Cytospin slides were subsequently stained for 5 min in May-Grünwald stain, shortly rinsed with ddH_2O, and then stained for 10 min in Wright-Giemsa stain. Afterwards, the slides were again shortly rinsed with ddH_2O, and cell morphology was determined using a light microscope. To further verify differentiation by CD markers, flow cytometric analysis was performed using antibodies specific for the following hematopoietic/myeloid markers: CD45 (leukocyte marker), CD34 (HSPC marker), CD33 (promyelocyte marker), CD11b (myeloid cell marker), CD14 (monocyte marker), and CD15 and CD16

(neutrophil markers). Neutrophil percentage was determined by gating on neutrophils as follows: $CD45^+CD11b^+CD15^+$, or $CD45^+CD11b^+CD16^+$, or $CD45^+CD15^+CD16^+$ cells.

2.2.13 Cell culture, transdifferentiation, and stimulation of BlaER1 cells

Culturing, transdifferentiation, and stimulation of BlaER1 cells was performed by Carsten Greve, a PhD student from the group of Alexander Weber, Department of Immunology, University of Tübingen. BlaER1 cells, originally derived from malignant B cells, were edited to monocytes/macrophages by the induction of a nuclear translocation of a C/EBPα transgene (Gaidt et al. 2018). Those cells (WT, *Unc93b*$^{-/-}$, and *Tlr8*$^{-/-}$) were a kind gift of Holger Heine, Borstel, Germany (Vierbuchen et al. 2017) and cultured, transdifferentiated, and stimulated for 18 h with the respective stimuli as previously described by our group (Herster et al. 2020). Therefore, 1 x 10^6 cells/well were seeded in a 6-well plate and differentiated into macrophage-like cells with 10 ng/mL hIL-3, 10 ng/mL hM-CSF and 150 nM β-estradiol in BlaER1 culture medium (see Table 2.5) for 7 days. 5 x 10^4 cells were then reseeded in a 96-well plate and rested for 1 h. Afterwards, macrophage-like cells were treated in a total volume of 125 µL/well with the respective stimuli (LPS (0.1 µg/mL), R848 (5 µg/mL), TL8 (100 ng/mL), ssRNA+LL37 complex (as described above), and Mock/PMA NETs +/-RNase inhibitor) in complete medium for 18 h. After stimulation, the supernatant was harvested, transferred into a new plate, and stored at -80°C until the IL-8 cytokine ELISA was performed.

2.2.14 Cell culture, differentiation, and stimulation of THP-1 cells

Culturing, differentiation, and stimulation of THP-1 cells was performed by Carsten Greve, a PhD student from AG Weber, Department of Immunology, University of Tübingen. THP-1 cells (a kind gift from Thomas Zillinger, Bonn, Germany (Coch et al. 2019)), derived from a human leukemia monocytic cell line (Chanput, Mes, and Wichers 2014), were cultured in complete RPMI (see Table 2.5) medium. For differentiation, 5 x 10^4 cells/well were seeded in a 96-well plate, subsequently treated with 300 ng/mL PMA and incubated for 16 h at 37°C and 5% CO_2 to induce differentiation into macrophage-like cells. Afterwards, the cells were washed with PBS three times and fresh medium was added. After 48 h of resting, the medium was removed and exchanged by medium containing 200 U/mL IFN-γ (Sigma, see Table 2.1), in which the cells were incubated for 6 h. After repeated washing and additional medium exchange, the differentiated and primed cells were treated in a total volume of 125 µL/well with the respective stimuli (PMA (25 µg/mL) + Ionomycin (0.375 µg/mL), LPS (0.1 µg/mL), R848 (5 µg/mL), TL8 (40 ng/mL), ssRNA+LL37 complex (as described above), Mock NETs+RNase inhibitor (1:50 dilution), PMA NETs (1:50 dilution), and PMA NETs+RNase inhibitor (1:50 dilution)) in complete medium for 18 h. The cells were centrifuged for 5 min after the stimulation, and the supernatant was transferred into a new plate which was stored at -80°C until the IL-8 cytokine ELISA was performed.

2.2.15 Cell culture and stimulation of N/TERT-1 keratinocytes

Culturing and stimulation of N/TERT-1 keratinocytes were performed by Carsten Greve, a PhD student from AG Weber, Department of Immunology, University of Tübingen. N/TERT-1 cells, which are immortalized keratinocytes (a kind gift from Prof. James Rheinwald (Dickson et al. 2000)), were always used in cultures lower than passage ten and kept in complete CnT-07 medium (see Table 2.1). Two days

prior to stimulation, a total amount of 2 x 10^4 cells/well was seeded in a 96-well plate and incubated at 37°C and 5% CO_2. For stimulation, fresh medium was added, and the cells were incubated in a total volume of 125 µL/well with the respective stimuli for 24 h diluted in culture medium (PMA (25 µg/mL) + Ionomycin (0.375 µg/mL), TL8 (200 ng/mL), ssRNA+LL37 complex (as previously described), as well as Mock and PMA NETs +/-RNase inhibitor at indicated dilutions). After the incubation, the cells were centrifuged, and the supernatant was stored in a new plate at -80°C until the IL-8 cytokine ELISA was performed.

2.2.16 Culturing and stimulation of primary normal human epidermal keratinocyte (NHEK) cells

Culturing and stimulation of NHEK cells was performed by Carsten Greve, a PhD student from AG Weber, Department of Immunology, University of Tübingen. NHEK cells (Normal Human Epidermal Keratinocytes (NHEK) single juvenile donor, proliferating, PromoCell, C-12002) were grown and stimulated in Keratinocyte Growth Medium 2 (PromoCell, see Table 2.1). A total amount of 2 x 10^4 cells/well was seeded in a 96-well plate and incubated at 37°C and 5% CO_2 two days before stimulation was performed. For stimulation, the medium was replenished with basal medium containing 1.7 mM $CaCl_2$ (Roth, see Table 2.1) and stimuli were added for 24 h diluted in medium in a final volume of 125 µL (R848 (20 µg/mL), TL8 (200 ng/mL), ssRNA+LL37 complex, as well as Mock NETs+RNase inhibitor (1:25 dilution) and PMA NETs +/-RNase inhibitor (1:25 dilution)). After the incubation was performed, the cells were centrifuged, and the supernatant was stored in a new plate at -80°C until the IL-8 cytokine ELISA was performed.

2.2.17 Preparation of the 3D human skin equivalent

The 3D human skin equivalent, as well as all reagents and cells needed for its generation, was kindly generated and were provided by Jasmin Scheurer from/and the group of Birgit Schittek, Division of Dermatooncology, Department of Dermatology, University Hospital Tübingen, as described (Bitschar et al. 2020). Therefore, primary fibroblasts were seeded on collagen and incubated in FF medium for five days. Subsequently, primary keratinocytes (NHEK) were added to the wells. After 12 days of coincubation, airlifting was performed. On day 22, the 3D skin model was stimulated for 24 h with NET content (Mock/PMA NETs +/-RNase inhibitor; 25 µL/well for one 3D construct grown in a 12-well chamber) or the respective water control (25 µL/well). Afterwards, the supernatant was harvested for ELISA and the RNA was isolated for qPCR analysis.

2.2.18 qPCR analysis of *IL-8* mRNA of the 3D human skin equivalent

qPCR analysis of *IL-8* mRNA of 3D human skin equivalent samples stimulated with NET content as described above was performed by Carsten Greve, a PhD student from AG Weber, Department of Immunology, University of Tübingen. Therefore, total RNA was isolated using the RNeasy Mini Kit (Qiagen, see Table 2.10) and the protocol for Animal Tissues and Cells. Subsequently, the High-Capacity RNA-to-cDNA-Kit (Thermo Fisher, see Table 2.10) was used according to the manufacturer's instructions for cDNA preparation. For performance of the qPCR, the TaqMan™ system was used: a master mix of TaqMan™ Universal Mastermix II (Thermo Fisher, see Table 2.1) and TaqMan™ Gene Expression Assay (Thermo Fisher, see Table 2.1) was prepared following the manufacturer's instructions. Hereby, 5.5 µL master mix and 4.5 µL of the respective cDNA (IL-8 and TBP, the latter was used as the housekeeping gene) were

mixed for one reaction and the qPCR was run. Analysis was performed in triplicates using QuantStudio Real-Time-PCR software version 1.3 (Thermo Fisher). Primers used for the qPCR are listed in Table 2.9.

2.2.19 Culturing and stimulation of NK-92 MI cells

Culturing and stimulation of NK-92 MI cells was performed by Pujan Engels, a PhD student from AG Weber, Department of Immunology, University of Tübingen. NK-92 MI cells (kindly provided by Melanie Märklin, University Hospital Tübingen), a NK cell line derived from a non-Hodgkin's lymphoma patient (Klingemann, Wong, and Maki 1996), were cultured in IMDM-Medium (Lonza, see Table 2.1). A total amount of 1 x 10^5 cells/well were seeded in a volume of 200 µL and incubated for 2 h at 37°C and 5% CO_2 for resting. For stimulation, the cells were incubated with LPS (100 ng/mL), CpG (2.5 µM) + DOTAP (25 µg/mL), R848 (5 µg/mL), TL8 (100 ng/mL), ssRNA (1.6 µg/mL) + DOTAP (50 µg/mL), ssRNA+LL37 complex (as described above), or NET content (Mock NETs+RNase inhibitor/PMA NETs +/-RNase inhibitor; 1:100 dilution) for 24 h. Afterwards, the plate was centrifuged for 5 min and the supernatant was transferred into a new plate, which was stored at -80°C until the cytokine ELISA for IFN-γ was performed.

2.2.20 Transient transfection of HEK293T cells

Transient transfection of HEK293T cells was performed by the former master student of AG Weber, Sirui Chen, Department of Immunology, University of Tübingen, under my supervision. Hereby, HEK293T cells were transiently transfected with the respective TLR8, TLR7, TLR9, and NF-κB reporter plasmids as previously described in literature (Colak et al. 2014) (see Table 2.8 for plasmids) using X-tremeGENE™ HP DNA Transfection Reagent (Merck, see Table 2.1). Therefore, one day prior to transfection, a total amount of 5 x 10^4 cells/well were seeded in a 24-well plate. For the transfection of one well, 100 ng of the according TLR plasmid, 100 ng of the firefly luciferase NF-κB reporter, and 10 ng *Renilla* luciferase control reporter was mixed in Opti-MEM™ Reduced Serum Medium (Thermo Fisher, see Table 2.1) in a total volume of 50 µL. After 15 min incubation at RT, the transfection mix was added to the cells and the cells were afterwards incubated for 48 h. Prior to subsequent stimulation, the medium was changed to complete DMEM medium (see Table 2.5), and the cells were incubated for 18 h at 37°C and 5% CO_2 with the respective NET content stimuli and TLR ligand controls (R848 (2.5 µg/mL; TLR7/8 ligand), TL8 (100 ng/mL; TLR8 ligand), CpG (1.25 µM) + DOTAP (25 µg/mL) (TLR9 ligand), ssRNA (0.6 µg/mL) + DOTAP (20 µg/mL) (TLR8 ligand), Mock NETs+RNase inhibitor (1:50 dilution), PMA NETs (1:50 dilution), PMA NETs+RNase inhibitor (1:50)). Supernatants were removed, and the cells frozen briefly at -80 °C. Subsequently, they were used for the dual luciferase reporter assay as described below.

2.2.21 Dual luciferase reporter assay

The dual luciferase reporter (DLR) assay was performed by the former master student of AG Weber, Sirui Chen, Department of Immunology, University of Tübingen, under my supervision, as described (Herster et al. 2020). In this assay, two reporters (*Renilla* and firefly luciferase) are transfected into the cells. At first, the luciferase activity of firefly is measured by luminescence. Afterwards, this signal is quenched which in turn activates the *Renilla* luciferase reaction in parallel. Thus, the *Renilla* luminescence can get measured to normalize the firefly experimental signal to this control reporter signal. Thereby, the DLR assay provides a fast measurement of two reporters in the same cell lysate (McNabb, Reed, and Marciniak 2005). In this study, the firefly activity was coupled to NF-κB expression as the experimental reporter for

TLR activation. In brief, supernatants were removed from the cells after stimulation and 60 µL/well of 1x passive lysis buffer (Promega, see Table 2.1) was added. The plate was then incubated for 15 min at RT on the plate shaker and subsequently stored at −80°C for at least 15 min to facilitate complete cell lysis. After thawing, the cell solution (60 µL) was transferred into a V-bottom 96-well plate (see Table 2.11) and centrifuged to pellet cell debris for 10 min at 2500 rpm and 4°C. Subsequently, 10 µL of supernatant were then transferred into a white microplate (glass bottom) and each condition was measured in triplicates using the FLUOstar OPTIMA device (BMG Labtech, see Table 2.11). Firefly and *Renilla* luciferase activity were determined using the Promega Dual luciferase kit (see Table 2.10). Both enzyme activities were measured for 12.5 s with 24 intervals of 0.5 s, respectively. The data was analyzed by calculating the ratio of the two measured signals, thereby normalizing each firefly luciferase signal to its corresponding *Renilla* luciferase signal. The ratios were represented as the relative light units (RLU) of NF-κB activation.

2.3 Immunochemical methods

2.3.1 Flow cytometry analysis of purity and pre-activation state of PMNs

After PMN isolation, the purity and activation state of the cells was determined by flow cytometry (FACS) as previously described by this group (Herster et al. 2020). Therefore, 200 µL of cells (1 x 10^6 cells/mL) were seeded in a 96-well plate (U-bottom, see Table 2.11) and centrifuged for 5 min at 448 x g. Afterwards, blocking was performed using 50 µL/well pooled human serum (see Table 2.1) diluted 1:10 in PBS for 15 min at 4°C. After washing with PBS (50 µL/well, centrifugation for 5 min at 448 x g), the samples were stained for 20 min at RT in the dark (50 µL antibody solution in PBS/well; each antibody used at 1:100 dilution) for CD15, CD66b, and CD62L in the first well, CD14 and CD66b in a second well, and PE-, FITC-, and BV421-isotypes in the third well (antibodies see Table 2.7). Subsequently, cells were washed again and fixed (100 µL/well fixation buffer, see Table 2.1) for 10 min at RT in the dark. After an additional washing step, the cell pellets were resuspended in 300 µL PBS and measurements were performed on a FACS Canto II (BD Bioscience, Diva software; see Table 2.11; settings see Table 2.13). Analysis was performed using FlowJo V10 analysis software (see Table 2.11).

2.3.2 Immunofluorescence (IF) microscopy of fixed human or murine primary neutrophils

For immunofluorescence microscopy (IF), 500 µL of 1.6 x 10^6 cells/mL of primary human blood PMNs, or 500 µL of 2 x 10^6 cells/mL of murine PMNs isolated from BM were seeded in a 24-well plate containing poly-L-lysine-coated glass coverslips (Electron Microscopy Sciences, see Table 2.11). After seeding, the cells were rested for 30 min and stimulated in PMN culture medium or BM-PMN culture medium at 37°C and 5% CO_2 (as described above) for 3 h (human) or 16 h (murine), respectively, as described and adapted from Brinkmann *et al.*, 2004 (Brinkmann et al. 2004). After stimulation, the cells were carefully washed three times for 5 min with 500 µL PBS/well. The cells were then fixed with 250 µL/well fixation buffer (Biolegend, see Table 2.1) for 10 min at RT in the dark and washed again. Afterwards, the cells were blocked with 200 µL/well IF blocking buffer (see Table 2.5) for 2 h at RT or alternatively overnight at 4°C. The primary antibodies (rRNA Y10b (incubated in the dark if conjugated antibody (AF647) was used), hLL37 (incubated in the dark because conjugated to Dylight550), see Table 2.7) were diluted 1:50 in blocking

buffer and 200 µL/well antibody solution was added. The cells were subsequently incubated for 2 h at RT while gently rocking. Afterwards, to get rid of unbound primary antibody, the cells were washed three times for 5 min with PBS (PBS was treated with 0.1% DEPC for RNase inactivation and subsequently autoclaved for DEPC inactivation) and incubated with 200 µL/well secondary antibody (rabbit anti-mouse AF647, see Table 2.7) in a 1:500 dilution in blocking buffer in the dark for 1 h (again gently rocking). After repeated washing, the cells were incubated with 1 µg/mL Hoechst 33342 (Thermo Fisher, see Table 2.7) for 5 min to stain nuclear DNA. Secondary antibodies alone were tested in the same way as described, substituting the primary antibody solution with blocking buffer. Those conditions did not yield any significant staining under identical microscopy acquisition conditions. The coverslips were mounted using 4 µL/coverslip mounting solution (ProLong™ Diamond Antifade Mountant, Thermo Fisher, see Table 2.1) on glass slides and left to dry overnight at RT in the dark. Subsequently, the samples were stored at 4°C before microscopy using a Zeiss LSM800 Confocal microscope (settings see Table 2.12) and image analysis using ImageJ-Win64 and Zen Blue3 software was performed (see Table 2.11).

2.3.3 Quantification of NET formation

When NETs are released by the PMNs, DNA (Hoechst) signals as well as naRNA (rRNA Y10b) signals showed up in a greater amount but smaller average size. Thus, the ratio of the signal number (amounts of regions of interest (ROIs)) and the average signal size can be used as a NET-related signal dispersion for quantification of nucleic acid-release during NET formation using both, DNA and RNA signal. Therefore, microscopy images were obtained using a Zeiss LSM800 Confocal microscope with a 40x objective and 3x3 tiles acquisition in AiryScan mode (settings see Table 2.12). Three images per sample of three biological replicates were acquired. Afterwards, ImageJ-Win64 software was used and a threshold (Triangle threshold) was applied as originally described (Zack, Rogers, and Latt 1977). Particles were analyzed with a ROI manager: size (micron^2): 100-infinity (pixel units) and circularity: 0.00-1.00. Hereby, the average size and number of particles (ROIs) was assessed. In another approach, to not check the signal dispersion but manually count the NET-forming cells, images were acquired as described above and ImageJ-Win64 software was used to create a PNG image of the Hoechst signal (DNA NET fibers visible). A grid with 8x8 tiles was manually applied to the images using PowerPoint (Microsoft, see Table 2.11). Tiles containing extracellular DNA structures were manually counted by a colleague in a blinded manner as NET-positive tiles. Data of both quantification approaches was transferred to and analyzed with Prism software (GraphPad, see Table 2.11).

2.3.4 Quantification of naRNA-LL37-colocalization by using Pearson's Correlation Coefficient

The Pearson's Correlation Coefficient is a widely used tool to determine the relation of two variables by their correlation behaving in a linear manner (Armstrong 2019). To assess the colocalization of neutrophil RNA (stained with anti-rRNA Y10b antibody) or DNA (stained with Hoechst 33342) with LL37 (stained with anti-hLL37 antibody) in resting and NET-forming PMNs, samples were prepared and stained as described above (for NET formation, cells were stimulated with PMA (600 nM) for 3 h). After NET-induction, staining, and mounting, images of fixed samples were taken using a Zeiss LSM800 Confocal microscope with a 40x objective and 3x3 tiles acquisition in AiryScan mode (settings see Table 2.12). For quantification, three images per sample of three biological replicates were acquired and ImageJ-Win64 software (see Table

2.11) was used for analysis. For PCC analysis, a threshold (Triangle threshold) was applied as originally described (Zack, Rogers et al. 1977), and analysis for Pearson's Correlation Coefficient (PCC) (Pearson 1895) between LL37 and rRNA, or LL37 and DNA signals, respectively, was performed. Data was transferred to and analyzed with Prism software (GraphPad, see Table 2.11).

2.3.5 Line plot analysis of high resolution and ultrathin section images

The line plot analysis tool provides intensity histograms of fluorescent signals measured in IF microscopy along a user-defined line, manually drawn through the region of interest of the IF image. This tool can be used in ImageJ-Win64 software or in Zen Blue 3 software. Therefore, resting and NET-forming PMNs were prepared as described (section 2.3.2 and 2.3.8). For NET formation, cells were stimulated for 3 h with 600 nM PMA for regular confocal IF, and with 1200 nM PMA for IF of ultrathin sections. Staining with anti-rRNA Y10b and anti-hLL37 antibodies, respective secondary antibodies, as well as Hoechst 33342 was performed as described (section 2.3.2 and 2.3.8), and images of fixed samples were taken using a Zeiss LSM800 Confocal microscope with a 63x objective, AiryScan mode, and high resolution acquisition (see Table 2.12 for settings), or Zeiss Axioplan microscope (63x objective) for ultrathin sections (see Table 2.11). Line plot analysis of high resolution IF images was performed using Zen Blue3 software. Line plot analysis of images of ultrathin sections was performed using ImageJ-Win64. The data was exported to and analyzed with Prism software (GraphPad, see Table 2.11).

2.3.6 Live fluorescence microscopy of RNase digest of human NETs

For live cell imaging of RNase A digest of naRNA, 500 µL of 1.6 x 10^6 cells/mL of human blood PMNs were seeded in a 4-well glass bottom microscopy cell culture dish (Greiner, see Table 2.11) and rested for 30 min. Afterwards, the PMNs were stimulated with 600 nM PMA at 37°C and 5% CO_2 for ~3 h. After stimulation, the medium was carefully removed, and the cells were washed three times with 500 µL PBS/well very carefully to not destroy the NET fibers. Afterwards, fresh culture medium without phenol red to avoid unspecific signals was added (RPMI culture medium without phenol red, see Table 2.1). 1 µg/mL Hoechst 33342 (Thermo Fisher, see Table 2.7) to stain nuclear DNA and 50 µM SYTO RNAselect green fluorescent dye (Thermo Fisher, see Table 2.7) to stain naRNA was added to the cells in a volume of 200 µL/well medium. After incubation of the cells for around 5-10 min at 37 °C and 5% CO_2 in the dark, the cells were transferred to the confocal microscope. The incubation chamber of the microscope was pre-heated to 37 °C and CO_2 flow (5%) was ensured before the experiment was run (for settings see Table 2.12). The experiment was started and 100 µg/mL RNase A (Thermo Fisher, see Table 2.6) was added between time point 0 and 5 min. Imaging was performed using a Zeiss LSM800 Confocal microscope with the 63x objective and z-stack acquisition (3 stacks), taking an image every 5 min for a duration of 30 min (for settings see Table 2.12). Image analysis and video creation was performed using ImageJ-Win64 (see Table 2.11).

2.3.7 Electron microscopy of NETs, naRNA, and LL37

For electron microscopy, 500 µL of 1.6 x 10^6 cells/mL of human blood-derived PMNs were seeded in a 24-well plate containing 8 mm diameter coverslips which were pre-coated for 15 min at 37°C with 0.01% poly-L-lysine (Sigma, see Table 2.1) for scanning electron microscopy (SEM). For transmission electron microscopy (TEM), 6 mm diameter coverslips were coated with a carbon layer, glow-discharged and UV-

treated overnight before cells were seeded. Coverslips were provided and prepared by the group of Katharina Hipp, Electron Microscopy Facility, Max Planck Institute for Biology Tübingen. After isolation of PMNs and seeding, cells were rested for 30 min at 37°C and 5% CO_2. Subsequent stimulation was carried out for 3 h with 1200 nM PMA to ensure that almost 100% of cells undergo NET formation and broad covering of the coverslips by the NET structures, thus making EM image acquisition more efficient. For unstimulated controls, PMNs were left untreated for 3 h. Afterwards, the cells were fixed in 2.5% EM-grade glutaraldehyde in PBS for 2 h at RT, followed by incubation at 4°C overnight. Further sample preparation and performance of electron microscopy was kindly done by the group of Katharina Hipp, Electron Microscopy Facility, Max Planck Institute for Biology Tübingen. Reagents and equipment therefore used were also kindly provided by Katharina Hipp.

For SEM, samples were post-fixed with 1% osmium tetroxide for 1 h on ice. Subsequently, samples were dehydrated in a graded ethanol series followed by critical point drying (Leica Microsystems, see Table 2.11) with CO_2. Finally, sputter-coating of the cells with a 4 nm thick layer of platinum (Safematic, see Table 2.11) was performed and the samples were examined with a field emission scanning electron microscope (Hitachi High Technologies, see Table 2.11) at an accelerating voltage of 3 kV. For antibody labeling, cells were treated as described above and washed after fixation. Subsequently, blocking in 0.2% gelatin in PBS was performed and for naRNA-staining, samples were incubated for 1 h at RT with anti-rRNA Y10b at a 1:50 dilution in blocking buffer. Secondary antibody labeling was afterwards performed using goat anti-mouse antibodies coupled to 6 nm gold at a 1:20 dilution (antibodies see Table 2.7) for 1 h at RT in blocking buffer (Jackson ImmunoResearch, see Table 2.1). After antibody labeling, silver enhancement of the gold-particles to induce signal amplification was performed. Following immunolabeling, the samples were treated with 1% uranyl acetate for 5 min at RT, dehydrated, and critical point dried as above described. Afterwards, the samples were sputter-coated with a 5 nm thick layer of carbon and analyzed in the SEM with an accelerating voltage of 5 kV.

For TEM, NET samples were prepared by the PLT method as described for IF of ultrathin sections (see following section 2.3.8). Samples were placed on grids (Cu, Ni) and subsequently sectioned into 50-60 nm ultrathin slices. Afterwards, immunolabeling was performed by incubation with the first primary antibody anti-rRNA Y10b (mouse) in a 1:50 dilution in blocking buffer (Jackson ImmunoResearch, see Table 2.1) at 4°C overnight. The second primary antibody, anti-hLL37 (rabbit), was incubated the next day in a 1:50 dilution in blocking buffer for 1 h at RT, yielding to better and more specific signals than simultaneous incubation of both primary antibodies. For immunogold labeling with the respective secondary antibodies, the samples were incubated afterwards with goat anti-mouse-6 nm gold and goat anti-rabbit-12 nm gold secondary antibodies in a 1:20 dilution in blocking buffer for 1 h at RT (antibodies see Table 2.7). Following immunolabeling, the samples were treated with 1% uranyl acetate for 5 min at RT before analysis with the transmission electron microscope was performed.

2.3.8 Preparation of ultrathin sections for IF

Ultrathin sections were kindly prepared and imaged by the group of Katharina Hipp, Electron Microscopy Facility, Max Planck Institute for Biology Tübingen. For IF of ultrathin sections, 6 mm diameter coverslips were coated with a carbon layer, glow-discharged and UV-treated overnight for sterilization. After isolation and stimulation of the cells as described above (section 2.3.7), the cells were fixed in 2.5% EM-

grade glutaraldehyde in PBS for 2 h at room temperature, followed by incubation at 4°C overnight. Samples were prepared by the progressive lowering of temperature method (PLT). Therefore, the fixed cells were incubated in ethanol for infiltration of Lowicryl HM20, which was followed by UV polymerization (hardening of the embedding medium). Subsequently, ultrathin sections of 50-60 nm slices were prepared. Afterwards, NETs were stained for naRNA with anti-rRNA Y10b (mouse) and anti-hLL37 (rabbit) primary antibodies in a 1:50 dilution in blocking buffer (Jackson ImmunoResearch, see Table 2.1) for 1 h at RT. Subsequently, the cells were incubated with the secondary antibodies goat anti-mouse Cy3 and goat anti-rabbit AF488 for 1 h at RT in the dark in a 1:500 dilution in blocking buffer (antibodies see Table 2.7). Following staining, the cells were treated with 1% uranyl acetate for 5 min at RT. Analysis was subsequently performed using a Zeiss Axioplan microscope (63x objective, Olympus SIS cell software, see Table 2.11) and image/line plot analysis was performed using ImageJ-Win64 (see Table 2.11) as described in section 2.3.5.

2.3.9 Click chemistry of stem cell-derived human PMNs and IF microscopy

In the click chemistry labeling, a copper-catalyzed cycloaddition reaction is used to connect azides (in this study the fluorescent label AF546-azide) to alkynes (here 5-ethynyluridine) (Presolski, Hong, and Finn 2011). To perform this antibody-independent labeling, 500 µL of 1.6 x 10^6 cells/mL of human stem cell-derived PMNs treated with 5-ethynyluridine or left untreated were seeded in a 24-well plate containing poly-L-lysine-coated glass coverslips (Electron microscopy Sciences, Table 2.11). After seeding, the cells were rested for 30 min before stimulation with 600 nM PMA was performed for 12 h at 37°C and 5% CO_2. Afterwards, the cells were washed three times with 500 µL/well PBS for 5 min and permeabilized for another 5 min with 500 µL/well ice-cold acetone (Applichem, see Table 2.1) 1:1 methanol (Honeywell, see Table 2.1) at RT. Subsequently, the click chemistry (reagents see Table 2.2) labeling of endogenous RNA was performed in a 24-well plate as described in literature (Presolski, Hong, and Finn 2011). Therefore, in a total volume of 500 µL PBS per well, 2 µL of AF546-azide, a pre-mixture of 1 mM $CuSO_4$ and 1.25 mM THPTA, 5 mM aminoguanidine-hydrochloride, and 5 mM Na-ascorbate were added to the cells. The wells were immediately sealed with plastic foil to ensure proper reaction and subsequently incubated in the dark for 1 h at RT while gently rocking. 5-ethynyluridine untreated cells incubated with complete click chemistry reagents and 5-ethynyluridine treated cells incubated with PBS and AF546-azide only were used as negative controls. Imaging those with the same microscopy settings as the regular click-labeled cells did not yield to significant signals. After the cycloaddition was performed, the cells were washed three times for 5 min with PBS in the dark and counterstained for 2 h at RT in the dark with the anti-rRNA Y10b primary antibody conjugated to AF647 (see Table 2.7) at a dilution of 1:50 in PBS. Afterwards, the cells were washed again three times for 5 min to remove unbound antibody, incubated with Hoechst 33342 (as previously described) to stain nuclear DNA, and mounted as described before. For control reasons, counterstaining with rRNA Y10b antibody was not performed on some samples. Those samples did not differ in the click-labeling derived fluorescence signals. Thus, antibody-counterstaining did not negatively affect the click chemistry labeling signal and imaging. Imaging was performed using a Zeiss LSM800 Confocal microscope with a 63x objective and AiryScan mode (settings see Table 2.12). Subsequent image analysis was performed using ImageJ-Win64 (Table 2.11).

2.3.10 Enzyme-linked Immunosorbent Assay (ELISA)

IL-8 cytokine ELISAs of supernatants of BlaER1, THP-1, N/TERT-1, NHEK, and 3D human skin equivalent were performed by Carsten Greve, a PhD student from AG Weber, Department of Immunology, University of Tübingen. IFN-γ cytokine ELISAs of supernatants of NK-92 MI cells were performed by Pujan Engels, a PhD student from AG Weber, Department of Immunology, University of Tübingen. IL-8, IL-6, and TNF ELISAs of supernatants of PBMCs were performed by Sirui Chen, a former master student from AG Weber, Department of Immunology, University of Tübingen, under my supervision. To measure cytokine release of the above mentioned cells and the 3D human skin equivalent after stimulation with NET content (Mock/PMA NETs +/-RNase inhibitor) and respective controls, ELISA kits for hIL-8, hIL-6, IFN-γ, and TNF (see Table 2.10) were used and assays were performed according to the manufacturer's instructions. Thereby, samples and standards were assessed in triplicates and absorption was measured at 450 nm with a standard plate reader. To safe supernatant and kit materials, half-area 96-well plates (see Table 2.11) were used, and therefore only half of the amounts of reagents and cell culture supernatants described in the manufacturer's instructions were needed.

2.3.11 Leukocyte RNA-ELISA for detection of anti-RNA autoantibodies

To investigate possible anti-RNA autoantibodies in sera of patients suffering from autoimmune diseases, in particular from SLE, a leukocyte RNA-ELISA was established. Hereby, RNA isolated from leukocytes was used as the target antigen, with which ELISA plates were coated with. Afterwards, patient sera and sera of healthy donors (as negative controls) were applied. Patient sera samples used were obtained from the group of Prof. Reinhild Klein, University Hospital Tübingen, and were of known autoantibody (antinuclear antibodies (ANA)) status. If those sera additionally contain autoantibodies directed against (neutrophil) RNA, they should bind to the leukocyte RNA coated onto the plate. Once bound, those anti-RNA antibodies were detected with a second antibody directed against IgG, coupled to HRP, and a subsequent substrate reaction. The detailed steps for this ELISA approach were performed as described below.

Buffy coats were acquired from the Transfusion medicine, University Hospital Tübingen. To get rid of erythrocytes, lysis was performed using 1x ACK (see Table 2.5). Therefore, 5 mL of blood were transferred into a 50 mL Falcon tube (get around 25 mL blood from one buffy coat, all of it was used), and the tube was filled up to 50 mL with 1x ACK. The cells were incubated for 20 min at 4°C on a roller shaker. Subsequently, the tube was centrifuged at 1600 rpm for 10 min and the supernatant was discarded. A second lysis was performed for 10 min at 4°C using 25 mL 1x ACK. After subsequent centrifugation for 5 min, the supernatant was removed and the cell pellet was resuspended in PBS. Around 30 x 10^7 cells were transferred into a 2 mL Eppendorf tube, centrifuged for 5 min, and resuspended in 1 mL TRIzol™ by thoughtfully pipetting the cell pellet up and down and vortexing (Thermo Fisher, see Table 2.1) (of note: around 30 x 10^8 cells were isolated from one buffy coat, all were used for RNA isolation). Afterwards, 200 µL chloroform (Merck, see Table 2.1) were added and the cells were vortexed for 30 sec, followed by 10 min incubation at RT. The suspension was shaken and centrifuged for 20 min at 4°C and 12,000 x g. After centrifugation and thus, separation of RNA and DNA, the upper, aqueous phase containing the RNA was transferred into a fresh tube, whereas the white and pink layer containing cell debris and DNA were left behind. Furthermore, 700 µL ice cold RNase-free isopropanol (VWR, see Table 2.1) were added. For RNA precipitation, the tube was inverted three times and stored at -20°C overnight. The tube was then

centrifuged at 4°C for 60 min at 14,000 rpm and the supernatant was carefully removed, to not disturb the RNA pellet. The RNA was then washed by adding 500 µL 75% ethanol (VWR, see Table 2.1) and 5 min centrifugation at 4°C and 12,000 x g. The washing step was repeated one more time and the RNA pellet was left to dry on ice for 3 h. At last, the RNA was dissolved in 1 mL RNase and DNase-free H_2O, the concentration was determined using a Nanodrop Spectrophotometer, and the RNA was stored at -80°C until the ELISA was performed. As mentioned above, this leukocyte RNA served as the coating antigen.

The RNA ELISA was kindly established and performed by Reinhild Klein and Beate Preuß, Immunopathologic Laboratory, University Hospital Tübingen. At first, the ELISA plates were coated for 1 h at 37°C with 0.05% poly-L-lysine (Sigma, see Table 2.1), followed by three washing steps with PBS. The antigen (RNA) was applied for 1 h at 37°C. For negative controls, wells with only PBS coating after poly-L-lysine treatment were used. The value of each sample hereby obtained was subtracted of the one measured for the respective serum sample of the wells with antigen coating at the end of the experiment (background signal subtraction). Additionally, it was investigated if RNA-stabilization with RNase inhibitor throughout the experiment can enhance the ELISA outcome. Since no differences were observed, RNase inhibitor was not further used. After antigen application, the wells were washed three times with PBS and blocking was performed. Therefore, 0.05 % BSA in PBS was applied for 1 h at 37°C. Subsequently, the serum samples of SLE patients or healthy donors were incubated at 4°C overnight. As a positive control, the rRNA Y10b antibody (see Table 2.7), which should readily bind to any blood cell-derived RNA bound to the plate as antigen, was added instead of serum. Of note, a positive signal of this positive control was achieved for every ELISA approach and used as an internal control for a successful experimental approach. After overnight incubation, the wells were washed three times with PBS + 0.2% Triton and the secondary antibody was added. For the patient/healthy donor samples, an anti-human IgG/HRP (Dianova, see Table 2.7) in a 1:3,000 dilution, and for the positive control (rRNA Y10 b antibody) an anti-mouse IgG/HRP antibody (Agilent, Dako, see Table 2.7) was used in a 1:1,000 dilution. At last, the substrate solution was added, and the OD was measured using a conventional plate reader. The background signal was subtracted of each sample as described above and the data was analyzed using Prism software (GraphPad, see Table 2.11).

2.3.12 Detection of autoantibody-binding to naRNA on resting/NET forming PMNs

To analyze whether autoantibodies contained in patient sera of SLE patients would specifically bind to neutrophil RNA, or even to naRNA, thus indicating that anti-naRNA autoantibodies might exist, patient sera were applied to fixed granulocytes. Thereby, resting and NET-forming neutrophils were used. Patient sera samples used were obtained from the group of Prof. Reinhild Klein, University Hospital Tübingen, and were of known autoantibody (antinuclear antibodies (ANA)) status. Fixed granulocytes were also kindly provided by the group of Prof. Reinhild Klein, University Hospital Tübingen.

In brief, 35 µL serum of SLE patients or healthy donors was added to the respective well containing fixed granulocytes mounted onto a multi-well (12 wells) coverslip in resting state or activated (NET-forming) conditions. Incubation was performed for 20 min at RT in a humidity chamber to prevent the cells from drying out. Subsequently, the cells were briefly rinsed with PBS and washed for 10 min in PBS. Afterwards, 35 µL/well FITC conjugate (BioRad, see Table 2.1) directed against IgG was added and incubation was performed in the dark in a humidity chamber for 20 min at RT. The cells were then rinsed with PBS, washed

as previously described and counterstained for naRNA with the rRNA Y10b antibody. Therefore, the procedure was performed as described in section 2.3.2, starting with the blocking step. After mounting, the cells were stored at 4°C until imaging using a Zeiss LSM800 Confocal microscope (settings see Table 2.12) was performed.

2.3.13 Quantification of autoantibody-binding to naRNA on resting PMNs

To analyze the binding of autoantibodies to whole PMN RNA, thus investigate by immunofluorescence microscopy if the SLE patient sera contain anti-PMN RNA directed autoantibodies, image quantification was performed. Therefore, three images per sample were acquired using a 40x objective and 3x3 tiles acquisition in AiryScan mode (settings see Table 2.12). ImageJ-Win64 software (see Table 2.11) was used for analysis. Regions of interest (ROIs) were analyzed with a ROI manager: size (micron^2): 100-infinity (pixel units) and circularity: 0.00-1.00. Hereby, the anti-rRNA Y10b-AF647 signal was used to define areas of PMN RNA. After defining the RNA ROIs, these ROIs were applied to the autoantibody (IgG)-derived FITC signal, and the overlapping area in percent was investigated. The data was exported and analyzed with Prism software (GraphPad, see Table 2.11).

2.4 *In vivo* experiments

All *in vivo* experiments were kindly performed by, and mice and reagents therefore used provided by Christine Youn, Yu Wang, and Nathan Archer, Department of Dermatology, Johns Hopkins University School of Medicine, Baltimore, USA.

2.4.1 Analysis of naRNA DAMP effects in skin inflammation

To investigate the effect of NETs with or without RNase inhibitors and the respective TLR signaling, 20 µL of NET content (Mock/PMA NETs +/-RNase inhibitor) and the respective controls (RPMI+RNase inhibitor as negative control, ssRNA+LL37 as positive control) were injected intradermally on day 0 into the ears of WT C57BL/6 control mice and *Tlr13*$^{-/-}$ mice lacking RNA-sensing. Afterwards, as a measure of inflammation, the ear thickness was assessed daily using a manual caliper (Peacock, see Table 2.11) until day 4. Data was transferred to and analyzed with Prism software (GraphPad, see Table 2.11).

2.4.2 Fluorescence imaging of neutrophil infiltration after intradermal NET-injection

The *in vivo* experiment for investigation of neutrophil infiltration after intradermal injection of NETs was performed as previously described by our group (Herster et al. 2020). Therefore, LysM$^{EGFP/+}$ mice expressing green fluorescent myeloid cells (Faust et al. 2000) were injected with 20 µL of PMA/Mock NETs with RNase inhibitor and respective controls (RPMI+RNase inhibitor as negative control, ssRNA+LL37 as positive control). LysM$^{EGFP/+}$ mice were subsequently anesthetized by applying isoflurane inhalation and *in vivo* fluorescence imaging was performed using the IVIS Lumina II imaging system (Caliper, see Table 2.11). EGFP fluorescence was measured using excitation at 465 nm, emission at 515–575 nm, and an exposure time of 0.5 s. Data were quantified as total radiant efficiency ([photons/s]/[µW/cm2]) within a circular region of interest using Living Image software (Caliper, see Table 2.11). Subsequently, data was transferred to and analyzed with Prism software (GraphPad, see Table 2.11).

2.4.3 Imiquimod model of psoriatic skin inflammation

To analyze the effect of RNA signaling in a more physiologically relevant setting using an *in vivo* model for psoriasis, the well-established imiquimod (IMQ) mouse model (previously described in section 1.3.3.4) was chosen (Gilliet et al. 2004). Therefore, WT C57BL/6 and *Tlr13*$^{-/-}$ mice, the latter lacking RNA-sensing, were used and 70 µL (62.5 mg) of IMQ (5%, Taro Pharmaceuticals Industries, see Table 2.1) was applied each day to both ears of the mice for 5 consecutive days (day 0 to 4). Ear thickness was daily measured with a manual caliper (Peacock, Tokyo, see Table 2.11) before subsequent IMQ application. Data was transferred to and analyzed with Prism software (GraphPad, see Table 2.11). One day after the last application of IMQ (day 5), full-thickness ear skin was excised with surgical scissors for histologic analysis as described in the following section.

2.4.4 Histologic analysis of mouse ear skin

Since epidermal thickening mediated by excessive keratinocyte proliferation is a hallmark of psoriasis (Benhadou, Mintoff, and Del Marmol 2019), this thickening of the ears of the mice used in the IMQ psoriasis mouse model was investigated. Therefore, ear skin specimens were excised with surgical scissors, afterwards fixed in 10% formalin, and finally embedded in paraffin. The embedded ears were then cut in 4 µm thick sections and mounted onto glass slides. The skin samples were further stained with H&E by the Johns Hopkins Reference Histology Laboratory. At last, 100 epidermal thickness measurements per mouse were performed and averaged from images taken at 200x magnification (Hamamatsu Nanozoomer) using ImageJ-Win64 software to assess epidermal thickening (see Table 2.11). Data was subsequently transferred to and analyzed with Prism software (GraphPad, see Table 2.11).

2.5 Data analysis and statistics

All experimental data acquired in this study were analyzed using Excel 2019 (Microsoft) and/or GraphPad Prism 8 software (see Table 2.11). Microscopy data were processed using ImageJ-Win64 or ZenBlue3 software (see Table 2.11), as stated above. Flow cytometry data to assess PMN purity were processed with FlowJo V10 (see Table 2.11). Statistical analysis was performed using GraphPad Prism 8 software (see Table 2.11). Therefore, normal distribution in each group was tested first using the Shapiro–Wilk test. Depending on the distribution of the assay, the subsequent choice of a parametric (ANOVA, Student's t-test for normally distributed data) or non-parametric (Mann–Whitney U) test was made, as indicated in the figure legends. P-values ($\alpha = 0.05$) were subsequently calculated. Hereby, values of $p < 0.05$ were generally considered statistically as significant and denoted by * throughout this study, even if considerably lower than 0.05. The comparisons were always made to unstimulated controls, unless indicated otherwise, as denoted by respective brackets and lines.

3 Results

3.1 naRNA is a highly abundant and canonical NET-component

Previous work of our group first observed NET-associated RNA, short naRNA, as an until then unknown NET component (Herster et al. 2020) besides well investigated constituents like chromatin, and antimicrobial and granule proteins (Brinkmann et al. 2004). Thus, little was known about the characteristics of naRNA at the start of this project: it was unknown, whether naRNA is released in suicidal and vital NET formation, as well as if naRNA-release is stimulus-dependent and what types of RNA naRNA is composed of.

3.1.1 naRNA is released independent of the stimulus and type of NET formation

It was described that, depending on the stimulus used, NET formation can either be a suicidal process, leading to the death of the neutrophil, or it may represent a vital process, leaving an anucleated but functional cell behind (Boeltz et al. 2019; Tan, Aziz, and Wang 2021). Whether the underlying process affects the release of naRNA was investigated first.

Whenever an experiment with primary human neutrophils was performed in this study, neutrophils were isolated as previously described and FACS analysis was run to ensure purity and non-pre-activated status of the cells. Hereby, $CD15^{+}CD66b^{+}CD14^{-}$ cells were considered as neutrophils. In the depicted example, 97.2% of cells were $CD15^{+}CD66b^{+}$ and 96.9% were $CD14^{-}CD66b^{+}$ (Fig. 3.1A), meaning around 97% of the isolated cells were indeed neutrophils. For all experiments performed in this study, a purity of >95% was achieved. Investigation of CD62L shedding, a sensitive and early activation marker of PMNs (Simon et al. 1995), was additionally performed. A shift of the CD62L peak towards the left-hand side would represent a loss of this surface marker from the respective cells, indicating a pre-activation of the neutrophils. This was not observed in the representative example (Fig. 3.1B) and only neutrophils which did not show pre-activation were used throughout this study.

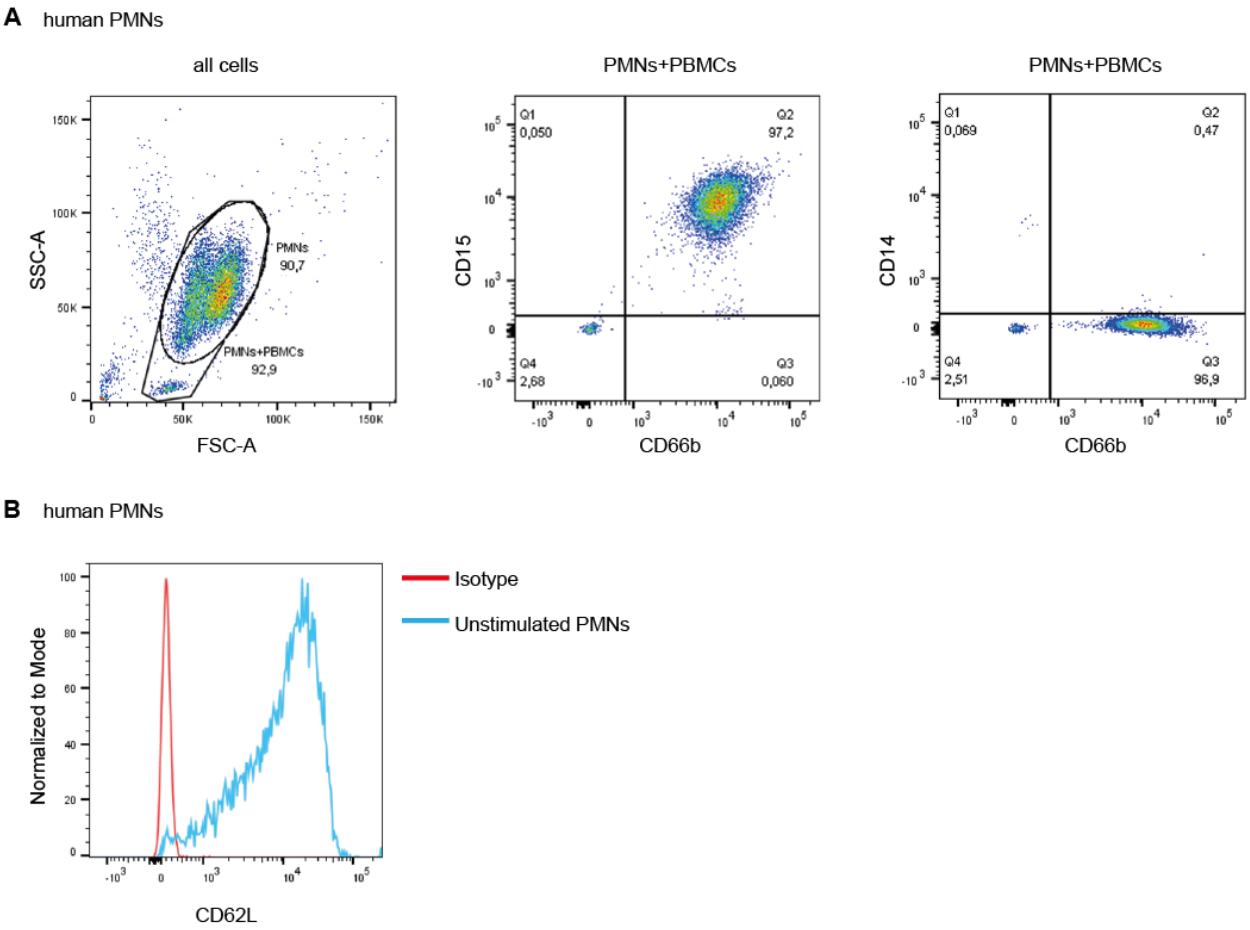

Figure 3.1: FACS analysis of human PMNs.

Primary human PMNs were stained with anti-CD66b (FITC) + anti-CD15 (PE) + anti-CD62L (BV421), or anti-CD66b (FITC) + anti-CD14 (PE), or FITC- + PE- + BV421-isotype control antibodies against surface antigens. **(A)** Gating strategy shown. $CD66b^{+}CD15^{+}CD14^{-}$ cells were considered as PMNs. A purity of >95% of cells was achieved for all experiments (representative example for one donor shown). **(B)** Histogram of CD62L analysis shown. Unstimulated PMNs do not show activation (no CD62L-shedding; representative example for one donor shown).

Human PMNs were then stimulated with the well-known and commonly used NET-inducing phorbol ester, PMA, which mediates a suicidal and ROS-dependent NET formation (Kenny et al. 2017), as a positive control. In addition, neutrophils were stimulated for 3 h with nigericin (suicidal NET formation (Kenny et al. 2017)), the live pathogen *C. albicans* (vital NET formation (Kenny et al. 2017)), and different complexes of LL37 with purified RNA (synthetic RNA (ssRNA), *S. aureus*-derived bacterial RNA (bRNA), and *C. albicans*-derived fungal RNA (fRNA)), similar to Herster et al. (Herster et al. 2020). Confocal microscopy of NETs was performed after staining with Hoechst 33342 for nuclear DNA and the well-characterized RNA-specific antibody rRNA Y10b (Lerner et al. 1981). To avoid unspecific binding of the secondary antibody, thorough blocking with serum derived from the same species as the secondary antibody (in this case chicken) was essential. Additionally, the blocking buffer was used during all incubation steps with the respective antibodies and RNase contamination was prevented by using an RNase inhibitor throughout the staining process. Furthermore, negative staining controls using the secondary antibody only were run and no

significant signals were observed. The IF microscopy revealed naRNA staining (magenta) in all NETs induced by the indicated stimuli, speckled on the DNA NET-backbone (white; Fig. 3.2A). Thus, naRNA appears to be a common component of NETs, released independent of the respective stimulus used and the NET-formation pathway thereby induced. Quantification of the RNA and DNA signals was performed using NET-related signal dispersion. Specifically, it was observed that during NET formation, when the nucleic acids are released, the DNA and RNA-derived signals showed up in smaller average size, but greater amounts compared when stained for in intact cells. Therefore, a ratio of the number of signals counted by the regions of interest (ROIs) defined with ImageJ-Win64 software and the average size of those ROIs can describe a NET-related signal dispersion. This signal dispersion provides an objective quantification of nucleic acid-release during NET formation using both, the RNA and DNA signals. The quantification showed that naRNA can be found in high abundance alongside of DNA in all forms of NETs (Fig. 3.2B).

In a next approach it was investigated whether naRNA is not only a component of human NETs but can be further found in extracellular traps released by murine neutrophils. Thus, BM-PMNs of C57BL/6 WT mice were isolated and stimulated for 16 h with PMA, nigericin, live *C. albicans*, and synthetic RNA-LL37 complex, respectively. Staining for DNA and naRNA as described above revealed the presence of naRNA in all murine NETs (magenta), which was observed to be stimulus-independent (Fig. 3.2C), just as discovered for human neutrophils (*cf.* Fig. 3.2A, B). These findings indicate that naRNA is a preserved NET component, independent of the species, and enables the usage of murine BM-PMNs for further investigation of the characteristics of naRNA.

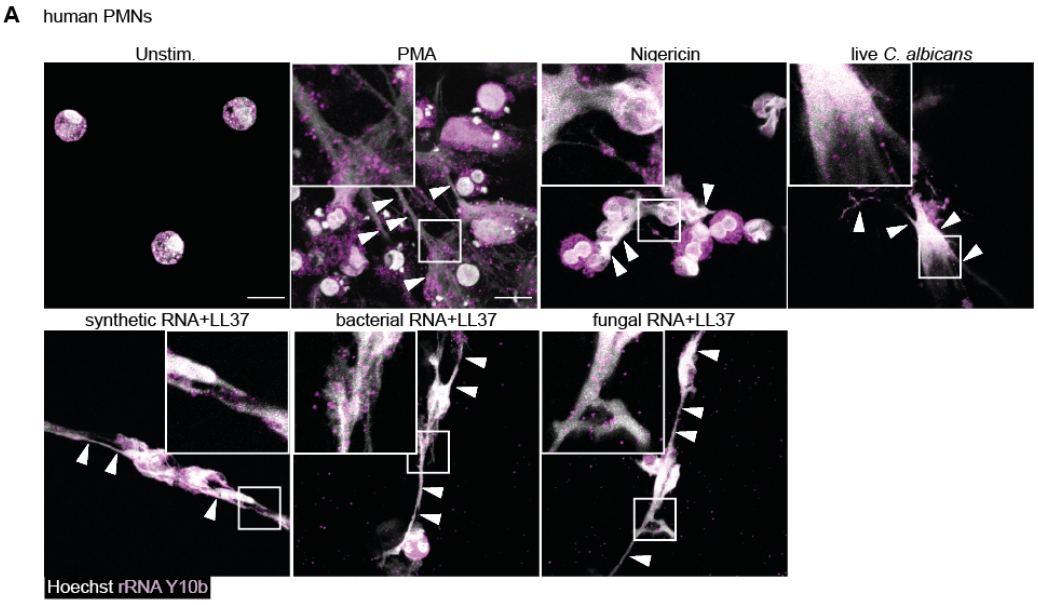
A
human PMNs
Unstim.
PMA
Nigericin
live C. albicans
synthetic RNA+LL37
bacterial RNA+LL37
fungal RNA+LL37
Hoechst rRNA Y10b

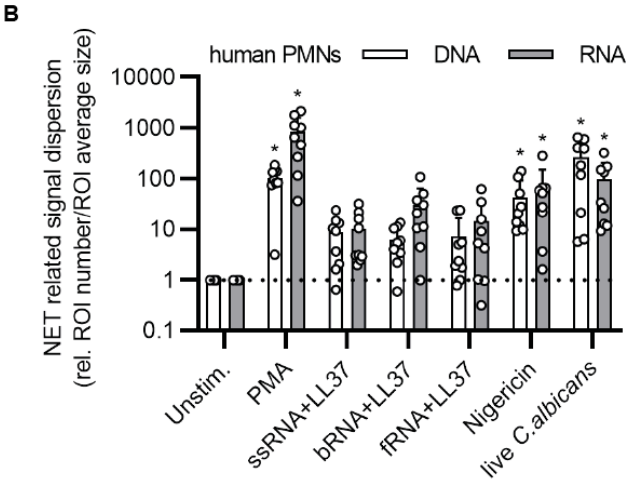
B
human PMNs
DNA
RNA
NET related signal dispersion
(rel. ROI number/ROI average size)
10000
1000
100
10
1
0.1
Unstim.
PMA
ssRNA+LL37
bRNA+LL37
fRNA+LL37
Nigericin
live C.albicans

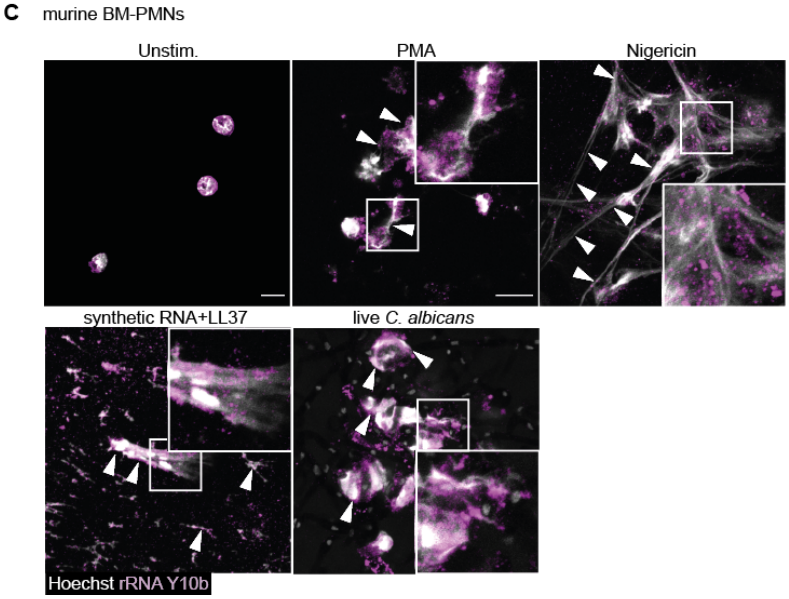
C
murine BM-PMNs
Unstim.
PMA
Nigericin
synthetic RNA+LL37
live C. albicans
Hoechst rRNA Y10b

Figure 3.2: naRNA is an abundant and common component of human and murine NETs.

(A, B) Confocal microscopy of primary human PMNs unstimulated (negative, resting control) or stimulated with PMA (600 nM), RNA+LL37 complex, nigericin (50 µM), or live *C. albicans* (MOI 2) for 3 h and stained for naRNA (anti-rRNA Y10b, magenta) and DNA (Hoechst 33342, white, n = 3, scale bar: 10 µm, arrowheads point to selected NET strands; representative images in **A**) were quantified in **B** (each dot represents one image (3 images/biological replicate), *p<0.05 according to one-way ANOVA). **(C)** Confocal microscopy of primary murine BM-PMNs of C57BL/6 WT mice unstimulated (negative, resting control) or stimulated with PMA (600 nM), ssRNA+LL37 complex, nigericin (50 µM), or live *C. albicans* (MOI 1) for 16 h and stained as in **A** (n = 3, representative images, scale bar: 10 µm).

3.1.2 Antibody-independent click chemistry labeling of naRNA validates its presence

Unspecific binding of antibodies to leukocytes due to their high amount of Fc receptors is a common issue encountered in immunofluorescence analysis of neutrophils (Hulspas et al. 2009). The precautions taken above excluded this concern, but to validate the presence of naRNA in NETs by another antibody-independent method, metabolic and subsequent click chemistry labeling was used. Metabolic labeling of endogenous RNA can be achieved with 5-ethynyluridine (5-EU), a nucleotide which is incorporated into RNA but not DNA (Darzynkiewicz et al. 2011), and which is amenable to subsequent click chemistry (a copper-catalyzed cycloaddition reaction connects azides (in this study the fluorescent label AF546-azide) to alkynes (here 5-ethynyluridine) (Presolski, Hong, and Finn 2011)). For efficient labeling, cells need to be cultured for several hours but blood-derived neutrophils are short-lived and should be used for experiments within 2 – 4 hours after isolation (Oh, Siano, and Diamond 2008). Metabolic labeling was therefore performed on human stem cell-derived neutrophils, differentiated *in vitro* from $CD34^+$ hematopoietic stem cells as described (Sioud 2020). In brief, bone marrow of healthy humans was used and $CD34^+$ cells were isolated using magnetic bead separation. Subsequently, the cells were differentiated using cytokines and growth factors (IL-3, IL-6, TPO, SCF, FLT-3L). For additional metabolic labeling, the cells were fed for 14 days with 5-EU during the differentiation process or left untreated as a negative control. The differentiation of the stem cell-derived neutrophils was first validated by Cytospin™ brightfield microscopy. Hereby, the characteristically segmented nucleus of neutrophils was used as a maker to identify successfully differentiated cells. It was observed that differentiation in all three experiments was successful and treatment with 5-EU did not affect it (Fig. 3.3A; of note: in experiment 2, Cytospin™ analysis was not performed for 5-EU treated cells). To investigate the differentiation by flow cytometry analysis, markers for myeloblasts, myelocytes, metamyelocytes, and neutrophils were used (CD45 (leukocyte marker), CD34 (HSPC marker), CD33 (promyelocyte marker), CD11b (myeloid cell marker), CD14 (monocyte marker), and CD15 and CD16 (neutrophil markers)). Percentage of fully differentiated neutrophils was determined by gating for $CD45^+CD11b^+CD15^+$, or $CD45^+CD11b^+CD16^+$, or $CD45^+CD15^+CD16^+$ cells. As observed by Cytospin™ analysis, no significant differences between cells treated with 5-EU and cells left untreated during differentiation could be detected (Fig. 3.3B). Thus, the differentiation of neutrophils was considered successful, and 5-EU metabolic labeling did not lead to adverse effects.

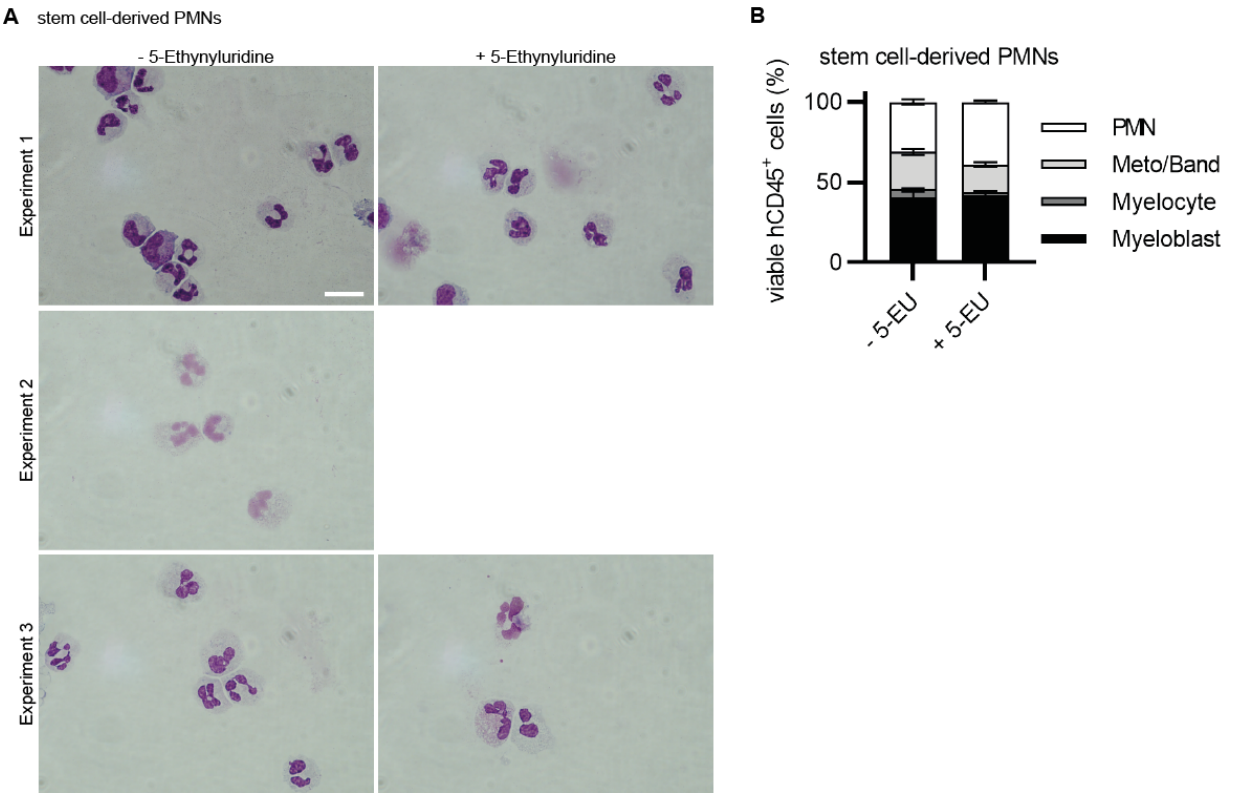

Figure 3.3: Validation of differentiation of stem cell-derived neutrophils.

(A) Brightfield microscopy analysis of cytospun control primary human stem cell-derived PMNs differentiated *in vitro* with/without 100 µM 5-Ethynyluridine (5-EU, n = 3, representative images, scale bar: 20 µm). **(B)** FACS analysis for cells shown in **A** (n=3, representative data). Differentiation of stem cells into neutrophils and 5-EU treatment, as well as subsequent validation was performed by Masoud Nasri, AG Skokowa, Division of Translational Oncology, Department of Oncology, Hematology, Clinical Immunology and Rheumatology, University Hospital Tübingen.

For NET formation assay and antibody-independent labeling of naRNA, the stem cell-derived neutrophils were stimulated with PMA for 12 h. Compared to mature peripheral blood neutrophils, these cells were observed to only form NETs after longer incubation with the respective stimulus in pilot experiments. Having established these conditions, subsequent click chemistry labeling was performed, as well as counterstaining with the previously used antibody for rRNA (anti-rRNA Y10b-AF647). Confocal microscopy analysis revealed that NETs formed by PMA-stimulated neutrophils treated with the 5-EU-alkyne were successfully stained for endogenous RNA released by those cells. This staining was achieved with the AF647-azide in a copper-catalyzed reaction as described in methods, thereby confirming the afore described findings of naRNA being an abundant NET component (5-EU metabolically labeled naRNA depicted in yellow, rRNA Y10b antibody-stained naRNA depicted in magenta, Fig. 3.4). The specificity of the antibody used (*cf.* Fig. 3.2) was further validated by the overlap of the click-labeled and antibody-labeled naRNA signals (Fig. 3.4). Since the antibody used throughout this study stains ribosomal RNA, but the click chemistry labeling used here stains the whole endogenous RNA, this overlapped staining further indicated that naRNA consists of rRNA but also of other types of cellular RNAs.

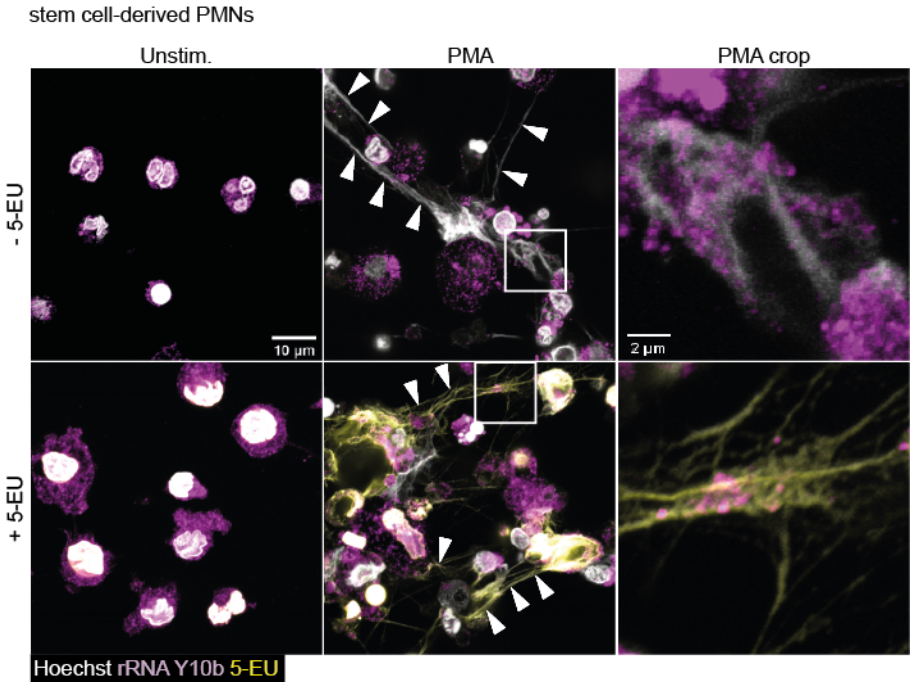

Figure 3.4: Metabolic labeling of naRNA in NETs of stem cell-derived neutrophils.

Confocal microscopy of primary human stem cells differentiated *in vitro* with/without 100 µM 5-ethynyluridine (5-EU, alkyne), incubated with 600 nM PMA for 12 h for NET formation or left unstimulated as negative controls, click-labeled with a AF647-azide (yellow, total RNA), and antibody-labeled for rRNA (anti-rRNA Y10b, magenta), as well as stained for DNA (Hoechst 33342, white; n = 3, representative images, scale bar: 10 µm, 2 µm in cropped image). Differentiation of stem cells into neutrophils and 5-EU treatment was performed by Masoud Nasri, AG Skokowa, Division of Translational Oncology, Department of Oncology, Hematology, Clinical Immunology and Rheumatology, University Hospital Tübingen.

3.1.3 Confirmation of naRNA in NET-fibers by high resolution imaging

High resolution imaging is a popular method for in-depth characterization of the composition and morphology of cellular structures, such as NETs (Isles et al. 2021). It was hence used in this study to further prove and visualize the existence of naRNA. Therefore, primary human PMNs were used, and PMA-induced NETs were stained as previously described. High resolution fluorescence microscopy and subsequent 3D analysis was performed using a confocal Microscope (Zeiss, LSM800) in AiryScan mode. Thereby, AiryScan imaging improves resolution and signal-to-noise simultaneously by the detector used in this setting, composed of a 32-channel array. The high resolution imaging is achieved since every channel functions as a very small pinhole compared to traditional systems (Huff et al. 2017). DNA fibers stained with Hoechst 33342 were observed to be 'speckled' with naRNA, stained with anti-rRNA Y10b antibody (Fig. 3.5A and Supplemental Movie S1). Thus, the high-resolution microscopy analysis and 3D reconstruction confirmed the previous findings of naRNA commonly decorating the characteristic DNA fibers of NETs (*cf.* Fig. 3.2)

By achieving a resolution roughly 100 times higher than light microscopy, electron microscopy (EM) can uncover the presence of the tiniest particles or structures (Wolff and Barcena 2021), therefore providing another popular method of choice for proof of existence of naRNA in this study. Therefore, neutrophils isolated of human healthy donors were used and samples of PMA-induced NETs were prepared as previously described. After stimulation of PMNs for 3 h with 1200 nM PMA, to ensure a broad coverage of the coverslip by NETs and thus simplify the imaging, scanning electron microscopy (SEM) was performed. SEM showed NETs as a mesh of fibers, which are easily interpreted as their DNA backbone (Doring, Libby, and Soehnlein 2020). To unequivocally reveal the presence of naRNA on those DNA fibers, immunogold labeling was used. Therefore, staining with anti-rRNA Y10b primary antibody, subsequent immunogold-labeling with the respective secondary antibody, and silver enhancement was performed. Secondary antibody controls only did not lead to significant signals (Fig. 5.1). This staining allowed the identification of naRNA in SEM microscopy, visualized by the bright appearing gold-particles (Fig. 3.3B, white arrows point to examples). Thus, SEM analysis was successfully used to further validate the presence of naRNA in NETs by high resolution imaging.

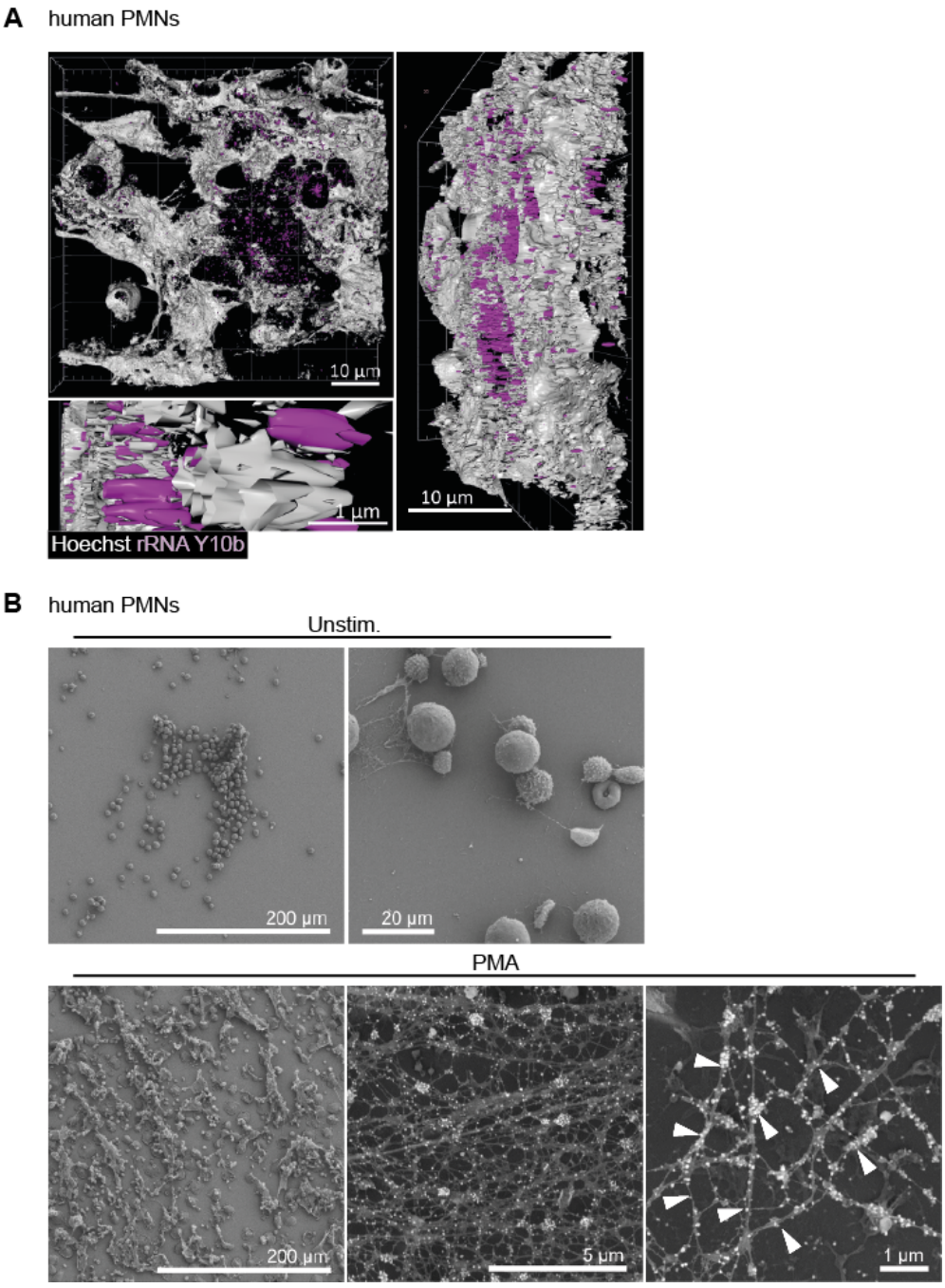

Figure 3.5: High resolution imaging of NETs proves existence of naRNA.

(A) 3D image reconstruction of z-stacks of confocal microscopy of primary human PMNs stimulated with 600 nM PMA for 3 h and stained for naRNA (anti-rRNA Y10b, magenta) and DNA (Hoechst 33342, white; n = 3, representative images, scale bar as indicated). **(B)** Scanning electron microscopy of human primary PMNs left unstimulated (negative control) or incubated with PMA (1200 nM) for 3 h and using anti-rRNA Y10b primary and immunogold (white arrow)-labeled secondary antibodies and silver enhancement (n = 3, representative images, scale bars as indicated; the two rightmost images of PMA-treated PMNs show composite images with signals from secondary electron and backscattered electron detectors for topography and additional material information, respectively). Electron microscopy was kindly performed by the group of Katharina Hipp, Electron Microscopy Facility, Max Planck Institute for Biology Tübingen.

3.1.4 naRNA consists of different types of RNA

Although Herster et al. (Herster et al. 2020) described the existence of naRNA in NETs, little was known about the exact composition of naRNA. Therefore, isolation of RNA from untreated neutrophils directly lysed in purification buffer (Mock control) and of naRNA harvested extracellularly from PMA-induced NETs from healthy donor neutrophils was performed as previously described. Significant amounts of almost 60 ng/µL naRNA could be thereby isolated from PMA-induced NETs (Fig. 3.6A). Besides the above-described microscopic proof of the existence of naRNA (*cf.* Fig. 3.2, 3.4, 3.5), these findings further validate its presence. To gain an insight into the composition of naRNA, RNA sequencing was performed. Annotation of reads to distinct RNA types revealed naRNA to vary from whole PMN RNA. It was observed that naRNA is composed of various types of RNA, such as mRNA, ncRNA, pseudogenes, nonsense mediated decay, alternatively spliced transcripts, and rRNA (Fig. 3.6B). However, the latter is clearly the main component of whole PMN RNA (Fig. 3.6B), which therefore differs in its composition in comparison to naRNA. This finding indicates that naRNA could be released as a canonical component of NETs, which could get specifically synthesized for its extrusion.

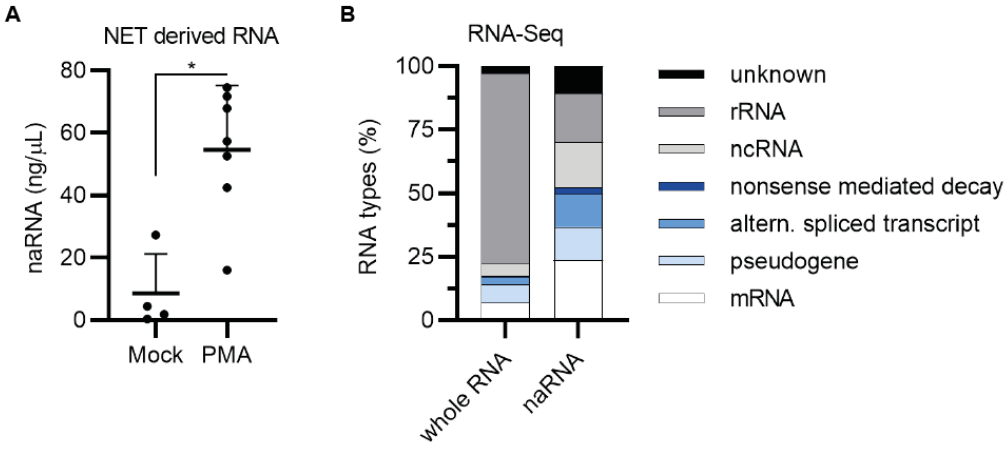

Figure 3.6: naRNA consists of different types of RNA.

(A) Agilent TapeStation quantification of naRNA isolated from Mock or PMA (600 nM) NETs of PMNs incubated for 4 h (from n = 4-6 donors, combined data, mean+SD, each dot represents one biological replicate/donor, *p<0.05 according to Mann-Whitney test). **(B)** RNAseq of PMA NET (600 nM, 4 h incubation) naRNA (n = 4) and whole PMN RNA (n = 1) (combined data). Data analysis of RNAseq results was performed with the help of Marissa Dubbelaar, Department of Immunology/Quantitative Biology Center (QbiC), University of Tübingen.

Taken together, this data provides a comprehensive proof of the existence of naRNA in NETs released upon incubation with various stimuli and independent of the NET formation pathway, based on complementary well-validated methods. As little is known about the function of naRNA to date, its effect on immune cells was investigated next.

3.2 NET formation in primary PMNs is propagated by naRNA, a potent DAMP

3.2.1 naRNA does not play a crucial role in the antibacterial properties of NETs

NETs were originally described by Brinkmann et al. in 2004 as a third host defense mechanism of neutrophils for protection against invading pathogens: it was observed that digestion of NETs with DNase I, thereby removing the DNA from the extracellular fibers, leads to impaired bacterial killing (Brinkmann et al. 2004). It was therefore examined in this study whether naRNA is a crucial component for the antimicrobial effects of NETs. During or after NET formation, respectively, PMA-induced NETs were treated with DNase I (control) or RNase A, to investigate the contribution of RNA to the described antibacterial effect. The extracellular traps-releasing cells were afterwards incubated with live *Staphylococcus aureus* as described (Brinkmann et al. 2004). Bacterial killing was assessed as the percentage of colony forming units (CFUs) of bacteria compared to CFUs formed in the presence of resting PMNs (normalized to 100%). DNA digestions during and after NET formation did not lead to a significant reduction of bacterial killing as evidenced by similar amounts of CFUs (Fig. 3.7). Moreover, no significant differences regarding the bactericidal properties of RNase A-treated PMNs and NETs compared to untreated were observed (Fig. 3.7). Thus, in contrast to the expected reduction of bacterial killing after DNase treatment as described (Brinkmann et al. 2004) and as assumed for RNase A incubation, digestion of the nucleic acid components of NETs did not impair their antimicrobial properties towards *S. aureus*. This indicates that naRNA is dispensable for bacterial killing of NETs.

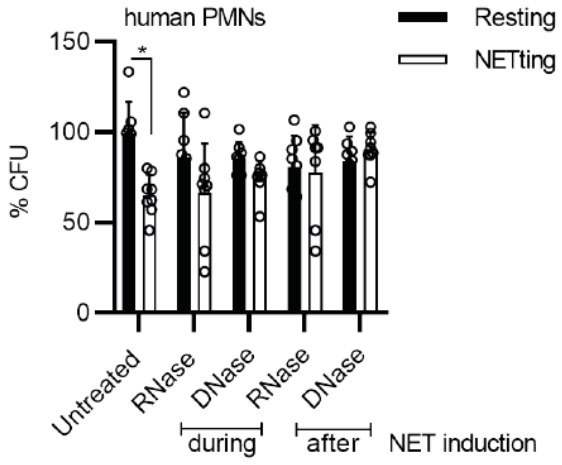

Figure 3.7: naRNA has no antibacterial properties on *Staphylococcus aureus*.

Extracellular bactericidal activity of human PMNs/NETs (600 nM PMA, 2 h) after infection with *S. aureus* (30 min) and treatment with 100 µg/mL RNase A and 1 U/10 µL DNase I during or after formation of PMA-induced NETs (n = 8, combined data, mean+SD, *p<0.05 according to one-way ANOVA). This assay was kindly performed by Jule Focken, AG Schittek, Division of Dermatooncology, Department of Dermatology, University Hospital Tübingen.

Given the fact that neutrophils readily exert pro-inflammatory responses upon stimulation with RNA-LL37 complexes and that both of these complex components are contained in NETs (Herster et al. 2020), as well as noting the aforementioned immune modulating properties of exRNAs (Quinn et al. 2015; Kim et

al. 2017; Happel, Ganguly, and Tagle 2020), it was rather focused on the possible roles of naRNA as a self-derived DAMP than on its properties in host defense for the further continuation of this study.

3.2.2 naRNA is the main driver of self-propagation of NETs

Instead of having antimicrobial properties, we considered that naRNA could be a potential driver of NET-induced inflammation. Therefore, NETs were isolated of PMA-treated neutrophils as previously described and depicted below (Fig. 3.8A). Those NETs were then used as a stimulus and their properties on other immune cells were investigated, starting with naïve neutrophils.

When adding NETs in different dilutions to freshly isolated $CD62L^+$ PMNs, it was observed that PMA-induced NETs readily induce NET formation in naïve PMNs at 1:50 dilution, as evidenced by fluorescence microscopy. Therefore, PMNs/NETs were stained with Hoechst 33342 for nuclear DNA and DNA fibers were used to identify NETs. The effect of NET-induced self-amplification could be enhanced by preserving naRNA through the addition of an RNase inhibitor during and after the formation and isolation process of NETs as a stimulus. In line with this observation, only NETs with RNase inhibitor-stabilized naRNA were still able to induce NET formation in naïve PMNs at higher dilutions (1:500) (Fig. 3.8B). Quantification of the dispersion of the DNA signal as a measure of NET formation (see section 2.2.3) revealed a significant difference in the stimulatory properties of naRNA-protected NETs (PMA NETs+RNase inhibitor) compared to regular PMA NETs, which was similar to the positive control PMA (Fig. 3.8C). Since no NET formation was induced for Mock NETs+RNase inhibitor, it can be ruled out that the observed stimulatory effects are artefacts caused by the RNase inhibitor (Fig. 3.8B, C). It was furthermore excluded that the stimulatory effects observed in Fig. 3.8B were caused by residual PMA (left from the stimulation during creation of NETs as a stimulus) by digesting naRNA in NETs with RNase A. PMA NETs were incubated with RNase A for 30 min before adding them as a stimulus to naïve neutrophils. Granula were stained somewhat more strongly, a finding indicating PMN activation and requiring further investigation, but clearly the NET-inducing properties of PMA NETs were completely abolished by RNase digestion (Fig. 3.8D, quantification in E). The successful degradation of naRNA in NETs by RNase A was additionally confirmed by live cell imaging. Here, NETs were stained with the RNA-selective dye SYTO RNAselect and time-lapse digestion analysis was performed, using a confocal microscope. Therefore, PMNs were pre-treated with PMA for 3 h before imaging, and the NET-forming cells were then placed in a heated incubation chamber of the microscope. Imaging was started and RNase A was added between time point 0 and 5 min. It was hereby observed that treatment of NETs with RNase A led indeed to the loss of the SYTO RNAselect signal, confirming efficient RNA digest under these conditions (Supplemental movie S2). Taken together, naRNA mediates self-amplifying properties of NETs and this data highlights the crucial function of naRNA in driving NET formation. Hence, naRNA rather acts as a host-derived DAMP with no antibacterial properties (*cf.* Fig. 3.7).

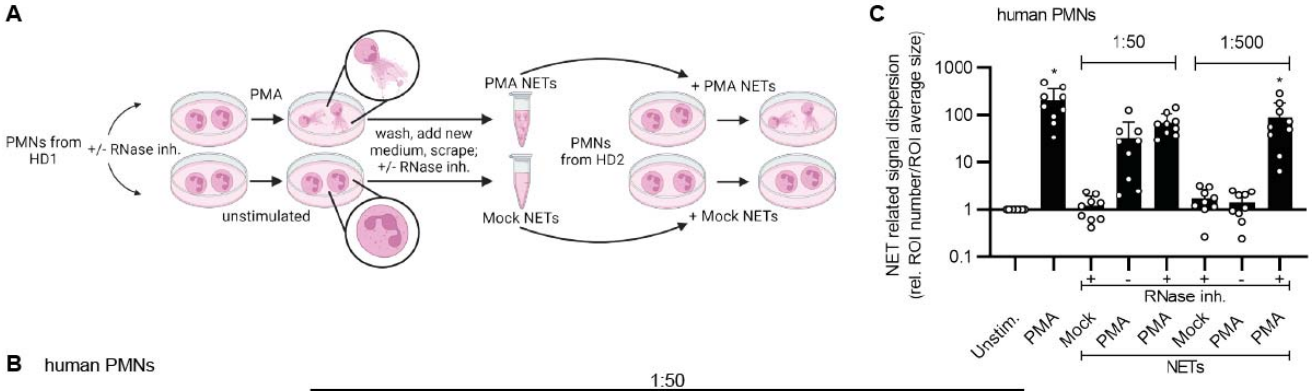
A
PMNs from HD1
+/- RNase inh.
PMA
unstimulated
wash, add new medium, scrape; +/- RNase inh.
PMA NETs
Mock NETs
PMNs from HD2
+ PMA NETs
+ Mock NETs
C
human PMNs
1:50
1:500
NET related signal dispersion (rel. ROI number/ROI average size)
1000
100
10
1
0.1
RNase inh.
Unstim.
PMA
Mock
PMA
PMA
Mock
PMA
PMA
NETs

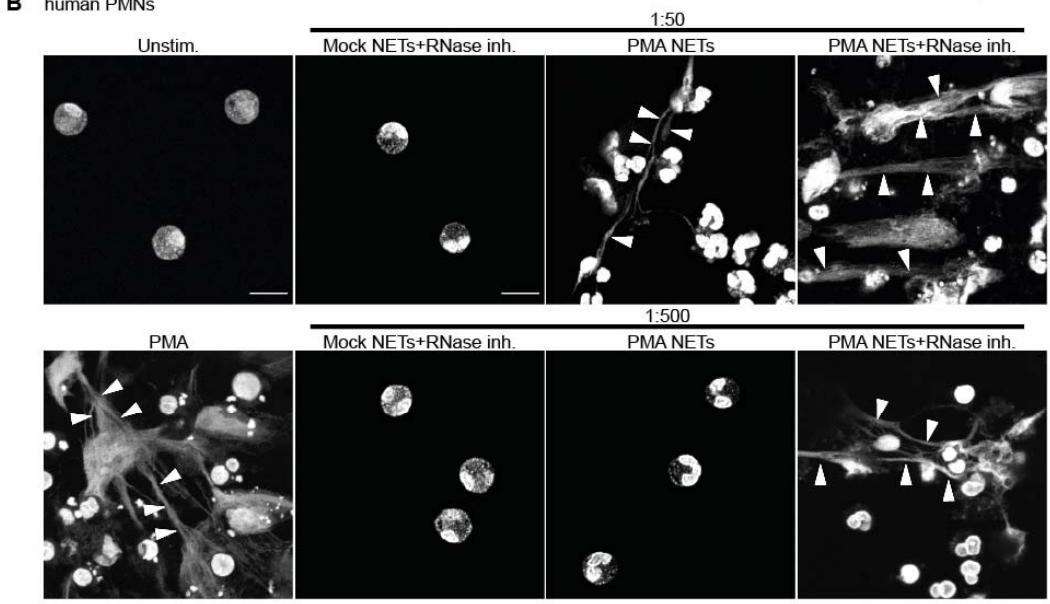
B
human PMNs
1:50
Unstim.
Mock NETs+RNase inh.
PMA NETs
PMA NETs+RNase inh.
1:500
PMA
Mock NETs+RNase inh.
PMA NETs
PMA NETs+RNase inh.

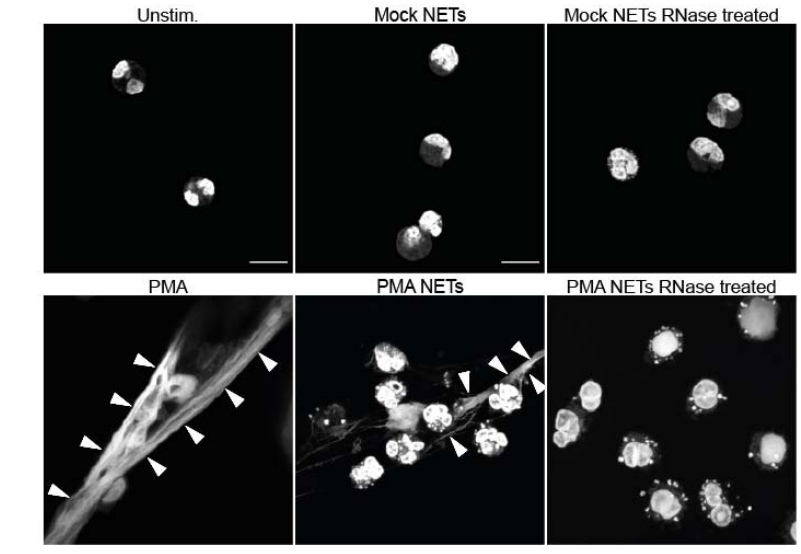
D
human PMNs
Unstim.
Mock NETs
Mock NETs RNase treated
PMA
PMA NETs
PMA NETs RNase treated

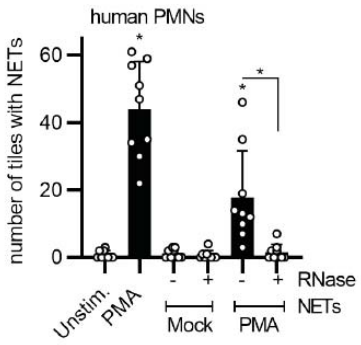
E
human PMNs
number of tiles with NETs
60
40
20
0
RNase
NETs
Unstim.
PMA
Mock
PMA

Figure 3.8: naRNA is the main driver of self-propagation of NETs.

(A) Workflow for NET content preparation from one donor and transfer to naïve human primary PMNs from a second donor. PMNs are seeded into an uncoated petri dish and stimulated with 600 nM PMA for 4 h. Subsequently, cells are carefully washed three times with 5 mL PBS. Only NET-forming PMNs adhere to the uncoated dish and unstimulated PMNs will be washed away during this step, as well as residual PMA and cytokines/chemokines released to the supernatant by activated PMNs. Afterwards, fresh medium is added to the dish and NETs are scraped from the plate and transferred into a new tube. NET content is stored at -80°C until stimulation of naïve PMNs. Where indicated, RNase inhibitor (10 U/µL) is added for naRNA protection during the 4 h stimulation and for storage. **(B)** Confocal microscopy of primary human PMNs left unstimulated (negative control) or stimulated with PMA (600 nM, positive control) or NET content (Mock/PMA, 3 h) harvested with/without RNase inhibitor and diluted 1:50 or 1:500, and then stained for NETs/DNA (Hoechst 33342, n = 9, representative images, scale bar: 10 µm). **(C)** Quantification of **B** using DNA (Hoechst 33342) signal to quantify NET formation (n = 3, combined data, mean+SD, each dot represents one image, *p<0.05 according to one-way ANOVA). **(D)** as in **B** but with/without pre-digestion of NET content (added at 1:100 dilution, 3 h) with 100 µg/mL RNase A for 30 min (n = 3, representative images, scale bar: 10 µm). **(E)** Quantification of **D** as in **C** (n = 3, combined data, mean+SD, each dot represents the number of NET-positive tiles in one image quantified from three images/condition, *p<0.05 according to one-way ANOVA).

3.3 Human TLR8 and murine Tlr13 are the DAMP-receptors sensing naRNA

3.3.1 NETs readily induce TLR8-sensing and self-amplification in a TLR8/Tlr13-dependent manner

To investigate the RNA receptors involved in NET sensing and thereby validate naRNA as the immunostimulatory component of NETs, HEK293T cells were first used. It was previously reported in literature that HEK293T cells do not respond to RNA-stimuli, except upon transfection with human TLR7 or TLR8-encoding plasmids (Colak et al. 2014). Of note, NETs were shown to activate TLR9 in DCs, indicating NET-associated DNA to be an immunomodulatory component of NETs (Garcia-Romo et al. 2011; Lande et al. 2011). Therefore, not only plasmids encoding the RNA-sensing endosomal TLRs (TLR7 and TLR8) were transfected, but furthermore a TLR9-encoding one, mediating expression of this DNA sensor. To assess TLR activation, HEK293T cells were further transfected with plasmids containing a *Renilla* luciferase coding sequence (CDS) under a control promoter and a plasmid of firefly luciferase under the control of a EF-1α promoter. Once a TLR is activated leading to downstream NF-κB expression, transcription leads to firefly luciferase mRNA expression and subsequent translation and release of the protein. The substrate turnover is measured in a plate reader and the signal is quenched by a second substrate, which in turn activates the *Renilla* luciferase reaction in parallel. The *Renilla* luminescence serves as the control reporter signal and is used to normalize the firefly experimental signal (see methods for details) (McNabb, Reed, and Marciniak 2005). After transfection, HEK293T cells were incubated with R848 (TLR7/8 ligand), TL8 (TLR8 ligand), and CpG+DOTAP (TLR9 ligand) for 24 h as controls, confirming the activation of the respective TLRs they were supposed to stimulate, as measured by NF-κB reporter activity (Fig. 3.9A). In addition, transfected HEK293T cells were stimulated with the Mock control (RNase inhibitor treated Mock NETs) or PMA NETs. Interestingly, TLR8-transfected cells reacted with considerably high NF-κB expression measured in relative light units (RLUs) of firefly luciferase signal (~30 RLUs) upon stimulation with PMA NETs, whereas TLR7 and TLR9-transfected cells only reached approximately the half of RLUs. Treatment with Mock NETs+RNase inhibitor as a negative control did not show any response. Upon using

PMA NETs with stabilized naRNA (PMA NETs+RNase inhibitor) for stimulation, TLR8-transfected HEK293T cells showed a significant activation, whereas TLR7-transfected cells only showed a slight increase. Both signals were significantly higher than the induction observed in TLR9-transfected cells incubated with this stimulus (Fig. 3.9A). It can therefore be concluded that the human RNA-sensing TLR8 is a key receptor which gets switched on upon stimulation with NETs, thereby emphasizing the crucial role of naRNA in the immunostimulatory effect of NETs.

To validate this finding more specifically for neutrophil sensing, primary human PMNs were used and incubated with the TLR8 inhibitor CU-CPT9a, which restricts TLR8-activation through stabilizing the receptor in its resting state (Zhang et al. 2018). NET release was assessed in the presence or absence of CU-CPT9a, which was added to the PMNs where indicated 30 min before stimulation with PMA (positive control), ssRNA-LL37 complex (TLR8 control (Herster et al. 2020)), and NET content. Neutrophils treated with CU-CPT9a did not release NETs upon stimulation with PMA NETs (1:100 dilution) or ssRNA-LL37 complexes. Of note, CU-CPT9a did not restrict NET formation in general as PMNs treated with the inhibitor but stimulated with PMA readily released extracellular traps (Fig. 3.9B, quantification Fig. 3.9D), confirming the TLR8-specific inhibitory properties of CU-CPT9a. These observations highlight the important role of TLR8-signaling in primary human PMNs in the context of self-amplification of NETs. In addition, the PAD4-inhibitor Cl-amidine was compared. This compound was reported to irreversibly inhibit PAD4 by covalently binding to the bioactive form of the enzyme bound to calcium (Lewis et al. 2015). By inhibition of PAD4, citrullination of histones is prevented and thus, subsequent chromatin decondensation which is critical for NET formation (Sorensen and Borregaard 2016). As expected, incubation with Cl-amidine led to unspecific blocking of NET formation of all stimuli tested here (PMA, ssRNA-LL37 complex, Mock NETs, PMA NETs), as no release of DNA was observed (Fig. 3.9C, quantification in D). These findings emphasize the specific TLR8-dependent detection of NETs in naïve PMNs and further indicate the involvement of PAD4 in this self-amplification.

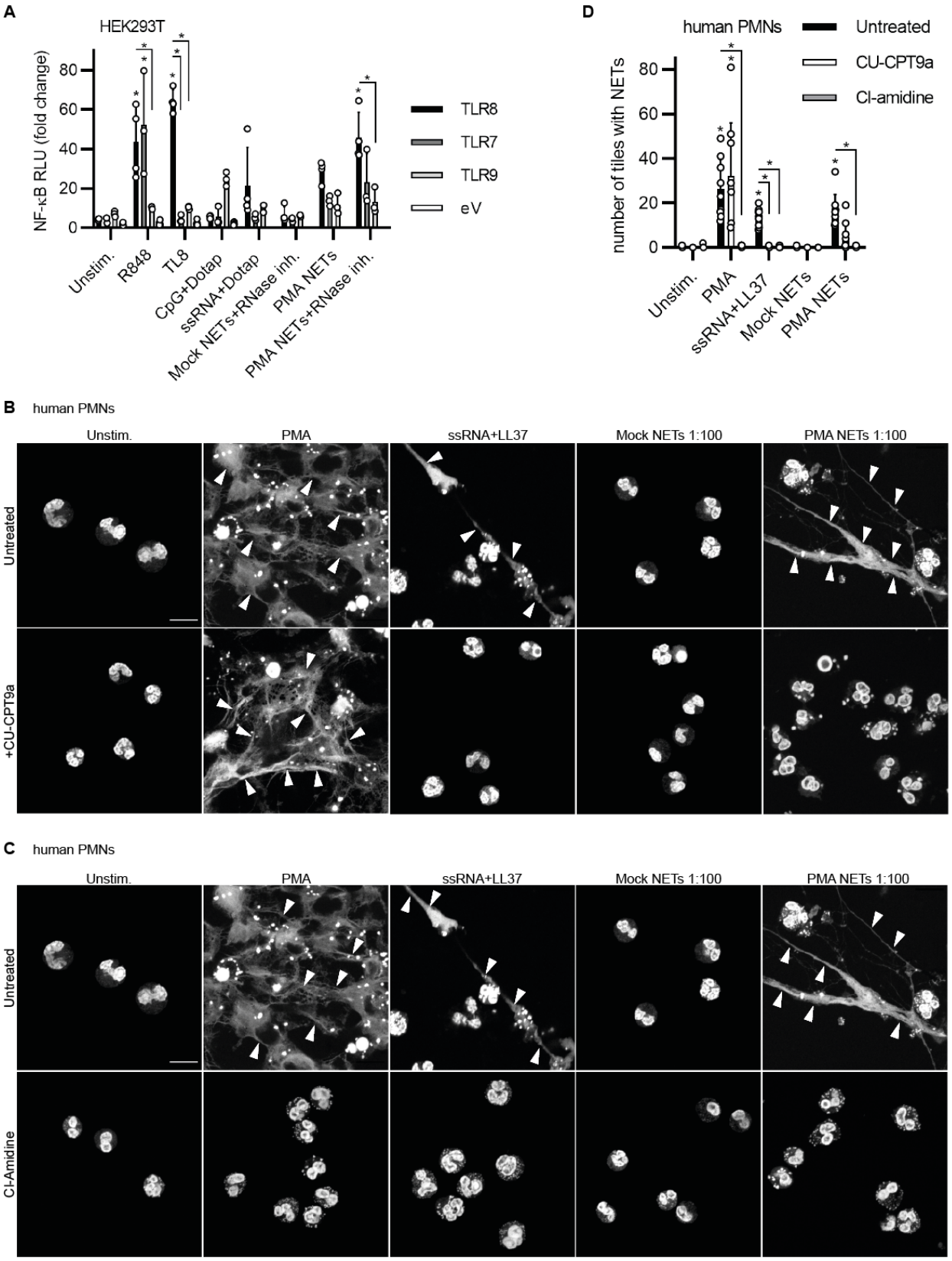
A
HEK293T
NF-κB RLU (fold change)
0
20
40
60
80
Unstim.
R848
TL8
CpG+Dotap
ssRNA+Dotap
Mock NETs+RNase inh.
PMA NETs
PMA NETs+RNase inh.
TLR8
TLR7
TLR9
eV
D
human PMNs
Untreated
CU-CPT9a
Cl-amidine
number of tiles with NETs
0
20
40
60
80
Unstim.
PMA
ssRNA+LL37
Mock NETs
PMA NETs
B
human PMNs
Unstim.
PMA
ssRNA+LL37
Mock NETs 1:100
PMA NETs 1:100
Untreated
+CU-CPT9a
C
human PMNs
Unstim.
PMA
ssRNA+LL37
Mock NETs 1:100
PMA NETs 1:100
Untreated
Cl-Amidine

Figure 3.9: NETs readily induce TLR8-sensing and self-amplification in a TLR8-dependent manner.

(A) NF-κB dual luciferase assay in HEK293T cells transiently transfected with human TLR7, TLR8, and TLR9 and stimulated with R848 (2.5 µg/mL), TL8 (100 ng/mL), CpG (1.25 µM) + DOTAP (25 µg/mL), ssRNA (0.6 µg/mL) + DOTAP (20 µg/mL), as well as Mock NETs+RNase inhibitor (RNase inh., 1:50 dilution), PMA NETs (1:50 dilution), PMA NETs+RNase inhibitor (1:50) for 24 h (eV = empty vector, n=3-5, combined data, mean+SD, *p<0.05 according to one-way ANOVA). **(B)** Confocal microscopy of human primary PMNs stimulated with PMA (600 nM), ssRNA-LL37 complex, and NET content (Mock/PMA, 1:100 dilution) for 3 h in the presence or absence of CU-CPT9a (100 nM) and stained for NETs/DNA (Hoechst 33342, white, n = 3, representative images, scale bar: 10 µm). **(C)** As in **B** but in the presence or absence of the PAD4-inhibitor Cl-amidine (200 µM, n = 3, representative images; scale bar 10 µm). **(D)** Quantification of **B,C** using DNA (Hoechst 33342) signal to quantify NET formation (n = 3, combined data, mean+SD, each dot represents the number of NET-positive tiles in one image, three images/condition, *p<0.05 according to non-parametric one-way ANOVA). The transfection of HEK293T cells and subsequent NF-κB dual luciferase assay was performed by Sirui Chen, former master student of AG Weber, Department of Immunology, University of Tübingen, under my supervision.

Knock-out mice provide a powerful way to examine the involvement and function of certain genes (Bello, Berry, and Smith 2020). Having observed that murine BM-PMN are responsive to RNA, this study sought to investigate naRNA sensing and the corresponding TLR in a further model. As aforementioned, mice lacking Unc93b1 activity are impaired in general endosomal Tlr-sensing (Lee and Barton 2014), i.e. Tlrs 7, 9, and 13 are impaired. Therefore, those mice were used to examine if endosomal Tlrs play a role in murine BM-PMN activation upon stimulation with NETs. BM-PMNs were isolated from C57BL76 WT mice as controls and *Unc93b1*$^{-/-}$ mice lacking functional endosomal Tlrs as described and stimulated for 16 h with PMA as the positive control, as well as human NET content. Afterwards, the cells were stained for nuclear DNA with Hoechst 33342 and NET formation was assessed using confocal microscopy. WT BM-PMNs readily responded with NET formation to the positive control PMA, as well as to PMA-induced human NET content (Fig. 3.10A), similar as observed for human PMNs (*cf.* Fig. 3.8B). As expected, *Unc93b1*$^{-/-}$ BM-PMNs did not respond upon stimulation with PMA NETs. However, *Unc93b1*$^{-/-}$ BM-PMNs were not generally impaired in NET formation as they readily responded to the PMA control (Fig. 3.10A). Of note, incubation of murine BM-PMNs with Mock NETs (negative control) did not lead to any unwanted NET release (Fig. 3.10A). Thus, endosomal Tlrs and therefore nucleic acid sensing seemed to be crucial for the activation of murine BM-PMNs upon stimulation with human NETs. To investigate specifically RNA sensing, BM-PMNs of *Tlr13*$^{-/-}$ mice were used. Tlr13 in mice is considered the equivalent for human TLR8 (Eigenbrod and Dalpke 2015), which is why *Tlr13*$^{-/-}$ mice provide an ideal system to investigate the naRNA-driven NET induction in mouse cells. BM-PMNs isolated from C57BL/6 WT mice as controls and *Tlr13*$^{-/-}$ mice were treated with PMA as the positive control and human NET content. When assessing NET release by confocal microscopy, it was observed that WT BM-PMNs responded with NET formation to stimulation with PMA NETs, whereas *Tlr13*$^{-/-}$ BM-PMNs did not. Of note, neutrophils derived of the knock-out mice were not generally impaired in NET formation as they still responded to PMA as a direct stimulus (Fig. 3.10B, quantified in Fig. 3.10C). Stimulation of the cells with Mock NETs as the negative control did not induce NET release (Fig. 3.10B). Therefore, Tlr13 seemed to be the NET-sensing Tlr in murine BM-PMNs, which indicated that naRNA is the crucial component for activation of naïve BM-PMNs upon contact with human NET content. This was in line with the findings that TLR8 is the key sensor of naRNA in human PMNs (*cf.* Fig. 3.9B, C). As a further control, *Tlr9*$^{-/-}$ mouse-derived neutrophils were investigated, which lack the DNA-sensing Tlr. Therefore, using those mice was helpful to exclude that DNA signaling of NETs is necessary to

induce activation of BM-PMNs. Thus, BM-PMNs were isolated from WT mice as controls and *Tlr9*$^{-/-}$ mice and stimulated with PMA and human NET content as described before. Stimulation with PMA as the positive control induced NET release in both, WT and KO BM-PMNs, whereas treatment with Mock NETs as the negative control did not lead to an activation of the cells. As expected, BM-PMNs of *Tlr9*$^{-/-}$ mice released NETs upon incubation with human PMA NETs, thereby responding just like WT cells (Fig. 3.10D). This indicated that DNA-sensing is dispensable for the responsiveness of BM-PMN to human NETs.

These findings unequivocally show that the DAMP-activity of naRNA is dependent on TLR8- and Tlr13-mediated neutrophil activation in human and in mice, respectively, and further identify naRNA as the primary immune stimulating component of NETs.

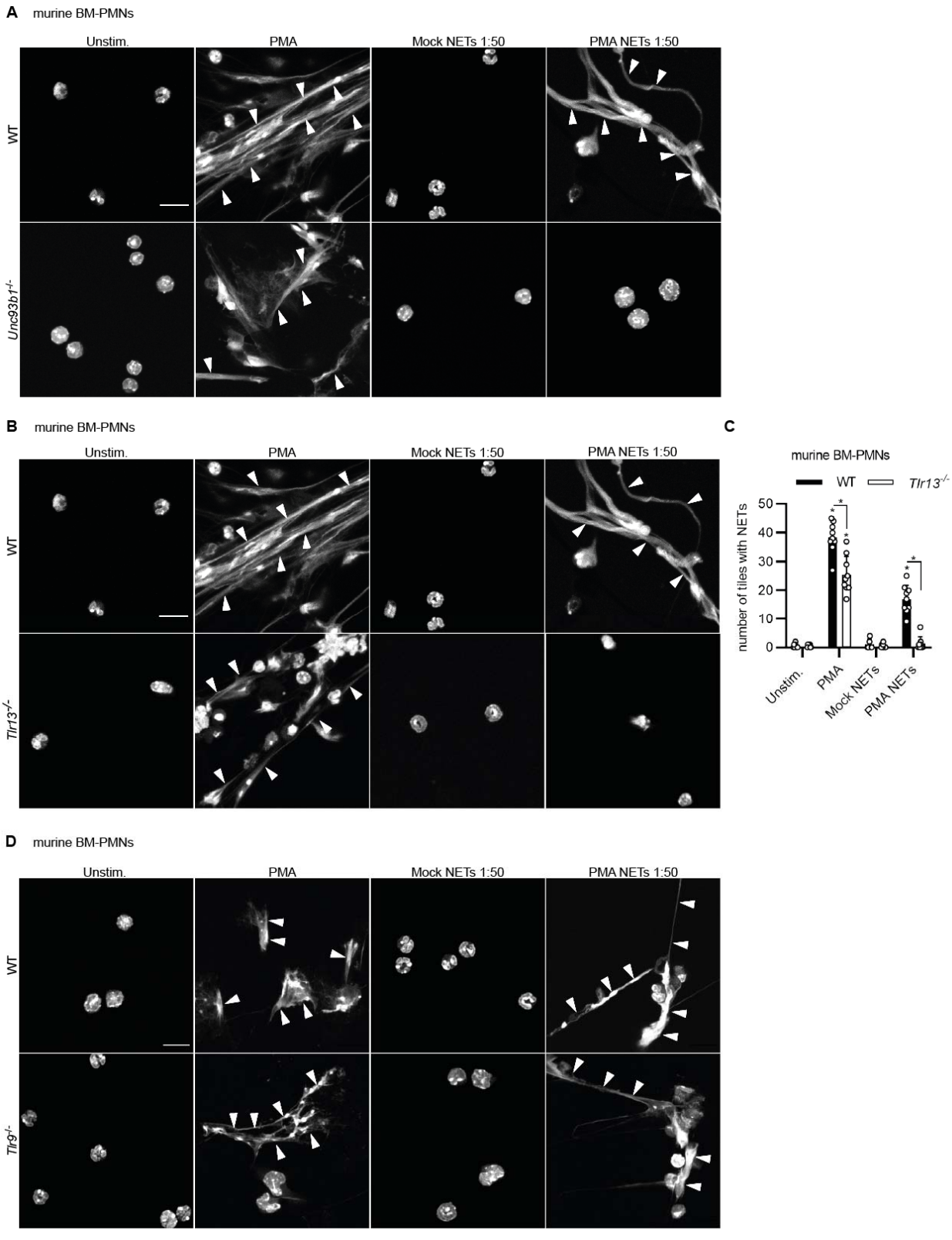
A
murine BM-PMNs
Unstim.
PMA
Mock NETs 1:50
PMA NETs 1:50
WT
Unc93b1-/-
B
murine BM-PMNs
Unstim.
PMA
Mock NETs 1:50
PMA NETs 1:50
WT
Tlr13-/-
C
murine BM-PMNs
WT
Tlr13-/-
number of tiles with NETs
50
40
30
20
10
0
Unstim.
PMA
Mock NETs
PMA NETs
D
murine BM-PMNs
Unstim.
PMA
Mock NETs 1:50
PMA NETs 1:50
WT
Tlr9-/-

Figure 3.10: NETs are sensed via Tlr13 in murine BM-PMNs.

(A) Confocal microscopy analysis of primary C57BL/6 WT or *Unc93b1*$^{-/-}$ murine BM-PMNs stimulated with PMA (600 nM) and NET content (Mock/PMA, 1:50 dilution) for 16 h and stained for NETs/DNA (Hoechst 33342, white, n = 3 WT, n = 1 *Unc93b1*$^{-/-}$, representative images, scale bar: 10 µm). **(B)** As in **A** but primary C57BL/6 WT or *Tlr13*$^{-/-}$ murine BM-PMNs (n = representative images, scale bar: 10 µm). **(C)** Quantification of **B** using DNA (Hoechst 33342) signal to quantify NET formation (n = 3, combined data, mean+SD, each dot represents the number of NET-positive tiles in one image, three images/condition, *p<0.05 according to non-parametric one-way ANOVA). **(D)** As in **A** but primary C57BL/6 WT or *Tlr9*$^{-/-}$ murine BM-PMNs (n = 3, representative images, scale bar: 10 µm). Bones for BM-PMN isolation from Tlr9 KO mice and corresponding WT mice were kindly provided by B. Schittek, Tübingen.

3.3.2 naRNA induces TLR8-dependent immune responses in macrophages, as well as activation of other immune cells

Since NETs were not only shown to activate neutrophils (Tan, Aziz, and Wang 2021), but were also reported to e.g. induce activation of macrophages (Papayannopoulos 2018) and keratinocytes (Shao et al. 2019), it was further anticipated in this study to investigate the role of naRNA in these inflammatory responses.

It was previously detected in this study that PMNs respond to naRNA in a TLR8-dependent manner and macrophages have been reported to sense ssRNA40 via TLR8 (Ishii et al. 2014). Therefore, it was hypothesized to observe similar findings for macrophages in regard of NET-sensing as found for PMNs. To examine this assumption, BlaER1 macrophages (Vierbuchen et al. 2017), which were genetically modified, were stimulated with respective controls (LPS (TLR4 ligand), R848 (TLR7/8 ligand), TL8 (TLR8 ligand), ssRNA-LL37 complexes (TLR8 ligand)), and NET content (Mock/PMA NETs +/-RNase inhibitor at different dilutions). Cellular responsiveness was assessed using a cytokine ELISA to detect IL-8 release. It was observed that BlaER1 macrophages lacking the RNA-sensor TLR8 (*TLR8*$^{-/-}$), as well as cells lacking endosomal TLR signaling (*UNC93B1*$^{-/-}$, both cell lines described by T. Vierbuchen and H. Heine et al. (Vierbuchen et al. 2017) and kindly provided by Holger Heine, Borstel, Germany), were unable to respond to stimulation with NET content, as depicted by significantly lower IL-8 release. WT macrophages responded to PMA NETs in a dilution-dependent manner, whereas Mock NETs did not induce IL-8 release. Of note, stimulation with PMA NETs containing RNase inhibitor (PMA NETs+RNase inhibitor) induced a greater IL-8 release in WT macrophages compared to PMA NETs without RNase inhibitor, in which naRNA is not additionally protected (Fig. 3.11A). Thus, TLR8 sensing of NETs in BlaER1 macrophages is essential for their activation as examined by IL-8 release in this study and occurs in a naRNA-dependent manner.

To assess these findings in another system, THP-1 macrophage-like cells with TLR7- and TLR8-editing were used (cells described by (Coch et al. 2019) and kindly provided by Thomas Zillinger, Bonn). After differentiation into macrophage-like cells as previously described, the cells were stimulated with the respective controls (PMA+Ionomycin, LPS (TLR4 ligand), R848 (TLR7/8 ligand), TL8 (TLR8 ligand), ssRNA-LL37 complexes (TLR8 ligand)) and NET content (Mock/PMA NETs +/-RNase inhibitor, 1:50 dilution). Their activation was subsequently investigated using an IL-8 cytokine ELISA. Similar to BlaER1 macrophage stimulation, high release of IL-8 was only observed in WT cells, whereas TLR8-deficient macrophage-like cells only barely responded to PMA NETs as a stimulus. Furthermore, TLR7-deficient cells showed a

significantly reduced IL-8 release upon stimulation with NET content. It was again found that protection of naRNA with RNase inhibitor drastically increased the stimulatory properties of PMA NETs on WT macrophages (Fig. 3.11B). Therefore, TLR8-sensing is also necessary for naRNA-dependent THP-1 activation upon stimulation with NET content.

This data highlights the critical role of naRNA in macrophage activation induced by NETs and the involvement of TLR8 in this inflammatory response.

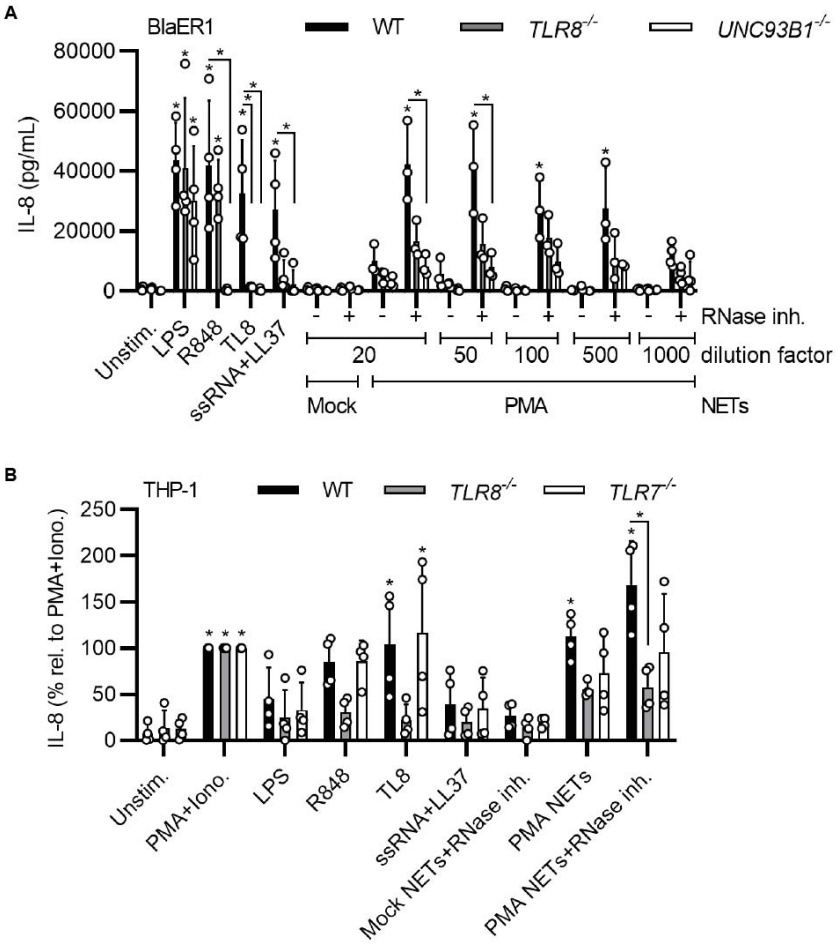

Figure 3.11: naRNA activates macrophages in a TLR8-dependent manner.

(A) Triplicate IL-8 ELISA from WT, *TLR8*$^{-/-}$ and *UNC93B1*$^{-/-}$ BlaER1 macrophage-like cells stimulated with LPS (0.1 µg/mL), R848 (5 µg/mL), TL8 (100 ng/mL), ssRNA+LL37 complex, and Mock/PMA NETs with/without RNase inhibitor at indicated dilutions for 18 h (n = 3-4, combined data, mean+SD, each dot represents one biological replicate, *p<0.05 according to one-way ANOVA). **(B)** As in **A** but from WT, *TLR8*$^{-/-}$, and *TLR7*$^{-/-}$ THP-1 cells stimulated with PMA (25 µg/mL)+Ionomycin (0.375 µg/mL), LPS (0.1 µg/mL), R848 (5 µg/mL), TL8 (40 ng/mL), ssRNA+LL37 complex, Mock NETs+RNase inhibitor (1:50 dilution), PMA NETs (1:50 dilution), and PMA NETs+RNase inhibitor (1:50 dilution) for 18 h, normalized to PMA+Ionomycin control (n = 4, combined data, mean+SD, each dot represents one biological replicate, *p<0.05 according to one-way ANOVA). Experiments with BlaER1 and THP-1 cells were performed by Carsten Greve, PhD student of AG Weber, Department of Immunology, University of Tübingen.

To further examine the role of naRNA in broad immune cell activation, human peripheral blood mononuclear cells (PBMCs) were isolated from healthy donors, stimulated with the respective controls (LPS (TLR4 ligand), R848 (TLR7/8 ligand), TL8 (TLR8 ligand), ssRNA-LL37/DOTAP complexes (TLR8 ligand)) and NET content (Mock/PMA NETs +/-RNase inhibitor, 1:20 dilution). Subsequently cytokine ELISAs for TNF, IL-6, and IL-8 were performed. Overall, stimulation of PBMCs with PMA NETs containing RNase inhibitor induced a higher release of TNF, IL-6, and IL-8 compared to PMA NETs. However, this effect could not be completely linked to TLR8-sensing, since the use of the TLR8-inhibitor CU-CPT9a did not lead to clear results (only used for TNF and IL-6 measurements) (Fig. 3.12A(TNF), B(IL-6) and C(IL-8)). The previous detected low TLR7-dependent NET sensing observed in transfected HEK cells (*cf.* Fig. 3.9A) could potentially explain why CU-CPT9a use in PBMCs was not sufficient to completely abolish naRNA signaling, as TLR7 sensing of RNA by e.g. conventional dendritic cells (Ganguly et al. 2009) might be left unaltered.

Furthermore, NK cells have been reported to sense RNA of *Plasmodium falciparum*-infected red blood cells via TLR8, leading to IFN-γ release (Coch et al. 2019). NK-92 MI cells, a frequently used cell line model of natural killer (NK) cells, were examined in this study to investigate if naRNA could induce IFN-γ release in a similar manner to the one reported in literature. Therefore, the cells were stimulated with the respective controls (LPS (TLR4 ligand), CpG+DOTAP (TLR9), R848 (TLR7/8 ligand), TL8 (TLR8 ligand), ssRNA-LL37/DOTAP complexes (TLR8 ligand)) and NET content (Mock/PMA NETs +/-RNase inhibitor, 1:100 dilution) and IFN-γ release was measured with a cytokine ELISA. Stimulation of the NK-92 MI cells with PMA NETs led to a mild release of IFN-γ, which was slightly greater upon stimulation of the cells with PMA NETs containing RNase inhibitor. However, no significant results were obtained (Fig. 3.11D). This indicates that naRNA might not be a very potent activator of NK cells, although investigation of the responsiveness of primary cells remains to be performed.

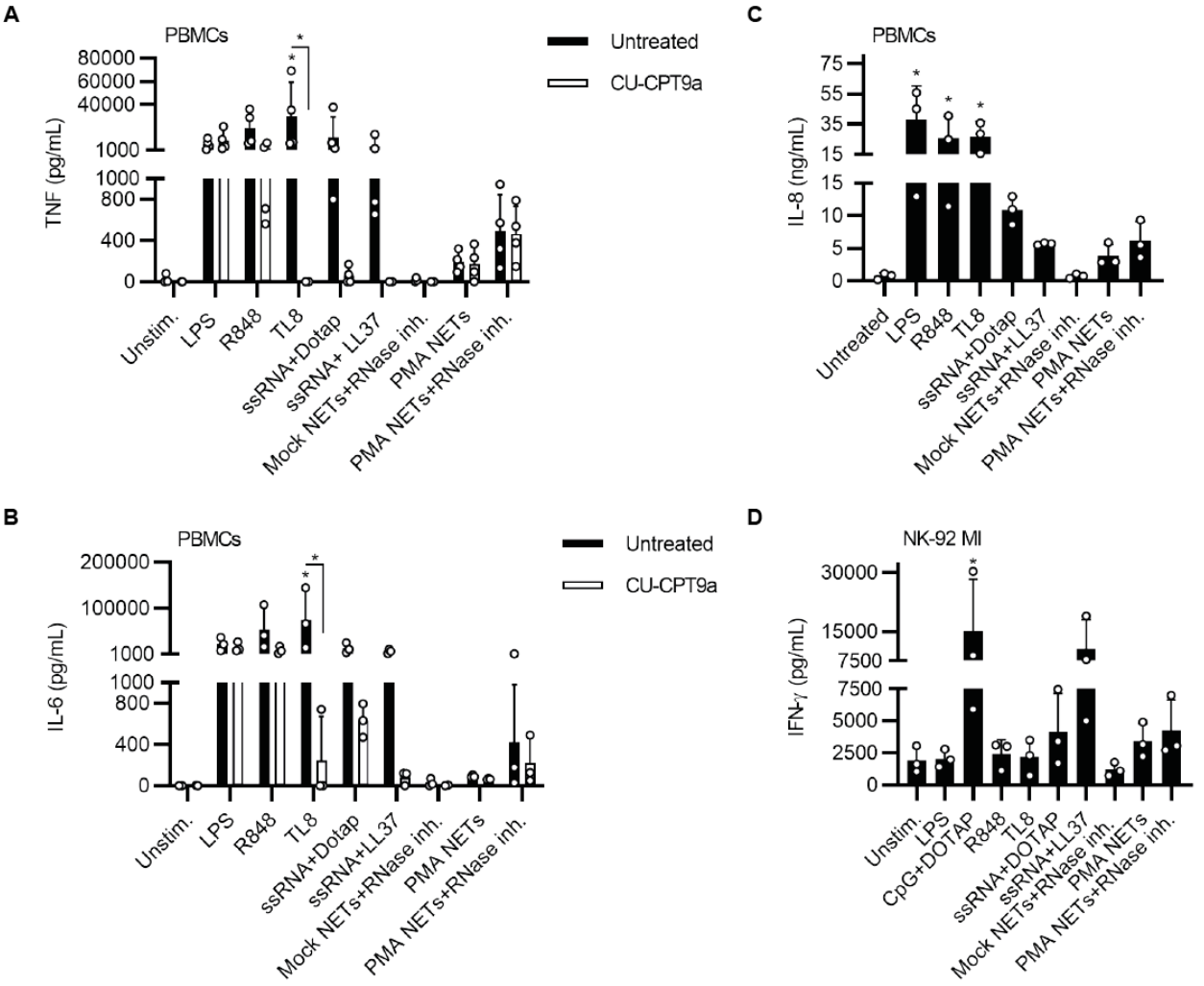

Figure 3.12: NETs induce a naRNA-dependent cytokine release in PBMCs and NK cells.

(A-C) Triplicate ELISA for TNF (**A**, n = 4), IL-6 (**B**, n = 3), and IL-8 (**C**, n = 3) from primary human PBMCs stimulated with LPS (100 ng/mL), R848 (5 µg/mL), TL8 (100 ng/mL), ssRNA (1.6 µg/mL)+DOTAP (50 µg/mL), ssRNA+LL37 complex, Mock NETs+RNase inhibitor (1:20 dilution), PMA NETs (1:20 dilution), or PMA NETs+RNase inhibitor (1:20 dilution) with/without CU-CPT9a (1 µM) for 24 h (combined data, mean+SD, each dot represents one biological replicate, *p<0.05 according to one-way ANOVA). **(D)** Triplicate IFN-γ ELISA from NK-92 MI cells stimulated with LPS (100 ng/mL), CpG (2.5 µM)+DOTAP (25 µg/mL), R848 (5 µg/mL), TL8 (100 ng/mL), ssRNA (1.6 µg/mL)+DOTAP (50 µg/mL), ssRNA+LL37 complex, Mock NETs+RNase inhibitor (1:100 dilution), PMA NETs (1:100 dilution), or PMA NETs+RNase inhibitor (1:100 dilution) for 24 h (n = 3, combined data, mean+SD, each dot represents one biological replicate, *p<0.05 according to one-way ANOVA). PBMC experiments were performed by Sirui Chen, former master student of AG Weber, Department of Immunology, University of Tübingen, under my supervision. Experiments with NK-92 MI cells were performed by Pujan Engels, PhD student of AG Weber, Department of Immunology, University of Tübingen.

Taken together, this data suggests that naRNA cannot only induce activation of naïve PMNs but may additionally induce responses in other immune cells, such as macrophages and NK cells, at least partially in a TLR8-dependent manner.

3.3.3 NETs induce naRNA-dependent keratinocyte activation

As previously mentioned, NETs actively drive diseases like psoriasis by activating keratinocytes (Shao et al. 2019). Therefore, this study aimed to investigate if these epidermal cells with immune functions (Piipponen, Li, and Landen 2020) also are activated by naRNA, as shown above for immune cells (*cf.* Fig. 3.11 and Fig. 3.12).

To address this question, N/TERT-1 keratinocytes were used. These cells were a kind gift from James Rheinwald, Harvard Medical School, Boston, USA (cells described by (Dickson et al. 2000)). Therefore, cells grown in monolayers were stimulated with PMA+Ionomycin (positive control), as well as TL8 (TLR8 ligand), ssRNA-LL37 complexes (TLR8 ligand), and NET content (Mock NETs 1:100 dilution +/-RNase inhibitor; PMA NETs 1:100-1:10,000 dilution +/-RNase inhibitor). It was observed that N/TERT-1 keratinocytes readily responded to ssRNA-LL37 complexes, as well as to PMA NETs at a 1:100 dilution, measured by IL-8 cytokine ELISA. Using PMA NETs without RNase inhibitor did not lead to IL-8 release at a dilution of 1:500 and higher, whereas PMA NETs+RNase inhibitor potently stimulated the keratinocytes dose-dependently up to a dilution of 1:5,000 (Fig. 3.13A). Thus, protecting naRNA greatly enhances the stimulatory properties of NETs in regard of N/TERT-1 keratinocyte activation, which indicates that the IL-8 response is RNA-dependent. Of note, Mock NETs +/-RNase inhibitor did not lead to detectable IL-8 release, ruling out unspecific stimulatory effects due to the RNase inhibitor (Fig. 3.13A).

In addition, primary normal human epidermal keratinocytes (NHEK, PromoCell), grown in monolayers, were tested. NHEK were stimulated in the same way as N/TERT-1 keratinocytes and an IL-8 cytokine ELISA was performed to investigate the activation status. Like N/TERT-1 keratinocytes, primary NHEK readily responded to ssRNA-LL37 complexes, as well as to PMA NETs (1:25 dilution). A significantly higher IL-8 release was induced upon stimulation of the cells with PMA NETs+RNase inhibitor, presumed to contain protected naRNA (Fig. 3.13B). Thus, NET-mediated activation of NHEK cells seems to be naRNA-dependent.

As a third system, a human skin equivalent 3D model was used. In this model, NHEK cells are used in combination with a fibroblast layer, and an air-lift step of initial 2D cultures leads to a 3D model in which the NHEKs adopt differentiation in layers that mimic natural keratinocyte differentiation in human skin (Bitschar et al. 2020). Stimulating the 3D skin model epicutaneously (i.e. by application on top) with PMA NETs induced the expression of *IL8* mRNA, as measured by qPCR (Fig. 3.13C), as well as the release of IL-8 cytokine, as measured by ELISA (Fig. 3.13D). Both was significantly elevated when stimulation was performed with PMA NETs containing protected naRNA (PMA NETs+RNase inhibitor; Fig. 3.13C, D). This is in line with the previous findings of naRNA-dependent keratinocyte activation measured by IL-8 release upon stimulation with NETs in the underlying study.

Using the three different systems to analyze keratinocyte responses to naRNA clearly shows that naRNA is a potent DAMP inducing keratinocyte activation and pro-inflammatory responses in those epidermal cells. Further studies are under way to investigate the PRR involved in these effects in keratinocytes.

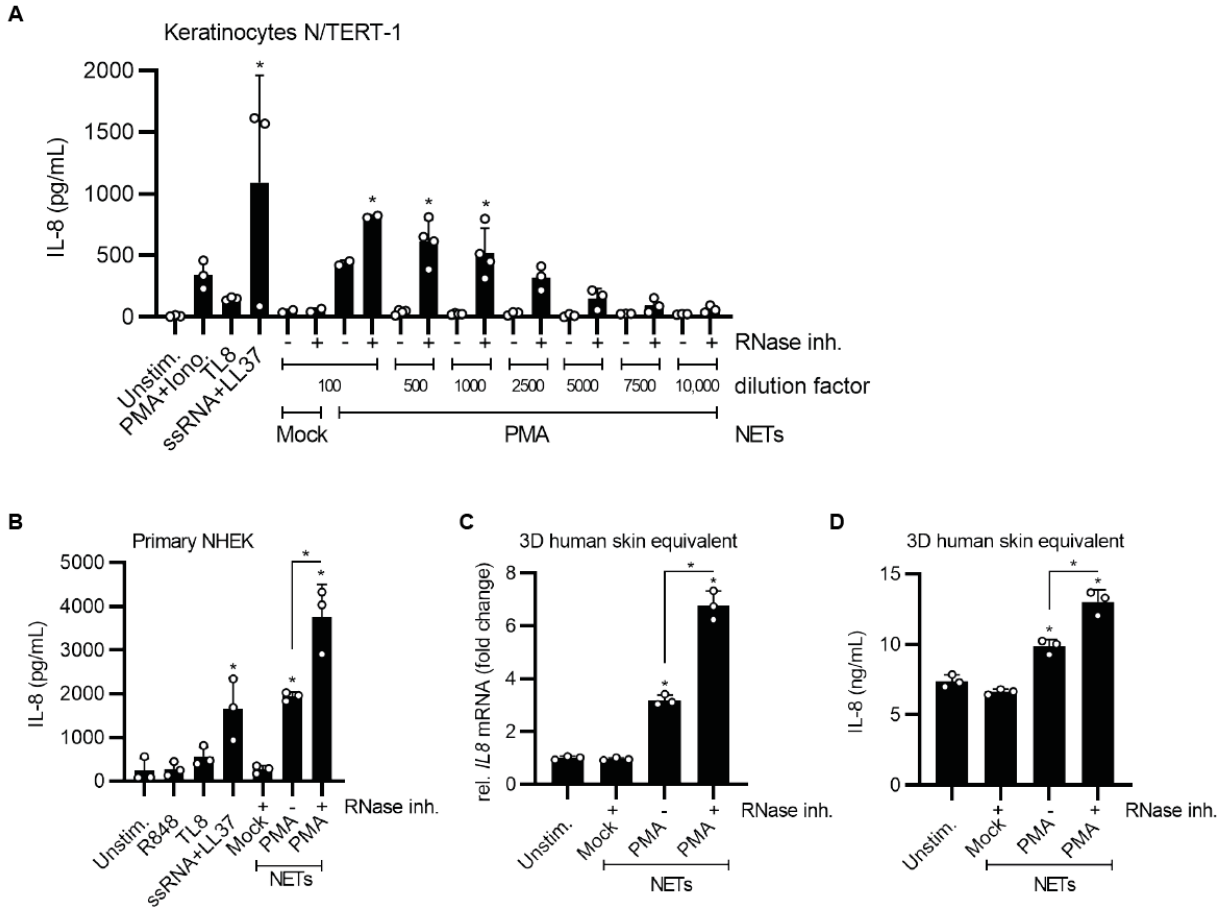

Figure 3.13: NETs induce naRNA-dependent keratinocyte activation.

(A) Triplicate IL-8 ELISA from N/TERT-1 keratinocytes stimulated with PMA (25 µg/mL)+Ionomycin (0.375 µg/mL), TL8 (200 ng/mL), ssRNALL37 complex, as well as Mock/PMA NETs with/without RNase inhibitor at the indicated dilutions for 24 h (n = 3, combined data, mean+SD, each dot represents one biological replicate, *p<0.05 according to one-way ANOVA). **(B)** As in **A** but with primary normal human epidermal keratinocytes (NHEK) stimulated with R848 (20 µg/mL), TL8 (200 ng/mL), ssRNA+LL37 complex, and Mock NETs+RNase inhibitor (1:25 dilution), PMA NETs with/without RNase inhibitor (1:25 dilution) for 24 h (n = 3, combined data, mean+SD, each dot represents one biological replicate, *p<0.05 according to one-way ANOVA). **(C, D)** Triplicate relative (to unstimulated) *IL8* mRNA qPCR or IL-8 ELISA from 3D human skin equivalent constructs stimulated Mock NETs+RNase inhibitor, PMA NETs, and PMA NETs+RNase inhibitor as previously described for 24 h (n = 3, representative of one biological replicate is shown, mean+SD, each dot represents one technical replicate, *p<0.05 according to one-way ANOVA). All experiments performed on N/TERT-1 keratinocytes and NHEK were done by Carsten Greve, PhD student of AG Weber, Department of Immunology, University of Tübingen. Preparation and stimulation of the 3D human skin equivalent was performed by Jasmin Scheurer, AG Schittek, Division of Dermatooncology, Department of Dermatology, University Hospital Tübingen. The corresponding *IL8* qPCR analysis and IL-8 cytokine ELISA was subsequently performed by Carsten Greve.

After proving the stimulatory role of naRNA in immune activation of neutrophils, macrophages, and keratinocytes *in vitro*, another important part of this study was the proof of principle *in vivo*.

3.4 NET-related *in vivo* inflammation is highly naRNA-dependent

NETs have been investigated as drivers of various autoimmune diseases, such as psoriasis (Lambert et al. 2019; Suzuki et al. 2014). More recently it has been reported that NET-derived serum MPO-DNA complexes are associated with disease severity and activity of psoriatic arthritis, highlighting the role of NETs in disease progression (Li, Li, et al. 2022). However, the exact underlying pathogenic mechanisms remain to be explored. With the well-established IMQ model (Gilliet et al. 2004) and the skin inflammation model induced by intradermal injection of RNA-LL37 complexes previously established and described (Herster et al. 2020), psoriasis provided an excellent disease background for *in vivo* experiments to investigate the pathophysiological role of naRNA in inflammation in this study.

3.4.1 naRNA potently triggers Tlr13-dependent inflammatory responses *in vivo*

As previously shown by this group, psoriasis-derived neutrophils are more prone to spontaneous NET formation *in vitro* compared to PMNs of healthy donors (Herster et al. 2020). In addition, NETs were found in high amounts in psoriatic skin lesions (Shao et al. 2019; Herster et al. 2020). Furthermore, the observation of naRNA as a novel component of NETs led to the hypothesis that NET-derived naRNA can form complexes with LL37 (Herster et al. 2020), which is known to accumulate in high abundance in psoriatic skin lesions (Zanetti 2004; Lande et al. 2014). These complexes were further suggested to drive disease progression (Herster et al. 2020). However, the final proof of principle was missing so far, why validation was performed in this research work.

As a first step to show naRNA was immunostimulatory *in vivo*, NET content was intradermally injected into the ears of C57BL/6 mice, as well as ssRNA-LL37 complexes, as previously described (Herster et al. 2020). Stimuli were injected once on day 0 and daily measurement of the ear swelling (thickness) as a marker of skin inflammation (Rizzo et al. 2011) with a manual caliper was performed on five consecutive days. The injection of Mock NETs +/-RNase inhibitor and the medium control (RPMI+RNase inhibitor, vector control) did not lead to significant ear swelling. The injection of PMA NETs led to a mild inflammation, significantly different from the skin reaction upon injection of Mock NETs. Importantly, this effect was drastically increased upon injection of PMA NETs containing RNase inhibitor, implicating naRNA as a vital stimulatory component. ssRNA-LL37 complex injection led to the highest ear swelling and was used as a positive control (Fig. 3.14A). Thus, naRNA was observed to indeed have immunostimulatory effects *in vivo*.

In a second approach, NET content containing RNase inhibitor (Mock (negative control) and PMA NETs), as well as ssRNA-LL37 complexes and RPMI+RNase inhibitor (positive and negative control, respectively) were injected intradermally into the ears of *LysM*$^{EGFP/+}$ mice, in which myeloid cells are GFP-positive. The fluorescent label of the cells thereby enables the observation of cellular influx *in vivo* (Faust et al. 2000). Interestingly, although ssRNA-LL37 complexes induced a greater inflammation than PMA NETs+RNase inhibitor (*cf.* Fig. 3.14A), injection of PMA NETs+RNase inhibitor led to a higher influx of naïve PMNs than

injection of the RNA complex, as measured over 0-6 h after injection of the stimuli at time point 0 (Fig. 3.14B). This indicates that naRNA acts *in vivo* as a more potent stimulus for attraction of PMNs compared to synthetic RNA. Of note, no neutrophil influx was observed upon injection of the negative control stimuli (Mock NETs+RNase inhibitor and RPMI+RNase inhibitor; Fig. 3.14B).

To investigate if Tlr13, i.e. an RNA sensor, mediates the inflammatory response *in vivo*, the immunostimulatory effect of NET content was compared in C57BL/6 and *Tlr13*$^{-/-}$ mice. Mock or PMA NETs+RNase inhibitor were intradermally injected into the ears on day 0 and inflammation was assessed by daily measurement of ear swelling with a manual caliper on five consecutive days. The injection of PMA NETs+RNase inhibitor in the ears of mice lacking RNA-sensing (*Tlr13*$^{-/-}$) led to a significantly reduced skin inflammation compared to WT mice (C57BL/6). Corresponding Mock controls did not induce skin inflammation (Fig. 3.14C). Thus, RNA-sensing seems to play a key role in propagation of NET-mediated skin inflammation *in vivo*.

Collectively this data highly suggests that naRNA is indeed the crucial NET component leading to *in vivo* skin inflammation, as naRNA-stabilized PMA NETs induced stronger ear swelling and mice without RNA sensing (Tlr13 KO) were partially protected from sustained inflammation.

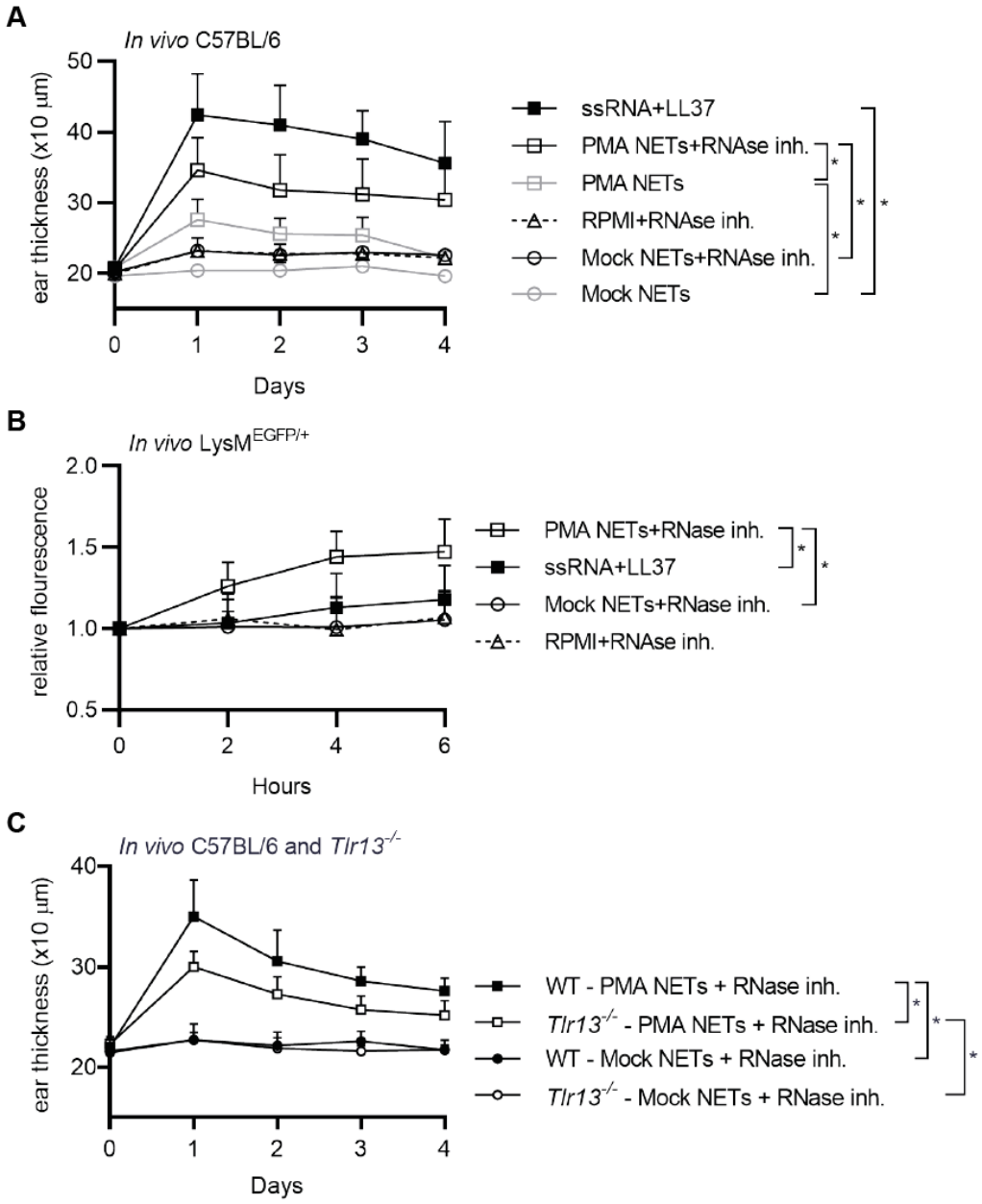

Figure 3.14: naRNA potently triggers Tlr13-dependent inflammatory responses *in vivo*.

(A) Ear thickness quantified daily in WT C57BL/6 mice injected intradermally with 20 µL NET content (Mock/PMA +/- RNase inhibitor), 20 µL medium control (RPMI+RNase inhibitor), or 20 µL ssRNA+LL37 complex *in vivo* on day 0 (n = 5 per group, combined data, mean+SD, *p<0.05 according to two-way ANOVA). **(B)** Fluorescence imaging monitored hourly in LysM$^{EGFP/+}$ mice injected intradermally *in vivo* at t=0 with 20 µL NET content (Mock/PMA +RNase inhibitor), 20 µL medium control (RPMI+RNase inhibitor), or 20 µL ssRNA+LL37 complex (n = 10 per group, combined data, mean+SD, *p<0.05 according to two-way ANOVA). **(C)** As in **A** but also using *Tlr13*$^{-/-}$ mice (injection of 20 µL Mock/PMA NETs+RNase inhibitor on day 0; n = 7, combined data, mean+SD, *p<0.05 according to two-way ANOVA). All *in vivo* experiments were kindly performed, and mice and reagents therefore used provided by Christine Youn, Yu Wang, and Nathan Archer, Department of Dermatology, Johns Hopkins University School of Medicine, Baltimore, USA.

3.4.2 RNA-sensing mediates disease progression in the IMQ psoriasis model

As reported in literature, topic treatment of murine skin with imiquimod (IMQ, TLR7 agonist) leads to skin inflammation, which has been used as tool to study to human psoriasis plaques, thereby providing a rapid and convenient disease model (Gilliet et al. 2004; van der Fits et al. 2009). It was earlier shown by our group that IMQ treatment also induces NET formation in murine tissue (Herster et al. 2020). Although the initial disease initiation is TLR7-dependent (Gilliet et al. 2004), it was aimed in this current study to investigate whether the further disease progression can be linked to naRNA, i.e. by a naRNA-mediated self-propagating effect.

Therefore, C57BL/6 WT and *Tlr13*$^{-/-}$ mice were treated with IMQ on day 0 to day 4 and ear swelling was measured daily with a manual caliper. Up to 48 hours after starting the treatment, WT and *Tlr13*-deficient animals showed similar ear swelling. From day 3 onwards, WT mice suffered from significantly greater skin inflammation compared to *Tlr13*$^{-/-}$ mice (Fig. 3.15A), as characterized by the ear thickness. This observation indicates that a lack of RNA-sensing provides protection against disease progression.

To investigate epidermal thickening mediated by excessive keratinocyte proliferation, a characteristic of psoriatic skin inflammation (Benhadou, Mintoff, and Del Marmol 2019), the mice were sacrificed on day 5 and histologic analysis of ear skin specimen was run. Therefore, H&E staining was performed, and images of the ears were acquired using brightfield microscopy. Measurements of epidermal thickness were subsequently taken using ImageJ-Win64 software. *Tlr13*$^{-/-}$ mice showed significantly reduced epidermal thickening compared to WT mice (Fig. 3.15B, histology example Fig. 3.15C), explaining the diminished ear swelling observed (*cf.* Fig. 3.15A). It can therefore be concluded that keratinocyte activation is minimized when RNA-sensing is missing.

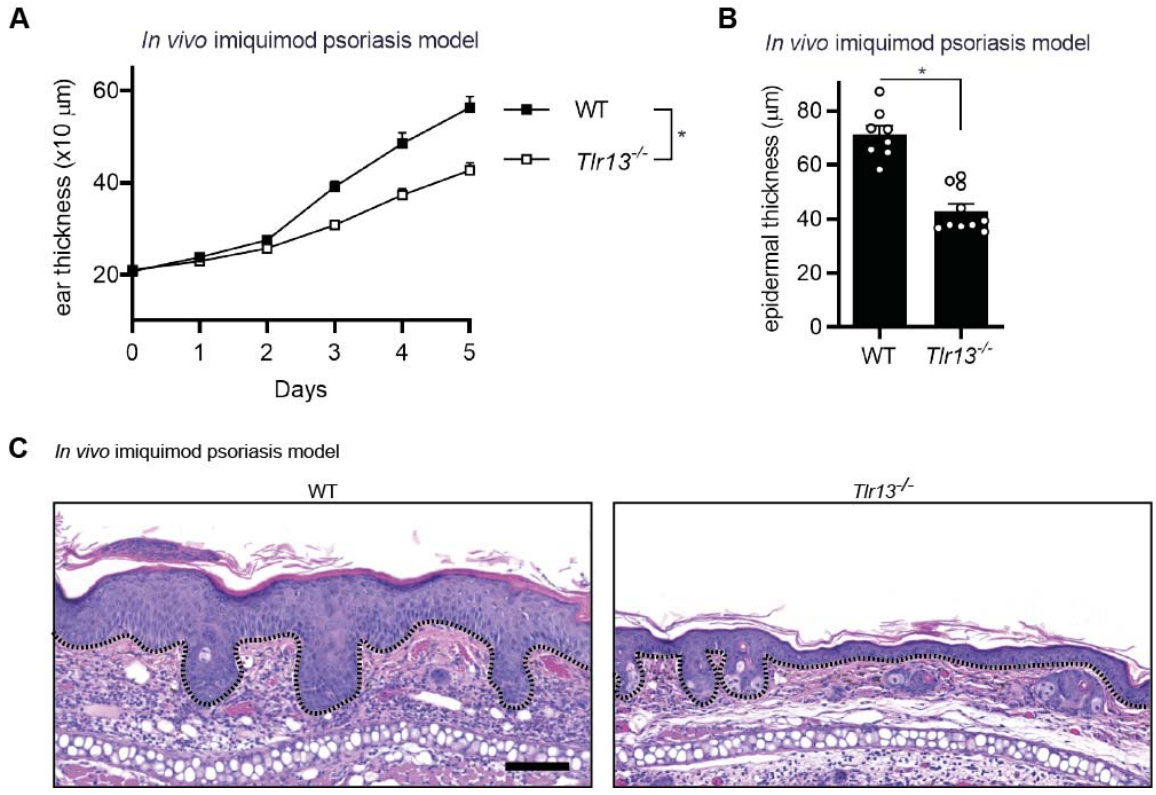

Figure 3.15: RNA-sensing mediates disease progression in the IMQ psoriasis model.

(A) Ear thickness quantified daily in WT C57BL/6 and *Tlr13*$^{-/-}$ mice with topical IMQ application (5%, 70 µL (62.5 mg)) on day 0–4 (C57BL/6 n = 8, *Tlr13*$^{-/-}$ n = 10, combined data, mean+SD, *p<0.05 according to two-way ANOVA). **(B)** Measurement of epidermal thickness of H&E-stained ear skin specimens of **A** (C57BL/6 n = 8, *Tlr13*$^{-/-}$ n = 10, combined data, mean+SD, *p<0.05 according to Student's t-test). **(C)** Histological analysis of H&E-stained ear skin specimens of **B** (C57BL/6 n = 8, *Tlr13*$^{-/-}$ n = 10, representative of one biological replicate is shown, scale bar: 100 µm). All *in vivo* experiments were kindly performed by, and mice and reagents therefore used provided by Christine Youn, Yu Wang, and Nathan Archer, Department of Dermatology, Johns Hopkins University School of Medicine, Baltimore, USA.

In summary, this *in vivo* data provides evidence that NETs induce a naRNA-dependent skin inflammation mediated by Tlr13-signaling in mice and that RNA-sensing can significantly contribute to disease progression in the psoriasis mouse model.

3.5 naRNA-LL37 complexes represent a pre-assembled composite DAMP

Former studies reported that RNA alone is no sufficient stimulus for neutrophils (Herster et al. 2020) or pDCs (Ganguly et al. 2009) but strictly required complexation with LL37. Knowing that LL37 is a common component of neutrophil granules (Lehrer and Ganz 2002) and NETs (Garcia-Romo et al. 2011) we sought to investigate and clarify the role of LL37 regarding the immunomodulatory effects of naRNA in more detail.

3.5.1 LL37 restores the NET-inducing properties of naRNA

To further validate that LL37 was involved in the effects of naRNA, 'naked' naRNA isolated from PMA NETs as described (*cf.* Fig. 3.6) was directly used as a stimulus for naïve PMNs. PMNs isolated from healthy donors were then stimulated with PMA (positive control), as well as naRNA alone or in complex with LL37. Afterwards, the cells were stained for nuclear DNA with Hoechst 33342 and NET formation as a sing for activation was assessed using confocal microscopy. Interestingly but in keeping with the aforementioned studies, naRNA alone did not induce NET formation. However, naRNA re-complexed (as performed for synthetic ssRNA, bRNA, and fRNA (*cf.* Fig. 3.2)) with exogenously added, synthetic LL37 was observed to be a potent stimulus (Fig. 3.16A). Of note, LL37 alone did not induce NET formation (Herster et al. 2020).

For naRNA to be active in NET contents, it could be postulated that it needed to be associated with LL37 in the NET. To investigate if naRNA and LL37 actually colocalized in NETs, PMA-treated neutrophils were stained for LL37 in addition to rRNA. Confocal microscopy revealed strong colocalization of both NET components (Fig 3.16B), as quantified by Pearson's (PCC) colocalization analysis (Fig. 3.16C). In this analysis 0 means that there is no linear association between two variables, whereas 1 means that there is a perfect linear correlation (Schober, Boer, and Schwarte 2018). This finding confirmed the assumption of the existence of NET-derived immune cell-activating naRNA-LL37 complexes, providing an explanation for the observed immunostimulatory properties of NETs.

As controls, unstimulated neutrophils had been included. Unexpectedly, colocalization of LL37 and naRNA was found to be significantly higher in intact, resting neutrophils (Fig. 3.16B, C) than in extracellular NETs. This was surprising and counter-intuitive because naRNA was stained with an anti-rRNA Y10b antibody, detecting ribosomal RNA (Lerner et al. 1981), which is mainly located in the nucleoli of intact cells (Pederson 2011) and LL37 is primarily found in specific granules (Lehrer and Ganz 2002), thus in another cellular compartment. This posed the intriguing possibility that naRNA is maybe localized to neutrophil granules, leading to a more detailed investigation into the localization of LL37 and rRNA (as a proxy for naRNA) in resting neutrophils.

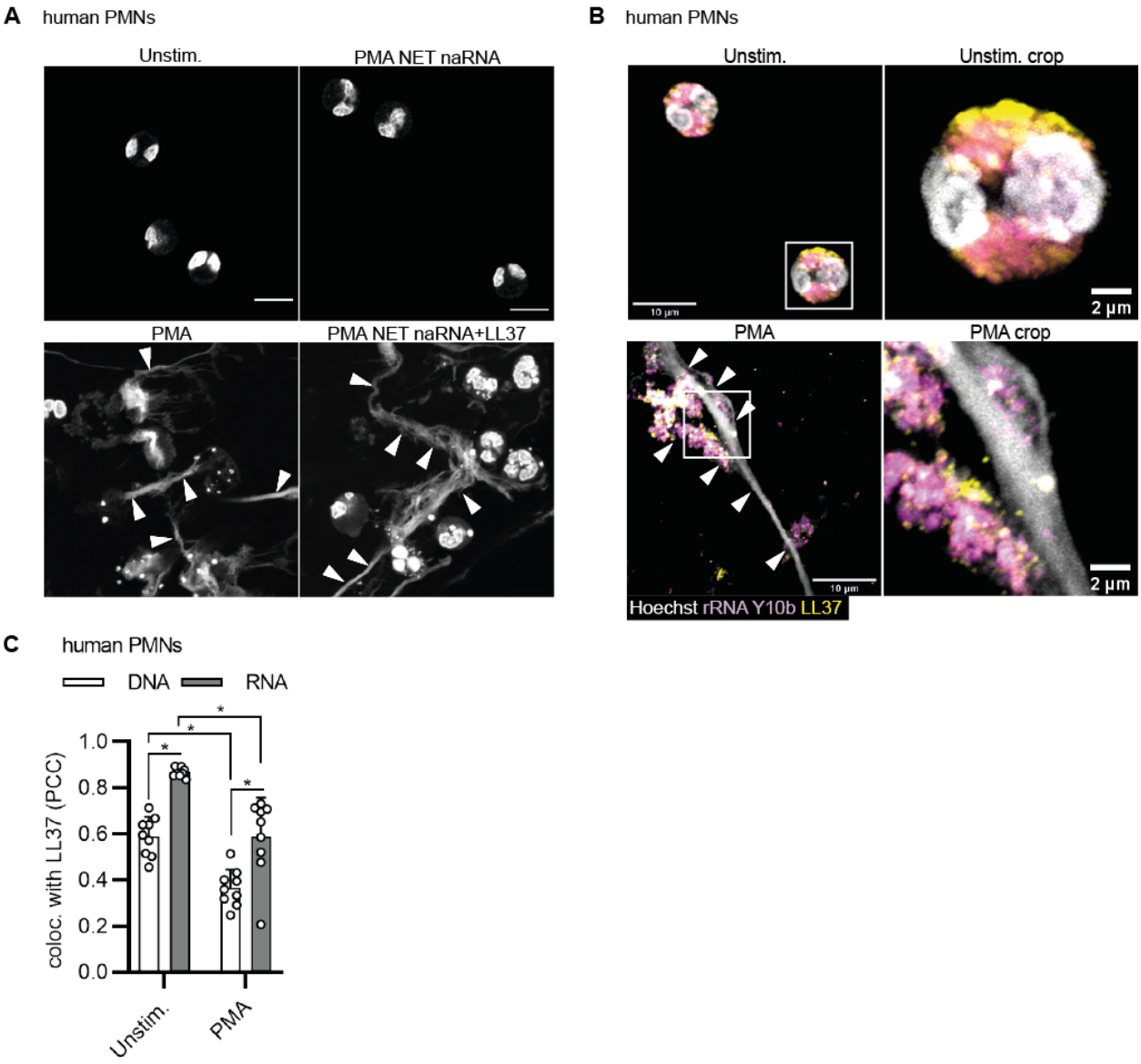

Figure 3.16: LL37 restores the NET-inducing properties of and co-localizes with naRNA.

(A) Confocal microscopy of primary human PMNs left unstimulated or stimulated (3 h) with PMA (600 nM, positive control), or purified naRNA (*cf.* Fig. 3.6) alone or in complex with exogenously added LL37 stained for NETs/DNA (Hoechst 33342; n = 3, representative images, scale bar: 10 µm). **(B)** Confocal microscopy of primary human PMNs stimulated with PMA (600 nM) for 3 h and stained for naRNA (anti-rRNA Y10b, magenta), LL37 (anti-hLL37-DyLight550, yellow), and DNA (Hoechst 33342, white, n = 3, representative images, scale bar 10 µm). **(C)** Pearson's correlation coefficient (PCC) (colocalization) analysis of **B** (n = 3, combined data, mean+SD, each dot represents one image, three images/condition, *p<0.05 according to one-way ANOVA).

3.5.2 naRNA-LL37 complexes are found in resting PMNs as a pre-assembled composite DAMP

It is of common knowledge that LL37 is localized in specific granules of neutrophils (Sorensen et al. 1997) and ribosomal RNA is mainly located in the nucleolus (Pederson 2011). Thus, both components were assumed to reside in distinct cell organelles prior to stimulation. Nevertheless, the PCC analysis of this study (*cf.* Fig. 3.16C) suggested a colocalization of naRNA (stained with anti-rRNA Y10b) and LL37 (stained with anti-LL37) in resting neutrophils. To investigate this colocalization in more detail, more precise line plot analysis was performed in order to pinpoint the exact origin of the two fluorescence signals of neutrophil rRNA and LL37 to gain information about their cellular localization. Therefore, primary human PMNs were stained for rRNA and LL37 as previously described and high-resolution confocal microscopy images were obtained. Line plot analysis (of the images obtained for Fig. 3.16B) was carried out with Zen Blue (Zeiss, Version 3). Here, shared co-localization maxima were observed, indicating that rRNA and LL37 are localized in very close proximity in the resting cell. This suggested further that some neutrophil rRNA and LL37 complexed already in intact neutrophils (Fig. 3.17A). In addition, in PMA-treated NET-forming neutrophils naRNA and LL37 were found to share colocalization maxima as well (Fig. 3.17B). This further indicated the existence of naRNA-LL37 complexes in NETs. Bearing in mind that z-resolution even for AiryScan analysis is far lower than x-/y-resolution, further investigations appeared necessary to corroborate this notion more fully.

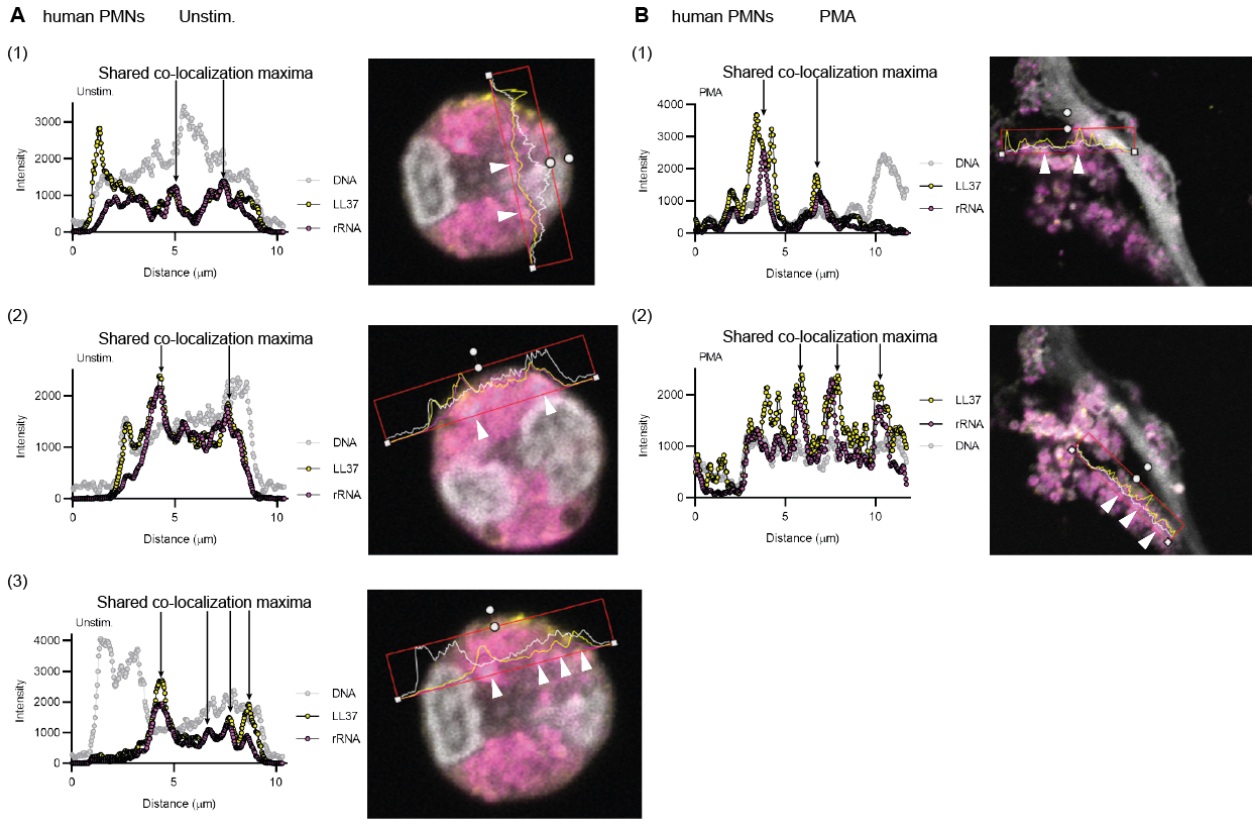

Figure 3.17: Line plot analysis of naRNA and LL37 in human PMNs reveals colocalization in unstimulated cells.

Confocal microscopy of primary human PMNs **(A)** unstimulated or **(B)** stimulated with PMA (600 nM) for 3 h and stained for naRNA (anti-rRNA Y10b, magenta), LL37 (anti-hLL37-DyLight550, yellow), and DNA (Hoechst 33342, white, n = 3, representative images). The line plot analysis of LL37, RNA, and DNA staining was performed using Zen Blue3 software. Two to three different line plots from representative images are shown.

First, using ultrathin sections of only approximately 50 nm thickness for IF permits the creation of extremely high resolution images and minimizes the risk for false location, since the signal is confined to originate from a very condensed volume (Takizawa and Robinson 2004). Thereby, IF microscopy of ultrathin sections provides an even more specific way to investigate the pre-association of naRNA and LL37. Hence, ultrathin sections (50-60 nm thickness) of primary human unstimulated PMNs were stained as described above, and line plot analysis was again performed using ImageJ-Win64 (NIH). Hereby, shared colocalization maxima of rRNA- and LL37-signals were found in punctate vesicle-like structures inside the cell, probably representing neutrophil granules (Fig. 3.18A). Thus, this specific IF microscopy analysis additionally revealed the presence of RNA-LL37 complexes in resting neutrophils and confirmed the previous findings of naRNA-LL37 pre-assembly in intact cells.

Last but not least, transmission EM (TEM), enabling a resolution of approximately 2 nm (Malatesta 2021), was used to investigate the cellular location and storage compartment of naRNA-LL37 complexes in resting neutrophils. To label LL37 and rRNA, staining of primary human PMNs with anti-rRNA Y10b and anti-LL37 antibodies and subsequent immunogold labeling with 6 nm (black arrows) and 12 nm (white arrow)-sized secondary antibodies, respectively, was performed. It has to be borne in mind that gold

particles repel each other (Flechsler et al. 2020), so that labeling of actual complexes is nearly impossible. Nevertheless, multiple granules were detected in which both 6 nm (rRNA, black arrows) and 12 nm particles (LL37, white arrows) were detected (Fig. 3.18B), indicating that rRNA and LL37 are found in the same subcellular compartment. This makes it highly likely that both are engaged in a novel composite DAMP complex.

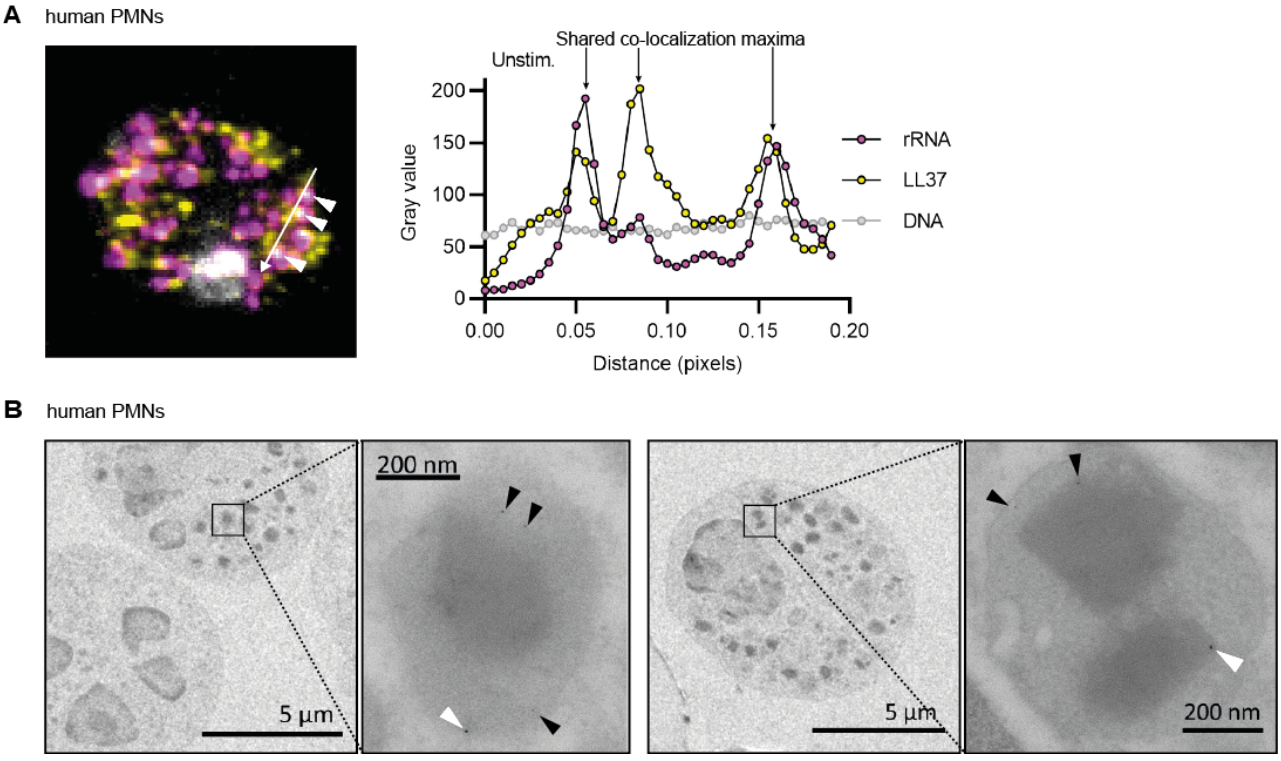

Figure 3.18: naRNA-LL37 complexes can be found pre-assembled in intact neutrophils.

(A) Confocal microscopy on ultrathin sections of primary human PMNs (unstimulated) stained for naRNA (anti-rRNA Y10b, magenta), LL37 (anti-hLL37, yellow), and DNA (Hoechst 33342, white, n = 3, representative image, scale bar 2 µm). Line plot analysis was performed using ImageJ-Win64 software (n=3, representative graph). **(B)** Transmission electron microscopy of unstimulated human primary PMNs using anti-rRNA and anti-hLL-37 primary and immunogold (6 nm (black arrow) and 12 nm (white arrow), respectively)-labeled secondary antibodies (n = 3, representative images, scale bars as indicated, high zoom images show one exemplary vesicle-like structure of the corresponding PMN). Electron microscopy and IF microscopy of ultrathin sections was performed by the group of Katharina Hipp, Electron Microscopy Facility, Max Planck Institute for Biology Tübingen.

Taken together, this data provides strong evidence that naRNA and LL37 not just complex 'by chance' during the extrusion in the process of NET formation, but that they rather represent a novel composite DAMP pre-stored for extrusion even in resting neutrophils from healthy donors.

4 Discussion

In summary, the key findings of this study were

- naRNA is a common component of human and murine NETs, independent of the stimulus and type of NET formation induced.
- naRNA mediates self-amplification of NETs in naïve primary human PMNs in a TLR8-dependent manner.
- naRNA activates naïve murine BM-PMNs dependent on Tlr13-signaling.
- naRNA induces TLR8-dependent macrophage activation, and further mediates cytokine release in PBMCs and NK cells, as well as activation of keratinocytes.
- naRNA induces skin inflammation *in vivo* dependent on Tlr13-signaling.
- RNA-sensing enhances disease progression in the IMQ mouse model for psoriasis.
- naRNA-mediated PMN activation is dependent on its complexation with LL37.
- naRNA-LL37 complexes are pre-assembled composite DAMPs which can be found in vesicle-like structures of resting neutrophils.

These discoveries are discussed in more detail in the following. Furthermore, open questions which arose from this study, such as the downstream signaling pathway of TLR8-induced NET formation, the pre-assembly process of naRNA and LL37, and the potential role of naRNA in NET-related diseases (Fig. 4.1), as well as possible therapeutic implications targeting naRNA are addressed (Fig. 4.4).

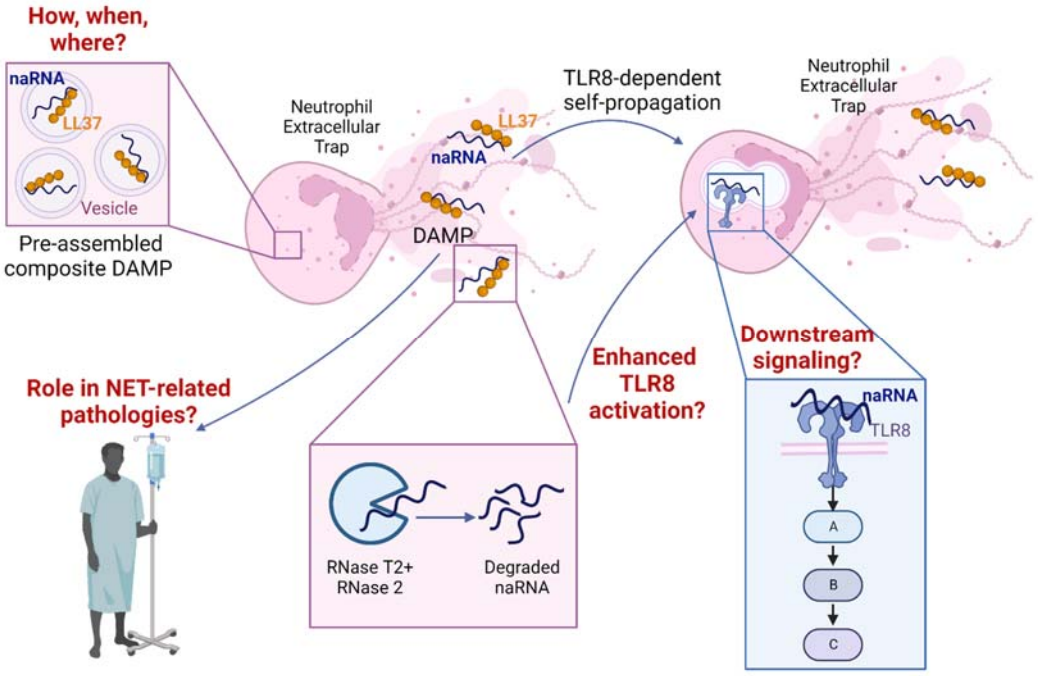

Figure 4.1: Open questions.

Dependent on the findings reported in this study, the following open questions arose: 1. What is the detailed structure of naRNA, what are possible modifications, and what strategies for naRNA-clearance to avoid adverse effects by e.g. digestion of naRNA with the wrong RNases, such as RNase T2 and RNase 2, could be applicable? 2. How is the TLR8-dependent NET formation mediated in detail and which molecules play a role in downstream signaling? 3. How, when, and in which cellular compartment do naRNA and LL37 pre-assemble to a composite DAMP? 4. What are the possible DAMP activities of naRNA in NET-related pathologies, since naRNA could be the so far undiscovered driver of such diseases? Created with BioRender.com.

4.1 The properties of naRNA

4.1.1 naRNA is a common component of NETs, independent of the NET-formation pathway

No matter if the NET formation process is suicidal, as e.g. after stimulation of PMNs with PMA, inducing a NADPH oxidase-dependent and ROS-producing pathway leading to chromatin decondensation, or if the release of NETs occurs in a vital way, e.g. upon contact with activated platelets, depending on PAD4 activity and leaving an almost completely functional, anucleated neutrophil behind, the outcome is the same: chromatin decondensation is caused by citrullination of histone H3 and the chromatin is released from the neutrophil together with granular proteins (Huang et al. 2022). The release of NET-associated RNA (naRNA) has been first described by Herster et al. in 2020, upon stimulation with PMA (suicidal NET formation (Kenny et al. 2017)) and ssRNA-LL37 complexes (Herster et al. 2020), whereby the basic NET formation pathway of the latter remains to be elucidated. In addition, NETs spontaneously formed by SLE patient-derived neutrophils were shown to release RNA more recently (Blanco et al. 2021), with elusive

underlying type of NET formation. This study is the first to show that naRNA is released in both types of NET formation: the suicidal one, induced herein by PMA and nigericin, as well as the vital NET formation, induced by live *C. albicans* (*cf.* Fig. 3.2A, B). It can therefore be concluded that naRNA is a common component of NETs, independent of the stimulus used to induce the extracellular trap release.

However, the third, less common, and poorly understood NET formation pathway, in which mitochondrial instead of nuclear DNA gets extruded by the living cell (de Buhr and von Kockritz-Blickwede 2016), has not been investigated in the present study. The mitochondrial NET formation has been observed upon GM-CSF priming and subsequent short-term receptor (TLR4 or C5a) stimulation (Yousefi et al. 2009), requiring the formation of mitochondrial ROS. Since this form of NET release is considered as non-suicidal and behaves similar to the vital form in which nuclear DNA gets extruded (Ravindran, Khan, and Palaniyar 2019), it can be hypothesized that naRNA is most likely also a component of mitochondrial NETs, although this remains to be investigated. To answer this question, one could prime and stimulate primary human PMNs as described in literature to induce mitochondrial NET formation (Yousefi et al. 2009) and stain for RNA as performed in the underlying study. Subsequent microscopy analysis could then possibly reveal the presence of naRNA in the mitochondrial type of NETs.

Moreover, extracellular traps (ETs) cannot only be released dependent on different pathways by neutrophils, but furthermore by other cells, like mast cells, eosinophils, basophils, and macrophages (Doster et al. 2018). Specifically, monocytes/macrophages have been shown to release extracellular traps (METs) upon stimulation with e.g. *Escherichia coli*, *Staphylococcus aureus*, *Candida albicans*, and PMA, amongst others. Similar to suicidal NET formation, METs are extruded upon a cell death mechanism in which DNA fibers complemented with cellular proteins are released. Given the similarities between NETs and METs (Doster et al. 2018) it is likely that MET-associated RNA could be revealed as a common component of these structures.

Besides macrophages, mast cells (MCs) have been shown to release their nuclear DNA in an antimicrobial host defense mechanism: the formation of MC extracellular traps (MCETs), to entrap and kill various microbes, such as *Staphylococcus aureus* or *Candida albicans*. This mechanism is dependent on the activity of NADPH oxidase and subsequent ROS production similar to suicidal NET formation. The nuclear DNA is released together with cytoplasmic and granular proteins in MCETs, which can induce enhanced proinflammatory responses in addition to their antimicrobial properties. Looking at the similarities between NETs and MCETs (Mollerherm, von Kockritz-Blickwede, and Branitzki-Heinemann 2016) it would not be surprising to observe RNA as a further MCET component, similar to naRNA.

Basophils and eosinophils, other members of the granulocyte family (Geering et al. 2013), have also been reported to release extracellular traps in an analogous fashion. In eosinophils, the release of mitochondrial DNA, similar to mitochondrial NET formation, was observed as an antibacterial defense mechanism (Yousefi et al. 2008). Comparable observations were made for basophils releasing basophil extracellular traps (BETs), independent of NADPH oxidase, containing mitochondrial DNA and granular proteins (Morshed et al. 2014). Since mitochondrial NET formation was not characterized regarding naRNA-release in this study, one can only speculate if RNA could be a common component of the mitochondria-related ETs released by eosinophils and basophils.

In the underlying study, complexation with the antimicrobial peptide LL37 emerged as vital in the context of inducing naïve NET formation (*cf.* Fig. 3.16A). Although macrophages, eosinophils, and mast cells have been reported to express LL37 (Lishko et al. 2016), it would therefore not only be of interest if ETs derived of those other immune cells contain RNA, but also if LL37 is found in their ETs, thereby enabling RNA-LL37 DAMP activities. The antibodies validated in this study could be used for such an analysis. Since the afore mentioned cells (macrophages and MCs) react with extracellular trap release upon interaction with the same pathogens, e.g. *Staphylococcus aureus* and *Candida albicans* (Doster et al. 2018; Mollerherm, von Kockritz-Blickwede, and Branitzki-Heinemann 2016), which are also known to induce NET formation (Kenny et al. 2017; Tan, Aziz, and Wang 2021), one could hypothesize the following: Even if METs and MCETs do not contain LL37, the RNA released by macrophages and MCs could also form complexes with the highly abundant NET-derived LL37, thus further contributing to inflammation. Investigating macrophages, MCs, eosinophils, and basophils in a microscopy approach regarding RNA and LL37 release during their ET formation would be a simple experiment to address those open questions.

4.1.2 The composition of naRNA

Throughout this whole study, an anti-rRNA Y10b antibody was used to stain naRNA in NETs. Thus, this research work clearly shows that naRNA consist of ribosomal RNA. However, RNA sequencing analysis revealed that the percentage of rRNA in naRNA is much lower than in whole PMN RNA (*cf.* Fig. 3.6B). Instead, higher amounts of mRNA, pseudogenes, ncRNA, and alternatively spliced transcripts were observed. This data indicates that neutrophil RNA transcription is remodeled before the release of this nucleic acid into the extracellular space. Moreover, metabolic labeling of naRNA additionally showed that rRNA is not the only type of RNA found in NETs: instead, all kinds of newly transcribed RNA seems to be extruded by the cells (*cf.* Fig. 3.4), since 5-EU incorporates in the latter (Bao et al. 2018). In the case of endosome-derived exRNAs released by various kinds of cells, the expression profiles of those have been reported to be different from their parental cells. Additionally, exRNAs are suggested to be actively selected and extruded (Tosar, Witwer, and Cayota 2021). Comparing the findings of naRNA to the state of the art of exRNAs in literature, naRNA should be considered as a type of exRNA, which gets actively selected and extruded into the extracellular space. Why naRNA is released as an immune-shaping exRNA remains to be elucidated and is further discussed in the following sections.

4.1.3 naRNA as an endogenous, sterile NET-inducing agent

It is also important to note that naRNA belongs to the group endogenous, sterile NET-inducing agents, which have not been frequently reported in literature. Although NETs are known to play roles and are commonly found in noninfectious diseases, such as autoimmune diseases, rheumatic diseases, thrombosis, and diabetes (Zhao and Jin 2022), little is known about the exact stimuli that induce the release of NETs. The following sterile agents for NET formation are described in literature (Table 4.1).

Table 4.1: Sterile NET-inducing agents.

Stimulus	Associated disease/pathology	Pathway	Experiment	Literature
Monosodium urate (MSU) crystals	Gout	ROS-dependent	*In vitro* and *in vivo* stimulation with MSU crystals	(Schauer et al. 2014)
Sialyl Lewis(X)	-	L-selectin	*In vitro* NET assay	(Mohanty et al. 2015)
Cathepsin C	Breast cancer	PR3-IL-1β axis, p38 activation and ROS production	*In vitro* and *in vivo* NET assay	(Xiao et al. 2021)
IL-8	Atherosclerosis	CXCR2, ERK, MAPK	*In vivo* model for atheroscleorisis	(An et al. 2019)
IL-17	Pancreatic cancer	-	*In vitro* NET assay	(Zhang et al. 2020)

As displayed in Table 4.1, only few sterile agents known to induce NET formation and their associated signaling pathways are described in literature. Monosodium urate (MSU) crystals have been reported to induce a ROS-dependent NET formation in patients suffering from gout, as shown by *in vitro* and *in vivo* analysis (Schauer et al. 2014). Moreover, sialyl Lewis(X) derived from saliva has been shown to induce *in vitro* NET formation via L-selectin binding (Mohanty et al. 2015) and cathepsin C was reported to induce the release of NETs by activating the PR3-IL-1β axis, subsequent p38 activation, and ROS production in breast cancer (Xiao et al. 2021). It has furthermore been demonstrated that the cytokines IL-8 and IL-17 can induce NET formation in sterile conditions. IL-8 was shown to induce neutrophil activation via CXCR2 and the ERK/MAPK pathway in atherosclerosis (An et al. 2019), whereas IL-17 was observed to induce NETs in pancreatic cancer (Zhang et al. 2020). This research work therefore provides an important comprehensive *in vitro* and *in vivo* study describing a novel, sterile NET-inducing agent and the related signaling receptor: naRNA via TLR8. Thereby, this study helps to gain deeper insights into NET-related non-infectious inflammatory processes. However, a big remaining open question is the detailed signaling pathway of naRNA acting as an endogenous TLR8-ligand, which is discussed in detail in the following section.

4.1.4 NET-related TLR8 signaling: which pathway does naRNA induce?

As observed in a previous study of this group, LL37 is capable of transferring RNA into human neutrophils, leading to the activation of TLR8 (Herster et al. 2020). It was shown in the current research work that NETs mainly induce TLR8 activation (only slight TLR7 activity was observed, *cf.* Fig. 3.9A), naRNA-dependent induction of NET formation can be blocked by a TLR8 inhibitor (*cf.* Fig. 3.9B, D), and that naRNA-sensing *in vivo* relies on Tlr13 (*cf.* Fig. 3.14C). Due to the observations of naRNA-LL37 complexes in NETs (*cf.* Fig. 3.16B, C, 3.17B), one can assume that naRNA transport into naïve PMNs, and possibly also into other cells, is mediated by LL37, as previously shown for other RNA types (Herster et al. 2020). Hence, the endosomal receptors TLR8 in human and Tlr13 in mice can get activated. Fluorescent labeling of NET-derived naRNA and LL37 and subsequent microscopy analysis to investigate the uptake of these complexes into other cells could help to further confirm this hypothesis. Although this study proves the role of TLR8 in naRNA-dependent self-propagation, little is known about TLR8-induced NET formation. The previous research

work published by our group (Herster et al. 2020) is one of very few so far to show that NET formation can be induced by TLR8-signaling (Saitoh et al. 2012; Lood et al. 2017; Smolarz et al. 2021). Thus, further research work investigating TLR8-mediated NET formation is necessary for subsequent therapeutic implications later on. The data presented in the current study already indicates that naRNA/TLR8-mediated NET formation is PAD4-dependent (*cf.* Fig. 3.9C). It should be additionally investigated if ROS production is mediated. This could be assessed by using carboxy-2', 7'-dichlorodihydrofluorescein diacetate, a molecule which becomes fluorescent after its oxidation, thus indicating the presence of ROS (Janke et al. 2009). To furthermore examine if the here presented process is glucose-dependent, PMNs could be cultured in glucose-free medium and the self-propagation NET assay could be performed *in vitro*, similar to assays reported in literature. In addition, NET formation has been reported to be blocked by CDK4/6 inhibitors, which would prevent the translocation from NE to the nucleus (Tan, Aziz, and Wang 2021). Using such inhibitors in the NET assay performed in this study could provide further insights in downstream events of naRNA-LL37 complex-induced NET formation. Assuming that naRNA activates the canonical TLR8 pathway, MYD88 and IRAKs would be downstream mediators (Murphey, Weaver, and Berg 2022). Thus, using small molecule inhibitors for MYD88 (e.g. M20 (Song et al. 2021) or compound 4210 (Saikh et al. 2020)) or IRAK (e.g. BAY1834845 for IRAK4 inhibition (Wiese, Manning-Bennett, and Abuhelwa 2020)) could reveal the role of those adaptor proteins. Taken together, deeper knowledge about naRNA-mediated TLR8 downstream signaling and factors involved in the subsequently induced NET formation would be advantageous for therapeutic implications targeting naRNA-induced inflammation, which are discussed in detail in section 4.5.

Besides the detailed TLR8-pathway, the ligand characteristics of naRNA should be investigated more thoroughly. Although application of RNase A has been reported to prevent the host from disease progression as previously described (Fruh et al. 2021; Lasch et al. 2020), digest of RNA with the 'wrong' enzyme could even enhance RNA-mediated immune responses. In 2019, the lysosomal endoribonuclease RNase T2 was described to be crucial for providing exogenous RNA-derived ligands detectable for TLR8 *in cellulo* (Greulich et al. 2019). One year later it was observed that the endolysosome-derived ribonucleases RNase T2 and RNase 2 cooperate to digest synthetic, bacterial, and protozoan RNA to release uridine, thus creating TLR8 ligands which potently activate this receptor (Ostendorf et al. 2020). In addition, TLR8 was reported to sense uridine- and guanosine-rich ssRNA, as well as RNA-derived short oligonucleotides, leading to its activation (Tanji et al. 2015). Thus, one should consider to investigate the sequence of naRNA and its degradation products created by RNases in detail to gain insights in possible adverse modulations, potentially enhancing TLR8-activation and thus resulting in greater immune responses.

4.2 naRNA acts as a novel class of composite DAMP

As previously mentioned, naRNA alone does not induce NET formation in naïve PMNs, only when complexed with LL37 (*cf.* Fig. 3.16A). Interestingly, naRNA-LL37 complexes were not only observed in NETs, but further found in vesicular structures in resting neutrophils (*cf.* Fig. 3.16B, C, 3.17, 3.18). This indicates that naRNA-LL37 complexes rather act as pre-assembled composite DAMPs than being 'accidentally' formed during the process of NET formation.

LL37, the only cathelicidin existing in humans, is constitutively expressed in neutrophils and stored in their cytoplasmic granules, which are released upon leukocyte activation (Zanetti, Gennaro, and Romeo 1995). Besides its antimicrobial properties, LL37 exerts chemoattractant functions, can inhibit apoptosis of neutrophils, and induce cytokine release, such as IL-8 (Bucki et al. 2010). That LL37 alone can trigger NET formation was, however, ruled out earlier (Herster et al. 2020).

For the performance of the LL37-colocalization experiments in this study (*cf.* Fig. 3.16B, C, 3.17, 3.18), naRNA was stained with an anti-rRNA Y10b antibody, detecting ribosomal RNA (Lerner et al. 1981), which is mainly located in the nucleoli of intact cells (Ali et al. 2021). Since LL37 is primarily found in specific granules (Minns et al. 2021), thus in another cellular compartment, the question of how naRNA and LL37 colocalize in neutrophil vesicles arises. To first further confirm the pre-complexation of naRNA and LL37 in resting cells by a validated method, the so-called proximity ligation assay (PLA) could be of use. In this assay, two primary antibodies of choice, which would be anti-rRNA Y10b and anti-LL37 in our case, which should be derived of different species (here mouse and rabbit, respectively), would be used in a first step to bind to the target antigens. Those primary antibodies would then be labeled with the respective secondary antibodies, which in turn are conjugated to so-called PLUS and MINUS probes. Those probes contain a unique DNA strand each, which hybridize to circular DNA once the two target antigens interact with each other, thus, are in very close proximity. Lastly, complementary oligonucleotides for this specific circular DNA which are fluorescently labeled would be used to visualize the interacting targets of interest (Alam 2022). Hence, naRNA-LL37 complexes could be detected using high resolution microscopy and defined as definitely colocalizing molecules by this approach.

In this underlying study, PMNs have not been characterized by their expression of the different types of granules (primary, secondary (Gierlikowska et al. 2021), or tertiary (Teng et al. 2017)), which might impact the colocalization of naRNA and LL37 as composite DAMPs, since LL37 was mainly reported to be part of secondary granules (Minns et al. 2021). For detailed investigation, one could add further antibodies to examine the specific granule status in immunofluorescence microscopy. Since MPO is found in high amounts in primary granules (Zhang et al. 2022) and gelatinase is only found in tertiary granules (Lawrence, Corriden, and Nizet 2018), using an anti-MPO antibody and an anti-matrix metallopeptidase 9 (MMP-9; also known as gelatinase B) antibody, respectively, could be of use to define the stage of granulopoiesis of the investigated cells (Zhang et al. 2022).

As before discussed, naRNA could be actively released as a form of exRNA, derived from vesicular structures (see section 4.1.2). Thus, PMNs might upregulate the expression of certain RNAs, followed by their re-localization to vesicular/granular structures, in which complex formation with LL37 as a composite DAMP occurs. To prove this hypothesis, further research needs to be performed, e.g. via a detailed

trafficking analysis of neutrophil RNA, to follow its production and localization to distinct cellular compartments. Therefore, stem-cell derived PMNs metabolically labeled with 5-EU as for the antibody-independent staining analysis of naRNA (*cf.* Fig. 3.4) performed in this study could be of use. Metabolically labeled endogenous neutrophil RNA could be investigated over time using click-chemistry labeling and live immunofluorescence microscopy, to follow its expression and localization to cellular compartments. However, labeling of the RNA without previous fixation and permeabilization of the cell would be a requirement to investigate live and physiologically relevant RNA-trafficking, which was not performed in the underlying study. Furthermore, to actually observe such delicate cellular structures like neutrophil granules, high resolution imaging is necessary. However, this is not applicable in live cell imaging in regular confocal microscopy due to intensive exposure times. To bypass these methodological problems, one could also switch from live cell imaging to analysis of cells which were fixed at different time points. Furthermore, isolation of neutrophil granules/vesicles and investigation of the contained components could reveal the presence of naRNA, which would be expected according to the findings presented in this study. Therefore, a similar approach as described in literature could be used: First, disruption of neutrophils in the according buffer could be performed, followed by subcellular fractionation of the released granules dependent on their densities and subsequent separation using a fraction collector. Afterwards, markers for the granular subsets (MPO: primary, LL37: secondary, MMP-9: tertiary) to identify the fractions could be investigated using ELISA (Rorvig et al. 2013). Subsequently, naRNA could be purified from the distinct granule subsets using an RNA-isolation kit as described in section 2.2.8 and additional analysis with a Nanodrop Spectrophotometer or RNA sequencing could be performed. In addition, cryo-EM, which is considered a revolutionary method to examine 3D structures of biomolecules (Danev, Yanagisawa, and Kikkawa 2019), could provide deeper insights in the structure of naRNA-LL37 complexes. Therefore, isolated naRNA (as described in section 2.2.8) complexed with LL37 (as described in section 2.2.1 and used for *cf.* Fig. 3.16A) could be added onto a cryo-EM grid and plunge-frozen as described in literature. Subsequently, EM imaging could be carried out followed by density mapping and structure remodeling (Yip et al. 2020). Taken together, further investigation of how, when, and where naRNA and LL37 assemble in the cell would help to shed light on and further prove this unexpected finding of naRNA-LL37 composite DAMPs, which is contradictory to the current knowledge of RNA and LL37 biology.

4.2.1 naRNA rather acts pro-inflammatory than providing host defense

It has been described in literature that LL37 loses its antimicrobial properties when bound to DNA (Weiner, Bucki, and Janmey 2003). In addition, DNA-LL37 complexes have been observed to induce proinflammatory responses in DCs leading to a break of tolerance to host-derived DNA (Lande et al. 2007). This concept implies that LL37 overrides normal compartmentalization-mediated tolerance to DNA. Two years later, similar findings have been made for host-derived RNA: in complex with LL37, self-RNA was found to induce DC activation in the context of psoriasis (Ganguly et al. 2009). Previous findings of our group showed that self-RNA or synthetic/bacterial RNA complexed with LL37 additionally lead to PMN activation and NET release (Herster et al. 2020). Moreover, in the current study, the observations made by Brinkmann et al. in 2004 that NET-associated DNA is crucial for the antibacterial effects of NETs (Brinkmann et al. 2004) could not be linked to naRNA (*cf.* Fig. 3.7). Thus, the research focus of the present study turned to the investigation of naRNA as a proinflammatory DAMP, which was indeed confirmed: it was shown in this research work that naRNA-LL37 complexes were sufficient to propagate NET formation

in naïve PMNs (*cf.* Fig. 3.16A) and that NET content induced various immune responses in a naRNA-dependent manner, such as skin inflammation *in vivo* (*cf.* Fig. 3.14), as well as additional NET release (*cf.* Fig. 3.8B-E) and cytokine extrusion (*cf.* Fig. 3.11-3.13). The induced IL-8 release in macrophages (TLR8-dependent) and keratinocytes possibly leads to subsequent PMN recruitment *in vivo*, as this chemokine is a potent neutrophil attractant (Metzemaekers, Gouwy, and Proost 2020), further highlighting the self-amplifying DAMP properties of naRNA. In literature, many NET-associated DAMPs have been described (see Table 4.2) (Block, Rossaint, and Zarbock 2022).

Table 4.2: NET-associated DAMPs.

Abbreviations: cfDNA – cell free DNA, HMGB1 – High-Mobility Group Box 1. Adapted from Block et al. (2022) (Block, Rossaint, and Zarbock 2022).

DAMP	NET-Association	TLRs involved	Experiments
Histones	Part of NETs Induce NET formation	TLR2, TLR3, TLR4, TLR9	Murine models; human NETs used as stimulus for *in vitro* experiments (Block, Rossaint, and Zarbock 2022)
cfDNA	Part of NETs	TLR9	*In vitro* stimulation with human genomic DNA or synthetic CpG-oligonucleotides (Lande et al. 2007)
LL37	Protects NET-DNA; Induction of NET formation through anti-LL37 autoantibodies	TLR4, TLR7, TLR8, TLR9, Tlr13	*In vitro* NET degradation assay (Neumann et al. 2014); anti-LL37 antibodies found in patient sera and suggested to be NET-related (O'Neil et al. 2021)
HMGB1	Induce NET formation; Part of NETs	TLR2, TLR4, TLR9	Elevated HMGB1 levels found in tissue of lupus nephritis patients suggested to be NET-related (Whittall-Garcia et al. 2019); *in vitro* co-culture of NET-forming PMNs and macrophages (Peng et al. 2017)

It has been shown that NET-derived histones induce TNF, IL-6, and IL-10 release in a TLR4-dependent manner in mice, and additionally trigger immune cell recruitment. In patients suffering from sepsis or various autoimmune diseases, elevated levels of NET-associated cell free (cf)DNA, contributing to sustained inflammation and inducing the release of proinflammatory cytokines, have been detected. LL37, which can be found in high abundance in NETs, was observed to induce polarization of macrophages to the M1 (proinflammatory) type, activation of the inflammasome, and release of type I IFN. Furthermore, anti-LL37 autoantibodies, directed against this cathelicidin expressed on neutrophil surfaces, have been identified to promote additional NET formation. HMGB1, also released during NET formation, can cause sterile inflammation. It is capable of inducing the recruitment of PMNs to the site of infection, as well as activation of macrophages and endothelial cells. In turn, proinflammatory cytokine, chemokine, or adhesion molecule production gets enhanced (Block, Rossaint, and Zarbock 2022). Comparing the observations made for naRNA as a potent stimulus of proinflammatory responses in this study to the other NET-derived DAMPs described in literature, it is simple to conclude that naRNA should be added to the list of DAMPs associated to NETs. Compared to the above-described reports, this underlying study is the

first to unequivocally show that the observed DAMP effects of naRNA are mediated by this NET component by using NETs as a direct stimulus not only *in vitro* but further *in vivo*. Thus, this study provides higher physiologically relevant insights into the immunomodulatory effects of naRNA than described for other NET-associated DAMPs. By using KO systems (e.g. *Unc93b1*$^{-/-}$ and *Tlr13*$^{-/-}$ mice, *cf.* Fig. 3.10) and an inhibitor to target human TLR8 (CU-CPT9a for TLR8 inhibition, *cf.* Fig. 3.9B, D) this study furthermore provides solid information about the underlying signaling of this novel DAMP, more specifically about the role of Tlr13 and TLR8 in mice and human, respectively.

However, naRNA was not investigated in this study regarding the described antiviral effects of NETs. Saitoh et al. (2012) showed that the infection efficiency of HIV was reduced when the virus was in contact with PMA-induced NETs, which could be recovered by digesting NETs with DNase (Saitoh et al. 2012). In a future approach, this experimental set up could be used to investigate the effects of NETs on the infection efficiency after RNase digest, thus giving information about the role of naRNA in antiviral responses.

4.2.2 naRNA-related DAMP activities could be linked to early NET responses

Given the previous findings of proinflammatory properties of NETs and naRNA, a mechanism to keep NET formation in check is needed to prevent sustained inflammation that could lead to autoimmunity, which is detrimental to the host (Block, Rossaint, and Zarbock 2022). It has been proposed that NETs get cleared by macrophages in a 'silent' process, without inducing further immune responses (Farrera and Fadeel 2013). More recently, macrophages have been observed to clear NETs in a LL37-signaling-dependent manner with the help of DCs, which provide DNase for digest of NETs (Lazzaretto and Fadeel 2019).

In recent studies, the effect of RNase A to prevent NET-related pathologies came into research focus. In a murine model of subarachnoid hemorrhage, intravenous application of RNase A significantly reduced the burden of NETs in brain parenchyma, thereby preventing further immune activation and inflammation (Fruh et al. 2021). Moreover, leukocyte recruitment and NET formation was significantly reduced by RNase A treatment in a murine model for ischemic muscle injury. In addition, reduced amounts of proinflammatory M1 macrophages and increased amounts of anti-inflammatory M2 macrophages were observed (Lasch et al. 2020). Furthermore, many RNases are known to be expressed in humans, with RNase1 being the human homologue of RNase A and playing crucial roles in different pathologies, such as autoimmune diseases and cancer (Huang et al. 2014).

Given those recent research observations and the knowledge about lymphocytic RNA as a rather short-lived molecule (Berger and Cooper 1975), one could hypothesize that naRNA serves as an early and transitory DAMP in NETs, inducing proinflammatory responses to help clear pathogens or a sterile insult shortly after NET extrusion, when naRNA and LL37 are associated with the NET. Over time, clearance of NETs and thus naRNA by macrophages or degradation of naRNA by serum RNases, i.e. RNase1, could lead to the eventual loss of the DAMP. In addition, DNase degradation of the NET-DNA backbone therefore making naRNA more accessible could also affect its extracellular presence. In consequence, naRNA-dependent immune activation would stop, and the inflammation could be resolved (Fig. 4.2). It would therefore be of interest to investigate the stability and life span of naRNA in further studies. For experimental assessment, one could induce NET-formation for IF and microscopy *in vitro* as described in

this study and add human serum to the cells. If serum-derived RNases digest naRNA over time, the naRNA-derived fluorescence signal should be lost, which could be detected by a time course analysis. In addition, one could perform a co-culture experiment of macrophages and NET-releasing neutrophils. Likewise, IF staining and microscopy analysis could reveal naRNA-uptake by macrophages. To be able to distinguish naRNA from macrophage self-RNA, metabolically labeled (5-EU) stem-cell derived PMNs could be used. Subsequently, click chemistry could be performed to only stain PMN RNA. Further knowledge about physiological naRNA-clearance processes could later on be useful to develop therapeutic strategies to target naRNA-induced inflammation.

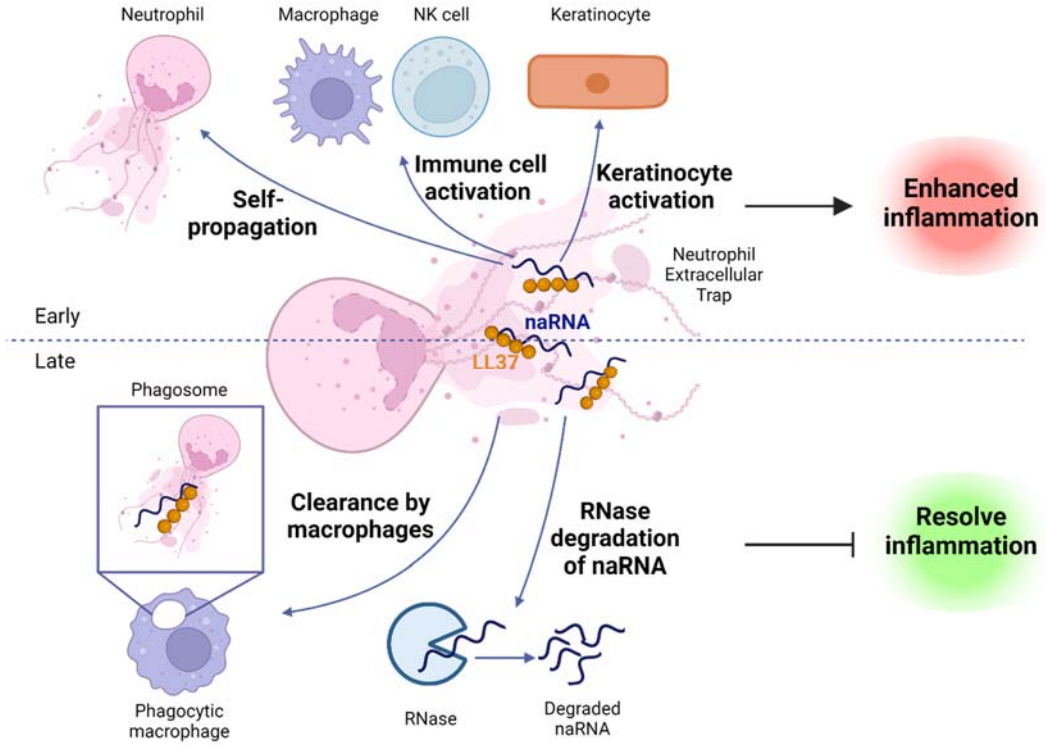

Figure 4.2: naRNA as an early inflammation-enhancing DAMP.

At early stages of inflammation, naRNA could act as an activator of immune cells and keratinocytes, and induce self-propagation of NETs, to enhance inflammation and thus, pathogen clearance. During later stages, naRNA could be removed by uptake and clearance of NETs through macrophages or degradation of naRNA by serum-derived RNases, e.g. RNase1. Thus, the DAMP-properties of naRNA would be lost and inflammation could be resolved. Created with BioRender.com.

4.3 Re-defining NETs: intentional release of DAMP webs

In the very first report by Brinkmann et al. (2004), NETs were initially defined as an antimicrobial host defense mechanism, capturing, and killing bacteria (Brinkmann et al. 2004). Following studies described NETs as an effective mechanism against a broad variety of pathogens, such as fungi like *C. albicans*, various kinds of gram-positive and gram-negative bacteria, as well as protozoa and viruses. However, the picture of NETs has changed: they are additionally regarded as highly pathogenic. NETs consist of a variety of active biomolecules, which are tightly bound together. If the amount of NETs released in the human body overgrows their removal, pathophysiological processes occur: thrombosis, cardiovascular diseases, autoimmune and autoinflammatory diseases, impaired fertility, lung diseases, and cancer progression due to enhanced metastasis (Brinkmann 2018). Thus, the findings reported in this study emphasize the pathogenic role of NETs by describing the DAMP activities of naRNA, which is a highly active, immunomodulatory, endogenous agent. Our findings could furthermore explain the often-missing associations between NETs and various pathologies by suggesting naRNA as the driving force of such, as discussed in more detail in the following sections.

4.4 naRNA as a potential driver of (autoimmune) diseases

4.4.1 naRNA as a source of exRNA modulating autoimmune diseases

Extracellular RNAs (exRNAs) are known to be elevated in serum of patients suffering from various diseases, such as autoimmune diseases or cancer (Quinn et al. 2015). To date, it is reported that exRNAs can exist in extracellular vesicles (EVs), actively released by the cells, or in unbound forms. However, the exact role of non-vesicular exRNAs is unknown but it is suggested that they are of physiological relevance modulating immunity, although the instability of those unpacked exRNAs complicates their study (Tosar, Witwer, and Cayota 2021). Due to the fact that neutrophils are the most abundant leukocytes in circulation (Rosales 2020), it is coherent to assume that they highly contribute to cell free RNAs found in serum as sources of exRNAs. Of note, NETs are associated with the same diseases (Demkow 2021; Fousert, Toes, and Desai 2020) in which exRNAs are commonly found. By showing that naRNA is a common component of all types of NETs (*cf.* Fig. 3.2A, B) and its link to LL37 (*cf.* Fig. 3.16-3.18), possibly providing stability and protection from degradation of this ribonucleic acid, it is indicated by this study that NETs are common sources of exRNAs due to naRNA release.

As mentioned, NETs have been linked to many autoimmune diseases, such as rheumatoid arthritis (RA), systemic lupus erythematosus (SLE), and anti-neutrophil cytoplasmic antibodies (ANCA)-associated vasculitis (AAV), being present at the inflammatory sites in high abundance. Interactions of NETs with other immune cells and the observation that various components of NETs provide a source of autoantigens for autoantibodies (see Table 4.3) are thought to break self-tolerance in those diseases (Fousert, Toes, and Desai 2020).

Table 4.3: NET-derived autoantigens and associated diseases.

Abbreviations: AAV - anti-neutrophil cytoplasmic antibodies (ANCA) vasculitis, Bb – complement factor b, C1q – complement component 1q, HMGB1 – high mobility group protein B, LAMP-2 – Lysosomal membrane protein 2, MMP8 – matrix metalloproteinases, MMP9 – matrix metalloproteinase 9, MPO – myeloperoxidase, PR3 – proteinase 3, RA – rheumatoid arthritis, RNP – ribonucleoprotein, SSA – Sjögren's syndrome antigen-A, SLE – systemic lupus erythematosus, Sm – Smith, TF – tissue factor. Adapted from Ahlin et al. (2012) and Fousert et al. (2020) (Fousert, Toes, and Desai 2020; Ahlin et al. 2012).

NET-derived autoantigens	Associated autoimmune diseases
α-enolase	SLE
Annexin A1	SLE, RA
Apolipoprotein A1	SLE
Bb	AAV
C1q	SLE
Catalase	SLE, RA
Citrullinated histones	SLE, RA
dsDNA	SLE
Histones	SLE
HMGB1	SLE
LAMP-2	AAV
LL37	SLE, Psoriasis
MMP8	RA
MMP9	SLE
MPO	AAV
PR3	AAV
Properdin	AAV
TF	SLE
RNP/Sm	SLE
SSA/Ro52	SLE

Additionally to the ones described in Table 4.3, circulating autoantibodies derived of patient sera were found to be directed against PAD4-deiminated histones in the case of Felty's syndrome. Moreover, they were observed to bind to activated neutrophils and NETs, providing evidence for direct contribution of NETs and associated nuclear autoantigens in the initiation and progression of this certain autoimmune disease (Dwivedi et al. 2012).

Furthermore, RNA associated antigens are known (ribonucleoprotein (RNP)/Smith (Sm) and Sjögren's syndrome antigen-A (SSA)/Ro52) and autoantibodies directed against those were e.g. found to be even greater enriched in SLE patients than anti-DNA autoantibodies (Ahlin et al. 2012). Autoantibodies directed against these RNA proteins can be divided into two groups, the ones targeting small nuclear ribonucleoprotein (snRNP) and the ones targeting small cytoplasmic ribonucleoprotein (scRNP) and were already described in the 1980s (Provost, Herrera-Esparza, and Diaz 1985). Additionally, NETs have been reported to induce the release of B cell activating factor (BAFF) by PMNs, which in turn activates B cells, thereby contributing to the formation of autoantibodies, again linking NETs directly to autoimmunity (Domer et al. 2021).

Taken together, many reports in literature provide evidence for the association of exRNA and NETs to the same autoimmune diseases and RNA-directed autoantibodies are described. However, a building piece was missing to date: naRNA. The findings of this study hypothesize that naRNA is released as a common component of NETs and a type of immune-active exRNA, which occurs in autoimmune diseases, serves as an additional source of autoantigens therefore driving disease progression. To examine this hypothesis, SLE-patient sera were investigated regarding the occurrence of RNA-directed autoantibodies and their link to NETs in preliminary experiments, as described in the following section.

4.4.2 SLE-patient sera contain anti-RNA autoantibodies with naRNA-binding affinities

The first question to be examined was if anti-RNA directed autoantibodies can be found in sera of patients suffering from autoimmune diseases. Therefore, SLE-patient sera were investigated, due to the knowledge about the association of this certain autoimmune disease to NETs (Fousert, Toes, and Desai 2020). It was hypothesized that anti-RNA directed autoantibodies in SLE patients could derive from naRNA as an autoantigen, as afore discussed. Hence, a RNA-ELISA to detected possible anti-RNA autoantibodies was performed. Therefore, RNA was isolated from leukocytes as described and used as the coating antigen. Subsequently, patient sera were added and autoantibodies binding to RNA were detected using an anti-IgG secondary antibody, coupled to HRP for followed substrate reaction. The absorbance was then measured with a standard plate reader. Of note, the patient sera used in this study were from human donors suffering from SLE with previous assessment of autoantibody (antinuclear antibodies (ANA)) status and positive outcome. Antibodies bound to leukocyte RNA were observed in 50% of SLE patients, whereas no healthy donor showed any response (Fig. 4.3A). Thus, leukocyte RNA seems to be indeed a potential autoantigen in SLE. However, it cannot be concluded that these anti-RNA autoantibodies definitely bind naRNA, since whole leukocyte RNA was used as a capture antigen due to the low amounts of naRNA which could be harvested from NETs. Collecting high amounts of naRNA and repeating the ELISA with naRNA as the coating antigen could reveal the presence of specific anti-naRNA autoantibodies in future experiments. In a further experiment, the patient sera were applied to neutrophils in resting conditions and cells which spontaneously underwent NET formation. Sera derived from healthy human donors were used as a negative control. Afterwards, the cells were stained for autoantibodies using a FITC-conjugated anti-IgG secondary antibody and for naRNA as previously described (anti-rRNA Y10b; Fig. 4.3B). It was hereby aimed to investigate if SLE autoantibodies would bind to PMN RNA, specifically to naRNA. If so, this finding would further highlight the possible role of naRNA as a source of autoantigens. When SLE patient sera were applied, overlapping areas of rRNA- and autoantibody-signals were observed, indicated by the white appearing staining (Fig. 4.3B). Quantification of this microcopy approach was additionally performed. Hereby, the RNA area of the resting cells was defined by ROIs of rRNA Y10b signal and ImageJ-Win64 was used to investigate the percentage of the PMN RNA area covered by autoantibodies (anti-IgG-FITC signal). It was detected that around 95% of autoantibody-derived signals overlap with PMN RNA signal when SLE patient sera were applied. This was significantly higher compared to the 60% overlap observed for sera of healthy donors (Fig. 4.3C). Of note, applying serum to PMNs and investigating subsequent autoantibody-binding requires staining with anti-IgG secondary antibodies without blocking to prevent unspecific binding of the secondary antibody to blocking-serum-derived IgGs. Thus, blocking before staining was only performed for the anti-rRNA Y10b staining part (performed after IgG detection with anti-IgG-FITC conjugate). Therefore, unspecific anti-IgG-FITC signals were observed, detected, and

quantified as false positive signals for healthy donor controls, as well as SLE patient samples. Since this background false-positive signal is the same for both, samples treated with serum of healthy donors and SLE patients, it can be ignored. Taken together, this data suggests that SLE patients express autoantibodies directed against neutrophil RNA and naRNA. However, further analysis is needed to validate those preliminary findings.

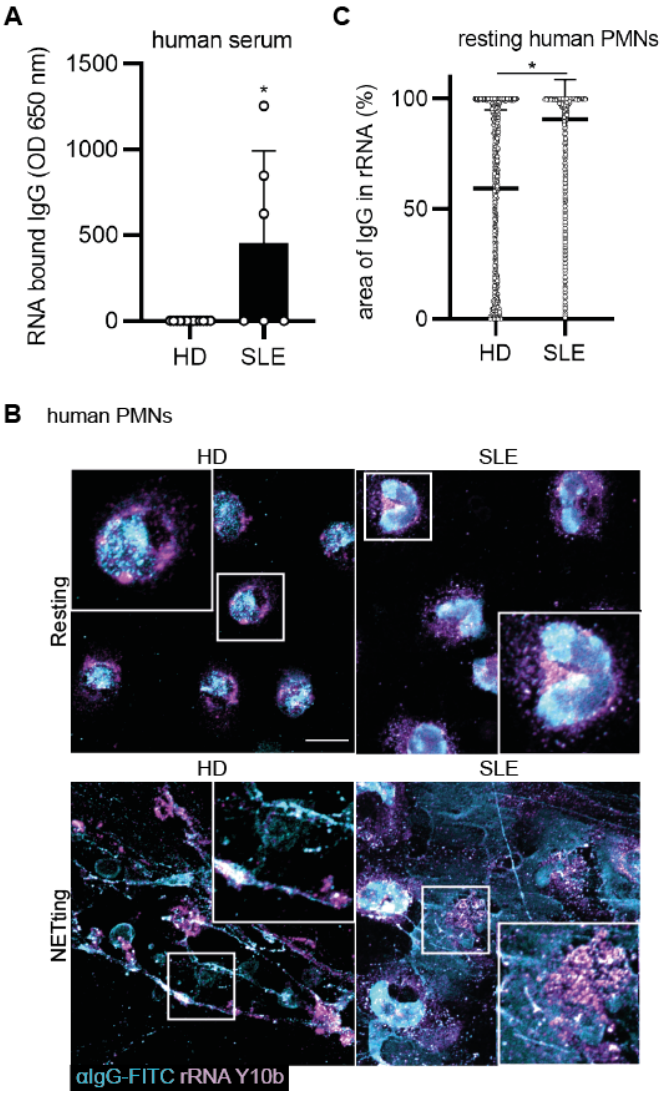

Figure 4.3: SLE patient sera contain autoantibodies directed against leukocyte RNA, specifically PMN RNA.

(A) Triplicate RNA-ELISA of human serum of healthy donors (HD) or Systemic lupus erythematosus (SLE) patients (HD: n = 13, SLE: n = 6; combined data, mean+SD, each dot represents one patient, *p<0.05 according to Kruskal-Wallis test). **(B)** Confocal microscopy of primary human PMNs incubated for 20 min with serum of HDs or SLE patients in resting or NETting (spontaneous NET formation) conditions and stained for IgG (anti-IgG-FITC, cyan) and RNA (anti-rRNA Y10b, magenta; HD: n = 4, SLE: n = 5, scale bar: 10 µm; representative images). **(C)** Quantification of **B** of binding to PMNs in resting conditions (HD: n = 4, SLE: n = 5; three images per biological replicate were analyzed; each dot represents one ROI, *p<0.05 according to one-way ANOVA).

Due to the reports in literature and the findings presented in this study, naRNA could be a notable novel source for RNA-autoantigens, leading to the development of autoantibodies, thereby driving autoimmune diseases. *In vivo* experiments performing a 'vaccination approach' with naRNA-containing NET content could possibly lead to the expression of anti-naRNA autoantibodies in mice. Therefore, BALB/c mice would be of use, since they are known to efficiently produce monoclonal antibodies and exceptionally respond to immunization due to easily triggered Th2 cell responses (Potter 1986). Detecting anti-RNA antibodies in a naRNA-ELISA after immunization of the animals with NETs could confirm the hypothesis of naRNA being a potential source of autoantigens.

4.4.3 naRNA as a possible driver of disease progression in psoriasis

In the special case of psoriasis, a skin inflammatory disease affecting around 2% of humans world-wide (Rendon and Schakel 2019), previous research has already linked the possible role of naRNA to disease progression. The first step was done in 2009 by the group of Michel Gilliet by observing that self-RNA-LL37 complexes can activate DCs and can be found in high abundance in psoriatic skin lesions, thereby contributing to disease progression (Ganguly et al. 2009). Moreover, as before mentioned, an earlier study of our group found NETs also to be present in great amounts in skin lesions of psoriasis patients and described naRNA for the first time, directly linking self-RNA-LL37 complex-associated inflammation in this disease to NETs (Herster et al. 2020). By naRNA-containing NET content induced inflammation and reduced severity observed in Tlr13-deficient mice (*cf.* Fig. 3.14C), as well as using the well-established IMQ psoriasis mouse model and observing significantly reduced progression of skin inflammation in mice lacking RNA-sensing (*cf.* Fig. 3.15), it was proven in this underlying study that RNA is a crucial contributor to disease progression. Thus, naRNA is a plausible source of host-derived RNA breaking immune tolerance. Thereby, the data presented herein links the previous findings and explains how NETs contribute to skin pathologies observed in this inflammatory disease.

4.4.4 COVID-19 pathologies might be naRNA-mediated

Regarding COVID-19 and associated thrombo-inflammatory states, like sepsis, thrombosis, and respiratory failure, NETs are of great research interest. Circulating NETs have been found in plasma of hospitalized COVID-19 patients (Zuo et al. 2020) and linked to thrombus formation by several research groups (Yaqinuddin and Kashir 2020; Cicco et al. 2020; Barnes et al. 2020; Golonka et al. 2020). Furthermore, ssRNA was described to play a role in platelet activation-mediated thrombosis (Fard et al. 2021), as well as exRNAs and micro RNAs have been reported as procoagulant cofactors in blood coagulation (Kannemeier et al. 2007; Sahu et al. 2017). However, the link between NET-related and RNA-induced thrombus formation has never been made. This current study can provide a starting point for bridging previous research by highlighting naRNA as the key factor of NET-induced thrombo-inflammatory states in COVID-19 disease pathogenesis. Similar to measuring MPO-DNA complexes in COVID-19 patient sera as a measure for circulating NETs (Middleton et al. 2020), one could detect naRNA-LL37 complexes in an ELISA-like approach to verify this assumption. Thereby, an anti-LL37 antibody could capture those complexes, which could be detected with the mouse anti-human rRNA Y10b antibody used in this study and verified to sufficiently bind naRNA. A secondary antibody directed against murine IgG and coupled to HRP could be used for subsequent substrate reaction.

Respiratory failure after SARS-CoV-2 virus infection can further lead to poor disease outcome (Xu, Shi, et al. 2020) and NETs have been tightly linked to lung tissue damage causing this disease pathology (Ackermann et al. 2021; Veras et al. 2020; Obermayer et al. 2021). The data presented herein indicate that naRNA could propagate tissue damage by its self-amplifying properties (*cf.* Fig. 3.8B-E), as well as by activating other immune cells and keratinocytes (*cf.* Fig. 3.11-3.13), or even endothelial cells (Blanco et al. 2021). Investigation of tissue by immunofluorescence microscopy could prove the presence of naRNA in COVID-19 patient lungs and thus verify the hypothesis of naRNA driving disease progression after SARS-CoV-2 infection.

4.5 Therapeutic implications – targeting naRNA to prevent disease progression

It was presented in this study that naRNA is the main driver of self-amplification of NET formation. Thus, naRNA should be considered as a therapeutic target in inflammatory diseases associated with excessive NET formation. By inhibiting naRNA-mediated self-amplification of NETs, additional naRNA release and thus, naRNA-induced sustained inflammation could be prevented (Fig. 4.4).

Application of RNA to the patient can be used as a very successful therapeutic option to e.g. mediate anti-cancer responses (Ling, Fabbri, and Calin 2013; Rupaimoole and Slack 2017), fight cardiovascular diseases (van Rooij and Olson 2012), or serve as a vaccine to induce immunity against COVID-19 (Chakraborty et al. 2021), as frequently reported in literature. In contrast, uncontrolled RNA-sensing has been observed to fuel autoinflammation, as e.g. lupus was found to be associated with a *TLR7* gain-of-function mutation (Brown et al. 2022). Furthermore, self-editing of dsRNA by adenosine deaminase RNA-specific binding protein (ADAR1) has been reported as a cellular mechanism to evade sensing by the cytosolic receptor MDA5 (Mannion et al. 2014) and mutations in *ADAR1* were found to be associated with autoimmune diseases (Rice et al. 2012). Genetic editing of *MDA5* could therefore serve as a potential therapeutic target to prevent uncontrolled sensing of dsRNA leading to autoinflammation in patients presenting *ADAR1* mutations (Li, Gloudemans, et al. 2022). These findings show that RNA-sensing and subsequent immune responses need to be kept in check to be advantageous and not detrimental to the host.

In the case of TLR7/8 sensing, which is more relevant for the data presented in this study, ADAR1 mediated editing of viral RNA to substitute adenosine with inosine was reported to lead to enhanced receptor recognition, due to its ability to form secondary structures with adenosine (A), cytidine (C), and uridine (U). In addition, TLR7/8-mediated sensing of ssRNA highly relies on uridine rich residues and their capability to form inter- and intramolecular secondary structures (Sarvestani et al. 2014). Thus, it would be of interest to gain detailed insights into the structure of naRNA and the residues presented to find possible targets to interfere with its binding to TLR8 by gene editing.

In the case of NET-related pathologies, as previously described, application of RNase A was successfully used to protect from disease progression in subarachnoid hemorrhage (Fruh et al. 2021) and ischemic muscle injury (Lasch et al. 2020). Of note, RNase A was reported to catalyze the cleavage of phosphate bonds of pyrimidine ring-containing nucleotides by binding to nucleobases (delCardayre and Raines 1994), thus acting on uridine (Xu, Chmela, et al. 2020). Therefore, it can be hypothesized that naRNA is rich in uridine residues which get impaired upon treatment with RNase A, thereby interfering with the binding

to TLR8 leading to protection of the host from excessive naRNA-propagated inflammation. However, the application of RNases as therapeutic options is challenging: the pharmacokinetics of RNases are rather bad, as they are small proteins which are easily eliminated from the human body. Furthermore, application of RNases leads to multiple targeting, since they non-specifically alter gene expression and regulation (Castro et al. 2021). Thus, application of RNases to therapeutically alter naRNA and its related signaling might not be the best option.

Besides the sequence of RNA and its residues, nucleoside modifications can have a high impact on receptor binding, providing the possibility to selectively distinguish between self and non-self. It was reported that modification of uridine, such as substitution with pseudo (Ψ)-uridine, can abolish TLR7/8 activation in primary, blood-derived DCs, as measured by cytokine release and CD markers. Moreover, dose-dependent suppression of RNA-mediated immune stimulation correlating with the amount of modifications applied was observed (Kariko et al. 2005). Accordingly, investigating modifications of naRNA, which is missing in this research work, could be later on used for target specific modulation and subsequent inhibition of the DAMP-effects mediated by this host-derived RNA. However, site-directed RNA modification in humans is still in its infancy. Currently, researchers work with the so-called RNA Editing for Programmable A to I Replacement (REPAIR) system, in which they can check if their technology could be used to fix RNA mutations. Nevertheless, too many technical challenges need to be overcome first, such as precise editing at the target site and the influence of endogenous enzymes. In addition, RNA-editing is debated regarding ethical justification (Ullah, Akbar, and Yannarelli 2020). In the special case of uridine modifications, pseudouridylation has been found to be associated with cancer, maternally inherited diabetes and deafness, as well as more severe disease progression in HIV-infected patients (Penzo et al. 2017). Therefore, substituting uridine with Ψ-uridine could lead to detrimental adverse effects. Due to the afore mentioned reasons and the fact that to date only few validated drugs targeting RNA exist and validation of further requires tedious and extensive investigation (Yu, Choi, and Tu 2020), targeting the naRNA receptor, specifically TLR8 or its downstream signaling molecules, might be more suitable for therapeutic interventions.

To target TLR8-mediated naRNA signaling, a PAD4 inhibitor, which was also used in this study to sufficiently block self-propagated NET formation and thereby additional release of naRNA (*cf.* Fig. 3.9C), could be of use. Blocking PAD4, which induces histone citrullination and thereby fuels chromatin decondensation and subsequent NET formation (Sorensen and Borregaard 2016), reduced NET-mediated vascular damage in a murine atherosclerosis model (Knight et al. 2014) and prevented NET formation in mice suffering from multiple myeloma, thereby delaying disease progression (Li et al. 2020). However, no physiological inhibitors of PAD4 are currently known and inhibition has to be performed with care. Isotypes of PAD4, which have a structural conserved active site, are involved in other biological pathways, and should therefore not be accidentally targeted to prevent adverse effects. In addition, blocking of PAD4 would block NET formation in general, which could be a potential threat to the host, since neutralization of pathogens would be affected (Liu et al. 2021).

Therefore, targeting naRNA-signaling more specifically by directly interfering with TLR8 or its downstream mediators could be advantageous. The *in vivo* data presented in this study unequivocally showed that inhibition of RNA-sensing can reduce disease progression in a psoriasis model (*cf.* Fig. 3.15). A synthetic

oligonucleotide, which was found to inhibit TLR7, 8, and 9, was reported to prevent the formation of skin lesions and mediated reduction of Th1 and Th17 responses in an IL-23-induced psoriatic mouse model (Jiang et al. 2013). Later on, IMO-8400, an oligonucleotide-based TLR7, 8, and 9 antagonist, was applied to patients suffering from moderate to severe psoriasis in a phase two clinical trial. Thereby, severity of the disease was reduced (Balak et al. 2017). Previous work of this group identified IRS661, an inhibitory oligonucleotide, to efficiently inhibit TLR8-dependent ssRNA-LL37-mediated NET formation in primary human PMNs (Herster et al. 2020).

Recently, in a mouse model for lupus, the selective TLR7/8 inhibitor M5049, a small molecule with drug-like properties, was observed to reduce disease progression. Due to its long duration of action and the possibility to oral administration, M5049 comprises advantages over synthetic oligodeoxynucleotide antagonists (Vlach et al. 2021). Another small molecular antagonist specific for TLR8, CU-CPT9a (Zhang et al. 2018), was shown in this study to inhibit naRNA-mediated self-propagation of NET formation (*cf.* Fig. 3.9B, D). In literature, CU-CPT9a was reported to block bacteria-mediated immunostimulatory effects on PBMCs (Venegas et al. 2019), to abrogate Icariside II, an active component of *Herba Epimedii*, -induced cell cycle arrest and differentiation in leukemia cells (Yang et al. 2019), and prevented *Plasmodium falciparum* TLR8-signaling (Kollisch et al. 2022). However, clinical studies investigating this TLR8-inhibitor in physiologically relevant settings are missing but could help to find therapeutics to block the adverse effects of naRNA-signaling in inflammatory diseases in human. In further research work, one could consider applying CU-CPT9a to WT mice before intradermal injection of NETs and check if the naRNA-mediated inflammation observed in this underlying study can be abolished.

Instead of targeting TLR8 directly, one could attempt to inhibit downstream signaling events. To date, little is known about the exact underlying pathways leading to NET formation after TLR8 activation, but it is suggested that NADPH oxidase gets stimulated, leading to subsequent ROS production, translocation of NE and MPO, additional PAD4 activation and chromatin decondensation, resulting in ET release (Chen et al. 2021). However, general suppression of NADPH-oxidase-dependent ROS formation could be detrimental to the host, due to the antimicrobial functions of ROS (Agita and Alsagaff 2017), as well as their roles as signaling molecules (Droge 2002). Thus, interreference with these pathways would likely lead to broad immunosuppression. It would therefore be of great interest to investigate downstream signaling events between TLR8 activation and NET formation in more detail to specifically inhibit TLR8-related adaptor proteins and directly target naRNA-induced NET propagation but leave other afferent signaling pathways and the general ability to form NETs in response to pathogens intact. If the canonical TLR8 pathway applies, downstream mediators would be MYD88 and IRAK kinases. Inhibitors for e.g. IRAK4 are currently used to treat rheumatoid arthritis (Wiese, Manning-Bennett, and Abuhelwa 2020), a disease in which NETs are also known to play a role (Khandpur et al. 2013). The four inhibitors PF-06650833 (Pfizer), CA-4949 (Curis and Aurigene), BAY1834845 and BAY1830839 (Bayer) have made it to phase I/II clinical trials, of which the one from Pfizer is the most advanced so far. Besides application in RA patients, BAY1834845 has been used in clinical trials for psoriasis treatment as well (Wiese, Manning-Bennett, and Abuhelwa 2020). Hypothesizing that IRAK4 plays a role in naRNA-dependent TLR8 activation, the beneficial effects of those inhibitors observed in RA and psoriasis could derive from impaired naRNA signaling. In a murine model for myocardial infarction, pharmacologic inhibition of MYD88 with ST2825 or IMG2005 has been reported to be beneficial (Van Tassell et al. 2010). Moreover, the small molecule

T6167923 was shown to inhibit dimer formation of MYD88, thus preventing cell proliferation in diffuse large B cell lymphoma (DLBCL) tumor isolates (Saikh 2021). Furthermore, compound 4210, a small molecule inhibitor of MYD88, was used in *in vitro* virus-infection assays, which led to a better antiviral response due to upregulation of type I interferon and suppression of viral replication (Saikh et al. 2020). More recently, the novel MYD88 inhibitor M20, a small molecule with a pyrazol pyridine skeleton, was successfully used in an *in vivo* model for acute lung injury (Song et al. 2021). Assuming a role of MYD88 in naRNA-mediated TLR8 signaling, application of such MYD88 inhibitors in a NET-assay could first reveal the role of this adaptor protein in naRNA-mediated self-propagation and later on be useful for therapeutic intervention of NET-mediated diseases in the future.

Taken together, this study offers many new therapeutic aspects for treatment options of NET-related inflammatory diseases by characterizing naRNA as an endogenous, sterile DAMP and its underlying signaling and immunomodulatory functions in more detail. However, much more research is needed to successfully implement those approaches in therapeutic applications in the future.

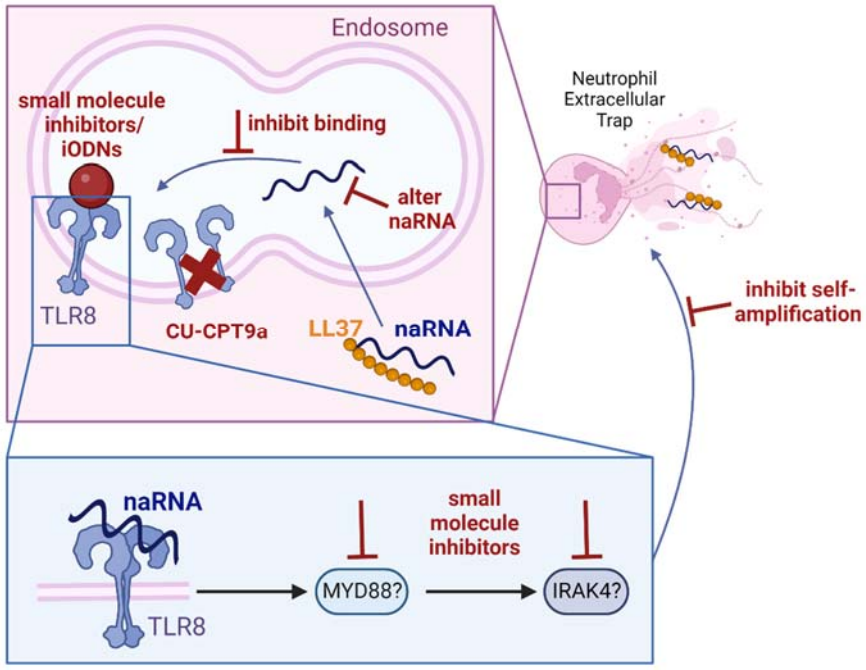

Figure 4.4: Therapeutic implications – targeting naRNA and its signaling to prevent disease progression.

naRNA-mediated self-propagation of NETs could be prevented by altering naRNA, thus hindering binding to the receptor. Additionally, small molecule inhibitors, such as CU-CPT9a, or iODNs could be used to inhibit TLR8, the naRNA-sensing receptor. Furthermore, depending on the downstream mediators of TLR8, small molecule inhibitors of e.g. MYD88 or IRAK4 could be used to prevent naRNA-mediated and TLR8-dependent NET formation. Overall, any of those strategies would hinder naRNA-driven self-amplification of NETs and thus stop sustained inflammation in NET-related pathologies. Created with BioRender.com.

4.6 Conclusion

This study unequivocally presents the various immunomodulatory properties of naRNA, a highly critical NET component which has not gotten much attention in research to date. Its pre-assembly with LL37 in resting neutrophils redefines NETs from an antimicrobial host defense mechanism to an inflammatory agent with possibly intentional DAMP release. The underlying research work therefore offers an explanation of the association of NETs to many diseases and their inflammation propagating nature by presenting the release of naRNA as a novel, endogenous source of immune activating exRNAs. Although many new open questions arose from this study and much more research is needed to confirm the herein presented findings in human pathologies, these intriguing insights in the characteristics of naRNA further pave the path for future research and potential therapeutic implications later on, targeting naRNA-induced molecular mechanisms for the treatment of NET-associated diseases.

5 Appendix

5.1 Secondary antibody controls of electron microscopy

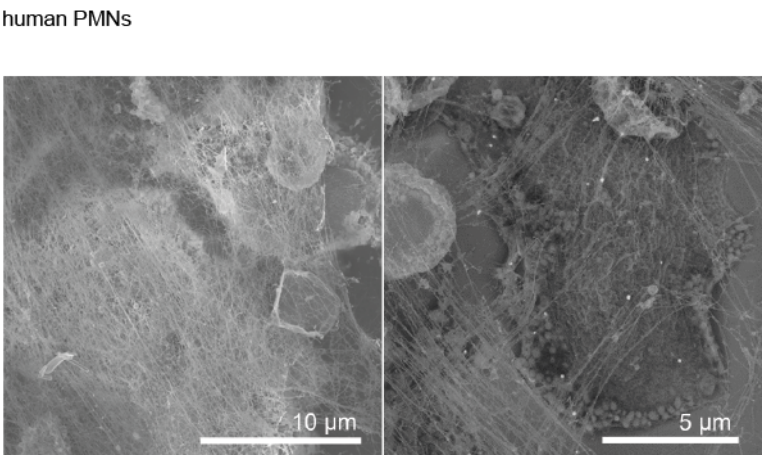

Figure 5.1: Secondary antibody controls of electron microscopy.

Scanning electron microscopy of PMA (1200 nM, 3 h)-treated human primary PMNs showing only secondary antibody staining (no primary antibody) control of Fig. **3.5B** (n = 1, representative data; the image on the right is a composite image with signals from secondary electron and backscattered electron detectors for topography and additional material information, respectively). Electron microscopy was performed by the group of Katharina Hipp, Electron Microscopy Facility, Max Planck Institute for Biology Tübingen.

5.2 Supplemental movies of 3D analysis of naRNA in NET-fibers and naRNA digest by RNase A

5.2.1 3D reconstruction of NETs: naRNA is speckled on DNA-fibers

https://www.dropbox.com/s/6cedodzh0rbv65u/Supplementary%20Movie%20S1.mp4?dl=0

Supplemental Movie S 1: 3D reconstruction of NETs: naRNA is speckled on DNA-fibers.

Confocal microscopy of primary human PMNs stimulated with PMA for 3 h, stained for naRNA (anti-rRNA Y10b, magenta) and DNA (Hoechst 33342, white, n = 3) and 3D analysis and animation were performed using Zen Blue3 software.

5.2.2 naRNA digest by RNase A in PMA-induced NETs

https://www.dropbox.com/s/7n1xlllg8gvmj0t/Supplementary%20Movie%20S2.mp4?dl=0

Supplemental Movie S 2: naRNA digest by RNase A in PMA-induced NETs.

Confocal live microscopy of RNase digestion of NETs obtained from primary human PMNs stimulated with PMA for 3 h, stained for naRNA (SYTO RNAselect, magenta) and DNA (Hoechst 33342, white, n = 3). 100 µg/mL RNase A was added between time point 0 and 5 min (n = 3, scale bar 20 µm). Video analysis and animation were performed using ImageJ-Win64 software.

Statutory Declaration

Ich erkläre hiermit, dass ich die zur Promotion eingereichte Arbeit mit dem Titel:

'Pre-assembled Complexes of naRNA and LL37 Redefine Neutrophil Extracellular Traps as Inflammatory Agents'

selbständig verfasst, nur die angegebenen Quellen und Hilfsmittel benutzt und wörtlich oder inhaltlich übernommene Stellen (alternativ: Zitate) als solche gekennzeichnet habe. Beiträge anderer wurden im Text als solche gekennzeichnet und sind zusätzlich in nachstehender Tabelle der mitwirkenden Wissenschaftlern gelistet. Ich erkläre, dass die Richtlinien zur Sicherung guter wissenschaftlicher Praxis der Universität Tübingen (Beschluss des Senats vom 25.5.2000) beachtet wurden. Ich versichere an Eides statt, dass diese Angaben wahr sind und dass ich nichts verschwiegen habe. Mir ist bekannt, dass die falsche Abgabe einer Versicherung an Eides statt mit Freiheitsstrafe bis zu drei Jahren oder mit Geldstrafe bestraft wird.

Mitwirkende Wissenschaftler

Scientist	**Affiliation**	**Data created**	**Data shown in this thesis in Figure**
Carsten Greve	Group of Prof. Weber, University of Tübingen	BlaER1 ELISA, THP-1 ELISA, N/TERT-1 ELISA, NHEK ELISA, qPCR and ELISA of 3D human skin equivalent supernatant	3.11, 3.13
Sirui Chen (unter meiner Betreuung)		HEK Dual luciferase assay, PBMC ELISA	3.9A, 3.12A-C
Pujan Engels		NK-MI92 ELISA	3.12D
Tzu-Hsuan Chang		Culturing of *C. albicans*	
Marissa Dubbelaar	Group of Prof. Walz, University of Tübingen	Analysis of RNASeq data	3.6B
Christine Youn	Group of Prof. Archer, Johns Hopkins University School of Medicine, Baltimore	*In vivo* experiments	3.14, 3.15
Yu Wang			
Nathan Archer			
Jule Focken	Group of Prof. Schittek, University Hospital Tübingen	*S. aureus* killing assay	3.7
Jasmin Scheurer		3D human skin equivalent	Preparation of 3D skin equivalent used for 3.13C, D
Birgit Schittek			
Masoud Nasri	Group of Prof. Skokowa, University Hospital Tübingen	*In vitro* transdifferentiation of human stem cells	3.3; Transdifferentiation of cells used for 3.4
Julia Skokowa			
Katharina Hipp	Electron Microscopy Facility, Max Planck Institute for Biology Tübingen	Scanning/Transmission Electron Microscopy, Immunofluorescence Microscopy of ultrathin sections	3.5B, 3.18A(image), B, 5.1
Natalya Korn	Group of Christiane Wolz, University of Tübingen	Preparation of bacterial RNA of *S. aureus*	
Reinhild Klein	Group of Reinhild Klein, University Hospital Tübingen	Providing patient sera and fixed granulocytes, performing RNA ELISA (data is not part of the publication noted below)	4.2
Beate Preuß			
Title of paper:	Release of the pre-assembled naRNA-LL37 composite DAMP re-defines neutrophil extracellular traps (NETs) as intentional DAMP webs		
Status in publication process:	Biorxiv; DOI: https://doi.org/10.1101/2022.07.26.499571		

Francesca Bork

_____

Tübingen, Germany

References

Ackermann, M., H. J. Anders, R. Bilyy, G. L. Bowlin, C. Daniel, R. De Lorenzo, M. Egeblad, T. Henneck, A. Hidalgo, M. Hoffmann, B. Hohberger, Y. Kanthi, M. J. Kaplan, J. S. Knight, J. Knopf, E. Kolaczkowska, P. Kubes, M. Leppkes, A. Mahajan, A. A. Manfredi, C. Maueroder, N. Maugeri, I. Mitroulis, L. E. Munoz, T. Narasaraju, E. Naschberger, I. Neeli, L. G. Ng, M. Z. Radic, K. Ritis, P. Rovere-Querini, M. Schapher, C. Schauer, H. U. Simon, J. Singh, P. Skendros, K. Stark, M. Sturzl, J. van der Vlag, P. Vandenabeele, L. Vitkov, M. von Kockritz-Blickwede, C. Yanginlar, S. Yousefi, A. Zarbock, G. Schett, and M. Herrmann. 2021. 'Patients with COVID-19: in the dark-NETs of neutrophils', *Cell Death Differ*, 28: 3125-39.

Agita, A., and M. T. Alsagaff. 2017. 'Inflammation, Immunity, and Hypertension', *Acta Med Indones*, 49: 158-65.

Aguila, S., A. M. de Los Reyes-Garcia, M. P. Fernandez-Perez, L. Reguilon-Gallego, L. Zapata-Martinez, I. Ruiz-Lorente, V. Vicente, R. Gonzalez-Conejero, and C. Martinez. 2021. 'MicroRNAs as New Regulators of Neutrophil Extracellular Trap Formation', *Int J Mol Sci*, 22.

Ahlin, E., L. Mathsson, M. L. Eloranta, T. Jonsdottir, I. Gunnarsson, L. Ronnblom, and J. Ronnelid. 2012. 'Autoantibodies associated with RNA are more enriched than anti-dsDNA antibodies in circulating immune complexes in SLE', *Lupus*, 21: 586-95.

Ai, Z., and I. A. Udalova. 2020. 'Transcriptional regulation of neutrophil differentiation and function during inflammation', *J Leukoc Biol*, 107: 419-30.

Alam, Muhammad S. 2022. 'Proximity Ligation Assay (PLA)Proximity ligation assay (PLA).' in Luis Del Valle (ed.), *Immunohistochemistry and Immunocytochemistry: Methods and Protocols* (Springer US: New York, NY).

Ali, M. A. M., J. A. Garcia-Vilas, C. R. Cromwell, B. P. Hubbard, M. J. Hendzel, and R. Schulz. 2021. 'Matrix metalloproteinase-2 mediates ribosomal RNA transcription by cleaving nucleolar histones', *FEBS J*, 288: 6736-51.

An, Z., J. Li, J. Yu, X. Wang, H. Gao, W. Zhang, Z. Wei, J. Zhang, Y. Zhang, J. Zhao, and X. Liang. 2019. 'Neutrophil extracellular traps induced by IL-8 aggravate atherosclerosis via activation NF-kappaB signaling in macrophages', *Cell Cycle*, 18: 2928-38.

Andersen, M. H., D. Schrama, P. Thor Straten, and J. C. Becker. 2006. 'Cytotoxic T cells', *J Invest Dermatol*, 126: 32-41.

Anderson, K. V., L. Bokla, and C. Nusslein-Volhard. 1985. 'Establishment of dorsal-ventral polarity in the Drosophila embryo: the induction of polarity by the Toll gene product', *Cell*, 42: 791-8.

Armstrong, A. W., and C. Read. 2020. 'Pathophysiology, Clinical Presentation, and Treatment of Psoriasis: A Review', *JAMA*, 323: 1945-60.

Armstrong, R. A. 2019. 'Should Pearson's correlation coefficient be avoided?', *Ophthalmic Physiol Opt*, 39: 316-27.

Arroyo, A. B., A. M. de Los Reyes-Garcia, J. M. Rivera-Caravaca, P. Valledor, N. Garcia-Barbera, V. Roldan, V. Vicente, C. Martinez, and R. Gonzalez-Conejero. 2018. 'MiR-146a Regulates Neutrophil Extracellular Trap Formation That Predicts Adverse Cardiovascular Events in Patients With Atrial Fibrillation', *Arterioscler Thromb Vasc Biol*, 38: 892-902.

Balak, D. M., M. B. van Doorn, R. D. Arbeit, R. Rijneveld, E. Klaassen, T. Sullivan, J. Brevard, H. B. Thio, E. P. Prens, J. Burggraaf, and R. Rissmann. 2017. 'IMO-8400, a toll-like receptor 7, 8, and 9 antagonist, demonstrates clinical activity in a phase 2a, randomized, placebo-controlled trial in patients with moderate-to-severe plaque psoriasis', *Clin Immunol*, 174: 63-72.

Bao, X., X. Guo, M. Yin, M. Tariq, Y. Lai, S. Kanwal, J. Zhou, N. Li, Y. Lv, C. Pulido-Quetglas, X. Wang, L. Ji, M. J. Khan, X. Zhu, Z. Luo, C. Shao, D. H. Lim, X. Liu, N. Li, W. Wang, M. He, Y. L. Liu, C. Ward, T. Wang, G. Zhang, D. Wang, J. Yang, Y. Chen, C. Zhang, R. Jauch, Y. G. Yang, Y. Wang, B. Qin, M. L. Anko, A.

P. Hutchins, H. Sun, H. Wang, X. D. Fu, B. Zhang, and M. A. Esteban. 2018. 'Capturing the interactome of newly transcribed RNA', *Nat Methods*, 15: 213-20.

Barnes, B. J., J. M. Adrover, A. Baxter-Stoltzfus, A. Borczuk, J. Cools-Lartigue, J. M. Crawford, J. Dassler-Plenker, P. Guerci, C. Huynh, J. S. Knight, M. Loda, M. R. Looney, F. McAllister, R. Rayes, S. Renaud, S. Rousseau, S. Salvatore, R. E. Schwartz, J. D. Spicer, C. C. Yost, A. Weber, Y. Zuo, and M. Egeblad. 2020. 'Targeting potential drivers of COVID-19: Neutrophil extracellular traps', *J Exp Med*, 217.

Bartels, M., A. M. Govers, V. Fleskens, A. R. Lourenco, C. E. Pals, S. J. Vervoort, R. van Gent, A. B. Brenkman, M. B. Bierings, S. J. Ackerman, J. van Loosdregt, and P. J. Coffer. 2015. 'Acetylation of C/EBPepsilon is a prerequisite for terminal neutrophil differentiation', *Blood*, 125: 1782-92.

Bello, S. M., M. L. Berry, and C. L. Smith. 2020. 'Know Your Model: How essential is that essential gene?', *Lab Anim (NY)*, 49: 9-10.

Benhadou, F., D. Mintoff, and V. Del Marmol. 2019. 'Psoriasis: Keratinocytes or Immune Cells - Which Is the Trigger?', *Dermatology*, 235: 91-100.

Berger, S. L., and H. L. Cooper. 1975. 'Very short-lived and stable mRNAs from resting human lymphocytes', *Proc Natl Acad Sci U S A*, 72: 3873-7.

Beutler, B. 2004. 'Innate immunity: an overview', *Mol Immunol*, 40: 845-59.

Bitschar, K., L. Staudenmaier, L. Klink, J. Focken, B. Sauer, B. Fehrenbacher, F. Herster, Z. Bittner, L. Bleul, M. Schaller, C. Wolz, A. N. R. Weber, A. Peschel, and B. Schittek. 2020. 'Staphylococcus aureus Skin Colonization Is Enhanced by the Interaction of Neutrophil Extracellular Traps with Keratinocytes', *J Invest Dermatol*, 140: 1054-65 e4.

Bitto, N. J., L. Cheng, E. L. Johnston, R. Pathirana, T. K. Phan, I. K. H. Poon, N. M. O'Brien-Simpson, A. F. Hill, T. P. Stinear, and M. Kaparakis-Liaskos. 2021. 'Staphylococcus aureus membrane vesicles contain immunostimulatory DNA, RNA and peptidoglycan that activate innate immune receptors and induce autophagy', *J Extracell Vesicles*, 10: e12080.

Blanco, L. P., X. Wang, P. M. Carlucci, J. J. Torres-Ruiz, J. Romo-Tena, H. W. Sun, M. Hafner, and M. J. Kaplan. 2021. 'RNA Externalized by Neutrophil Extracellular Traps Promotes Inflammatory Pathways in Endothelial Cells', *Arthritis Rheumatol*, 73: 2282-92.

Blasius, A. L., and B. Beutler. 2010. 'Intracellular toll-like receptors', *Immunity*, 32: 305-15.

Block, H., J. Rossaint, and A. Zarbock. 2022. 'The Fatal Circle of NETs and NET-Associated DAMPs Contributing to Organ Dysfunction', *Cells*, 11.

Boeltz, S., P. Amini, H. J. Anders, F. Andrade, R. Bilyy, S. Chatfield, I. Cichon, D. M. Clancy, J. Desai, T. Dumych, N. Dwivedi, R. A. Gordon, J. Hahn, A. Hidalgo, M. H. Hoffmann, M. J. Kaplan, J. S. Knight, E. Kolaczkowska, P. Kubes, M. Leppkes, A. A. Manfredi, S. J. Martin, C. Maueroder, N. Maugeri, I. Mitroulis, L. E. Munoz, D. Nakazawa, I. Neeli, V. Nizet, E. Pieterse, M. Z. Radic, C. Reinwald, K. Ritis, P. Rovere-Querini, M. Santocki, C. Schauer, G. Schett, M. J. Shlomchik, H. U. Simon, P. Skendros, D. Stojkov, P. Vandenabeele, T. V. Berghe, J. van der Vlag, L. Vitkov, M. von Kockritz-Blickwede, S. Yousefi, A. Zarbock, and M. Herrmann. 2019. 'To NET or not to NET:current opinions and state of the science regarding the formation of neutrophil extracellular traps', *Cell Death Differ*, 26: 395-408.

Bonaventura, A., A. Vecchie, A. Abbate, and F. Montecucco. 2020. 'Neutrophil Extracellular Traps and Cardiovascular Diseases: An Update', *Cells*, 9.

Bonilla, F. A., and H. C. Oettgen. 2010. 'Adaptive immunity', *J Allergy Clin Immunol*, 125: S33-40.

Borzova, E. 2020. 'The Absolute Basophil Count', *Methods Mol Biol*, 2163: 109-24.

Bouchery, T., and N. Harris. 2019. 'Neutrophil-macrophage cooperation and its impact on tissue repair', *Immunol Cell Biol*, 97: 289-98.

Brinkmann, V. 2018. 'Neutrophil Extracellular Traps in the Second Decade', *J Innate Immun*, 10: 414-21.

Brinkmann, V., U. Reichard, C. Goosmann, B. Fauler, Y. Uhlemann, D. S. Weiss, Y. Weinrauch, and A. Zychlinsky. 2004. 'Neutrophil extracellular traps kill bacteria', *Science*, 303: 1532-5.

Brown, G. D., J. A. Willment, and L. Whitehead. 2018. 'C-type lectins in immunity and homeostasis', *Nat Rev Immunol*, 18: 374-89.

Brown, G. J., P. F. Canete, H. Wang, A. Medhavy, J. Bones, J. A. Roco, Y. He, Y. Qin, J. Cappello, J. I. Ellyard, K. Bassett, Q. Shen, G. Burgio, Y. Zhang, C. Turnbull, X. Meng, P. Wu, E. Cho, L. A. Miosge, T. D. Andrews, M. A. Field, D. Tvorogov, A. F. Lopez, J. J. Babon, C. A. Lopez, A. Gonzalez-Murillo, D. C. Garulo, V. Pascual, T. Levy, E. J. Mallack, D. G. Calame, T. Lotze, J. R. Lupski, H. Ding, T. R. Ullah, G. D. Walters, M. E. Koina, M. C. Cook, N. Shen, C. de Lucas Collantes, B. Corry, M. P. Gantier, V. Athanasopoulos, and C. G. Vinuesa. 2022. 'TLR7 gain-of-function genetic variation causes human lupus', *Nature*, 605: 349-56.

Bucki, R., K. Leszczynska, A. Namiot, and W. Sokolowski. 2010. 'Cathelicidin LL-37: a multitask antimicrobial peptide', *Arch Immunol Ther Exp (Warsz)*, 58: 15-25.

Burn, G. L., A. Foti, G. Marsman, D. F. Patel, and A. Zychlinsky. 2021. 'The Neutrophil', *Immunity*, 54: 1377-91.

Cassatella, M. A., E. Gardiman, F. Arruda-Silva, F. Bianchetto-Aguilera, S. Gasperini, M. Bugatti, W. Vermi, F. Larousserie, O. Devergne, and N. Tamassia. 2020. 'Human neutrophils activated by TLR8 agonists, with or without IFNgamma, synthesize and release EBI3, but not IL-12, IL-27, IL-35, or IL-39', *J Leukoc Biol*, 108: 1515-26.

Castro, J., M. Ribo, M. Vilanova, and A. Benito. 2021. 'Strengths and Challenges of Secretory Ribonucleases as AntiTumor Agents', *Pharmaceutics*, 13.

Chakraborty, C., A. R. Sharma, M. Bhattacharya, and S. S. Lee. 2021. 'From COVID-19 to Cancer mRNA Vaccines: Moving From Bench to Clinic in the Vaccine Landscape', *Front Immunol*, 12: 679344.

Chamilos, G., J. Gregorio, S. Meller, R. Lande, D. P. Kontoyiannis, R. L. Modlin, and M. Gilliet. 2012. 'Cytosolic sensing of extracellular self-DNA transported into monocytes by the antimicrobial peptide LL37', *Blood*, 120: 3699-707.

Chang, Tzu-Hsuan, Yamel Cardona Gloria, Margareta J. Hellmann, Carsten Leo Greve, Didier Le Roy, Thierry Roger, Lydia Kasper, Bernhard Hube, Stefan Pusch, Neil Gow, Morten Sørlie, Anne Tøndervik, Bruno M. Moerschbacher, and Alexander N.R. Weber. 2022. 'Transkingdom mechanism of MAMP generation by chitotriosidase (CHIT1) feeds oligomeric chitin from fungal pathogens and allergens into TLR2-mediated innate immune sensing', *bioRxiv*: 2022.02.17.479713.

Chanput, W., J. J. Mes, and H. J. Wichers. 2014. 'THP-1 cell line: an in vitro cell model for immune modulation approach', *Int Immunopharmacol*, 23: 37-45.

Chaplin, D. D. 2010. 'Overview of the immune response', *J Allergy Clin Immunol*, 125: S3-23.

Chehboun, S., J. Labrecque-Carbonneau, S. Pasquin, Y. Meliani, B. Meddah, W. Ferlin, M. Sharma, A. Tormo, J. F. Masson, and J. F. Gauchat. 2017. 'Epstein-Barr virus-induced gene 3 (EBI3) can mediate IL-6 trans-signaling', *J Biol Chem*, 292: 6644-56.

Chen, C. Y., J. Chen, L. He, and B. L. Stiles. 2018. 'PTEN: Tumor Suppressor and Metabolic Regulator', *Front Endocrinol (Lausanne)*, 9: 338.

Chen, J. Q., P. Szodoray, and M. Zeher. 2016. 'Toll-Like Receptor Pathways in Autoimmune Diseases', *Clin Rev Allergy Immunol*, 50: 1-17.

Chen, T., Y. Li, R. Sun, H. Hu, Y. Liu, M. Herrmann, Y. Zhao, and L. E. Munoz. 2021. 'Receptor-Mediated NETosis on Neutrophils', *Front Immunol*, 12: 775267.

Chiang, C. C., W. J. Cheng, M. Korinek, C. Y. Lin, and T. L. Hwang. 2019. 'Neutrophils in Psoriasis', *Front Immunol*, 10: 2376.

Cicco, S., G. Cicco, V. Racanelli, and A. Vacca. 2020. 'Neutrophil Extracellular Traps (NETs) and Damage-Associated Molecular Patterns (DAMPs): Two Potential Targets for COVID-19 Treatment', *Mediators Inflamm*, 2020: 7527953.

Cieutat, A. M., P. Lobel, J. T. August, L. Kjeldsen, H. Sengelov, N. Borregaard, and D. F. Bainton. 1998. 'Azurophilic granules of human neutrophilic leukocytes are deficient in lysosome-associated membrane proteins but retain the mannose 6-phosphate recognition marker', *Blood*, 91: 1044-58.

Claushuis, T. A. M., L. E. H. van der Donk, A. L. Luitse, H. A. van Veen, N. N. van der Wel, L. A. van Vught, Jjth Roelofs, O. J. de Boer, J. M. Lankelma, L. Boon, A. F. de Vos, C. van 't Veer, and T. van der Poll. 2018. 'Role of Peptidylarginine Deiminase 4 in Neutrophil Extracellular Trap Formation and Host Defense during Klebsiella pneumoniae-Induced Pneumonia-Derived Sepsis', *J Immunol*, 201: 1241-52.

Coch, C., B. Hommertgen, T. Zillinger, J. Dassler-Plenker, B. Putschli, M. Nastaly, B. M. Kummerer, J. F. Scheunemann, B. Schumak, S. Specht, M. Schlee, W. Barchet, A. Hoerauf, E. Bartok, and G. Hartmann. 2019. 'Human TLR8 Senses RNA From Plasmodium falciparum-Infected Red Blood Cells Which Is Uniquely Required for the IFN-gamma Response in NK Cells', *Front Immunol*, 10: 371.

Colak, E., A. Leslie, K. Zausmer, E. Khatamzas, A. V. Kubarenko, T. Pichulik, S. N. Klimosch, A. Mayer, O. Siggs, A. Hector, R. Fischer, B. Klesser, A. Rautanen, M. Frank, A. V. Hill, B. Manoury, B. Beutler, D. Hartl, A. Simmons, and A. N. Weber. 2014. 'RNA and imidazoquinolines are sensed by distinct TLR7/8 ectodomain sites resulting in functionally disparate signaling events', *J Immunol*, 192: 5963-73.

Danev, R., H. Yanagisawa, and M. Kikkawa. 2019. 'Cryo-Electron Microscopy Methodology: Current Aspects and Future Directions', *Trends Biochem Sci*, 44: 837-48.

Darzynkiewicz, Z., F. Traganos, H. Zhao, H. D. Halicka, and J. Li. 2011. 'Cytometry of DNA replication and RNA synthesis: Historical perspective and recent advances based on "click chemistry"', *Cytometry A*, 79: 328-37.

de Buhr, N., and M. von Kockritz-Blickwede. 2016. 'How Neutrophil Extracellular Traps Become Visible', *J Immunol Res*, 2016: 4604713.

delCardayre, S. B., and R. T. Raines. 1994. 'Structural determinants of enzymatic processivity', *Biochemistry*, 33: 6031-7.

Demkow, U. 2021. 'Neutrophil Extracellular Traps (NETs) in Cancer Invasion, Evasion and Metastasis', *Cancers (Basel)*, 13.

Dhawan, U. K., P. Bhattacharya, S. Narayanan, V. Manickam, A. Aggarwal, and M. Subramanian. 2021. 'Hypercholesterolemia Impairs Clearance of Neutrophil Extracellular Traps and Promotes Inflammation and Atherosclerotic Plaque Progression', *Arterioscler Thromb Vasc Biol*, 41: 2598-615.

Diaz-Godinez, C., Z. Fonseca, M. Nequiz, J. P. Laclette, C. Rosales, and J. C. Carrero. 2018. 'Entamoeba histolytica Trophozoites Induce a Rapid Non-classical NETosis Mechanism Independent of NOX2-Derived Reactive Oxygen Species and PAD4 Activity', *Front Cell Infect Microbiol*, 8: 184.

Dickson, M. A., W. C. Hahn, Y. Ino, V. Ronfard, J. Y. Wu, R. A. Weinberg, D. N. Louis, F. P. Li, and J. G. Rheinwald. 2000. 'Human keratinocytes that express hTERT and also bypass a p16(INK4a)-enforced mechanism that limits life span become immortal yet retain normal growth and differentiation characteristics', *Mol Cell Biol*, 20: 1436-47.

Domer, D., T. Walther, S. Moller, M. Behnen, and T. Laskay. 2021. 'Neutrophil Extracellular Traps Activate Proinflammatory Functions of Human Neutrophils', *Front Immunol*, 12: 636954.

Doring, Y., P. Libby, and O. Soehnlein. 2020. 'Neutrophil Extracellular Traps Participate in Cardiovascular Diseases: Recent Experimental and Clinical Insights', *Circ Res*, 126: 1228-41.

Doster, R. S., L. M. Rogers, J. A. Gaddy, and D. M. Aronoff. 2018. 'Macrophage Extracellular Traps: A Scoping Review', *J Innate Immun*, 10: 3-13.

Droge, W. 2002. 'Free radicals in the physiological control of cell function', *Physiol Rev*, 82: 47-95.

Dwivedi, N., J. Upadhyay, I. Neeli, S. Khan, D. Pattanaik, L. Myers, K. A. Kirou, B. Hellmich, B. Knuckley, P. R. Thompson, M. K. Crow, T. R. Mikuls, E. Csernok, and M. Radic. 2012. 'Felty's syndrome autoantibodies bind to deiminated histones and neutrophil extracellular chromatin traps', *Arthritis Rheum*, 64: 982-92.

Eigenbrod, T., and A. H. Dalpke. 2015. 'Bacterial RNA: An Underestimated Stimulus for Innate Immune Responses', *J Immunol*, 195: 411-8.

Fard, M. B., S. B. Fard, S. Ramazi, A. Atashi, and Z. Eslamifar. 2021. 'Thrombosis in COVID-19 infection: Role of platelet activation-mediated immunity', *Thromb J*, 19: 59.

Farrera, C., and B. Fadeel. 2013. 'Macrophage clearance of neutrophil extracellular traps is a silent process', *J Immunol*, 191: 2647-56.

Faust, N., F. Varas, L. M. Kelly, S. Heck, and T. Graf. 2000. 'Insertion of enhanced green fluorescent protein into the lysozyme gene creates mice with green fluorescent granulocytes and macrophages', *Blood*, 96: 719-26.

Flechsler, Jennifer, Thomas Heimerl, Carolin Pickl, Reinhard Rachel, York-Dieter Stierhof, and Andreas Klingl. 2020. '2D and 3D immunogold localization on (epoxy) ultrathin sections with and without osmium tetroxide', *Microscopy Research and Technique*, 83: 691-705.

Fousert, E., R. Toes, and J. Desai. 2020. 'Neutrophil Extracellular Traps (NETs) Take the Central Stage in Driving Autoimmune Responses', *Cells*, 9.

Fruh, A., K. Tielking, F. Schoknecht, S. Liu, U. C. Schneider, S. Fischer, P. Vajkoczy, and R. Xu. 2021. 'RNase A Inhibits Formation of Neutrophil Extracellular Traps in Subarachnoid Hemorrhage', *Front Physiol*, 12: 724611.

Futosi, K., S. Fodor, and A. Mocsai. 2013. 'Neutrophil cell surface receptors and their intracellular signal transduction pathways', *Int Immunopharmacol*, 17: 638-50.

Gabius, H. J., H. Kaltner, J. Kopitz, and S. Andre. 2015. 'The glycobiology of the CD system: a dictionary for translating marker designations into glycan/lectin structure and function', *Trends Biochem Sci*, 40: 360-76.

Gaidt, M. M., F. Rapino, T. Graf, and V. Hornung. 2018. 'Modeling Primary Human Monocytes with the Trans-Differentiation Cell Line BLaER1', *Methods Mol Biol*, 1714: 57-66.

Gan, T., Y. Yang, F. Hu, X. Chen, J. Zhou, Y. Li, Y. Xu, H. Wang, Y. Chen, and M. Zhang. 2018. 'TLR3 Regulated Poly I:C-Induced Neutrophil Extracellular Traps and Acute Lung Injury Partly Through p38 MAP Kinase', *Front Microbiol*, 9: 3174.

Ganguly, D., G. Chamilos, R. Lande, J. Gregorio, S. Meller, V. Facchinetti, B. Homey, F. J. Barrat, T. Zal, and M. Gilliet. 2009. 'Self-RNA-antimicrobial peptide complexes activate human dendritic cells through TLR7 and TLR8', *J Exp Med*, 206: 1983-94.

Garcia-Romo, G. S., S. Caielli, B. Vega, J. Connolly, F. Allantaz, Z. Xu, M. Punaro, J. Baisch, C. Guiducci, R. L. Coffman, F. J. Barrat, J. Banchereau, and V. Pascual. 2011. 'Netting neutrophils are major inducers of type I IFN production in pediatric systemic lupus erythematosus', *Sci Transl Med*, 3: 73ra20.

Gay, N. J., and F. J. Keith. 1991. 'Drosophila Toll and IL-1 receptor', *Nature*, 351: 355-6.

Geering, B., C. Stoeckle, S. Conus, and H. U. Simon. 2013. 'Living and dying for inflammation: neutrophils, eosinophils, basophils', *Trends Immunol*, 34: 398-409.

Gewurz, H., C. Mold, J. Siegel, and B. Fiedel. 1982. 'C-reactive protein and the acute phase response', *Adv Intern Med*, 27: 345-72.

Gierlikowska, B., A. Stachura, W. Gierlikowski, and U. Demkow. 2021. 'Phagocytosis, Degranulation and Extracellular Traps Release by Neutrophils-The Current Knowledge, Pharmacological Modulation and Future Prospects', *Front Pharmacol*, 12: 666732.

Gilliet, M., C. Conrad, M. Geiges, A. Cozzio, W. Thurlimann, G. Burg, F. O. Nestle, and R. Dummer. 2004. 'Psoriasis triggered by toll-like receptor 7 agonist imiquimod in the presence of dermal plasmacytoid dendritic cell precursors', *Arch Dermatol*, 140: 1490-5.

Golonka, R. M., P. Saha, B. S. Yeoh, S. Chattopadhyay, A. T. Gewirtz, B. Joe, and M. Vijay-Kumar. 2020. 'Harnessing innate immunity to eliminate SARS-CoV-2 and ameliorate COVID-19 disease', *Physiol Genomics*, 52: 217-21.

Greb, J. E., A. M. Goldminz, J. T. Elder, M. G. Lebwohl, D. D. Gladman, J. J. Wu, N. N. Mehta, A. Y. Finlay, and A. B. Gottlieb. 2016. 'Psoriasis', *Nat Rev Dis Primers*, 2: 16082.

Greulich, W., M. Wagner, M. M. Gaidt, C. Stafford, Y. Cheng, A. Linder, T. Carell, and V. Hornung. 2019. 'TLR8 Is a Sensor of RNase T2 Degradation Products', *Cell*, 179: 1264-75 e13.

Guiducci, E., C. Lemberg, N. Kung, E. Schraner, A. P. A. Theocharides, and S. LeibundGut-Landmann. 2018. 'Candida albicans-Induced NETosis Is Independent of Peptidylarginine Deiminase 4', *Front Immunol*, 9: 1573.

Happel, C., A. Ganguly, and D. A. Tagle. 2020. 'Extracellular RNAs as potential biomarkers for cancer', *J Cancer Metastasis Treat*, 6.

Hawez, A., A. Al-Haidari, R. Madhi, M. Rahman, and H. Thorlacius. 2019. 'MiR-155 Regulates PAD4-Dependent Formation of Neutrophil Extracellular Traps', *Front Immunol*, 10: 2462.

Herster, F., Z. Bittner, N. K. Archer, S. Dickhofer, D. Eisel, T. Eigenbrod, T. Knorpp, N. Schneiderhan-Marra, M. W. Loffler, H. Kalbacher, T. Vierbuchen, H. Heine, L. S. Miller, D. Hartl, L. Freund, K. Schakel, M. Heister, K. Ghoreschi, and A. N. R. Weber. 2020. 'Neutrophil extracellular trap-associated RNA and LL37 enable self-amplifying inflammation in psoriasis', *Nat Commun*, 11: 105.

Hirai, H., A. Yokota, A. Tamura, A. Sato, and T. Maekawa. 2015. 'Non-steady-state hematopoiesis regulated by the C/EBPbeta transcription factor', *Cancer Sci*, 106: 797-802.

Hopfner, K. P., and V. Hornung. 2020. 'Molecular mechanisms and cellular functions of cGAS-STING signalling', *Nat Rev Mol Cell Biol*, 21: 501-21.

Hoppenbrouwers, T., A. S. A. Autar, A. R. Sultan, T. E. Abraham, W. A. van Cappellen, A. B. Houtsmuller, W. J. B. van Wamel, H. M. M. van Beusekom, J. W. van Neck, and M. P. M. de Maat. 2017. 'In vitro induction of NETosis: Comprehensive live imaging comparison and systematic review', *PLoS One*, 12: e0176472.

Houseley, J., and D. Tollervey. 2009. 'The many pathways of RNA degradation', *Cell*, 136: 763-76.

Hsieh, Y. T., Y. C. Chou, P. Y. Kuo, H. W. Tsai, Y. T. Yen, A. L. Shiau, and C. R. Wang. 2022. 'Down-regulated miR-146a expression with increased neutrophil extracellular traps and apoptosis formation in autoimmune-mediated diffuse alveolar hemorrhage', *J Biomed Sci*, 29: 62.

Huang, J., W. Hong, M. Wan, and L. Zheng. 2022. 'Molecular mechanisms and therapeutic target of NETosis in diseases', *MedComm (2020)*, 3: e162.

Huang, W., M. Zhao, N. Wei, X. Wang, H. Cao, Q. Du, and Z. Liang. 2014. 'Site-specific RNase A activity was dramatically reduced in serum from multiple types of cancer patients', *PLoS One*, 9: e96490.

Huff, Joseph, Annette Bergter, Jan Birkenbeil, Ingo Kleppe, Ralf Engelmann, and Uros Krzic. 2017. 'The new 2D Superresolution mode for ZEISS Airyscan', *Nature Methods*, 14: 1223-23.

Hugon, P., J. C. Dufour, P. Colson, P. E. Fournier, K. Sallah, and D. Raoult. 2015. 'A comprehensive repertoire of prokaryotic species identified in human beings', *Lancet Infect Dis*, 15: 1211-19.

Hulspas, R., M. R. O'Gorman, B. L. Wood, J. W. Gratama, and D. R. Sutherland. 2009. 'Considerations for the control of background fluorescence in clinical flow cytometry', *Cytometry B Clin Cytom*, 76: 355-64.

Ishii, N., K. Funami, M. Tatematsu, T. Seya, and M. Matsumoto. 2014. 'Endosomal localization of TLR8 confers distinctive proteolytic processing on human myeloid cells', *J Immunol*, 193: 5118-28.

Isles, H. M., C. A. Loynes, S. Alasmari, F. C. Kon, K. M. Henry, A. Kadochnikova, J. Hales, C. F. Muir, M. C. Keightley, V. Kadirkamanathan, N. Hamilton, G. J. Lieschke, S. A. Renshaw, and P. M. Elks. 2021. 'Pioneer neutrophils release chromatin within in vivo swarms', *Elife*, 10.

Janeway, C. A., Jr. 1989. 'Approaching the asymptote? Evolution and revolution in immunology', *Cold Spring Harb Symp Quant Biol*, 54 Pt 1: 1-13.

———. 1992. 'The immune system evolved to discriminate infectious nonself from noninfectious self', *Immunol Today*, 13: 11-6.

Janeway, C. A., Jr., and R. Medzhitov. 2002. 'Innate immune recognition', *Annu Rev Immunol*, 20: 197-216.

Janiuk, K., E. Jablonska, and M. Garley. 2021. 'Significance of NETs Formation in COVID-19', *Cells*, 10.

Janke, M., J. Poth, V. Wimmenauer, T. Giese, C. Coch, W. Barchet, M. Schlee, and G. Hartmann. 2009. 'Selective and direct activation of human neutrophils but not eosinophils by Toll-like receptor 8', *J Allergy Clin Immunol*, 123: 1026-33.

Jiang, W., F. G. Zhu, L. Bhagat, D. Yu, J. X. Tang, E. R. Kandimalla, N. La Monica, and S. Agrawal. 2013. 'A Toll-like receptor 7, 8, and 9 antagonist inhibits Th1 and Th17 responses and inflammasome activation in a model of IL-23-induced psoriasis', *J Invest Dermatol*, 133: 1777-84.

Kahlenberg, J. M., C. Carmona-Rivera, C. K. Smith, and M. J. Kaplan. 2013. 'Neutrophil extracellular trap-associated protein activation of the NLRP3 inflammasome is enhanced in lupus macrophages', *J Immunol*, 190: 1217-26.

Kannemeier, C., A. Shibamiya, F. Nakazawa, H. Trusheim, C. Ruppert, P. Markart, Y. Song, E. Tzima, E. Kennerknecht, M. Niepmann, M. L. von Bruehl, D. Sedding, S. Massberg, A. Gunther, B. Engelmann, and K. T. Preissner. 2007. 'Extracellular RNA constitutes a natural procoagulant cofactor in blood coagulation', *Proc Natl Acad Sci U S A*, 104: 6388-93.

Kanwar, S., D. C. Bullard, M. J. Hickey, C. W. Smith, A. L. Beaudet, B. A. Wolitzky, and P. Kubes. 1997. 'The association between alpha4-integrin, P-selectin, and E-selectin in an allergic model of inflammation', *J Exp Med*, 185: 1077-87.

Kariko, K., M. Buckstein, H. Ni, and D. Weissman. 2005. 'Suppression of RNA recognition by Toll-like receptors: the impact of nucleoside modification and the evolutionary origin of RNA', *Immunity*, 23: 165-75.

Kawai, T., and S. Akira. 2010. 'The role of pattern-recognition receptors in innate immunity: update on Toll-like receptors', *Nat Immunol*, 11: 373-84.

Kennedy, A. D., and F. R. DeLeo. 2009. 'Neutrophil apoptosis and the resolution of infection', *Immunol Res*, 43: 25-61.

Kenny, E. F., A. Herzig, R. Kruger, A. Muth, S. Mondal, P. R. Thompson, V. Brinkmann, H. V. Bernuth, and A. Zychlinsky. 2017. 'Diverse stimuli engage different neutrophil extracellular trap pathways', *Elife*, 6.

Kessenbrock, K., M. Krumbholz, U. Schonermarck, W. Back, W. L. Gross, Z. Werb, H. J. Grone, V. Brinkmann, and D. E. Jenne. 2009. 'Netting neutrophils in autoimmune small-vessel vasculitis', *Nat Med*, 15: 623-5.

Khandpur, R., C. Carmona-Rivera, A. Vivekanandan-Giri, A. Gizinski, S. Yalavarthi, J. S. Knight, S. Friday, S. Li, R. M. Patel, V. Subramanian, P. Thompson, P. Chen, D. A. Fox, S. Pennathur, and M. J. Kaplan. 2013. 'NETs are a source of citrullinated autoantigens and stimulate inflammatory responses in rheumatoid arthritis', *Sci Transl Med*, 5: 178ra40.

Kim, K. M., K. Abdelmohsen, M. Mustapic, D. Kapogiannis, and M. Gorospe. 2017. 'RNA in extracellular vesicles', *Wiley Interdiscip Rev RNA*, 8.

Kim, S. J., and C. N. Jenne. 2016. 'Role of platelets in neutrophil extracellular trap (NET) production and tissue injury', *Semin Immunol*, 28: 546-54.

Klingemann, H. G., E. Wong, and G. Maki. 1996. 'A cytotoxic NK-cell line (NK-92) for ex vivo purging of leukemia from blood', *Biol Blood Marrow Transplant*, 2: 68-75.

Knight, J. S., W. Luo, A. A. O'Dell, S. Yalavarthi, W. Zhao, V. Subramanian, C. Guo, R. C. Grenn, P. R. Thompson, D. T. Eitzman, and M. J. Kaplan. 2014. 'Peptidylarginine deiminase inhibition reduces vascular damage and modulates innate immune responses in murine models of atherosclerosis', *Circ Res*, 114: 947-56.

Kollisch, G., F. V. Solis, H. L. Obermann, J. Eckert, T. Muller, T. Vierbuchen, T. Rickmeyer, S. Muche, J. M. Przyborski, H. Heine, A. Kaufmann, S. Baumeister, K. Lingelbach, and S. Bauer. 2022. 'TLR8 is activated by 5'-methylthioinosine, a Plasmodium falciparum-derived intermediate of the purine salvage pathway', *Cell Rep*, 39: 110691.

Kruger, P., M. Saffarzadeh, A. N. Weber, N. Rieber, M. Radsak, H. von Bernuth, C. Benarafa, D. Roos, J. Skokowa, and D. Hartl. 2015. 'Neutrophils: Between host defence, immune modulation, and tissue injury', *PLoS Pathog*, 11: e1004651.

Kubo, T., and M. Fujii. 2001. 'Specific binding and stabilization of DNA and phosphorothioate DNA by amphiphilic alpha-helical peptides', *Nucleosides Nucleotides Nucleic Acids*, 20: 1313-6.

Kwak, H. J., P. Liu, B. Bajrami, Y. Xu, S. Y. Park, C. Nombela-Arrieta, S. Mondal, Y. Sun, H. Zhu, L. Chai, L. E. Silberstein, T. Cheng, and H. R. Luo. 2015. 'Myeloid cell-derived reactive oxygen species externally regulate the proliferation of myeloid progenitors in emergency granulopoiesis', *Immunity*, 42: 159-71.

Lakschevitz, F. S., S. Hassanpour, A. Rubin, N. Fine, C. Sun, and M. Glogauer. 2016. 'Identification of neutrophil surface marker changes in health and inflammation using high-throughput screening flow cytometry', *Exp Cell Res*, 342: 200-9.

Lambert, S., C. A. Hambro, A. Johnston, P. E. Stuart, L. C. Tsoi, R. P. Nair, and J. T. Elder. 2019. 'Neutrophil Extracellular Traps Induce Human Th17 Cells: Effect of Psoriasis-Associated TRAF3IP2 Genotype', *J Invest Dermatol*, 139: 1245-53.

Lande, R., E. Botti, C. Jandus, D. Dojcinovic, G. Fanelli, C. Conrad, G. Chamilos, L. Feldmeyer, B. Marinari, S. Chon, L. Vence, V. Riccieri, P. Guillaume, A. A. Navarini, P. Romero, A. Costanzo, E. Piccolella, M. Gilliet, and L. Frasca. 2014. 'The antimicrobial peptide LL37 is a T-cell autoantigen in psoriasis', *Nat Commun*, 5: 5621.

Lande, R., D. Ganguly, V. Facchinetti, L. Frasca, C. Conrad, J. Gregorio, S. Meller, G. Chamilos, R. Sebasigari, V. Riccieri, R. Bassett, H. Amuro, S. Fukuhara, T. Ito, Y. J. Liu, and M. Gilliet. 2011. 'Neutrophils activate plasmacytoid dendritic cells by releasing self-DNA-peptide complexes in systemic lupus erythematosus', *Sci Transl Med*, 3: 73ra19.

Lande, R., J. Gregorio, V. Facchinetti, B. Chatterjee, Y. H. Wang, B. Homey, W. Cao, Y. H. Wang, B. Su, F. O. Nestle, T. Zal, I. Mellman, J. M. Schroder, Y. J. Liu, and M. Gilliet. 2007. 'Plasmacytoid dendritic cells sense self-DNA coupled with antimicrobial peptide', *Nature*, 449: 564-9.

Lasch, M., K. Kumaraswami, S. Nasiscionyte, S. Kircher, D. van den Heuvel, S. Meister, H. Ishikawa-Ankerhold, and E. Deindl. 2020. 'RNase A Treatment Interferes With Leukocyte Recruitment, Neutrophil Extracellular Trap Formation, and Angiogenesis in Ischemic Muscle Tissue', *Front Physiol*, 11: 576736.

Lauber, K., S. G. Blumenthal, M. Waibel, and S. Wesselborg. 2004. 'Clearance of apoptotic cells: getting rid of the corpses', *Mol Cell*, 14: 277-87.

Lawrence, S. M., R. Corriden, and V. Nizet. 2018. 'The Ontogeny of a Neutrophil: Mechanisms of Granulopoiesis and Homeostasis', *Microbiol Mol Biol Rev*, 82.

Lazzaretto, B., and B. Fadeel. 2019. 'Intra- and Extracellular Degradation of Neutrophil Extracellular Traps by Macrophages and Dendritic Cells', *J Immunol*, 203: 2276-90.

Lee, B. L., and G. M. Barton. 2014. 'Trafficking of endosomal Toll-like receptors', *Trends Cell Biol*, 24: 360-9.

Lehrer, R. I., and T. Ganz. 2002. 'Cathelicidins: a family of endogenous antimicrobial peptides', *Curr Opin Hematol*, 9: 18-22.

Lemaitre, B., E. Nicolas, L. Michaut, J. M. Reichhart, and J. A. Hoffmann. 1996. 'The dorsoventral regulatory gene cassette spatzle/Toll/cactus controls the potent antifungal response in Drosophila adults', *Cell*, 86: 973-83.

Lerner, E. A., M. R. Lerner, C. A. Janeway, Jr., and J. A. Steitz. 1981. 'Monoclonal antibodies to nucleic acid-containing cellular constituents: probes for molecular biology and autoimmune disease', *Proc Natl Acad Sci U S A*, 78: 2737-41.

Lewis, H. D., J. Liddle, J. E. Coote, S. J. Atkinson, M. D. Barker, B. D. Bax, K. L. Bicker, R. P. Bingham, M. Campbell, Y. H. Chen, C. W. Chung, P. D. Craggs, R. P. Davis, D. Eberhard, G. Joberty, K. E. Lind, K. Locke, C. Maller, K. Martinod, C. Patten, O. Polyakova, C. E. Rise, M. Rudiger, R. J. Sheppard, D. J. Slade, P. Thomas, J. Thorpe, G. Yao, G. Drewes, D. D. Wagner, P. R. Thompson, R. K. Prinjha, and D. M. Wilson. 2015. 'Inhibition of PAD4 activity is sufficient to disrupt mouse and human NET formation', *Nat Chem Biol*, 11: 189-91.

Li, B., G. Li, X. Yang, Z. Song, Y. Wang, and Z. Zhang. 2022. 'NETosis in Psoriatic Arthritis: Serum MPO-DNA Complex Level Correlates With Its Disease Activity', *Front Immunol*, 13: 911347.

Li, M., C. Lin, H. Deng, J. Strnad, L. Bernabei, D. T. Vogl, J. J. Burke, and Y. Nefedova. 2020. 'A Novel Peptidylarginine Deiminase 4 (PAD4) Inhibitor BMS-P5 Blocks Formation of Neutrophil Extracellular Traps and Delays Progression of Multiple Myeloma', *Mol Cancer Ther*, 19: 1530-38.

Li, Q., M. J. Gloudemans, J. M. Geisinger, B. Fan, F. Aguet, T. Sun, G. Ramaswami, Y. I. Li, J. B. Ma, J. K. Pritchard, S. B. Montgomery, and J. B. Li. 2022. 'RNA editing underlies genetic risk of common inflammatory diseases', *Nature*, 608: 569-77.

Li, X. D., and Z. J. Chen. 2012. 'Sequence specific detection of bacterial 23S ribosomal RNA by TLR13', *Elife*, 1: e00102.

Liew, P. X., and P. Kubes. 2019. 'The Neutrophil's Role During Health and Disease', *Physiol Rev*, 99: 1223-48.

Ling, H., M. Fabbri, and G. A. Calin. 2013. 'MicroRNAs and other non-coding RNAs as targets for anticancer drug development', *Nat Rev Drug Discov*, 12: 847-65.

Linhares-Lacerda, L., J. R. Temerozo, M. Ribeiro-Alves, E. P. Azevedo, A. Mojoli, M. T. C. Nascimento, G. Silva-Oliveira, W. Savino, D. Foguel, D. C. Bou-Habib, and E. M. Saraiva. 2020. 'Neutrophil extracellular trap-enriched supernatants carry microRNAs able to modulate TNF-alpha production by macrophages', *Sci Rep*, 10: 2715.

Lishko, V. K., B. Moreno, N. P. Podolnikova, and T. P. Ugarova. 2016. 'Identification of Human Cathelicidin Peptide LL-37 as a Ligand for Macrophage Integrin alphaMbeta2 (Mac-1, CD11b/CD18) that Promotes Phagocytosis by Opsonizing Bacteria', *Res Rep Biochem*, 2016: 39-55.

Liu, X., T. Arfman, K. Wichapong, C. P. M. Reutelingsperger, J. Voorberg, and G. A. F. Nicolaes. 2021. 'PAD4 takes charge during neutrophil activation: Impact of PAD4 mediated NET formation on immune-mediated disease', *J Thromb Haemost*, 19: 1607-17.

Lood, C., S. Arve, J. Ledbetter, and K. B. Elkon. 2017. 'TLR7/8 activation in neutrophils impairs immune complex phagocytosis through shedding of FcgRIIA', *J Exp Med*, 214: 2103-19.

Malatesta, M. 2021. 'Transmission Electron Microscopy as a Powerful Tool to Investigate the Interaction of Nanoparticles with Subcellular Structures', *Int J Mol Sci*, 22.

Mannion, N. M., S. M. Greenwood, R. Young, S. Cox, J. Brindle, D. Read, C. Nellaker, C. Vesely, C. P. Ponting, P. J. McLaughlin, M. F. Jantsch, J. Dorin, I. R. Adams, A. D. Scadden, M. Ohman, L. P. Keegan, and M. A. O'Connell. 2014. 'The RNA-editing enzyme ADAR1 controls innate immune responses to RNA', *Cell Rep*, 9: 1482-94.

Manz, M. G., and S. Boettcher. 2014. 'Emergency granulopoiesis', *Nat Rev Immunol*, 14: 302-14.

McNabb, D. S., R. Reed, and R. A. Marciniak. 2005. 'Dual luciferase assay system for rapid assessment of gene expression in Saccharomyces cerevisiae', *Eukaryot Cell*, 4: 1539-49.

Medzhitov, R., P. Preston-Hurlburt, and C. A. Janeway, Jr. 1997. 'A human homologue of the Drosophila Toll protein signals activation of adaptive immunity', *Nature*, 388: 394-7.

Metzemaekers, M., M. Gouwy, and P. Proost. 2020. 'Neutrophil chemoattractant receptors in health and disease: double-edged swords', *Cell Mol Immunol*, 17: 433-50.

'Microbiology by numbers'. 2011. *Nat Rev Microbiol*, 9: 628.

Middleton, E. A., X. Y. He, F. Denorme, R. A. Campbell, D. Ng, S. P. Salvatore, M. Mostyka, A. Baxter-Stoltzfus, A. C. Borczuk, M. Loda, M. J. Cody, B. K. Manne, I. Portier, E. S. Harris, A. C. Petrey, E. J. Beswick, A. F. Caulin, A. Iovino, L. M. Abegglen, A. S. Weyrich, M. T. Rondina, M. Egeblad, J. D. Schiffman, and C. C. Yost. 2020. 'Neutrophil extracellular traps contribute to immunothrombosis in COVID-19 acute respiratory distress syndrome', *Blood*, 136: 1169-79.

Minns, D., K. J. Smith, V. Alessandrini, G. Hardisty, L. Melrose, L. Jackson-Jones, A. S. MacDonald, D. J. Davidson, and E. Gwyer Findlay. 2021. 'The neutrophil antimicrobial peptide cathelicidin promotes Th17 differentiation', *Nat Commun*, 12: 1285.

Mohanty, T., J. Sjogren, F. Kahn, A. H. Abu-Humaidan, N. Fisker, K. Assing, M. Morgelin, A. A. Bengtsson, N. Borregaard, and O. E. Sorensen. 2015. 'A novel mechanism for NETosis provides antimicrobial defense at the oral mucosa', *Blood*, 126: 2128-37.

Mollerherm, H., M. von Kockritz-Blickwede, and K. Branitzki-Heinemann. 2016. 'Antimicrobial Activity of Mast Cells: Role and Relevance of Extracellular DNA Traps', *Front Immunol*, 7: 265.

Mora, C., D. P. Tittensor, S. Adl, A. G. Simpson, and B. Worm. 2011. 'How many species are there on Earth and in the ocean?', *PLoS Biol*, 9: e1001127.

Moran, N. A. 2006. 'Symbiosis', *Curr Biol*, 16: R866-71.

Morshed, M., R. Hlushchuk, D. Simon, A. F. Walls, K. Obata-Ninomiya, H. Karasuyama, V. Djonov, A. Eggel, T. Kaufmann, H. U. Simon, and S. Yousefi. 2014. 'NADPH oxidase-independent formation of extracellular DNA traps by basophils', *J Immunol*, 192: 5314-23.

Munzer, P., R. Negro, S. Fukui, L. di Meglio, K. Aymonnier, L. Chu, D. Cherpokova, S. Gutch, N. Sorvillo, L. Shi, V. G. Magupalli, A. N. R. Weber, R. E. Scharf, C. M. Waterman, H. Wu, and D. D. Wagner. 2021. 'NLRP3 Inflammasome Assembly in Neutrophils Is Supported by PAD4 and Promotes NETosis Under Sterile Conditions', *Front Immunol*, 12: 683803.

Murao, A., A. Arif, M. Brenner, N. L. Denning, H. Jin, S. Takizawa, B. Nicastro, P. Wang, and M. Aziz. 2020. 'Extracellular CIRP and TREM-1 axis promotes ICAM-1-Rho-mediated NETosis in sepsis', *FASEB J*, 34: 9771-86.

Murphey, K., C. Weaver, and L. Berg. 2022. *Janeway's Immunobiology 10th Edition* (Norton).

Mysore, V., X. Cullere, J. Mears, F. Rosetti, K. Okubo, P. X. Liew, F. Zhang, I. Madera-Salcedo, F. Rosenbauer, R. M. Stone, J. C. Aster, U. H. von Andrian, A. H. Lichtman, S. Raychaudhuri, and T. N. Mayadas. 2021. 'FcgammaR engagement reprograms neutrophils into antigen cross-presenting cells that elicit acquired anti-tumor immunity', *Nat Commun*, 12: 4791.

Nauseef, W. M., and N. Borregaard. 2014. 'Neutrophils at work', *Nat Immunol*, 15: 602-11.

Neumann, A., L. Vollger, E. T. Berends, E. M. Molhoek, D. A. Stapels, M. Midon, A. Friaes, A. Pingoud, S. H. Rooijakkers, R. L. Gallo, M. Morgelin, V. Nizet, H. Y. Naim, and M. von Kockritz-Blickwede. 2014. 'Novel role of the antimicrobial peptide LL-37 in the protection of neutrophil extracellular traps against degradation by bacterial nucleases', *J Innate Immun*, 6: 860-8.

Newton, K., and V. M. Dixit. 2012. 'Signaling in innate immunity and inflammation', *Cold Spring Harb Perspect Biol*, 4.

Ngou, B. P. M., P. Ding, and J. D. G. Jones. 2022. 'Thirty years of resistance: Zig-zag through the plant immune system', *Plant Cell*, 34: 1447-78.

Nicholson, L. B. 2016. 'The immune system', *Essays Biochem*, 60: 275-301.

O'Brien, K. L., and D. K. Finlay. 2019. 'Immunometabolism and natural killer cell responses', *Nat Rev Immunol*, 19: 282-90.

O'Neil, L. J., C. B. Oliveira, D. Sandoval-Heglund, A. Barrera-Vargas, J. Merayo-Chalico, E. Aguirre-Aguilar, M. J. Kaplan, and C. Carmona-Rivera. 2021. 'Anti-Carbamylated LL37 Antibodies Promote Pathogenic Bone Resorption in Rheumatoid Arthritis', *Front Immunol*, 12: 715997.

O'Neill, L. A., D. Golenbock, and A. G. Bowie. 2013. 'The history of Toll-like receptors - redefining innate immunity', *Nat Rev Immunol*, 13: 453-60.

Obermayer, A., L. M. Jakob, J. D. Haslbauer, M. S. Matter, A. Tzankov, and W. Stoiber. 2021. 'Neutrophil Extracellular Traps in Fatal COVID-19-Associated Lung Injury', *Dis Markers*, 2021: 5566826.

Oh, H., B. Siano, and S. Diamond. 2008. 'Neutrophil isolation protocol', *J Vis Exp*.

Ostendorf, T., T. Zillinger, K. Andryka, T. M. Schlee-Guimaraes, S. Schmitz, S. Marx, K. Bayrak, R. Linke, S. Salgert, J. Wegner, T. Grasser, S. Bauersachs, L. Soltesz, M. P. Hubner, M. Nastaly, C. Coch, M. Kettwig, I. Roehl, M. Henneke, A. Hoerauf, W. Barchet, J. Gartner, M. Schlee, G. Hartmann, and E. Bartok. 2020. 'Immune Sensing of Synthetic, Bacterial, and Protozoan RNA by Toll-like Receptor 8 Requires Coordinated Processing by RNase T2 and RNase 2', *Immunity*, 52: 591-605 e6.

Pan, L., M. P. Lu, J. H. Wang, M. Xu, and S. R. Yang. 2020. 'Immunological pathogenesis and treatment of systemic lupus erythematosus', *World J Pediatr*, 16: 19-30.

Papayannopoulos, V. 2018. 'Neutrophil extracellular traps in immunity and disease', *Nat Rev Immunol*, 18: 134-47.

Parker, D. C. 1993. 'T cell-dependent B cell activation', *Annu Rev Immunol*, 11: 331-60.

Parkin, J., and B. Cohen. 2001. 'An overview of the immune system', *Lancet*, 357: 1777-89.

Pearson, Karl. 1895. 'Note on Regression and Inheritance in the Case of Two Parents', *Proceedings of the Royal Society of London*, 58: 240-42.

Pederson, T. 2011. 'The nucleolus', *Cold Spring Harb Perspect Biol*, 3.

Peng, H. H., Y. J. Liu, D. M. Ojcius, C. M. Lee, R. H. Chen, P. R. Huang, J. Martel, and J. D. Young. 2017. 'Mineral particles stimulate innate immunity through neutrophil extracellular traps containing HMGB1', *Sci Rep*, 7: 16628.

Penzo, M., A. N. Guerrieri, F. Zacchini, D. Trere, and L. Montanaro. 2017. 'RNA Pseudouridylation in Physiology and Medicine: For Better and for Worse', *Genes (Basel)*, 8.

Piipponen, M., D. Li, and N. X. Landen. 2020. 'The Immune Functions of Keratinocytes in Skin Wound Healing', *Int J Mol Sci*, 21.

Potter, M. 1986. *The Wild Mouse in Immunology*.

Preissner, K. T., S. Fischer, and E. Deindl. 2020. 'Extracellular RNA as a Versatile DAMP and Alarm Signal That Influences Leukocyte Recruitment in Inflammation and Infection', *Front Cell Dev Biol*, 8: 619221.

Presolski, S. I., V. P. Hong, and M. G. Finn. 2011. 'Copper-Catalyzed Azide-Alkyne Click Chemistry for Bioconjugation', *Curr Protoc Chem Biol*, 3: 153-62.

Prince, L. R., M. K. Whyte, I. Sabroe, and L. C. Parker. 2011. 'The role of TLRs in neutrophil activation', *Curr Opin Pharmacol*, 11: 397-403.

Prochazkova, P., R. Roubalova, J. Dvorak, N. I. Navarro Pacheco, and M. Bilej. 2020. 'Pattern recognition receptors in annelids', *Dev Comp Immunol*, 102: 103493.

Provost, T. T., R. Herrera-Esparza, and L. A. Diaz. 1985. 'Nucleoprotein autoantibodies in lupus erythematosus', *J Invest Dermatol*, 85: 133s-39s.

Quinn, J. F., T. Patel, D. Wong, S. Das, J. E. Freedman, L. C. Laurent, B. S. Carter, F. Hochberg, K. Van Keuren-Jensen, M. Huentelman, R. Spetzler, M. Y. Kalani, J. Arango, P. D. Adelson, H. L. Weiner, R. Gandhi, B. Goilav, C. Putterman, and J. A. Saugstad. 2015. 'Extracellular RNAs: development as biomarkers of human disease', *J Extracell Vesicles*, 4: 27495.

Rauta, P. R., B. Nayak, and S. Das. 2012. 'Immune system and immune responses in fish and their role in comparative immunity study: a model for higher organisms', *Immunol Lett*, 148: 23-33.

Ravindran, M., M. A. Khan, and N. Palaniyar. 2019. 'Neutrophil Extracellular Trap Formation: Physiology, Pathology, and Pharmacology', *Biomolecules*, 9.

Ray, A., M. Cot, G. Puzo, M. Gilleron, and J. Nigou. 2013. 'Bacterial cell wall macroamphiphiles: pathogen-/microbe-associated molecular patterns detected by mammalian innate immune system', *Biochimie*, 95: 33-42.

Rendon, A., and K. Schakel. 2019. 'Psoriasis Pathogenesis and Treatment', *Int J Mol Sci*, 20.

Rice, G. I., P. R. Kasher, G. M. Forte, N. M. Mannion, S. M. Greenwood, M. Szynkiewicz, J. E. Dickerson, S. S. Bhaskar, M. Zampini, T. A. Briggs, E. M. Jenkinson, C. A. Bacino, R. Battini, E. Bertini, P. A. Brogan, L. A. Brueton, M. Carpanelli, C. De Laet, P. de Lonlay, M. del Toro, I. Desguerre, E. Fazzi, A. Garcia-Cazorla, A. Heiberg, M. Kawaguchi, R. Kumar, J. P. Lin, C. M. Lourenco, A. M. Male, W. Marques, Jr., C. Mignot, I. Olivieri, S. Orcesi, P. Prabhakar, M. Rasmussen, R. A. Robinson, F. Rozenberg, J. L. Schmidt, K. Steindl, T. Y. Tan, W. G. van der Merwe, A. Vanderver, G. Vassallo, E. L. Wakeling, E. Wassmer, E. Whittaker, J. H. Livingston, P. Lebon, T. Suzuki, P. J. McLaughlin, L. P. Keegan, M. A. O'Connell, S. C. Lovell, and Y. J. Crow. 2012. 'Mutations in ADAR1 cause Aicardi-Goutieres syndrome associated with a type I interferon signature', *Nat Genet*, 44: 1243-8.

Richardson, I. M., C. J. Calo, and L. E. Hind. 2021. 'Microphysiological Systems for Studying Cellular Crosstalk During the Neutrophil Response to Infection', *Front Immunol*, 12: 661537.

Rieckmann, J. C., R. Geiger, D. Hornburg, T. Wolf, K. Kveler, D. Jarrossay, F. Sallusto, S. S. Shen-Orr, A. Lanzavecchia, M. Mann, and F. Meissner. 2017. 'Social network architecture of human immune cells unveiled by quantitative proteomics', *Nat Immunol*, 18: 583-93.

Rizzo, H. L., S. Kagami, K. G. Phillips, S. E. Kurtz, S. L. Jacques, and A. Blauvelt. 2011. 'IL-23-mediated psoriasis-like epidermal hyperplasia is dependent on IL-17A', *J Immunol*, 186: 1495-502.

Rorvig, S., O. Ostergaard, N. H. Heegaard, and N. Borregaard. 2013. 'Proteome profiling of human neutrophil granule subsets, secretory vesicles, and cell membrane: correlation with transcriptome profiling of neutrophil precursors', *J Leukoc Biol*, 94: 711-21.

Rosales, C. 2020. 'Neutrophils at the crossroads of innate and adaptive immunity', *J Leukoc Biol*, 108: 377-96.

Rosazza, T., J. Warner, and G. Sollberger. 2021. 'NET formation - mechanisms and how they relate to other cell death pathways', *FEBS J*, 288: 3334-50.

Rupaimoole, R., and F. J. Slack. 2017. 'MicroRNA therapeutics: towards a new era for the management of cancer and other diseases', *Nat Rev Drug Discov*, 16: 203-22.

Sahu, A., P. K. Jha, A. Prabhakar, H. D. Singh, N. Gupta, T. Chatterjee, T. Tyagi, S. Sharma, B. Kumari, S. Singh, V. Nair, S. Goel, and M. Z. Ashraf. 2017. 'MicroRNA-145 Impedes Thrombus Formation via Targeting Tissue Factor in Venous Thrombosis', *EBioMedicine*, 26: 175-86.

Saikh, K. U. 2021. 'MyD88 and beyond: a perspective on MyD88-targeted therapeutic approach for modulation of host immunity', *Immunol Res*, 69: 117-28.

Saikh, K. U., E. M. Morazzani, A. E. Piper, R. R. Bakken, and P. J. Glass. 2020. 'A small molecule inhibitor of MyD88 exhibits broad spectrum antiviral activity by up regulation of type I interferon', *Antiviral Res*, 181: 104854.

Saitoh, T., J. Komano, Y. Saitoh, T. Misawa, M. Takahama, T. Kozaki, T. Uehata, H. Iwasaki, H. Omori, S. Yamaoka, N. Yamamoto, and S. Akira. 2012. 'Neutrophil extracellular traps mediate a host defense response to human immunodeficiency virus-1', *Cell Host Microbe*, 12: 109-16.

Sarma, J. V., and P. A. Ward. 2011. 'The complement system', *Cell Tissue Res*, 343: 227-35.

Sarvestani, S. T., M. D. Tate, J. M. Moffat, A. M. Jacobi, M. A. Behlke, A. R. Miller, S. A. Beckham, C. E. McCoy, W. Chen, J. D. Mintern, M. O'Keeffe, M. John, B. R. Williams, and M. P. Gantier. 2014. 'Inosine-mediated modulation of RNA sensing by Toll-like receptor 7 (TLR7) and TLR8', *J Virol*, 88: 799-810.

Schauer, C., C. Janko, L. E. Munoz, Y. Zhao, D. Kienhofer, B. Frey, M. Lell, B. Manger, J. Rech, E. Naschberger, R. Holmdahl, V. Krenn, T. Harrer, I. Jeremic, R. Bilyy, G. Schett, M. Hoffmann, and M.

Herrmann. 2014. 'Aggregated neutrophil extracellular traps limit inflammation by degrading cytokines and chemokines', *Nat Med*, 20: 511-7.

Schober, P., C. Boer, and L. A. Schwarte. 2018. 'Correlation Coefficients: Appropriate Use and Interpretation', *Anesth Analg*, 126: 1763-68.

Schon, M. P., S. M. Broekaert, and L. Erpenbeck. 2017. 'Sexy again: the renaissance of neutrophils in psoriasis', *Exp Dermatol*, 26: 305-11.

Shan, L., D. Yang, F. Feng, D. Zhu, and X. Li. 2021. 'miR-3146 induces neutrophil extracellular traps to aggravate gout flare', *J Clin Lab Anal*, 35: e24032.

Shao, S., H. Fang, E. Dang, K. Xue, J. Zhang, B. Li, H. Qiao, T. Cao, Y. Zhuang, S. Shen, T. Zhang, P. Qiao, C. Li, J. E. Gudjonsson, and G. Wang. 2019. 'Neutrophil Extracellular Traps Promote Inflammatory Responses in Psoriasis via Activating Epidermal TLR4/IL-36R Crosstalk', *Front Immunol*, 10: 746.

Silvestre-Roig, C., Z. G. Fridlender, M. Glogauer, and P. Scapini. 2019. 'Neutrophil Diversity in Health and Disease', *Trends Immunol*, 40: 565-83.

Simon, S. I., A. R. Burns, A. D. Taylor, P. K. Gopalan, E. B. Lynam, L. A. Sklar, and C. W. Smith. 1995. 'L-selectin (CD62L) cross-linking signals neutrophil adhesive functions via the Mac-1 (CD11b/CD18) beta 2-integrin', *J Immunol*, 155: 1502-14.

Sioud, M. 2020. 'RNA Interference and CRISPR Technologies Technical Advances and New Therapeutic Opportunities Preface', *Rna Interference and Crispr Technologies: Technical Advances and New Therapeutic Opportunities*, 2115: V-Vii.

Skokowa, J., D. C. Dale, I. P. Touw, C. Zeidler, and K. Welte. 2017. 'Severe congenital neutropenias', *Nat Rev Dis Primers*, 3: 17032.

Smolarz, M., M. Zawrotniak, D. Satala, and M. Rapala-Kozik. 2021. 'Extracellular Nucleic Acids Present in the Candida albicans Biofilm Trigger the Release of Neutrophil Extracellular Traps', *Front Cell Infect Microbiol*, 11: 681030.

Song, J., D. Chen, Y. Pan, X. Shi, Q. Liu, X. Lu, X. Xu, G. Chen, and Y. Cai. 2021. 'Discovery of a Novel MyD88 Inhibitor M20 and Its Protection Against Sepsis-Mediated Acute Lung Injury', *Front Pharmacol*, 12: 775117.

Sorensen, O., K. Arnljots, J. B. Cowland, D. F. Bainton, and N. Borregaard. 1997. 'The human antibacterial cathelicidin, hCAP-18, is synthesized in myelocytes and metamyelocytes and localized to specific granules in neutrophils', *Blood*, 90: 2796-803.

Sorensen, O. E., and N. Borregaard. 2016. 'Neutrophil extracellular traps - the dark side of neutrophils', *J Clin Invest*, 126: 1612-20.

Suzuki, E., E. D. Mellins, M. E. Gershwin, F. O. Nestle, and I. E. Adamopoulos. 2014. 'The IL-23/IL-17 axis in psoriatic arthritis', *Autoimmun Rev*, 13: 496-502.

Tabeta, K., K. Hoebe, E. M. Janssen, X. Du, P. Georgel, K. Crozat, S. Mudd, N. Mann, S. Sovath, J. Goode, L. Shamel, A. A. Herskovits, D. A. Portnoy, M. Cooke, L. M. Tarantino, T. Wiltshire, B. E. Steinberg, S. Grinstein, and B. Beutler. 2006. 'The Unc93b1 mutation 3d disrupts exogenous antigen presentation and signaling via Toll-like receptors 3, 7 and 9', *Nat Immunol*, 7: 156-64.

Taguchi, A., Y. Suei, M. Ohtsuka, K. Otani, K. Tanimoto, and M. Ohtaki. 1996. 'Usefulness of panoramic radiography in the diagnosis of postmenopausal osteoporosis in women. Width and morphology of inferior cortex of the mandible', *Dentomaxillofac Radiol*, 25: 263-7.

Takeuchi, O., and S. Akira. 2010. 'Pattern recognition receptors and inflammation', *Cell*, 140: 805-20.

Takizawa, T., and J. M. Robinson. 2004. 'Thin is better!: ultrathin cryosection immunocytochemistry', *J Nippon Med Sch*, 71: 306-7.

Tamassia, N., F. Arruda-Silva, H. L. Wright, R. J. Moots, E. Gardiman, F. Bianchetto-Aguilera, S. Gasperini, M. Capone, L. Maggi, F. Annunziato, S. W. Edwards, and M. A. Cassatella. 2019. 'Human neutrophils activated via TLR8 promote Th17 polarization through IL-23', *J Leukoc Biol*, 105: 1155-65.

Tan, C., M. Aziz, and P. Wang. 2021. 'The vitals of NETs', *J Leukoc Biol*, 110: 797-808.

Tanji, H., U. Ohto, T. Shibata, M. Taoka, Y. Yamauchi, T. Isobe, K. Miyake, and T. Shimizu. 2015. 'Toll-like receptor 8 senses degradation products of single-stranded RNA', *Nat Struct Mol Biol*, 22: 109-15.

Teng, T. S., A. L. Ji, X. Y. Ji, and Y. Z. Li. 2017. 'Neutrophils and Immunity: From Bactericidal Action to Being Conquered', *J Immunol Res*, 2017: 9671604.

Tosar, J. P., K. Witwer, and A. Cayota. 2021. 'Revisiting Extracellular RNA Release, Processing, and Function', *Trends Biochem Sci*, 46: 438-45.

Touraine, J. L., H. Betuel, C. Pouteil-Noble, and C. Royo. 1989. 'HLA class II antigens: structure, function, and expression in immunodeficiencies, autoimmune diseases, and allograft rejection', *Adv Nephrol Necker Hosp*, 18: 325-34.

Ullah, M., A. Akbar, and G. Yannarelli. 2020. 'Clinical Applications of RNA Editing Technology for the Early Detection of Cancer and Future Directions', *Technol Cancer Res Treat*, 19: 1533033820964194.

van der Fits, L., S. Mourits, J. S. Voerman, M. Kant, L. Boon, J. D. Laman, F. Cornelissen, A. M. Mus, E. Florencia, E. P. Prens, and E. Lubberts. 2009. 'Imiquimod-induced psoriasis-like skin inflammation in mice is mediated via the IL-23/IL-17 axis', *J Immunol*, 182: 5836-45.

van Rooij, E., and E. N. Olson. 2012. 'MicroRNA therapeutics for cardiovascular disease: opportunities and obstacles', *Nat Rev Drug Discov*, 11: 860-72.

Van Tassell, B. W., I. M. Seropian, S. Toldo, F. N. Salloum, L. Smithson, A. Varma, N. N. Hoke, C. Gelwix, V. Chau, and A. Abbate. 2010. 'Pharmacologic inhibition of myeloid differentiation factor 88 (MyD88) prevents left ventricular dilation and hypertrophy after experimental acute myocardial infarction in the mouse', *J Cardiovasc Pharmacol*, 55: 385-90.

Vellai, T., and G. Vida. 1999. 'The origin of eukaryotes: the difference between prokaryotic and eukaryotic cells', *Proc Biol Sci*, 266: 1571-7.

Venegas, F. A., G. Kollisch, K. Mark, W. E. Diederich, A. Kaufmann, S. Bauer, M. Chavarria, J. J. Araya, and A. J. Garcia-Pineres. 2019. 'The Bacterial Product Violacein Exerts an Immunostimulatory Effect Via TLR8', *Sci Rep*, 9: 13661.

Veras, F. P., M. C. Pontelli, C. M. Silva, J. E. Toller-Kawahisa, M. de Lima, D. C. Nascimento, A. H. Schneider, D. Caetite, L. A. Tavares, I. M. Paiva, R. Rosales, D. Colon, R. Martins, I. A. Castro, G. M. Almeida, M. I. F. Lopes, M. N. Benatti, L. P. Bonjorno, M. C. Giannini, R. Luppino-Assad, S. L. Almeida, F. Vilar, R. Santana, V. R. Bollela, M. Auxiliadora-Martins, M. Borges, C. H. Miranda, A. Pazin-Filho, L. L. P. da Silva, L. D. Cunha, D. S. Zamboni, F. Dal-Pizzol, L. O. Leiria, L. Siyuan, S. Batah, A. Fabro, T. Mauad, M. Dolhnikoff, A. Duarte-Neto, P. Saldiva, T. M. Cunha, J. C. Alves-Filho, E. Arruda, P. Louzada-Junior, R. D. Oliveira, and F. Q. Cunha. 2020. 'SARS-CoV-2-triggered neutrophil extracellular traps mediate COVID-19 pathology', *J Exp Med*, 217.

Vierbuchen, T., C. Bang, H. Rosigkeit, R. A. Schmitz, and H. Heine. 2017. 'The Human-Associated Archaeon Methanosphaera stadtmanae Is Recognized through Its RNA and Induces TLR8-Dependent NLRP3 Inflammasome Activation', *Front Immunol*, 8: 1535.

Vlach, J., A. T. Bender, M. Przetak, A. Pereira, A. Deshpande, T. L. Johnson, S. Reissig, E. Tzvetkov, D. Musil, N. T. Morse, P. Haselmayer, S. C. Zimmerli, S. L. Okitsu, R. L. Walsky, and B. Sherer. 2021. 'Discovery of M5049: A Novel Selective Toll-Like Receptor 7/8 Inhibitor for Treatment of Autoimmunity', *J Pharmacol Exp Ther*, 376: 397-409.

Warnatsch, A., M. Ioannou, Q. Wang, and V. Papayannopoulos. 2015. 'Inflammation. Neutrophil extracellular traps license macrophages for cytokine production in atherosclerosis', *Science*, 349: 316-20.

Weiner, D. J., R. Bucki, and P. A. Janmey. 2003. 'The antimicrobial activity of the cathelicidin LL37 is inhibited by F-actin bundles and restored by gelsolin', *Am J Respir Cell Mol Biol*, 28: 738-45.

Whittall-Garcia, L. P., J. Torres-Ruiz, A. Zentella-Dehesa, M. Tapia-Rodriguez, J. Alcocer-Varela, N. Mendez-Huerta, and D. Gomez-Martin. 2019. 'Neutrophil extracellular traps are a source of extracellular

HMGB1 in lupus nephritis: associations with clinical and histopathological features', *Lupus*, 28: 1549-57.

Wiese, M. D., A. T. Manning-Bennett, and A. Y. Abuhelwa. 2020. 'Investigational IRAK-4 inhibitors for the treatment of rheumatoid arthritis', *Expert Opin Investig Drugs*, 29: 475-82.

Wolff, G., and M. Barcena. 2021. 'Multiscale Electron Microscopy for the Study of Viral Replication Organelles', *Viruses*, 13.

Xiao, Y., M. Cong, J. Li, D. He, Q. Wu, P. Tian, Y. Wang, S. Yang, C. Liang, Y. Liang, J. Wen, Y. Liu, W. Luo, X. Lv, Y. He, D. D. Cheng, T. Zhou, W. Zhao, P. Zhang, X. Zhang, Y. Xiao, Y. Qian, H. Wang, Q. Gao, Q. C. Yang, Q. Yang, and G. Hu. 2021. 'Cathepsin C promotes breast cancer lung metastasis by modulating neutrophil infiltration and neutrophil extracellular trap formation', *Cancer Cell*, 39: 423-37 e7.

Xu, J., V. Chmela, N. J. Green, D. A. Russell, M. J. Janicki, R. W. Gora, R. Szabla, A. D. Bond, and J. D. Sutherland. 2020. 'Selective prebiotic formation of RNA pyrimidine and DNA purine nucleosides', *Nature*, 582: 60-66.

Xu, Z., L. Shi, Y. Wang, J. Zhang, L. Huang, C. Zhang, S. Liu, P. Zhao, H. Liu, L. Zhu, Y. Tai, C. Bai, T. Gao, J. Song, P. Xia, J. Dong, J. Zhao, and F. S. Wang. 2020. 'Pathological findings of COVID-19 associated with acute respiratory distress syndrome', *Lancet Respir Med*, 8: 420-22.

Yang, J., J. Lan, H. Du, X. Zhang, A. Li, X. Zhang, Y. Liu, J. Zhang, C. Zhang, Y. Ding, and T. Zhang. 2019. 'Icariside II induces cell cycle arrest and differentiation via TLR8/MyD88/p38 pathway in acute myeloid leukemia cells', *Eur J Pharmacol*, 846: 12-22.

Yang, L., L. M. Qiu, Q. Fang, D. W. Stanley, and G. Y. Ye. 2021. 'Cellular and humoral immune interactions between Drosophila and its parasitoids', *Insect Sci*, 28: 1208-27.

Yaqinuddin, A., and J. Kashir. 2020. 'Novel therapeutic targets for SARS-CoV-2-induced acute lung injury: Targeting a potential IL-1beta/neutrophil extracellular traps feedback loop', *Med Hypotheses*, 143: 109906.

Yasuda, K., M. Rutz, B. Schlatter, J. Metzger, P. B. Luppa, F. Schmitz, T. Haas, A. Heit, S. Bauer, and H. Wagner. 2006. 'CpG motif-independent activation of TLR9 upon endosomal translocation of "natural" phosphodiester DNA', *Eur J Immunol*, 36: 431-6.

Ye, W., and Y. Murata. 2016. 'Microbe Associated Molecular Pattern Signaling in Guard Cells', *Front Plant Sci*, 7: 583.

Yip, K. M., N. Fischer, E. Paknia, A. Chari, and H. Stark. 2020. 'Atomic-resolution protein structure determination by cryo-EM', *Nature*, 587: 157-61.

Yipp, B. G., B. Petri, D. Salina, C. N. Jenne, B. N. Scott, L. D. Zbytnuik, K. Pittman, M. Asaduzzaman, K. Wu, H. C. Meijndert, S. E. Malawista, A. de Boisfleury Chevance, K. Zhang, J. Conly, and P. Kubes. 2012. 'Infection-induced NETosis is a dynamic process involving neutrophil multitasking in vivo', *Nat Med*, 18: 1386-93.

Yousefi, S., J. A. Gold, N. Andina, J. J. Lee, A. M. Kelly, E. Kozlowski, I. Schmid, A. Straumann, J. Reichenbach, G. J. Gleich, and H. U. Simon. 2008. 'Catapult-like release of mitochondrial DNA by eosinophils contributes to antibacterial defense', *Nat Med*, 14: 949-53.

Yousefi, S., C. Mihalache, E. Kozlowski, I. Schmid, and H. U. Simon. 2009. 'Viable neutrophils release mitochondrial DNA to form neutrophil extracellular traps', *Cell Death Differ*, 16: 1438-44.

Yu, A. M., Y. H. Choi, and M. J. Tu. 2020. 'RNA Drugs and RNA Targets for Small Molecules: Principles, Progress, and Challenges', *Pharmacol Rev*, 72: 862-98.

Zack, G. W., W. E. Rogers, and S. A. Latt. 1977. 'Automatic measurement of sister chromatid exchange frequency', *J Histochem Cytochem*, 25: 741-53.

Zanetti, M. 2004. 'Cathelicidins, multifunctional peptides of the innate immunity', *J Leukoc Biol*, 75: 39-48.

Zanetti, M., R. Gennaro, and D. Romeo. 1995. 'Cathelicidins: a novel protein family with a common proregion and a variable C-terminal antimicrobial domain', *FEBS Lett*, 374: 1-5.

Zerial, M., and H. McBride. 2001. 'Rab proteins as membrane organizers', *Nat Rev Mol Cell Biol*, 2: 107-17.

Zhang, N., X. Aiyasiding, W. J. Li, H. H. Liao, and Q. Z. Tang. 2022. 'Neutrophil degranulation and myocardial infarction', *Cell Commun Signal*, 20: 50.

Zhang, S., Z. Hu, H. Tanji, S. Jiang, N. Das, J. Li, K. Sakaniwa, J. Jin, Y. Bian, U. Ohto, T. Shimizu, and H. Yin. 2018. 'Small-molecule inhibition of TLR8 through stabilization of its resting state', *Nat Chem Biol*, 14: 58-64.

Zhang, Y., V. Chandra, E. Riquelme Sanchez, P. Dutta, P. R. Quesada, A. Rakoski, M. Zoltan, N. Arora, S. Baydogan, W. Horne, J. Burks, H. Xu, P. Hussain, H. Wang, S. Gupta, A. Maitra, J. M. Bailey, S. J. Moghaddam, S. Banerjee, I. Sahin, P. Bhattacharya, and F. McAllister. 2020. 'Interleukin-17-induced neutrophil extracellular traps mediate resistance to checkpoint blockade in pancreatic cancer', *J Exp Med*, 217.

Zhao, J., and J. Jin. 2022. 'Neutrophil extracellular traps: New players in cancer research', *Front Immunol*, 13: 937565.

Zuchtriegel, G., B. Uhl, D. Puhr-Westerheide, M. Pornbacher, K. Lauber, F. Krombach, and C. A. Reichel. 2016. 'Platelets Guide Leukocytes to Their Sites of Extravasation', *PLoS Biol*, 14: e1002459.

Zuo, Y., S. Yalavarthi, H. Shi, K. Gockman, M. Zuo, J. A. Madison, C. Blair, A. Weber, B. J. Barnes, M. Egeblad, R. J. Woods, Y. Kanthi, and J. S. Knight. 2020. 'Neutrophil extracellular traps in COVID-19', *JCI Insight*, 5.